Exploring the Pre-B cell receptor checkpoint as a therapeutic target in acute lymphoblastic leukaemia

Ali Haider Alhammer

Thesis submitted in part requirement for the degree of Doctor of Philosophy (PhD)

Wolfson Childhood Cancer Research Centre

Northern Institute for Cancer Research

Herschel Building, Level 6

Faculty of Medical Sciences

Newcastle University

Newcastle upon Tyne

NE1 7RU

January 2018

Abstract

Acute lymphoblastic leukaemia (ALL) is a clonal disorder of developing lymphocytes and is the most common malignancy in children and adolescents. While cure rates are high, treatment is associated with significant morbidity and relapsed ALL remains one of the leading causes of cancer-related deaths in children. New, less toxic therapies are clearly needed for refractory ALL.

There are number of lines of evidence to suggest that ALL cells hijack component of Pre-B cell receptor signalling and that this dependency may be amenable to therapeutic exploitation. There are a number of tyrosine kinase inhibitors (TKIs) targeting Pre-BCR signalling that are showing great promise in the clinic for other leukaemic subtypes which warrant preclinical evaluation in childhood ALL. These include CAL-101 (PI3K-δ inhibitor), Ibrutinib (BTK inhibitor), Fostamatinib (SYK inhibitor) and Dasatinib (BCR-ABL/SRC inhibitor).

TKIs were evaluated in ALL cells, including cell lines and patient derived xenograft samples (PDX) from 15 predominantly high risk/relapse primary ALLs. ALL cell lines were generally resistant to all drugs but modest sensitivity was seen to the active form of fostamatinib, R406 and dasatinib in Pre-BCR^{+} cells. CAL-101 and dasatinib were shown to be cytostatic, while ibrutinib and R406 were associated with cell cycle arrest and induction of apoptosis. Pharmacodynamic assessments using phospho-flow cytometry and western blotting showed inhibition of the relevant targets at the GI_{50} concentrations. PDX ALL cells were generally more sensitive than the cell lines; CAL-101 (2 from 14 PDXs); ibrutinib (3 from 14 PDXs); R406 (6 from 15 PDXs) and dasatinib (4 from 15 PDXs). Pre-BCR^{+} ALL cells were more likely to be sensitive to dasatinib and fostamatinib. Some Pre-BCR^{-} ALL were also sensitive to some TKIs, although predictive biomarkers remain to be established.

Significant synergism was seen after co-treatment of the TKIs with the glucocorticoid (GC), dexamethasone. This was most marked for the dexamethasone and dasatinib combination and significantly potentiated G1 arrest and apoptosis in both GC sensitive and resistant ALL cells. Synergism was associated with a significant increase in expression of the GR target, *GILZ* and enhanced induction of proapoptotic BIM. *In vivo* preclinical confirmation of these data may offer new therapies for refractory ALL.

Acknowledgements

First and foremost, I would like to thank God for the mercy and never-ending grace.

My deep gratitude to my supervisor Prof. Julie Irving, who encouraged me to pursue this study and taught me the art of exploring targeted therapies in ALL. I truly enjoyed working under your research atmosphere which stimulate initiative and critical thinking. Great appreciation to my second supervisor Prof. Josef Vormoor for his innovative ideas and sympathetic attitude at every point throughout my research. Many thanks for Liz Matheson `the queen of western blotting` , Marian Case and Lynne Minto for their help from the very beginning of my PhD study and for giving me a lot of precious suggestions. I`m very grateful to Helen Blair who assisted me in the mouse work in CBC. Thanks to Zach Dixon and Rosie Jackson, it was a great pleasure working with you in the same lab and thanks for offering me the help when needed. I would also like to acknowledge my progression panel Prof. Christine Harrison and Prof. Sophie Hambleton for their helpful suggestions. I'm also thankful to everyone who I was working with throughout my study at Newcastle University.

This work would not materialise without the financial support from the Iraqi Cultural Attaché-London, the official representative of Iraqi ministry of higher education and scientific research. Also my deepest appreciation for Biotechnology research centre at Al-Nahrain University for nominating me to have this scholarship.

I`m very grateful to my parents, without whom I was nothing, and my brothers and sister for their moral and emotional support, in spite of being far away from me. Finally, I`m very grateful to my wife, Dunya, for always being so encouraging and supportive during tough and difficult times, without you, this work might not come into this shape.

Table of contents

List of figures

List of tables

List of abbreviations

Abbreviation	Meaning
µHC	Igµ heavy chain
ALL	Acute lymphoblastic leukaemia
BACH2	bric-a`-brac, tramtrack and broad complex and cap‟n‟collar homology
BCA	Bicinchoninic acid
BCAP	B cell PI3K adapter
BCL-6	B cell lymphoma-6
BCP-ALL	B-cell precursor acute lymphoblastic leukemia
BCR	B cell receptor
BLNK	B cell linker protein
B-NHL	B-non Hodgkin lymphoma
BSA	Bovine serum albumin
BTK	Bruton`s tyrosine kinase
CAN	Copy number alteration
CAR T	T cells with chimeric antigen receptor
CCD	Charge coupled device
CD	Clusters of differentiation
cDNA	copy DNA
CI	Combination index
CLL	Chronic lymphocytic leukaemia
C_{max}	The maximum drug concentration achieved in the serum
CML	Chronic myeloid leukaemia

CNAs	Copy number alterations
CREB1	cyclic AMP-responsive element-binding protein 1
CRLF2	Cytokine receptor like-factor 2
C_T	Threshold cycle
CV	Control vehicle
D_H	Diversity segment
DHFR	Dihydrofolate reductase
DLBCL	Diffuse large B-cell lymphoma
DMSO	Dimethyl sulphoxide
DNA	Deoxy-ribonucleic acid
ECACC	European Collection of Cell Cultures
ED	Effective dose
EPOR	Erythropoietin receptor
ERK	Extracellular signal-regulated kinase
FA	Fraction affected
FAM	6-carboxyfluorescein
FBS	Foetal bovine serum
FDA	Food and drug administration
FL	Follicular lymphoma
FLT3	fms-Related tyrosine kinase 3
FOXO1	Forkhead box protein O1
FRET	Fluorescence Resonance Energy Transfer
GC	Glucocorticoid
GCR	Glucocorticoid receptor complex

GI_{50}	The drug dose that decreases cells proliferation to 50% when compared to the control
GILZ	Glucocorticoid-Induced Leucine Zipper
GR	Glucocorticoid receptor
GRB2	Growth factor receptor bound protein 2
GRE	Glucocorticoid response element
HCL	Hairy cell leukemia
HRP	Horseradish peroxidase
iAMP21	intrachromosomal amplification of chromosome 21
IC_{50}	The drug concentration that inhibits half maximal protein kinase activity
Ig	Immunoglobulin
Igμ	Ig heavy chain
IgH	Ig heavy chain
IgL	Ig light chain
Igκ	Immunoglobulin light chain
IL-7R	Interleukin-7 receptor
IRF4	Interferon regulatory factor-4
ITAMs	Immuno-receptor tyrosine-based activation motifs
JAK3	Janus kinase3
J_H	Joining segment
LCIS	Live Cell Imaging Solution
L-GILZ	Long variant of GILZ
MCL	Mantle cell lymphoma

MFI	Mean fluorescent intensity
MRD	Minimal residual disease
NICR	Northern Institute for Cancer Research
NOD/SCID	Non-obese diabetic/severe combined immunodeficiency
NSG	IL-2R common gamma chain null
PBS	Phosphate buffered saline
PBSA	0.2% BSA in PBS
PDX	Primary-derived xenograft cells
Ph^+	Philadelphia chromosome positive
PI	Propidium iodide
PI3K-δ	Phosphatidylinositol 3-kinase-δ
PKB	Phosphoinositide-3 kinase-Protein kinase B
PLC-ɣ2	Phospholipase C-ɣ2
Pre-BCR	Precursor B cell receptor
PS	Phosphatidyl serine
PtdIns (3,4,5)P3	Phosphatidylinositol 3,4,5-triphosphate
PtdIns (4,5)P2	Phosphatidylinositol-4,5-biphosphate
PVDF	Polyvinylidine difluoride
QRT-PCR	Quantitative reverse-transcriptase polymerase chain reaction
RAG	Recombination activation gene
RAS	Rat sarcoma kinase
RF10	RPMI 1640, supplemented with 10% heat-inactivated foetal bovine serum

RF15	RPMI 1640, supplemented with 15% heat-inactivated foetal bovine serum
RPM	Revolutions per minute
RPPA	Reverse phase protein array
SDS	Sodium dodecyl sulphate
SFKs	SRC-family kinases
SLC	Surrogate light chain
SLL	Small lymphocytic lymphoma
SNP	Single nucleotide polymorphism
STAT5	Signal transducer and activator of transcription 5
STR	Short tandem repeat
SYK	Spleen tyrosine kinase
T-ALL	T-leneage acute lymphoblastic leukaemia
TAMRA	6-carboxy-tetramethyl-rhodamine
TBP	TATA-box binding Protein
TBS	Tris-Buffered Saline
TBST	Tris-Buffered Saline supplemented with Tween-20
TKI	Tyrosine kinase inhibitor
TP53	Tumour protein P53
UV	Ultra violet
V_H	Variable segment
WM	Waldenström macroglobulinemia
WBC	White blood cells count
ZAP70	ζ-chain associated protein kinase of 70 KDa

Chapter 1: Introduction

Chapter 1: Introduction

Acute lymphoblastic leukaemia (ALL)

Leukaemia is a form of cancer derived from hematopoietic stem cells with an abnormal proliferative mechanism. Like other kinds of cancer, blood malignancy emerges from a genetically altered single cell that then propagates the leukaemia. Generally, leukaemia is sub grouped into chronic or acute, occurring as either myeloid or lymphoid forms. The term chronic is used to depict leukaemia of a slow propagation of well differentiated cells, whilst acute refers to the fast proliferation of undifferentiated progenitor cells (Passegue *et al.*, 2003; Popat and Abraham, 2011; Arber *et al.*, 2016). ALL is the most prevalent childhood Cancer and is one of the most common causes of cancer-related demises (Inaba *et al.*, 2013). The haematological malignancy of focus in this study is acute lymphoblastic leukaemia (ALL).

1.1 Biology of ALL

ALL is a malignancy of blood forming cells in the bone marrow and is characterised by continuously dividing cells with maturation arrest, which leads to blast accumulation (Popat and Abraham, 2011) and is often a consequence of chromosomal abnormalities (Mullighan *et al.*, 2007; Mårtensson *et al.*, 2010; Harrison, 2011). The accumulation of immature lymphoblastoid cells in the bone marrow hinders normal haematopoiesis and over population may lead to spilling of the malignant cells into the peripheral blood and organ infiltration (Passegue *et al.*, 2003; Larson and Anastasi, 2008). ALL is characterized by bone marrow overproduction of white blood cells, and depending on immunophenotypic features, it is categorized as B-cell precursor ALL (BCP-ALL), the most common type, with fewer cases presenting as mature B or T-cell immunophenotypes (Winick *et al.*, 2004; Pui *et al.*, 2008).

1.2 Incidence of ALL

ALL is the most common childhood malignancy, representing about one quarter of childhood cancers (Ries *et al.*, 1999; Pui *et al.*, 2008; Ward *et al.*, 2014). In the United States, the incidence of this disease is 37-49 cases in 1 million children per year, with the 2-5 years age group registering the greatest incidence (Howlader *et al.*, 2013).

Over the last two decades, the incidence of ALL has gradually increased, but developments in both diagnosis and treatment with risk-adapted treatment regimens have raised the cure rate to around 90% (Conter *et al.*, 2010; Hunger *et al.*, 2012; Howlader *et al.*, 2013).

1.3 Causes of ALL

Although the specific causes of ALL in most patients are still not known and may be multifactorial, exposure to certain drugs or ionizing radiation, acquired or congenital immune deficiencies (such as ataxia-telangiectasia) and chromosomal abnormalities are implicated (Pui *et al.*, 2008; Pui *et al.*, 2012a). Interestingly, studies using Guthrie cards and monozygotic twins have shown that the development of ALL may be caused by pre and post-natal events (Wiemels *et al.*, 1999; Greaves, 2005). A variety of genetic alterations associated with leukaemic cells were identified in blood spots taken a few days after birth (Wiemels *et al.*, 1999; McHale *et al.*, 2003). Moreover, another study found that the existence of the *ETV6-RUNX1* fusion in cord blood was 100 times greater than the incidence in children with *ETV6-RUNX1* ALL (Mori *et al.*, 2002), suggesting that the development of ALL required additional postnatal events, such as wild type *ETV6* deletion (Mori *et al.*, 2002; Wiemels, 2012). Also, twin studies demonstrated that the transfer of pre-leukaemic clones between monozygotic twins was occurring *in utero* through the placenta and hence provided evidence of prenatal origin of ALL. However, other events are needed for the development of ALL disease (Greaves *et al.*, 2003; Maia *et al.*, 2003).

1.4 Classification of ALL

ALL is a heterogeneous blood disease but it can be classified depending on cytogenetics, sub-microscopic genetic lesions and immunophenotyping.

1.4.1 Cytogenetics

The hallmark of BCP-ALL is the presence of genetic abnormalities that affect differentiation (Mullighan *et al.*, 2007; Pui *et al.*, 2008; Iacobucci and Mullighan, 2017). Childhood ALL is grouped into subtypes depending on gross cytogenetic aberrations. These genetic alterations include numerical (ploidy) or structural changes of the chromosomes. The cytogenetic subgroup high hyperdiploidy (>50 chromosomes) is present in 30% of BCP-ALL cases, while hypodiploid (<44 chromosomes) is much rarer, being found in less than 1% of BCP-ALL patients (Moorman, 2012; Mullighan, 2012) (Figure 1.1).

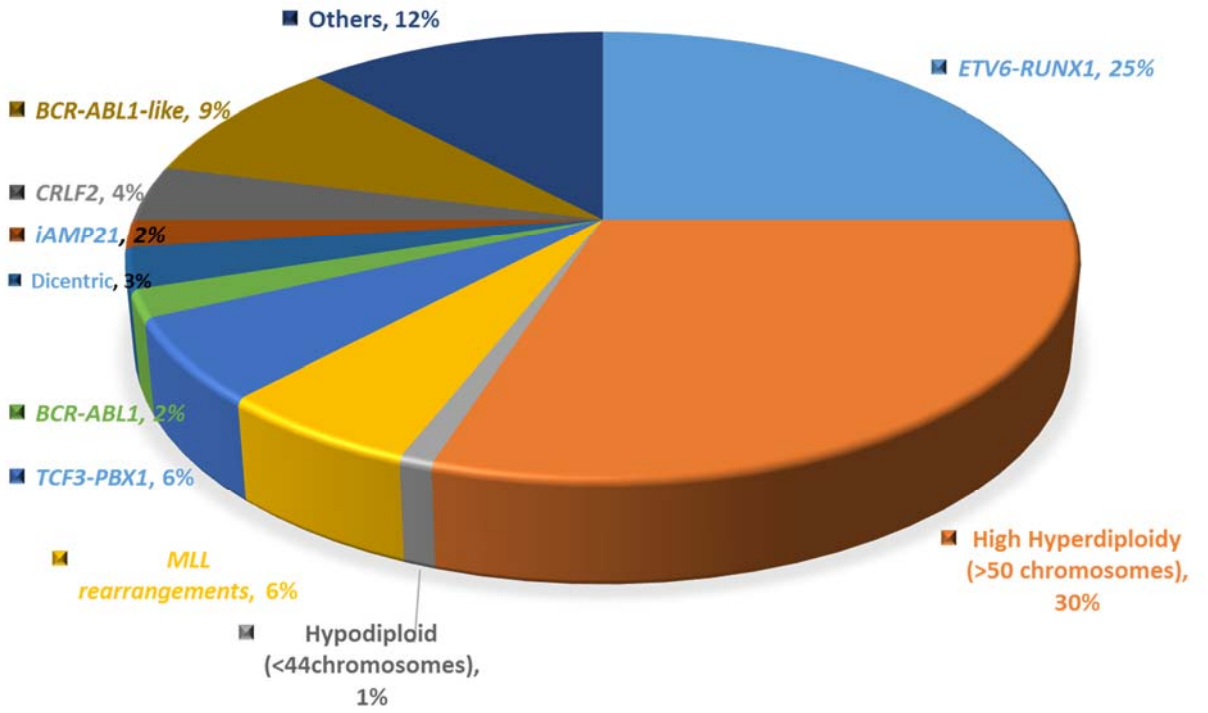

Figure 1.1: Estimated frequencies of selected chromosomal rearrangements and other genetic lesions in childhood BCP-ALL patients, adapted from: (Inaba *et al.*, 2013).

Chromosomal translocations can lead to the formation of fusion proteins and such structural genetic alterations are considered defining features of leukaemia. In BCP-ALL cell malignancy, four of the most common recurrent genetic alterations include *ETV6-RUNX1*, *MLL* rearrangement at 11q23 linked with a variety of fusion genes, *TCF3-PBX1* and *BCR-ABL1* (Figure 1.1). While the *BCR-ABL1* fusion gene encodes a constitutively active tyrosine kinase, oncogenic transcription factors are also encoded by *ETV6-RUNX1* and *MLL-AF4* fusion genes (Look, 1997; Mullighan, 2012; Woo *et al.*, 2014).

The most common translocation in childhood BCP-ALL cell malignancy is the t(12;21)(p13;q22), which results in the ETV6-RUNX1 (Rubnitz *et al.*, 2008; Mullighan, 2012) fusion protein and is found in about 25% of children with ALL and grants an excellent prognosis (Figure 1.1) (Moorman *et al.*, 2010; Gandemer *et al.*, 2012). While the *ETV6* and *RUNX1* are transcription factors important for normal production of blood cells (Okuda *et al.*, 1996), the fusion protein (ETV6-RUNX1) disrupts the normal expression of genes regulated by *RUNX1* by altering its function into a transcriptional repressor leading to the unlimited proliferation of haematopoietic cells with differentiation arrest at BCP stage (Hiebert *et al.*, 1996; Morrow *et al.*, 2004; Fischer *et al.*, 2005).

TCF3-PBX1 is a chimeric transcriptional factor resulting from the chromosomal translocation t(1;19)(q23;p13), in which Homebox protein (PBX1) is converted into a trans-activating factor and the expression of *TCF3* encoded proteins (E12 and E47), which are essential factors in B lymphopoiesis, are reduced (Lu and Kamps, 1997; Aspland *et al.*, 2001). This translocation exists in 6% of childhood BCP-ALL malignancy (Figure 1.1), but because of the contemporary advanced treatment regimens, the clinical outcomes of children with this aberration have changed from poor to intermediate prognosis (Schmiegelow *et al.*, 2010).

The chromosomal rearrangement t(9;22)(q34;q11) is traditionally called the Philadelphia chromosome (Ph^+) and is very common in chronic myeloid leukaemia and also present in 2-5 % of childhood ALL (Ribeiro *et al.*, 1987; Armstrong and Look, 2005; Moorman, 2012). This translocation encodes for the oncogenic fusion protein BCR-ABL1 which is sufficient to transform B-precursors into malignant cells due to its constitutive activity (Huettner *et al.*, 2000) leading to hyper activation of RAS pathway, unlike normal ABL1 kinase in which kinase activity is tightly regulated (Melo, 1996; Cilloni and Saglio, 2012). This cytogenetic group was traditionally characterized by the worst clinical prognosis but the clinical outcome has

improved with the introduction of tyrosine kinase inhibitors (TKIs) such as imatinib and dasatinib (Schultz *et al.*, 2009; Ravandi *et al.*, 2010; Schultz *et al.*, 2014). In addition, a subgroup has been found recently and exists in 15-20% of ALL patients called *BCR-ABL1-like* (Ph-like). This subgroup is characterised by having a genetic signature similar to that of *BCR-ABL1*, but without the Ph^+ translocation (Den Boer *et al.*, 2009; Mullighan and Downing, 2009). Recently, it was found that patients with *BCR-ABL1-like* had higher percentage of kinase activating lesions, and a patient with the novel fusion *EBFI-PDGFRB* was sensitive to the TKI, imatinib *in vivo* (Roberts *et al.*, 2014; Ishibashi *et al.*, 2016).

The *MLL* (Mixed-lineage leukaemia) gene that locates at band 11q23 on chromosome 11 is a promiscuous gene that can fuse with a large number of partner genes (Meyer *et al.*, 2009; Meyer *et al.*, 2013). It is generally held that the leukaemogenic effect is owed to the fusion of the *MLL* 5` portion to the 3` portion of chimeric partner gene on chromosome 11. *MLL* rearrangements are present in 6% of children with BCP-ALL (Figure 1.1) and 70-80% of all infant acute BCP-leukaemia (Moorman, 2012). *MLL-AFF1* (formerly *AF4*) is the most common MLL translocation t(4;11)(q21;q23) in infants, followed by *MLL-MLLT3* (*AF9*) encoded by t(9;11)(p22;q23), *MLL-ENL* encoded by t(11;19)(q23;p13.3), and *MLL-MLLT10* (*AF10*) encoded by t(10;11)(p13-14;q14-21) (Chessells *et al.*, 2002; Moorman *et al.*, 2005; Winters and Bernt, 2017). Infants are categorised as high risk because they have very poor prognosis and international trials are underway to improve their outcome (Pieters *et al.*, 2007; Brown, 2013).

Additionally, the gain of >3 extra copies of the *RUNX1*-containing region of chromosome 21, defines a subgroup known as intrachromosomal amplification of chromosome 21 (*iAMP21*), which was recently identified in 2% of patients with BCP-ALL (Rand *et al.*, 2011; Mullighan, 2012; Li *et al.*, 2014; Ryan *et al.*, 2016). Although it was associated previously with poor outcome, recently it was shown that intensive therapy could improve the outcome of iAMP21 patients significantly (Heerema *et al.*, 2013; Moorman *et al.*, 2013; Harrison *et al.*, 2014; Harrison, 2015).

1.4.2 Sub-microscopic genetic lesions

Recent developments in single nucleotide polymorphism (SNP) microarray have highlighted sub microscopic copy number alterations (CNAs) in BCP-ALL (Mullighan *et al.*, 2007; Mullighan, 2012). Compared to chromosomal translocations, which are generally initiating

leukaemogenesis events, these sub-microscopic lesions are collaborating aberrations that associate with a particular cytogenetic group (Schwab *et al.*, 2013). In patients with *ETV6-RUNX1* translocation, for example, there are 6-8 cooperative mutations (Sun *et al.*, 2017). The majority of the involved genes play crucial roles in lymphocytic malignancy development (*IKZF1, PAX5*), lymphoid signalling (*NR3C1*), tumor suppression and cell cycle regulation (*PTEN, CDKN2A/CDKN2B, RB1*) and co-activation and regulation of transcription (*ETV6*). The most mutated genes in BCP-ALL include *IKZF1, PAX5* and *CRLF2* (Moorman, 2012; Woo *et al.*, 2014).

The transcriptional factors genes *IKZF1* and *PAX5* were found to be involved the development of BCP-ALL disease. Maturation arrest may arise after loss of function, due to deletion or mutations in the *IKZF1* gene (codes for Ikaros protein). *IKZF1* mutations are found in 80% of *BCR-ABL1* positive ALL patients and in 15% of BCP-ALLs overall (Mullighan *et al.*, 2007; Mullighan *et al.*, 2008; Mullighan, 2012). Mutations in *PAX5* are present in about 32% of childhood ALL patients (Kuiper *et al.*, 2007; Mullighan *et al.*, 2008).

Mutations in *JAK1* in addition to *JAK2* may lead to constitutive activation of the JAK-STAT pathway, which play an important role in the proliferation of malignant ALL cells. Such mutations are frequent in patients with Down`s syndrome ALL (Bercovich *et al.*, 2008; Mullighan *et al.*, 2009b). In addition, overexpression of *CRLF2* also activated the JAK-STAT pathway which is found in about 15% of ALL patients (Mullighan *et al.*, 2009a; Cario *et al.*, 2010; Rand *et al.*, 2011).

In addition, mutations in genes which activate the RAS pathway (RAS/RAF/MEK/ERK) are very commonly mutated in BCP-ALL patients at both presentation and relapse and are associated with high risk (Case *et al.*, 2008; Zhang *et al.*, 2011; Irving *et al.*, 2014; Irving, 2016). Activation of the RAS pathway may alter proliferation, survival and differentiation of lymphoid precursor-B cells.

1.4.3 Immunophenotyping

Immunophenotyping allows the detection of intracellular and cell surface antigens and thus classifies the lineage and differentiation stage at which leukaemic cells were arrested during leukaemogenesis. Surface antigens, called clusters of differentiation (CD), markers are often key to ALL immunophenotyping. Classification based on this method revealed that the vast

majority of childhood ALL is B-Lineage (85%) and the remaining is T-lineage (15%) ALL (Onciu, 2009). For BCP-ALL leukaemia cells, CD19, CD20, CD22, CD24 and CD79a markers are used for classification, whereas, CD1a, CD2, CD3, CD4, CD5, CD7 and CD8 markers are used in the diagnosis and classification of T-ALL (Onciu, 2009; Chiaretti *et al.*, 2014). Depending on the expression pattern of B-lineage markers, B cell malignancy can be categorised into four stages; early Pre-B, Pre-B, transitional Pre-B and mature B cells (Chiaretti *et al.*, 2014). Moreover, It has been found that the Pre-BCR is only expressed in about 15% of BCP-ALL patients cells, therefore, depending on the expression of Pre-BCR components (see section 1.6 for further details), BCP-ALL leukaemia can be classified into two main groups; Pre-BCR^{+} and Pre-BCR^{-}. Expression of the receptor was associated with *TCF3-PBX1* positive cases as Pre-BCR gene upregulation was mediated by *TCF3-PBX1* directly (Geng *et al.*, 2015).

1.5 Prognosis of ALL

Prognostic factors at diagnosis include key clinical parameters as well as ALL specific features and assist the stratification of patients for the optimal intensity of therapy. For example, low risk patients could avoid the toxicity of unnecessary intensive therapy that needs to be given to patients with higher risk disease. Both initial white blood cell (WBC) count and age are relevant for outcome prediction. For patients to be classified as standard risk, the initial WBC count should be less than 50 000 WBC/mm3 and age from 1-9 years, however, anything above the ranges of standard risk is indicative of high risk (Smith *et al.*, 1996).

Favourable outcomes are associated with *ETV6-RUNX1* and high hyperdiploidy, whereas, *CRLF2* rearrangement is associated with intermediate risk group (Ensor *et al.*, 2011). Moreover, *MLL* rearrangements, hypodiploidy, *BCR-ABL1, BCR-ABL1-like* and *iAMP21* are associated with poor outcome (Nachman *et al.*, 2007; Arico *et al.*, 2010; Moorman *et al.*, 2010; Harrison *et al.*, 2014).

The clinical response to glucocorticoid (GC) treatment is a key prognostic factor for ALL. In separate Berlin-Frankfurt-Münster trials, a good response to prednisolone monotherapy treatment for seven days was predictive of good overall prognosis (Dordelmann *et al.*, 1999). In addition, several studies have highlighted minimal residual disease (MRD) levels, for example, sub-microscopic disease serve as a powerful prognostic marker (Coustan-Smith *et*

al., 2000; Borowitz *et al.*, 2008). Both PCR or flow cytometry techniques can be used to detect MRD and require a sensitivity to detect at least 1 blast cell in 10 000 normal cells (Campana, 2012; Pui *et al.*, 2015) . It has been found in MRD positive (MRD>0.01% at the end of induction treatment) patients, the risk of relapse is 3-5 times higher than MRD negative patients (MRD<0.01%), but intensification of therapy can improve the outcome for the latter group of patients (Coustan-Smith *et al.*, 2000; Conter *et al.*, 2010; Vora *et al.*, 2014). In addition, classification of very good risk patients as identified by MRD negativity, has led to dose de-escalation in these patients, without compromising overall survival rates (Vora *et al.*, 2014; Pui *et al.*, 2015; Schaink A, 2016).

1.6 B cell development

B cell lymphopoiesis is a stepwise maturation process of pluripotent haematopoietic stem cells into distinct stages (Pro-B, Pre-B and mature B lymphocytes), which is mediated by sequential DNA recombination of immunoglobulin (Ig) genes, leading to the expression of a highly diverse repertoire of antibodies (Herzog *et al.*, 2009; Rickert, 2013).

Ig heavy chain (*IgH*) gene rearrangement is initiated at early Pro-B or common lymphoid progenitor stage, in which a diversity (D_H) segment is recombined with a joining (J_H) segment. Subsequently, variable gene region (V_H) is joined with the recombined (DJ_H), hence, a productive gene recombination will give rise to the Ig heavy chain (Igμ or μHC) (Figures 1.2 and 1.3). Recombination is primarily mediated by recombination activating genes (*RAG-1* and *RAG-2*). μHC in association with a germline-encoded heterodimer called surrogate light chain (SLC), composed of VPREB and λ 5 invariant proteins, will form the Pre-BCR that is expressed at the precursor B cell stage (Melchers, 2005; Geier and Schlissel, 2006; Herzog *et al.*, 2009; Mårtensson *et al.*, 2010). A schematic of the Pre-BCR is shown in figure 1.2.

Early Pre-B cells are selected when they have a successful IgH rearrangement, a productive rearrangement allows transient expression of the Pre-BCR. A productive Pre-BCR mediates survival signaling that rescues the cells which were programmed to die (Osmond, 1991). In mice, 10 million of Pre-B cells are produced daily in the bone marrow, however, the Pre-BCR checkpoint eliminates the majority of them (Sakaguchi and Melchers, 1986; Osmond, 1991). Hence, Pre-BCR acts as a key checkpoint regulator for monitoring VDJ recombination on one

hand and triggering the proliferation machinery on the other hand (Hendriks and Middendorp, 2004; Melchers, 2005; Johnson *et al.*, 2008). Pre-BCR then activates several protein tyrosine kinases that orchestrate the downstream signalling responsible for proliferation and differentiation (Figure 1.4A) (Guo *et al.*, 2000; Burrows *et al.*, 2002; Rickert, 2013; Clark *et al.*, 2014). Therefore, tight regulation of the signal transduction cascade downstream of the Pre-BCR-induced proliferation and differentiation is vital to prevent uncontrolled cellular expansion which might result in neoplastic transformation and development of leukaemia (Herzog *et al.*, 2009; Mårtensson *et al.*, 2010; Perez-Vera *et al.*, 2011; Zhou *et al.*, 2012; Rickert, 2013).

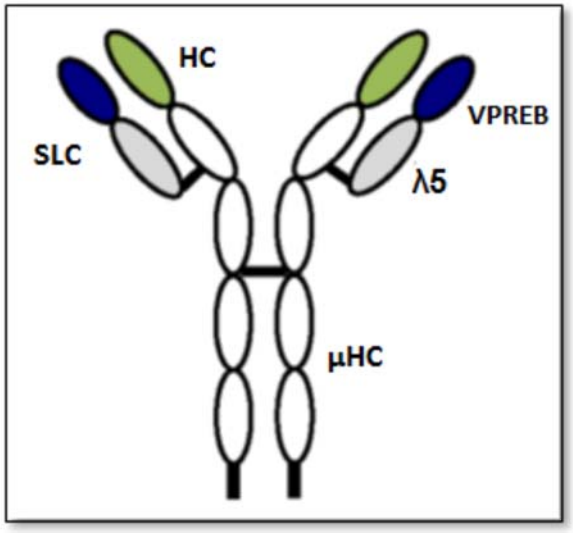

Figure 1.2: Schematic representation of Pre-BCR complex.

Pre-BCR is assembled from μHC (Igμ) and SLC, the latter chain is constructed from VPREB and λ5 invariant polypeptides. [Adapted from: (Mårtensson *et al.*, 2010)].

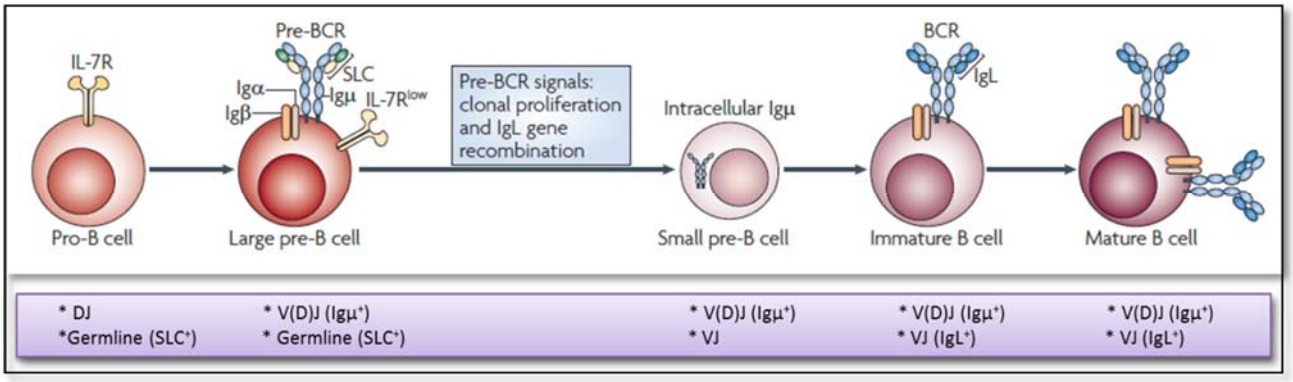

Figure 1.3: A simplified scheme of Pre-BCR and B-cell lymphopoiesis.

V(D)J recombination of *IgH* gene is initiated at the pro-B cell or common-lymphoid-progenitor stage, and productive rearrangement yields cell surface µHC chain which together with SLC gives rise to the Pre-BCR at the large pre B cell stage. Both clonal expansion that is followed by cell cycle exit and *IgH* gene recombination are downstream events of Pre-BCR signalling. B cell receptor (BCR) is expressed following *IgL* gene rearrangement on immature B cells, and eventually, mature long-living B cells repertoire is selected from the immature B cell pool. [Adapted from: (Herzog *et al.*, 2009; Clark *et al.*, 2014)].

1.7 Pre-BCR checkpoint

The Pre-BCR checkpoint is the first crucial element at which the cell navigates its maturation processes, such as clonal selection, proliferation and subsequent development to the stage of precursor B cell. Moreover, the cells with incompetent µHC are negatively selected and undergo apoptosis (clonal distinction) (Hendriks and Middendorp, 2004; Rickert, 2013; Eswaran *et al.*, 2015).

Upon assembly of a transient Pre-BCR, its downstream signalling cascade drives clonal expansion of µHC$^+$ Pre-B cells (Clark *et al.*, 2014). Spleen tyrosine kinase (SYK)-induced constitutive activation of phosphoinositide-3 kinase-Protein kinase B (PI3K-AKT) pathway leads to downstream suppression of RAG gene expression in addition to the κ-chain of the immunoglobulin light chain (Igκ) recombination. Thereby, it inhibits differentiation and induces a short clonal expansion for four to five cycles (Okkenhaug and Vanhaesebroeck, 2003; Deane and Fruman, 2004; Geier and Schlissel, 2006; Reth and Nielsen, 2014; Eswaran *et al.*, 2015).

After a short burst of proliferation, the signalling of progenitor B cells stops the cell cycle to allow re-expression of RAG genes and rearrangement of the Ig light chains to ensure further cellular maturation (clonal differentiation). RAG gene expression is induced by Forkhead box

protein O1 (FOXO1), downstream of B cell linker protein (BLNK), leading to Igκ recombination in collaboration with Interferon regulatory factor-4 (IRF4), which is expressed downstream of SYK-BLNK signalling. IRF4 downregulates λ5 gene expression and eventually terminates SLC expression (Figure 1.4 A). Taken together, the dual role of BLNK mediates the switch from proliferation to differentiation of Pre-BCR$^+$ into BCR$^+$ cells (Flemming *et al.*, 2003; Lu *et al.*, 2003; Parker *et al.*, 2005; Hendriks and Kersseboom, 2006; Johnson *et al.*, 2008; Ochiai *et al.*, 2012; Eswaran *et al.*, 2015).

In addition to this role in proliferation and differentiation in Pre-B cell stage, the Pre-BCR checkpoint also eliminates progenitor B cells with non-functional Igμ heavy chain recombination. Robust expression of bric-a`-brac, tramtrack and broad complex and cap‟n‟collar homology (BACH2) is triggered upon absence of a functional Igμ chain, leading to activation of tumour protein P53 (TP53) and induction of apoptosis (Figure 1.4A). Therefore, cells are negatively selected and die off (clonal extinction) (Oyake *et al.*, 1996; Muto *et al.*, 1998; Herzog *et al.*, 2009; Martensson *et al.*, 2010). Taken together, the Pre-BCR checkpoint allows eligible Pre-B cells to progress development, and if not, initiates cell death (Herzog *et al.*, 2009; Almqvist and Martensson, 2012; Ochiai *et al.*, 2012; Clark *et al.*, 2014; Eswaran *et al.*, 2015).

1.8 Pre-BCR signalling

1.8.1 Normal signalling

It has been reported that Interleukin-7 receptor (IL-7R) signalling is important for both survival and proliferation of early maturation stages of B cells, by activating PI3K and Janus kinase3-signal transducer and activator of transcription 5 (JAK3-STAT5) pathways (Corfe and Paige, 2012; O'Shea and Plenge, 2012). But, during clonal expansion in later B cell developmental stages, recent articles have revealed a collaborative role between IL-7R and Pre-BCR dependent downstream signalling cascade (Hendriks and Middendorp, 2004; Rickert, 2013; Clark et al., 2014). Two mechanisms have been proposed for the triggering of Pre-BCR signaling. A potential ligand candidate (Galectin-1) for Pre-BCR, was identified by an earlier work (Gauthier et al., 2002) and is expressed on the surface of stromal cells in the bone marrow. However, a recent study suggested activation of Pre-BCR signaling autonomously in

a ligand-independent manner (Ubelhart et al., 2010). Ligand-independent auto cross-linkage of surrogate light chain component (λ5) and N-linked glycosylated molecule of the μHC on the cell surface of Pre-B cells induces the transphosphorylation of Immuno-receptor tyrosine-based activation motifs (ITAM`s) tyrosine residues Igα (also known CD 79A) and Igβ (also known CD 79B) by SRC-family kinases (SFKs), which in turn become docking and activation sites for SYK. Additionally to some extent, they recruit ζ-chain associated protein kinase of 70 KDa (ZAP 70) (Ohnishi and Melchers, 2003; Crespo *et al.*, 2006; Monroe, 2006; Ubelhart *et al.*, 2010; Eschbach *et al.*, 2011) (Figure 1.4 A).

BLNK is the primary substrate of SYK and ZAP 70 and acts as a docking site for both Bruton`s tyrosine kinase (BTK). BTK is a downstream kinase of both PI3K and Phospholipase C-ɣ2 (PLC-ɣ2), PLC-ɣ2 also promotes calcium ion flux (Guo *et al.*, 2000; Kurosaki and Tsukada, 2000; Marshall *et al.*, 2000; Kouro *et al.*, 2001; Kurosaki and Okada, 2001; Scharenberg *et al.*, 2007a). PI3K is activated and phosphorylated by active SYK either directly or indirectly via CD19 and B cell PI3K adapter (BCAP) (Deane and Fruman, 2004; Aiba *et al.*, 2008). Hence, PI3K phosphorylates phosphatidylinositol-4,5-biphosphate (PtdIns (4,5)P2) into the second messenger phosphatidylinositol 3,4,5-triphosphate (PtdIns (3,4,5)P3) and attracts AKT to the plasma membrane (Okkenhaug and Vanhaesebroeck, 2003).

Extracellular signal-regulated kinase (ERK) is then promoted upon PLC-ɣ2 binding to activate active rat sarcoma kinase (RAS) pathway (Imamura *et al.*, 2009). Though, BLNK is more likely to play a significant role in orchestrating the cell cycle either positively via activating RAS-RAF-MEK-ERK (proliferation pathway) (Shaw *et al.*, 1999a; Nagaoka *et al.*, 2000; Imamura *et al.*, 2009) or negatively (Figure 1.4 A) (Flemming *et al.*, 2003). In terms of its negative role, BLNK indirectly promotes FOXO1 translocation into the nucleus (Herzog *et al.*, 2008) and antagonises the AKT activation through the IL-7R/PI3K/AKT proliferation signalling cascade (Milne and Paige, 2006; Herzog *et al.*, 2008; Ochiai *et al.*, 2012), consequently, FOXO1 upregulates B cell lymphoma-6 gene (*BCL-6*), RAG and BLNK. BCL-6 suppresses cell cycle genes [G1/S- specific cyclin D2 (*CCND2*) and *MYC*] in addition to *TP53* (Figure 1.4 A), thereby halting the cellular proliferation machinery and inducing a quiescence state (clonal rescue) (Tang *et al.*, 2002; Duy *et al.*, 2010; Nahar *et al.*, 2011). Additionally, it has been suggested that BLNK may play a tumour suppressor function in association with BTK to regulate IL-7 mediated survival and proliferation (Kersseboom *et al.*, 2003; Middendorp *et al.*, 2005). Moreover, this

is also achieved when BLNK suppresses STAT5 activation via its interaction and inhibition of JAK3 (Figure 1.4 A) (Nakayama *et al.*, 2009).

1.8.2 Malignant signalling

ALL cells are arrested at the Pre-B stage and most do not express a Pre-BCR (or BCR) and have thus escaped clonal extinction or differentiation (Trageser *et al.*, 2009; Geng *et al.*, 2015). It has been noted that BCP-ALL children patients have a high frequency of somatic mutations which activate certain key signalling cascades, particularly, RAS/ERK, PI3K, JAK-STAT. These aberrant pathways grant survival and continued proliferation of Pre-B cells as shown in figure 1.4 B (Klein *et al.*, 2004a; Nakayama *et al.*, 2009; Zhang *et al.*, 2011; Knight and Irving, 2014). Patients with BCP-ALL malignancy have increased autocrine and paracrine stimulation of IL-7, which enhances robust activation of JAK3-STAT5 and PI3K pathways, thereby allow survival and proliferation of leukaemic Pre-B cells (Figure 1.4 B) (Fisher *et al.*, 1993; Mertsching *et al.*, 1996; Rickert, 2013). Moreover, aberrant expression or splicing of *BLNK* gene was found in a large proportion of BCP-ALL patients. In agreement with this observation, higher expression level of Pre-BCR, which allow higher proliferation of BCP-ALL cells, was associated with BLNK-deficiency (Flemming *et al.*, 2003; Jumaa *et al.*, 2003).

BLNK deficiency restores IL-7 mediated stimulation of JAK3-STAT5 and PI3K-AKT pathways leading to BCL-6 downregulation due to prevention of FOXO1 protein translocation into the nucleus (Figure 1.4 B). Diminished expression of BCL-6 releases the repression of the cell cycle progression genes (*MYC* and *CCND2*) (Flemming *et al.*, 2003; Herzog *et al.*, 2008; Nakayama *et al.*, 2009; Duy *et al.*, 2010; Nahar *et al.*, 2011; Geng *et al.*, 2015).

Moreover, gain of function mutations downstream of RAS and SHP2, leading to hyper activated RAS-ERK pathway, have been reported in cases with high risk BCP-ALL (Case *et al.*, 2008; Yasuda *et al.*, 2008; Irving *et al.*, 2014). Functional studies have revealed two important transcriptional activators promoted by activated ERK (downstream of RAS), namely cyclic AMP-responsive element-binding protein 1 (CREB1) and ELK1, which upregulate expression of Monocyte enhancer factor 2c (*MEF2C*) and *MEF2D* or *MYC* respectively leading to proliferation (Yasuda *et al.*, 2008), as shown in figure 1.4 A and B. In addition, *BACH2* gene, which serve as tumor suppressor, was found to be downregulated in 30% of BCP-ALL patients with *PAX5*

lesions and low expression levels of BACH2 was associated with relapse (Mullighan *et al.*, 2007; An *et al.*, 2008; Kawamata *et al.*, 2012; Swaminathan *et al.*, 2013b).

By using a similar evasive strategy of replacing the role of Pre-BCR, aberrant precursor B cells in patients with Ph^+ chromosome express the *BCR-ABL1* oncoprotein (Klein *et al.*, 2004a), which binds to growth factor receptor bound protein 2 (GRB2) adapter to promote activation of RAS and PI3K pathways, whereas STAT5 is activated via direct phosphorylation by *BCR-ABL1* (Figure 1.4 B) (Roberts *et al.*, 2012; Rickert, 2013). As a result, the requirement for Pre-BCR expression is bypassed and cell cycle proceeds with clonal expansion (Iritani *et al.*, 1997; Shaw *et al.*, 1999b).

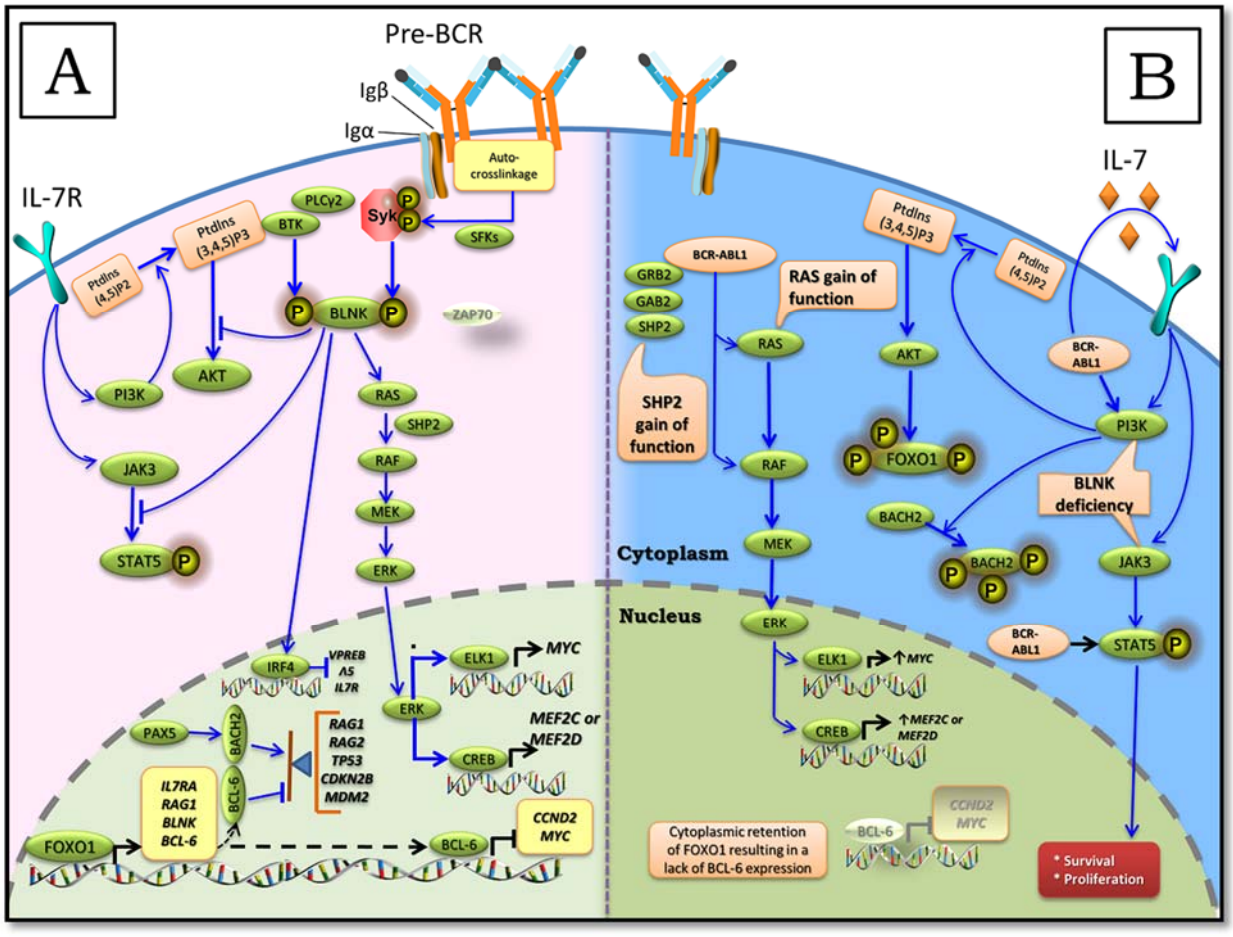

Figure 1.4: Signalling events in normal and malignant Pre-B cells.

A) Normal Pre-B cell signalling cascades leading to clonal proliferation and differentiation. **B)** Malignant Pre-B cell events summarising the possible perturbed signalling pathways leading to BCP-ALL malignancy, adapted from (Rickert, 2013; Eswaran *et al.*, 2015).

1.9 Exploitation of Pre-BCR in favour of B-cell derived childhood leukaemia

There are several lines of evidence suggest that key genetic aberrations in BCP-ALL, such as chromosomal translocations and gene deletions/mutations, interfere with Pre-BCR signaling (Eswaran *et al.*, 2015) to achieve the following:

1.9.1 Inhibit Pre-BCR mediated maturation and cell cycle arrest

It is well known that Pre-BCR mediated differentiation is arrested in BCP-ALL cells (Klein *et al.*, 2004b), thus, the BCP-derived malignancy is assumed to stem from pro-proliferative mechanisms of the Pre-B cells in association with inhibited differentiation mechanisms. However, it has been found that *BCR-ABL1* harbouring cells have a non-functional *IgH* gene rearrangement and, therefore, can escape clonal extinction by downregulating Pre-BCR encoded genes, including *VPREB1* and *IgHM* (Klein *et al.*, 2004b; Trageser *et al.*, 2009), thereby, they are eligible to avoid normal B cell differentiation and can survive by evading the Pre-BCR checkpoint (Klein *et al.*, 2004a; Klein *et al.*, 2004b). Interestingly, recent findings have shown that reconstitution of normal Pre-BCR signalling in Ph^+ cells through re-expression of BLNK and µHC in deficient mice can exert a tumor suppressor activity and leads to cell death (Trageser *et al.*, 2009).

When BCP-ALL cells escape the Pre-BCR checkpoint, they modify the clonal extinction mechanism, which eliminates the cells with non-productive Ig heavy chain rearrangement, in favour of progenitor B cell malignancy development (Swaminathan *et al.*, 2013a). As mentioned earlier in section 1.8, the player of clonal extinction mechanism, BACH2, is commonly downregulated in some malignant ALL cells compared to normal Pre-B cells, especially in relapsed cases with PAX5 abnormalities (Swaminathan *et al.*, 2013a). Additionally, BLNK deletion may involve inhibition of *CDK2NA/MDM2/P53* mediated apoptosis, due to increased cytoplasmic retention of FOXO1 which leads to diminished BCL-6 expression (Figure 1.4 B) (Jumaa *et al.*, 2003; Ta *et al.*, 2010).

1.9.2 Activate Pre-BCR mediated pro-survival/pro-proliferative signalling

As pointed out earlier (section 1.8.1), the triggering of Pre-BCR signalling is initiated by auto-crosslinkage of SLC components, which then recruits the major player of downstream signalling, SYK, leading to clonal expansion and differentiation in normal progenitor B cells. SYK may act as an oncoprotein when it is constitutively expressed leading to continuous proliferation associated with suppression of apoptosis, via constitutive activation of PI3K/AKT and FOXO1 signalling pathways, which eventually involve inhibition of BCL-6 (mediator of suppression of cell cycle genes and *TP53*) as shown in figure 1.4 (Wossning *et al.*, 2006; Duy *et al.*, 2011; Ochiai *et al.*, 2012). BCL-6 is a key survival factor that ensures clonal rescue for μHC^{+} normal Pre-B cells (Duy *et al.*, 2010). It has been found that SYK can drive Pre-BCR malignancy via MYC. Therefore, BCP-ALL cell death could be promoted by SYK inhibition (Wossning *et al.*, 2006; Perova *et al.*, 2014; Uckun and Qazi, 2014).

1.9.3 Override the Pre-BCR checkpoint and activate pro-survival signalling through aberrant mechanisms

Malignant Pre-B cells may harness pro survival pathways independently of the Pre-BCR. For example, aberrant expression of the Erythropoietin receptor (EPOR) in *ETV6-RUNX1* positive ALL cells induce JAK-STAT signalling which ensures outgrowth of malignant cells (Fine *et al.*, 2004; van Delft *et al.*, 2005; Inthal *et al.*, 2008; Roberts *et al.*, 2012). Moreover, approximately 25% of IgH rearrangement cases involve over-expression of *CRLF2* and are associated with IL-7R and JAK gene family mutations (Russell *et al.*, 2009). Consequently, JAK-STAT signalling in addition to PI3K/mTOR pro-survival and pro-proliferation pathways are activated (Tasian *et al.*, 2012). Additionally, mutations in IL-7R, and (fms-Related tyrosine kinase 3) (*FLT3*) can cause activation of JAK-STAT pathway (Roberts *et al.*, 2012; Loh *et al.*, 2013).

1.10 Treatment of ALL

Contemporary advances in treatment regimens have pushed the 5 year event free survival up to 90% due to the use of multi-agent chemotherapy, improved supportive care and precise risk stratification (Pui *et al.*, 2009; Pui *et al.*, 2012b; Pui, 2013). However, some children ultimately relapse and survival outcomes at this stage are poor (Parker *et al.*, 2010; Eckert *et al.*, 2011). Treatment still needs optimising, as both early and late therapeutic-related adverse events reduce the quality of life significantly. Certain aberrant cellular pathways activated by genetic abnormalities may allow the introduction of targeted drugs that may improve prognosis and reduce toxicity (Pui and Jeha, 2007; Szczepanski *et al.*, 2010; Irving *et al.*, 2014).

1.10.1 Chemotherapy

The conventional treatment of paediatric ALL used drugs that either inhibit nucleic acid synthesis or target the DNA directly and some drugs interfere with the mitotic spindle while others block protein synthesis (Table 1.1). As such, these non-specific treatments overwhelmingly contribute to adverse events in normal tissues (Pui and Jeha, 2007). Even though treatment regimens differ across the globe, therapy stages for paediatric ALL are separated into three major phases (Table 1.2). These are (1) remission-induction therapy (to eliminate about 95-99% of the initial malignant cells burden and to re-establish the normal haematopoiesis) followed by (2) consolidation therapy, which eradicates the residual leukaemic cells, and (3) prolonged continuation treatment that usually lasts for 2 years or more (Pui and Evans, 2006; Pui *et al.*, 2008; Inaba *et al.*, 2013).

Drug (approval year)	Mechanism of action
Glucocorticoids: dexamethasone (1958)	Transrepression or transactivation of genes after binding with glucocorticoid receptor elements (GRE) at the promoter regions of genes.
Anthracyclines: doxurobicin (1989)	Damages DNA after free radicals formation; Forms complexes with topoisomerase-IIα enzyme and DNA leading to breakage of both DNA strands; Induces apoptosis through caspases activation.
Vincristine (1963)	Binds to tubulin and hence inhibits formation of mitotic spindle
Methotrexate (1953)	Inhibits formation of *de novo* purine; blocks folate metabolism enzymes and hence inhibits DNA synthesis.
Cytarabine (1969)	Blocks polymerisation of DNA after incorporating into it.
Asparaginase (1978)	Catalyses asparagine depletion and hence inhibits protein synthesis
Thiopurines (1953)	Inhibits new purine synthesis and pathway of purine salvage
Alkylators: cyclophosphamide (1959)	Changes DNA function and structure through fragmenting or crosslinking of DNA strands

Table 1.1: Standard chemotherapeutic agents with their mechanisms of action used in childhood acute lymphoblastic leukaemia, adapted from: (Pui and Jeha, 2007)].

Treatment phase	Typically used Chemotherapies
Remission/ Induction	* Vincristine * Corticosteroids (e.g. Dexamethasone) * L-Asparaginase * +/- Anthracycline (High risk patients)
Consolidation/ Intensification	* Vincristine * Cytarabine (Ara-C) * Cyclophosphamide * Mercaptopurine * Methotrexate
Maintenance	* Mercaptopurine (daily) * Methotrexate weekly

Table 1.2: General outline for chemotherapeutic regime used for BCP-ALLs. Adapted from (Pui *et al.*, 2004).

1.10.2 Targeted therapies

Researchers have proven that tyrosine kinases are impressive therapeutic targets in several kinds of cancer (Druker *et al.*, 2001; Pui and Jeha, 2007; Rebecca and Smalley, 2014). During the last decade, several tyrosine kinase inhibitors (TKIs) have been introduced in haemato-oncology to reduce the adverse effects of cancer therapy and to enhance its effectiveness. Tyrosine kinases are key elements in signal transduction of cellular pathways, which transmit information from extracellular or cytoplasmic domains to the nucleus. As many malignant cells show aberrant activity of particular tyrosine kinases, this could be exploited using TKIs in cases where kinases are therapeutic targets (Krause and Van Etten, 2005; Rebecca and Smalley, 2014; Sun and Bernards, 2014).

TKIs were given continuously, as single agents or in combination with classical chemotherapies, for patients as maintenance therapy (de Labarthe *et al.*, 2007; Foa *et al.*, 2011; Fielding *et al.*, 2014). For example, the combination of imatinib mesylate, a small molecule TKI, with conventional chemotherapy has revolutionised the therapy for ALL patients harbouring Ph chromosome, and therefore, survival has increased from 30-70% compared to historical controls. Importantly, there was no increase in toxicity (Schultz *et al.*, 2009; Ravandi *et al.*, 2010; Schultz *et al.*, 2014). However, if patients became resistant to imatinib, they transitioned to dasatinib, a second generation TKI which has better CNS penetration. Dasatinib targets the mutated form(s) of *BCR-ABL1* and SRC signalling (Talpaz *et al.*, 2006; Brave *et al.*, 2008; Porkka *et al.*, 2008).

Most recently, the treatment of B-cell malignancies has gained exciting momentum by the use of targeted therapies to key proximal tyrosine kinases downstream of BCR, including BTK, PI3K and SYK. So far, the preclinical drug testing and clinical trials have shown promising results (Choi and Kipps, 2012; Fowler and Davis, 2013; Rickert, 2013; Young and Staudt, 2013; Sun and Bernards, 2014). Therefore, the analogy between Pre-BCR and BCR mediated signalling cascades (Guo *et al.*, 2000) may represent an appealing therapeutic avenue in childhood ALL.

1.10.2.1 PI3K-δ inhibitor (CAL-101)

In B lineage cells, PI3K signalling can be promoted by Pre or B cell-dependent or independent mode, for instance, via other cytokine receptors (Werner *et al.*, 2010; Herman and Johnson, 2012). Perturbed PI3K signalling is recurrent in different malignancies, however, the PI3K-δ isoform is primarily expressed in cells of haematopoietic origin (Ramadani *et al.*, 2010; Tasian *et al.*, 2012; Kandoth *et al.*, 2013). It recruits downstream AKT enzyme during Pre-B and BCR signalling, which in turn activates multiple signalling effectors orchestrating proliferation and survival (Deane and Fruman, 2004; Yuan and Cantley, 2008). Taken together, it is emerging as a therapeutic target in multiple B cell malignancies (Vanhaesebroeck *et al.*, 1997; Herman *et al.*, 2010; Lannutti *et al.*, 2011).

CAL-101 or GS-1101 (also called idelalisib) is a highly selective small molecule inhibitor of PI3K-δ, it inhibits p110δ isoform and was developed by Gilead Sciences (Figure 5.1 A). CAL-101 has been found to inhibit BCR signalling and also abrogate the chemokine microenvironment niche effect in lymph nodes (Herishanu *et al.*, 2011; Hoellenriegel *et al.*, 2011; Burger, 2012). Recently, CAL-101 was approved by FDA as a monotherapy for the treatment of follicular lymphoma (FL) and relapsed small lymphocytic lymphoma (SLL). In addition, CAL-101 was used in combination with rituximab in the treatment of relapsed chronic lymphocytic leukaemia (CLL) (Furman *et al.*, 2014; Miller *et al.*, 2015). Although CAL-101 was well tolerated in patients, there were some adverse effects such as diarrhea, hepatotoxicity and pneumonitis (Do *et al.*, 2016). Moreover, recent preclinical studies have suggested that relapsed BCP-ALL patients with *TCF3-PBX1* lesion may benefit from CAL-101 monotherapy (Eldfors *et al.*, 2017).

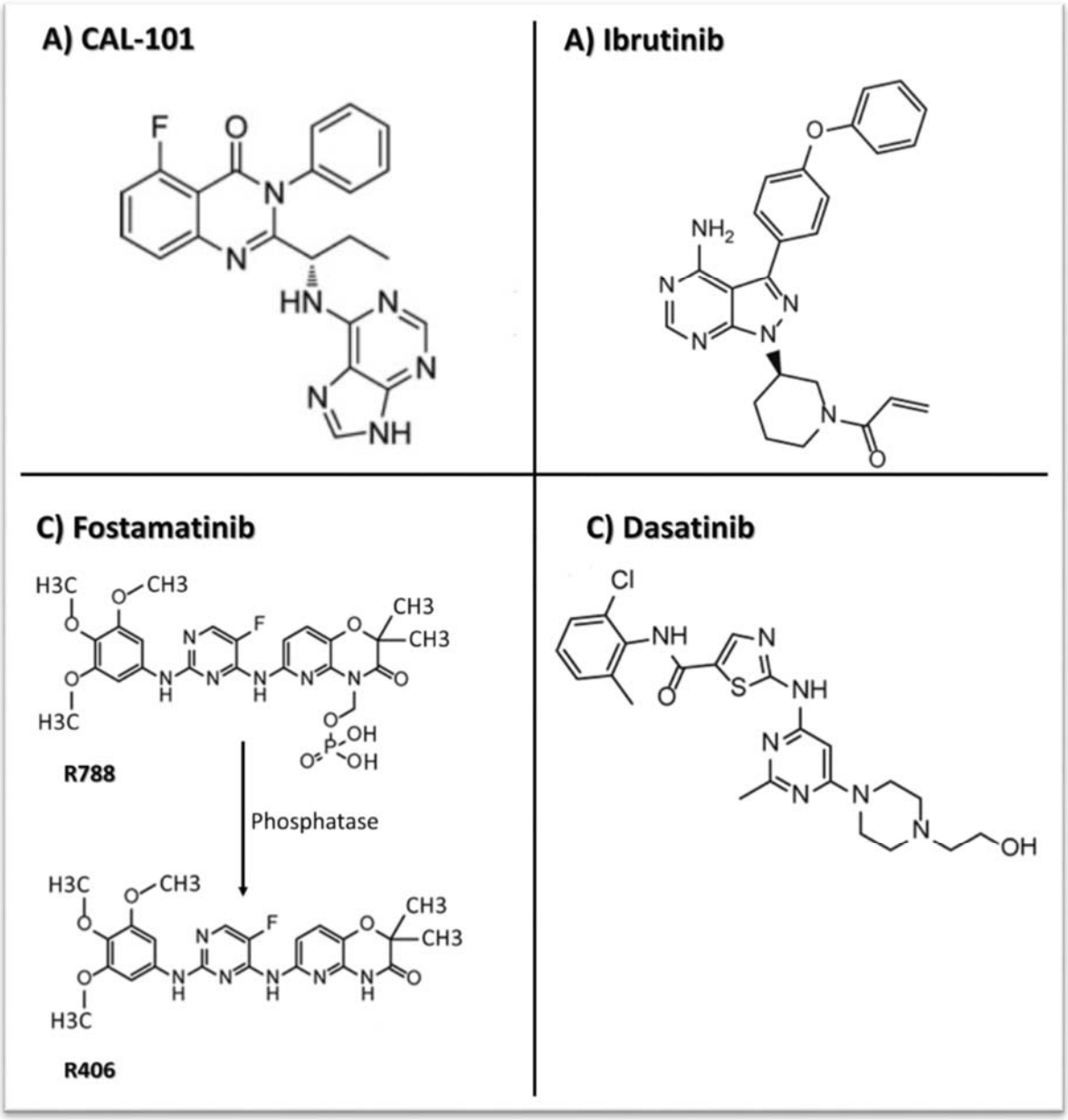

Figure 1.5: Chemical structures of small molecule inhibitors targeting BCR signalling.

(A) CAL-101 [PI3K-δ inhibitor], **(B)** Ibrutinib [BTK inhibitor], **(C)** Fostamatinib [SYK inhibitor] and **(D)** Dasatinib [BCR-ABL1/SRC inhibitor]. Adapted from (Kantarjian *et al.*, 2006; Sweeny *et al.*, 2010; Lannutti *et al.*, 2011; Tucker and Rule, 2015).

1.10.2.2 BTK inhibitor (Ibrutinib)

It is known that BTK is a cytoplasmic tyrosine kinase expressed in different haematopoietic lineages (Brunner *et al.*, 2005). It plays a central role in survival and proliferation in normal and malignant blood cells (de Weers *et al.*, 1993; Katz *et al.*, 1994). Recently, several small-molecule BTK inhibitors have been introduced into clinical trials of lymphoid malignancies, including Ibrutinib (Young and Staudt, 2013). A potent,-irreversible inhibitor of BTK, Ibrutinib (PCI-32765) (Figure 5.1 B) was approved by FDA for clinical anti-tumour activity in various B cell malignancies, including mantle cell lymphoma (MCL), waldenström macroglobulinemia (WM) and CLL, with no discernible side effects (Pan *et al.*, 2007; Staudt *et al.*, 2011; Byrd *et al.*, 2012; Advani *et al.*, 2013; Hendriks *et al.*, 2014; van der Veer *et al.*, 2014; Raedler, 2016). Most recently, preclinical studies in ALL proposed Ibrutinib as a potential therapy for Pre-BCR$^+$ and *TCF3*-rearranged ALL (van der Veer *et al.*, 2014; Geng *et al.*, 2015; Kim *et al.*, 2017).

1.10.2.3 SYK inhibitor (Fostamatinib R406)

As mentioned earlier, SYK triggers downstream signalling cascades important for proliferation and survival in all B-lineage stages (Mocsai *et al.*, 2010; Uckun *et al.*, 2010b). Constitutive activity of SYK promotes survival or proliferation in multiple subtypes of BCP-ALL and may be associated with relapse (Ding *et al.*, 2000; Takano *et al.*, 2002; Uckun and Qazi, 2014), therefore, inhibition of SYK may induce cell cycle arrest and apoptosis (Uckun *et al.*, 2010a; Perova *et al.*, 2014; Geng *et al.*, 2015). Fostamatinib R788, oral SYK inhibitor, is metabolised *in vivo* from the pro-drug form (R788) to the active form (R406) (Braselmann *et al.*, 2006; Rolf *et al.*, 2015) (Figure 1.5 C). The BCR pathway was shown to be selectively inhibited by fostamatinib (Riccaboni *et al.*, 2010). Fostamatinib has shown efficacy in rheumatoid arthritis and also reduced the growth of blast B cells in mouse model of CLL (Suljagic *et al.*, 2010; Weinblatt *et al.*, 2014; Newland *et al.*, 2018). Fostamatinib was tested in phase I and phase II clinical trials in patients with B-non Hodgkin lymphoma (B-NHL) and CLL (Friedberg *et al.*, 2010; Suljagic *et al.*, 2010). Objective response rates were obtained in 55% of CLL patients, 24% of diffuse large B-cell lymphoma (DLBCL) patients, 11% of MCL patients and also patients with FL (10%) (Friedberg *et al.*, 2010). However, fatigue, nausea and diarrhea were the most side effects of fostamatinib upon treating DLBCL patients using high doses (200mg, twice daily)

(Flinn *et al.*, 2016) and its thought that these adverse effects were because of 'off target' effect of fostamatinib (Rolf *et al.*, 2015). In addition to its role in inhibiting BCR signalling pathway, it impairs BCR- dependent secretion of chemokines such as CCL3 and CCL4 (Hoellenriegel *et al.*, 2012). In addition, tumour burden in mice transplanted with high risk and relapsed BCP-ALL cells was decreased after fostamatinib treatment (Perova *et al.*, 2014).

1.10.2.4 BCR-ABL1/SRC inhibitor (Dasatinib)

The second generation *BCR-ABL1* inhibitor, dasatinib (Figure 1.5 D), was approved in 2006 by FDA for the treatment of adults with chronic myeloid leukaemia (CML) and Ph^+ ALL who were resistant or intolerant to imatinib (Kantarjian *et al.*, 2006; Foa *et al.*, 2011). Dasatinib is potent multi-kinase inhibitor of different kinases, including SFKs, PDGFR-β, C-KIT, BTK in addition to *BCR-ABL1* (Lombardo *et al.*, 2004; Hantschel *et al.*, 2007; Kantarjian *et al.*, 2010a; Amrein *et al.*, 2011). In B-cell malignancies, dasatinib induced apoptosis in DLBCL cell lines (Davis *et al.*, 2010a), and in the clinic, there was 20% response rate when CLL patients were treated with the drug (Amrein *et al.*, 2011). Interestingly, both clinical and preclinical findings suggested that dasatinib is effective in Ph-like, *TCF3-PBX1* and Pre-BCR^+ ALL (Bicocca *et al.*, 2012; Geng *et al.*, 2015; Kobayashi *et al.*, 2015; Welsh *et al.*, 2017).

1.10.2.5 Synthetic glucocorticoid (Dexamethasone)

The synthetic glucocorticoid, dexamethasone, has played a pivotal role in the treatment of lymphoid malignancies since the late 1950s, because of its ability to induce programmed cell death in lymphoid cells, but its use is associated with life-threatening infections and osteonecrosis (Pui and Evans, 2006; Inaba and Pui, 2010). The glucocorticoid receptor (GR), also called NR3C1, mediates the anti-leukaemic effect of dexamethasone (Kofler, 2000). In the cytosol, GR heterocomplexes with several proteins when not bound with ligand (Nicolaides et al., 2010). Dexamethasone molecules are lipophilic and relatively small in size, therefore they passively enter the cell and bind to the GR which enables dissociation of the GR from the cytoplasmic heterocomplexes. The ligand bound GR has dual effects. Firstly, as a monomer, the GR-dexamethasone complex makes protein-protein interactions with transcription factors, such as NFkB, leading to transrepression of genes indirectly (Kofler, 2000; Schaaf and

Cidlowski, 2002; Inaba and Pui, 2010). Secondly, as a dimer, the GR-dexamethasone complex transactivates the gene expression directly, by interaction with the DNA binding sites, also called glucocorticoid response elements (GREs) (Schaaf and Cidlowski, 2002; Oakley and Cidlowski, 2013a). Ultimately, this transrepression and gene transactivation effect of dexamethasone leads to the induction of apoptosis or cell cycle arrest (Inaba and Pui, 2010).

1.11 Hypothesis and objectives of the work

Given the clear necessity of ALL cells to escape from normal Pre-BCR checks, the mechanism they rely on may serve as an Achilles' heel that could be exploited to offer new therapeutic approaches. There are a number of drugs targeting Pre-BCR signalling in the clinic that are showing efficacy in other leukaemic subtypes and thus warrant preclinical evaluation in childhood ALL. Therefore, in this project, the hypothesis to be tested is that malignant blasts in B lineage ALL hijack Pre-BCR signalling pathways and that this dependence may be amenable to therapeutic exploitation.

The objectives are:-

1 To preclinically evaluate small molecule inhibitors targeting Pre-BCR pathways in ALL cell lines and primary derived ALL cells *in vitro*

2 To investigate predictive biomarkers of response, including Pre-BCR expression, function and downstream signalling activity

3 To assess synergism of the small molecule inhibitors with pivotal ALL drugs, such as glucocorticoids

Chapter 2: Materials and Methods

Chapter 2: Materials and Methods

2.1 General

2.1.1 Equipment

- 7500 Fast Real-Time PCR System (Applied Biosystems, Warrington, UK)
- Magnetic stirrer UC151 (Bibby Scientific Limited, Staffordshire, UK)
- Heating block (Grant QBD2, Cambridge, UK)
- Water Bath (Grant Instruments, Cambridge, UK)
- Mini Trans-Blot Electrophoretic Transfer Cell (BioRad, USA)
- Mini-PROTEAN 11 Electrophoresis Cell (BioRad, USA)
- Gyro-Rocker STR9 (Fisher Scientific, Loughborough, UK)
- Gel Electrophoresis Tank (Pharmacia Biotech, Amersham Biosciences, UK)
- FLUOStar Omega Microplate Reader (BMG Labtech, Aylesbury, UK)
- FACSCalibur (Becton Dickinson, Oxford, UK)
- FACSCanto II (Becton Dickinson, Oxford, UK)
- BIOMAT-2 class II microbiological safety cabinet (Medical Air Technology Ltd., Manchester, UK)
- BioRad Power Pac 200 (Bio-Rad Laboratories Ltd, Watford, UK)
- Analogue Tube Roller SRT9 (Stuart Scientific, Staffordshire, UK)
- Bead Bath (Gallenkamp/Weiss, Loughborough, UK)
- WhirliMixer (Fisons Scientific Equipment, Leicestershire UK)
- Thermomixer comfort (Eppendorf, Hamburg, Germany)
- Humidified CO_2 incubator (Panasonic healthcare, Japan)
- GeneAmp PCR System 27000 (Applied Biosystems, USA)
- Roller mixer (SRT9) Stuart (BIBBY scientific Ltd. Staffordshire, UK)
- BioRad ChemiDoc^{TM} MP imaging system (BioRad, USA)
- Julabo U3 water bath (JULABO LABORTECHNIK GMBH, West Germany)
- Nanodrop 1000 spectrophotometer (Thermo Fisher Scientific, UK)
- Automatic X-ray Film Processor (JPI Healthcare Co. Ltd. Huddersfield, UK)

2.1.2 Centrifuges

- MSE Mistral 3000i Refrigerated Centrifuge (Fisher Scientific, UK)
- MSE Mistral 1000 centrifuge (Fisher Scientific, UK)
- SciSpin ONE centrifuge (SciQuip, Shropshire, UK)
- Eppendorf 5804 centrifuge (Fisher Scientific, Hamburg, Germany)
- Eppendorf refrigerated centrifuge 5417R (Fisher Scientific, Hamburg, Germany)

2.1.3 Microscopes

- Olympus transmitted light microscope (Olympus, Japan)
- Zeiss transmitted light microscope (Carl Zeiss Ltd., Welwyn Garden City, Herts., UK)
- Olympus CKX53 inverted light microscope (Olympus, Tokyo, Japan)

2.1.4 General chemicals and reagents

All reagents and chemicals were obtained from Thermo Fisher (Loughborough, UK) or Sigma Chemical Company (Dorset, UK) unless otherwise stated. Phosphate buffered saline (PBS) was made from tablets purchased from Invitrogen (Paisley, UK) and then autoclaved prior to use.

2.1.5 Software

- Graphpad Prism software (6.0) (GraphPad Software, Inc., San Diego, CA, USA)
- CalcuSyn software (2) (Cambridge, UK)
- CellQuest software (5.2) (BD Biosciences, San Jose CA, USA)
- FlowJo software (10.0.8) (Tree Star, Ashland, USA)
- MARS Data Analysis Software (3.20 R2) (BMG Labtech, Aylesbury, UK)
- Image Lab™ Software 6.0 (Bio-Rad Laboratories, USA)
- ImageJ FIJI software (National Institutes of Health, Rockville, MD, USA)

2.2 Tissue culture

2.2.1 Materials for tissue culture

RPMI-1640 cell culture media were obtained from Sigma Chemical Company (Dorset, UK). All plastic ware for tissue culture was purchased from Corning (Corning, High Wycombe, UK). Foetal bovine serum (FBS) was purchased from Gibco (Gibco by Life Technologies, Paisley, UK).

2.2.2 Cell lines characteristics

A number of haematopoietic cell lines were used: (a) TK6; (b) PreB 697; (c) R3F9; (d) REH; (e) Nalm-6; (f) Daudi and (g) Ramos. Cells were obtained from the European Collection of Cell Cultures (ECACC). ALL cell lines (PreB 697, R3F9, REH and Nalm-6) were selected as they were derived from patients at relapse and previously characterised for Pre-BCR expression (Geng *et al.*, 2015). All cell lines were authenticated by Short tandem repeat (STR) profiling by the company LGC Standards, UK. STR are loci at the human genome and considered the most informative genetic markers which help ensuring integrity and quality of human cell lines. All cells were routinely tested for mycoplasma using MycoAlert™ PLUS Assay (Lonza, Basel, Switzerland) and were cultured in RF10 (RPMI 1640, supplemented with 10% heat-inactivated FBS) in a 5% CO_2 and humidified atmosphere at 37˚C.

a) **TK6:** A lymphoblastoid cell line, was derived from WIL-2 cells that have been isolated from spleen cells of a 5 years old male patient with hereditary spherocytic anaemia, but with no evidence of malignancy and have normal B cell characteristics ((ECACC); Levy *et al.*, 1968; Skopek *et al.*, 1978).
b) **PreB 697:** Pre-B cell line derived from the bone marrow cells of a 12 year old boy with relapsed ALL in 1979 (Findley *et al.*, 1982).
c) **R3F9:** Glucocorticoid resistant clone of PreB 697 incubated with dexamethasone for 21 to 28 days (Schmidt *et al.*, 2006).
d) **REH:** A cell line derived from a pro-B ALL in 1974 from the peripheral blood of a 15 year old female at relapse (Han *et al.*, 1978).

e) **Nalm-6:** Human PreB-cell line of ALL established from the peripheral blood of a 19 year old male at relapse (Hurwitz *et al.*, 1979).

f) **Daudi:** Human immature B-lymphoblast cell line, established in 1967 from 16-year old male patient with Burkitt`s lymphoma (Klein *et al.*, 1968).

g) **Ramos:** Human B-lymphoblast cell line derived from a 3 year male patient with Burkitt`s lymphoma (Klein *et al.*, 1975).

2.2.3 Cell line growth

All cell lines listed in section 2.2.2 were grown in suspension. They were cultured in RF10. Class II safety microbiological safety cabinets (Section 2.1.1) were used to perform tissue culture and sterile plastic and glassware were utilised. Flasks or multi-well plates were used for growing cells. Cells were incubated at 37°C with 5% CO_2 in a humidified tissue culture incubator. To ensure cells are always in the logarithmic phase of growth, cell lines were fed routinely with fresh medium every 48 to 72 hours and the final cells concentration was adjusted to less than $5x10^5$ cells per ml after RF10 addition.

2.2.4 Mycoplasma test

Mycoplasma is the simplest form of bacteria as they have very basic genome and lack the cell wall. In order to meet their demands of biosynthesis and energy, they must function as parasites by exploiting their host`s cells. Therefore, cell lines infection with mycoplasma can affect cell metabolism, growth characteristics and the effects are not predictable and vary between cell lines (Drexler and Uphoff, 2002). To ensure that all cell lines were mycoplasma free, MycoAlert (Lonza, Basel, Switzerland) assays was performed periodically by Elizabeth Matheson, a member of the Northern Institute for Cancer Research (NICR) staff. The selective activity of mycoplasma enzymes were exploited in this assay to detect infection. The released enzymes from any lysed viable mycoplasma react with the MycoAlert substrate and mediate the transformation of ADP to ATP. After quantifying ATP levels in a cell line sample before and after MycoAlert addition, the

presence or absence of mycoplasma infection is effectively detected by calculating the substrate ratio. All cell lines used in this project were mycoplasma free.

2.2.5 Cell harvesting

Cells were harvested for RNA and protein studies when in exponential growth phase. Cell suspensions were centrifuged for 5 minutes at 1000 RPM at room temperature. The supernatant was aspirated and the pelleted cells were resuspended in PBS and pelleted again by centrifugation. Washing was repeated again and PBS was aspirated and the pelleted cells were either resuspended again in the appropriate medium or stored at -80°C until required.

2.2.6 Counting of cells and viability assessment

To calculate both the total number of cells and their viability, a small aliquot of cell suspension was mixed with an equal volume of 0.4% w/v Trypan Blue solution. This mixture was loaded in an improved Neubauer haemocytometer and cells counted using a light microscope at 20x magnification. This method is based on the dye exclusion principle, where dead cells take up Trypan blue dye and appear blue under microscopy, while viable cells do not (Strober, 2001). Viability was expressed as a percentage of live cells within the total population.

2.2.7 Freezing of cells

In order to make frozen stocks, cells proliferating exponentially were counted and their viability was assessed as described above (Section 2.2.6). Cells were centrifuged at room temperature for 5 minutes at 1000 RPM and $5x10^6$-$1X10^7$ cells were resuspended in 1ml of FBS containing 10% (v/v) dimethyl sulphoxide (DMSO). One ml aliquots were added into 2ml polypropylene labelled cryovials (Thermo Fisher Scientific, Loughborough, UK) and then kept in a polystyrene box filled with cotton wool before freezing at -80°C. This to make sure that the sample cooling rate is approximately 1°C per minute. Cells were then

moved to a-150°C freezer or liquid nitrogen for long term storage after being temporarily kept at -80°C for 2-14 days.

In order to recover frozen cells, cryovials were warmed rapidly in a 37°C waterbath to thaw and then diluted in 5ml of pre-warmed RF10 medium. Cells were then pelleted by centrifugation at 1000 RPM for 5 minutes prior to resuspending in fresh RF10 medium and seeding in a cell culture flask.

2.3 Flow cytometry

Background

Flow cytometry is a tool which enables detection of a variety of cellular components on the cell surface or intracellular in each individual cell within a complex population. A standard flow cytometer machine is equipped with one to two lasers, however, modern machines are more sophisticated with more lasers to detect large numbers of parameters at the same time. Flow cytometry is composed of three modules; fluidics, optics and electronics. The fluidics system produces single cell stream which passes through an interrogation point. The scattered laser light at this point then enables detection of various cellular parameters labelled with fluorochromes. The physical parameters of cells, including granularity and cell size are detected by side and forward scattering respectively. At the interrogation point, the laser beams excite fluorochromes to emit light of longer wavelength. Various dichroic mirrors then divert the emitted light into a series of filters before collecting by photomultiplier tubes. The analogue signals are then digitised to be analysed by specialised software on a computer (Henel and Schmitz, 2007). In order to analyse several cellular properties in parallel, different antibodies conjugated to different fluorochromes can be used. Fluorochromes can be excited by similar laser but emit different wavelengths (Henel and Schmitz, 2007).

Bandpass filters within the flow cytometer are selective for the appropriate excitation and emission wavelengths. However, fluorescence could be detected from more than one fluorochrome when emission spectra overlap. To overcome spill over issue, fluorescence compensation process was employed. This process ensures that the signal collected by a

particular photomultiplier tube is originated from the fluorochrome that is being analysed (Roederer, 2001).

2.3.1 Measurement of calcium release from cytoplasmic stores

Background

Intracellular calcium flux is considered an important indicator of several biological processes including B cell function. Also, large cellular modifications can occur due to minor alterations in intracellular calcium levels (Berridge *et al.*, 2003). Ca^{2+} is a downstream signal following phosphorylation and recruitment of BLNK to PLC- ɣ2 upon engagement of Pre-BCR (Scharenberg *et al.*, 2007a; Hogan *et al.*, 2010). Ca^{2+} mobilisation can be detected by Fluo-4, AM imaging assay. This assay involves loading of Fluo-4, AM dye inside the cells and then `AM` moiety is cleaved by esterases cellular enzymes. After removal of AM group from the dye, free Fluo-4 is then able to bind Ca^{2+} and fluoresce. Given that the dye may be actively extruded outside the cell as it`s unbound to any cellular compartment, therefore, probenecid was added to minimise the dye efflux (Gee *et al.*, 2000).

Reagents

- Live Cell Imaging Solution (LCIS) (Life Technologies, USA, Cat#: A14291DJ)
- Fluo-4 Calcium imaging kit (Table 2.1) (Life Technologies, USA, Cat#: F10489)
- F(ab`)2 goat anti-µHC antibody (life Technologies, USA, Cat #: A24484)
- Ionomycin (Sigma-Aldrich, USA)

Procedure

One million cells were washed by resuspending the cells in pre-warmed LCIS Solution followed by centrifugation for 5 minutes at 450g and then the supernatant removed. Washing was repeated again and visible light-excitable calcium indicator Fluo-4 solution was prepared freshly according to the manufacturer`s instructions (see table 2.1). A 500µl aliquot of this solution was added to each cell suspension and incubated for 60 minutes in the dark at room temperature. Following incubation, the samples were washed once and resuspended in 0.5ml of LCIS and analysed on a FACSCalibur. FITC detectors can detect the Ca^{2+}-bounded Fluo-4 dye emission (excitation 494nm/emission 506 nm). Over

the first 60 seconds, cells were acquired to indicate the baseline fluorescence signal, the acquisition paused and a 20µg/ml F(ab`)2 goat anti-µHC antibody was added to the sample to stimulate the PreB/B cell receptor signalling. The event acquisition was then restarted for an additional 4 minutes before a final pause for the addition of Ionomycin which acted as a positive control (final concentration of 10 µg/ml) and further acquisition for 90 seconds. Ionomycin served to enhance moderate and transient Ca^{2+} concentration in the cytosol through increasing the endoplasmic reticulum store discharge of Ca^{2+} (Beeler *et al.*, 1979; Kauffman *et al.*, 1980; Feske, 2007; Dellis *et al.*, 2009). Daudi or Ramos B cells which express mature BCR acted as a positive control for their proven calcium flux and, therefore, they were included in all test runs (Kuwahara *et al.*, 1996). The data are shown as dot plots of y-axis (FL1-FITC) over x-axis (time) and analysed by FlowJo software.

Volume for 1 sample	Material	Purpose
5µl	PowerLoad™ Concentrate, 100X (Component B)	Minimizes the unfavourable effect of medium replacement
0.5µl	Fluo-4, AM, 1000X in DMSO (Component A)	Calcium indicator excited by visible light
Vortex		
0.5ml	LCIS	Physiological buffer for cell maintenance
Invert the tube to mix		
10µl	Probenecid, water soluble (Component D)	To decrease the baseline signal and prevent extrusion of intracellular dye (Fluo-4, AM)

Table 2.1: Fluo-4 solution preparation from Fluo-4 kit. Fluo-4 solution was prepared by mixing Fluo-4 kit components in LCIS solution (purchased separately). The purpose of each material is shown and the volumes depicted are per sample.

2.3.2 Annexin V staining for detecting apoptosis

Background

Annexin V is a protein dye that binds to phosphatidyl serine (PS) with high affinity in the presence of calcium (Aubry *et al.*, 1999). Once programed cell death is initiated, PS

molecules are translocated from the inner to the outer face of the plasma membrane. When PS become exposed to cell surface, it can be easily detected by staining with fluorescent conjugated Annexin V and analysed by flow cytometry (Fadok *et al.*, 1992; Vermes *et al.*, 1995).

The apoptosis assay was performed using Annexin V-FITC Apoptosis Detection Kit (Abcam, UK, Cat#: ab14085)

Reagents

- Annexin V-FITC
- 1X Binding Buffer

Procedure

After inducing apoptosis, $2.5x10^5$ cells were collected by centrifugation at 450g for 5 minutes and the supernatant was removed. Pelleted cells were then resuspended in PBS and centrifuged at 450g for 5 minutes at room temperature. Then, PBS was removed completely and cells were resuspended in 250µl of 1x binding buffer. Following that, 2.5µl of Annexin V-FITC was added and cells were incubated in the dark for 5 minutes at room temperature. Annexin V-FITC binding was analysed by flow cytometry on a FACSCalibur (Ex=488 nm; Em=530 nm) using the FITC detector (FL1). BD CellQuest software was used to analyse the data.

2.3.3 Cell cycle analysis using propidium iodide DNA staining

Background

Analysis of cell cycle by flow cytometry is a method to discriminate cells in three major cell cycle phases (G1, S and G2/M) in addition to the possibility of detecting dead cells by their fractioned DNA at sub-G1 phase (Pozarowski and Darzynkiewicz, 2004). Propidium iodide (PI) is a fluorescent dye (Ex: 488 nm; Em: 600 nm) that intercalates into the major grooves of DNA quantitatively. It can also bind double stranded RNA, therefore, RNAse A is added for optimal results (Crissman and Steinkamp, 1973; Krishan, 1975).

Reagents

- Cold 70% ethanol
- Propidium iodide solution (stock of 1 mg/ml); (Sigma, Dorset, UK)
- RNAse A (stock of 1 mg/ml); (Sigma, Dorset, UK)

Procedure

After incubating cells for the required time point, $0.5x10^6$ of cells were collected and washed once in PBS (450g for 4 minutes) and the supernatant then removed. One ml of cold 70% ethanol was added in a dropwise fashion to fix the cells whilst gently vortexing to minimise clumping of cells. Cells were then placed on ice for half an hour before washing once in PBS (450g for 4 minutes) and the supernatant completely removed. Pelleted cells were then resuspended in 250µl of working PI solution (Table 2.2) and stored at room temperature in the dark for 20 minutes before analysis by flow cytometry.

Material	Volume (µl)	Final concentration
RNAse A	6	24µg/ml
Propidium iodide	10	32µg/ml
PBS	234	N/A

Table 2.2: Working PI solution components per sample.

2.3.4 Surface marker detection

2.3.4.1 Determining Pre-BCR expression

Background

To investigate Pre-BCR expression in different cell lines and primary-derived xenograft (PDX) cells, Pre-BCR components were detected by flow cytometry. VPREB (CD179a) is an Ig V-like protein expressed on the surface of cells at pro-B and early pre-B developmental stages which can associates non-covalently with the Ig C-like protein, λ5 (CD179b) to form

SLC. In turn, the membrane bound protein µHC is complexed with SLC to form the Pre-BCR complex (Pillai and Baltimore, 1987; Karasuyama *et al.*, 1990).

In antibody staining experiments, it is important to rule out the background noise by using isotype controls. An isotype control is an antibody raised against an epitope not expressed in the cells being tested. It ensures that the measured signal is due to specific binding with the target rather than an artefact. The optimum isotype control should match the species of the host, the primary antibody fluorophore and concentration and Ig subclass. Moreover, the addition of BSA to the staining buffer reduces the non-specific binding of antibody (Hulspas *et al.*, 2009).

Reagents

- 1x Dulbecco`s PBS [prepared from diluting 10x Dulbecco`s PBS in distilled water]
- Bovine serum albumin fraction V (BSA) (Sigma, Dorset, UK)
- Fluorescent labelled antibodies (Table 2.3)

Protein target	Fluorochrome	Antibody species	Concentration (µg/ml)	Volume per sample (µl)	Clone	Isotype	Supplier	Cat#
IgM (µHC)	APC	Mouse Anti-Human	3	20	G20-127	Mouse IgG1, κ	BD Biosciences	561010
VPREB	PE	Mouse Anti-Human	400	5	HSL96	Mouse IgG1, κ	BioLegend	347404
λ5	PE	Mouse Anti-Human	200	5	HSL11	Mouse IgG1, κ	BioLegend	349803
Isotype control	PE	Mouse Anti-Human	200	5 or 10*	MOPC-21	Mouse IgG1, κ	BD Biosciences	554680
Isotype control	Alexa Fluor® 647	Mouse Anti-Human	1.5	40	MOPC-21	Mouse IgG1, κ	BD Biosciences	557783

Table 2.3: Antibodies used in Pre-BCR expression determination by flow cytometry.

*5µl for λ5 and 10µl for VPREB isotype matched control.

Procedure

Cell lines growing exponentially or PDX cells harvested from mouse spleen were counted and two flow cytometry tubes (one million cells each) per each sample were prepared and then centrifuged at 450g for 4 minutes to remove the supernatant. Pelleted cells were then resuspended in 2ml of filtered Dulbecco`s PBSA (0.2% BSA in Dulbecco`s PBS) and centrifuged at 450g for 4 minutes. After removing the supernatant, cells were resuspended in 100µl of Dulbecco`s PBSA. The relevant amount of target antibody (Table 2.3) was added to one tube and a similar concentration of matched isotype control antibody was added to the other tube. After incubation for 20 minutes at room temperature in the dark, cells were washed twice in 3.5ml of Dulbecco`s PBSA (450g for 5 minutes) and then analysed on the FACSCalibur. FlowJo software was used to analyse the acquired raw data of Pre-BCR molecules expression through determining the geometric mean fluorescent intensity (MFI) from histogram statistics.

2.3.4.2 Surface marker staining for detection of leukaemia blasts

Background

Commercial monoclonal antibodies against certain human or mouse immunophenotypes of interest were directly bound to fluorochromes and utilised for multicolour flow cytometry.

Reagents

- 1x Dulbecco`s PBS (prepared from diluting 10x Dulbecco`s PBS in distilled water)
- 10x red cell lysis buffer (1.55M ammonium chloride, 99.88mM potassium bicarbonate and 10.2mM EDTA disodium). 1x buffer is obtained after diluting in water.
- Bovine serum albumin fraction V (BSA) (Sigma, Dorset, UK)
- Florescent labelled antibodies (Table 2.4)

Target surface antigen	Target species	Clone	Florochrome	Volume (µl) per 50 µl of blood	Supplier	Cat #
CD38	Human	HB7	FITC	5	BD Biosciences	340909
CD45	Human	2D1	FITC	5	BD Biosciences	345808
CD10	Human	HI10a	PE	5	BD Biosciences	332776
CD34	Human	8G12	PerCP	5	BD Biosciences	345803
CD19	Human	SJ25C1	APC	2.5	BD Biosciences	345791
Mouse CD45	Mouse	30-F11	PE-Cy™7	2.5	BD Biosciences	552848
CD58	Human	1C3	FITC	5	BD Biosciences	555920
CD66c (KOR-SAR3544)	Human	KOR-SA3544	FITC	5	BECKMAN COULTER	IM2039U

Table 2.4: Monoclonal antibodies used for immunophenotyping by Flow cytometry.

Procedure

After blood (around 50µl) has been taken from mouse tail vein (Section 2.7.3), a cocktail of antibodies (Table 2.4) were added to the blood sample directly and mixed by pipetting before incubation in the dark for 15 minutes at room temperature. CD10, CD34, CD19 and mouse CD45 were added to all samples, but FITC conjugated antibodies were patient specific, and selected based on known expression of CD45, CD38, CD58 or CD66c (KOR-SAR3544). Following this, 1.2 ml of 1x red cell lysis buffer was added and mixed gently by inversion for 5 minutes. Samples were then centrifuged for 4 minutes at 450g and the supernatant was discarded. After pelleting the cells, samples were washed twice in 3.5ml of filtered Dulbecco`s PBSA and centrifuged for 5 minutes at 450g prior to analysis on a BD FACSCanto II machine. To assess human blast cell engraftment in mouse spleen, double the amount of antibodies (Table 2.4) were utilised and no red cell lysis was needed.

2.3.5 Intracellular phospho-protein staining

Background

Phospho-specific flow cytometry is a quick and effective method to quantify phosphorylated proteins which enables the determination of signalling cascades in samples where cell numbers are limiting, unlike lysate-based methods (Schulz et al., 2007; Schulz et al., 2012). Hence, identifying aberrant signaling pathways may serve as prognostic factor in some leukaemic malignancies (Calo *et al.*, 2003; Krutzik *et al.*, 2004; Brown *et al.*, 2015). Unlike the detection of surface proteins, phospho-specific intracellular flow cytometry is more problematic. The antibody is inaccessible to the intracellular target and the phosphorylation of protein is a transient mechanism and therefore unstable (Krutzik *et al.*, 2004). To overcome these challenges, proteins are stabilised by fixing with paraformaldehyde. Also, alcohol or detergent is used to permeabilize cells to allow entry of antibodies to intracellular phospho-epitopes of target proteins (Krutzik *et al.*, 2004) (Figure 2.1). For all phospho targets listed in table 2.5, Ramos cells were used as a positive control and were ran side by side with any experiment involving intracellular phospho flow cytometry.

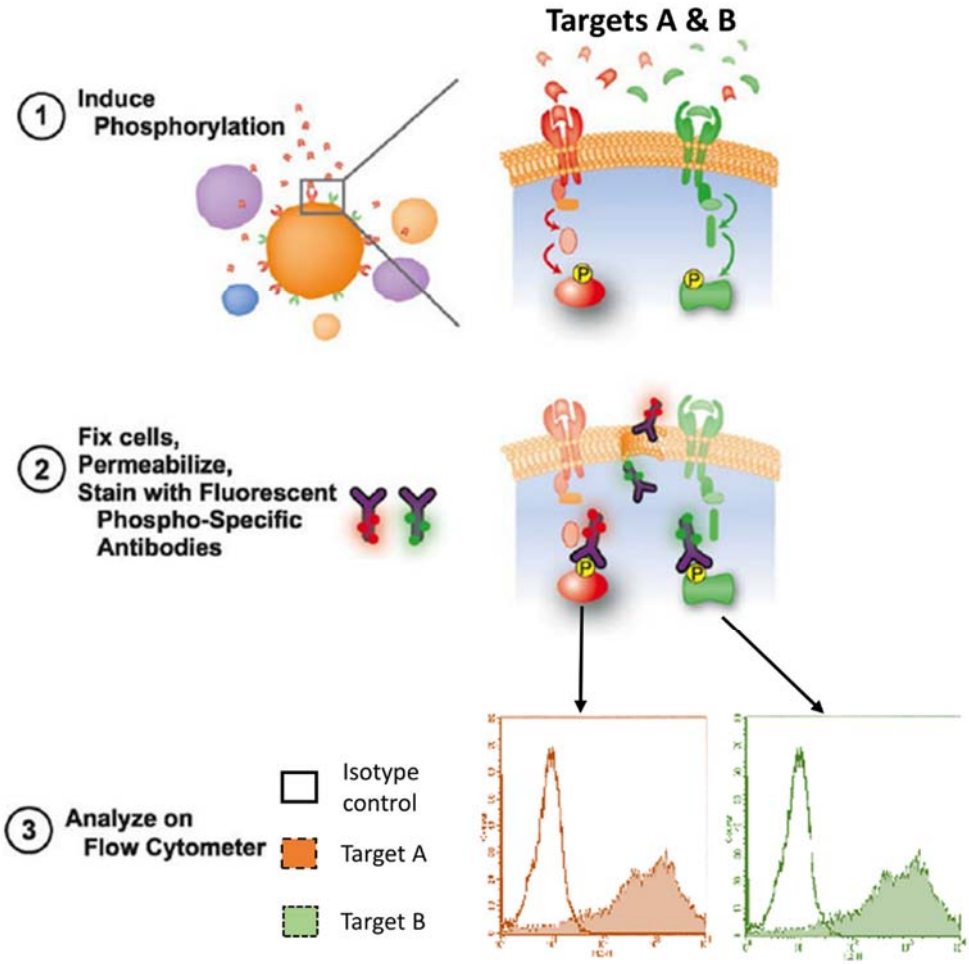

Figure 2.1: Summary of phospho-specific antibody flow cytometry technique. Adapted from (Krutzik *et al.*, 2004) .

Reagents

- Bovine serum albumin fraction V (BSA) (Sigma Aldrich, USA)
- BD Cytofix™ buffer (BD Biosciences, Belgium, Cat#:554655)
- Perm III buffer (BD Biosciences, Belgium, Cat#:558050)
- Fluorescent labelled antibodies (Table 2.5)

Protein target	Fluorochrome	Concentration (µg/ml)	Volume per sample (µl)	Clone	Isotype	Cat#
BTK (pY223)/Itk (pY180)	PE	12.6	5	N35-86	Mouse IgG1, κ	562753
AKT (ps473)	PE	1.5	20	M89-61	Mouse (BALB/c) IgG1, κ	560378
BLNK (pY84)	PE	0.75	20	J117-1278	Mouse (BALB/c) IgG2b, κ	558442
ZAP70 (Y319)/SYK (Y352)	PE	1.5	20	17A/P-ZAP70	Mouse IgG1	557881
SYK (pY348)	Alexa Fluor® 488	25	20	I120-722	Mouse (BALB/c) IgG1, κ	560081
ERK1/2 (pT202-pY204)	Alexa Fluor® 647	3	20	20A	Mouse IgG1	612593
PLC-γ2 (PY759)	Alexa Fluor® 647	3	20	K86-689.37	Mouse IgG1, κ	558498
Isotype control	PE	100	*	MOPC-21	Mouse IgG1, κ	554680
Isotype control	Alexa Fluor® 647	1.5	40	MOPC-21	Mouse IgG1, κ	557783
Isotype control	Alexa Fluor® 488	25	20	MOPC-21	Mouse IgG1, κ	557782

Table 2.5: List of antibodies and their concentrations used in phospho flow cytometry, all purchased from BD Biosciences.

* This Isotype control is diluted in PBS to match the concentrations of antibodies of interest.

A. Procedure for measuring basal and anti-µHC stimulated phosphorylation of cell lines and PDX cells

This procedure involves 6 main steps.

a. ***Harvesting and washing***: For cells being tested, 3 million cells were harvested and divided into 3 round bottom polystyrene test tube (also called FACS tubes) (Falcon, Mexico) equally (isotype control, baseline and stimulated). In addition, 2 FACS tubes each containing $1x10^6$ Ramos cells (baseline, stimulated) were used. After pelleting cells and discarding the supernatant medium, cells were washed once in 2ml of filtered 0.2% of BSA in PBS (termed PBSA) and then cells in all tubes were resuspended in 200µl of pre-warmed PBSA after removing supernatant.

b. ***Stimulation***: Twenty µg/ml of F(ab')2-Goat anti-Human IgM Heavy Chain antibody (anti-µHC) was added only to stimulated tubes for 4 minutes at 37 °C to activate the Pre-BCR/BCR and downstream signalling.

c. ***Fixation***: After stimulation, 750µl of Cytofix buffer was directly added to all the tubes (including recently stimulated cells) on top of cells suspended in 200µl PBSA and were directly incubated at 37 °C for 10-15 minutes. The samples were then centrifuged for 4 minute at 450g and the supernatant was removed.

d. ***Permeabilisation***: To the pelleted cells in all tubes, 1ml of cold perm buffer III was added while vortexing at mild speed and then incubated on ice for 30 minutes. Following that, cells were washed twice using 3.5ml of PBSA for 5 minutes at 450g and supernatant was decanted. Pelleted cells were then resuspended in 100µl of PBSA.

e. ***Antibody staining***: Cells were then stained with relevant amount of phospho antibody or matched isotype control (Table 2.5) and left for one hour at room temperature in the dark. Following incubation, samples were washed twice with 2ml of PBSA for 4 minutes at 450g.

f. ***Acquisition on Flow cytometry***: Ten thousand events were then acquired on FACSCalibur machine and analysed using CellQuest™ or Flowjo software.

B. Procedure for measuring the pharmacodynamic effects of drugs on cell lines and PDX cells

This procedure is very similar to the protocol for measuring basal and anti-µHC stimulated phosphorylation (Section 2.3.5.A) with the exception of non-stimulation of cells being tested (Isotype control, control vehicle treated cells, drug(s) treated cells).

2.4 Quantitative reverse-transcriptase polymerase chain reaction

Quantitative reverse-transcriptase polymerase chain reaction (QRT-PCR) is a sensitive and fast technique to measure relative gene expression at the mRNA level. The technique involves 3 stages:

1. RNA extraction from the cells
2. Reverse transcription of the RNA to synthesise copy DNA (cDNA)
3. Polymerase chain reaction using the cDNA

2.4.1 Total RNA extraction

Background

Qiagen RNeasy Mini kit (Qiagen, Crawley, UK) was used to extract total RNA from cell pellets. The selective binding features of a silica-based membrane is the basis of this method. Cell pellets were lysed and homogenised in the presence of a buffer containing guanidine-isothiocyanate. This buffer is highly denaturing which inactivates RNAases immediately and ensures intact RNA purification. To provide optimum binding conditions, ethanol was added prior to applying the cell lysate to the silica membrane. Contaminants were then removed efficiently and RNA was eluted in RNAse free water (Tan and Yiap, 2009).

Reagents

- Buffer RLT
- Buffer RW1
- Buffer RPE
- 2-Mercaptoethanol

- 70% ethanol
- RNase free water

Procedure

Cell lines growing in exponential phase were harvested and then $3x10^6$ to $10x10^6$ cells were exposed to single or combination of drugs. Cells were then pelleted and washed in PBS at 1000 RPM for 5 minutes. An appropriate amount of buffer RLT (containing 2-Mercaptoethanol) was added to lyse the cells and pipetting was applied to loosen the pellets. Cell lysates were then homogenised by passing the samples 5-10 times through a 20-gauge needle fitted to a one ml hypodermic syringe. A similar volume of 70% ethanol was added to the lysate and pipetted vigorously prior to transfer onto the spin column. A 2ml collection tube was then fitted to the spin column and centrifuged for 15 seconds at 10,000 RPM at room temperature and the flow-through was discarded. Following that, 700µl of buffer RW1 was added into RNeasy column and centrifuged for 15 seconds at 10,000 RPM at room temperature and then flow-through was removed. 0.5ml of buffer RPE was added and then spin column was centrifuged at 10,000 RPM for 15 seconds at room temperature. After decanting the flow-through, further washing was carried out by adding 500µl of buffer RPE and then RNeasy column was centrifuged at room temperature for 2 minutes. The flow-through was then decanted and the column was centrifuged at 14,000g for 1 minute to get rid of any leftover ethanol. RNeasy column was then transferred to a new 1.5ml eppendorf tube and 30-50µl of RNAse free water was added before centrifugation at 10,000 RPM for 1 minute to elute RNA. The purity and concentration of RNA was then determined spectrophotometry.

2.4.2 RNA samples quantification

The RNA concentration was assessed by measuring the absorbance of spectrophotometer (Nano Drop 1000 spectrophotometer) at 260nm and 280nm against an RNAse free water blank. Since nucleic acids absorb light at 260nm and proteins at 280nm, the purity was assessed through calculating the ratio of 260:280nm readings. A ratio between 1.8 and 2.0 is indicative of pure RNA, while lower ratios indicate contamination with protein (Tataurov *et al.*, 2008).

2.4.3 Synthesis of copy DNA

Background

This method involves synthesis of complementary cDNA using random primers that hybridise along several points along the mRNA template. This reaction is catalysed by the reverse transcriptase enzyme. The resulting cDNA can then be used in QRT-PCR reaction.

High-Capacity Reverse Transcription Kit purchased from Applied Biosystems (Thermo Fisher, UK) and the provided protocol were used for cDNA synthesis.

Reagents

- 10x RT Buffer
- 10x RT Random Primers
- 25x dNTP Mix (100mM)
- Multiscribe™ Reverse Transcriptase (50U/µl)
- RNase Inhibitor
- RNase free water

Procedure

According to the manufacturer instructions, the final concentration of each RNA sample was adjusted to 200µg/ml in RNAse free water. The reaction buffer was prepared on ice as detailed in table 2.6.

Component	Volume (µl)/Reaction
10x RT Buffer	2.0
25x dNTP Mix (100mM)	0.8
10x Random Primers	2.0
MultiScribe™ Reverse Transcriptase	1.0
RNase Inhibitor	1.0
Nuclease-free H2O	3.2

Table 2.6: Components of reaction buffer utilised in the synthesis of cDNA.

Ten microliters of RNA (at 200µg/ml) were then mixed with 10µl of reaction buffer in a PCR reaction tube (Applied Biosystems, USA) and mixed by pipetting. A short spin was applied to the PCR tubes to remove any bubbles formed. The tubes were then placed into a thermocycler (Gene Amp PCR System 2700) set with temperatures outlined in table 2.7 to complete the reaction. cDNA was then kept at 4°C for short term storage.

Step	Temperature (°C)	Time (min)
1	25	10
2	37	120
3	85	5
4	4	∞

Table 2.7: Thermal cycler program for cDNA synthesis using High-Capacity Reverse Transcription Kit.

2.4.4 QRT-PCR amplification of cDNA

Background

Real Time RT-PCR is a highly sensitive and reproducible technique which relies on quantification of PCR product via the fluorescent signal generated after each cycle. The number of PCR product molecules proportionate directly with fluorescent signals.

TaqMan® real-time PCR, the commercially available method, was used in this project. In this technique, accurate measurement of PCR product was achievable after inclusion of a fluorogenic oligonucleotide probe to components of a standard PCR. TaqMan® probes involve 2 types of fluorophores; the reporter attached at the 5', such as 6-carboxyfluorescein (FAM) and a quencher attached at the 3' end 6-carboxy-tetramethyl-rhodamine (TAMRA).

After each PCR cycle, samples are irradiated by ultra violet (UV) light and the fluorescent signal is then determined by a charge coupled device (CCD) camera logged by a computer. As long as the probes are intact, the fluorescent output is significantly reduced due to the close proximity of the reporter to the quencher. However, the fluorescent emission is increased once the probe is cleaved depending on the principle of Fluorescence Resonance Energy Transfer (FRET) (Cardullo *et al.*, 1988). If the target DNA sequence is present, the exonuclease

activity of *Taq* polymerase in the direction of 5' to 3' degrades the probe downstream of the target during PCR extension phase. This degradation allows continuance of primer extension to the end of DNA template strand and also releases the reporter dye molecule from its quencher. Thus, the intensity of the florescent signal increases with each additional PCR cycle and is proportional to the DNA template amount formed in the PCR.

In the course of PCR amplification, the fluorescent intensity is quantified allowing formation of an amplification plot. The amount of target DNA present in the PCR product can be measured from this amplification plot and is proportional to the level of mRNA expression. The initial 10-15 cycles of amplification are linear, where the fluorescent intensity is below the minimal detectable limit of the CCD camera, and defined as amplification plot baseline (Dorak, 2006). However, the fluorescent intensity exceeds the baseline upon increase of target DNA template and therefore, the higher the initial copy number of the target nucleic acid, the sooner there is detectable fluorescent intensity, above the baseline.

The threshold is the most important factor for numerical quantification which distinguishes between background signal and relevant amplification. It is calculated by multiplying the standard deviation of baseline fluorescence signal by ten (Arya *et al.*, 2005). The threshold cycle (C_T) is the PCR cycle number when the fluorescent signal crosses the threshold value (Walker, 2002). The C_T value is inversely proportional with the starting copy number of nucleic acid.

In this project, relative gene quantification method [also called comparative C_T threshold method ($\Delta\Delta C_T$)] was used, where changes in expression of target gene were measured in relation to expression of a housekeeping reference gene without calculating a standard curve (Schmittgen and Livak, 2008; Bustin *et al.*, 2009). For this method, the following formula was used:

$$\Delta CT = C_T \text{ Target Gene} - C_T \text{ Reference Gene}$$

$$\Delta\Delta C_T = \Delta C_T \text{ Treated} - \Delta C_T \text{ Untreated}$$

Reagents

- 2x TaqMan Universal PCR Master Mix (Applied Biosystems, UK, Cat#: 4304437)
- Human TBP (TATA-box binding Protein) Endogenous Control (VIC®/TAMRA™ probe, primer limited) (Applied Biosystems, UK, Cat#: 4310891E)

- TSC22 domain family; member 3 (TSC22D3), also known *GILZ* (Glucocorticoid-Induced Leucine Zipper) TaqMan primer (FAM-MGB) (Applied Biosystems, UK, Cat#: 4331182)
- RNase free water (Qiagen, Crawley, UK)

Procedure to measurement of glucorticoid target gene (*GILZ*)

Cell lines growing exponentially were harvested and treated for 24 hours with combination of dexamethasone plus fostamatinib R406 or dexamethasone plus dasatinib to investigate transcription of the glucocorticoid receptor (GR) target gene *GILZ*. After incubation, cells were then collected for RNA extraction and cDNA synthesis (Sections 2.4.1 and 2.4.3). Human *GILZ or* (*TSC22D3*) gene was then measured by QRT-PCR method, with human TATA-box binding Protein (*TBP*) housekeeping gene was used as an endogenous control. *TBP* was broadly used by our group as a reference gene in studies involving treatment of ALL cells with dexamethasone as it was proven to be stable in lymphocytes (Ledderose *et al.*, 2011).

2.5 Drug sensitivity

Background

To monitor the effect of treating cells with a drug, Alamar blue assay was used in this project. This assay quantitatively measures cells viability/proliferation depending on the reducing metabolic activity within living cells. Resazurin, the active compound of Alamar blue, is non-fluorescent and blue in colour and is metabolised by the mitochondrial enzyme (diaphorase) into the highly fluorescent red in colour Resorufin compound (Schreer *et al.*, 2005). The florescent intensity is relative to the number of living cells and therefore less metabolic activity is expected from apoptotic/necrotic cells.

Reagents

- RF10 medium: RPMI 1640 containing L-glutamine supplemented with 10% of FBS
- RF15 medium: RPMI 1640 containing L-glutamine supplemented with 15% of FBS and 0.05% v/v Penicillin-Streptomycin with 10,000 units penicillin and 10mg streptomycin) (Sigma, Dorset, UK)
- AlamarBlue® Cell Viability reagent (Thermo Fisher, UK, Cat#: DAL1100)

- CAL-101 (Stratech, UK, Cat#: S2226-SEL)
- Ibrutinib (PCI-32765) (Stratech, UK, Cat#: S2680-SEL)
- Fostamatinib R406 (Selleckchem, UK, Cat#: S2194)
- Dasatinib (Stratech, UK, Cat#: S1021-SEL)
- Dexamethasone (Sigma, Dorset, UK, Cat#: D-1756)

Drug	Cells	Concentration range	Control vehicle (CV)
CAL-101	PreB 697	0.1-100µM	0.5% DMSO
	Nalm-6	0.1-100µM	0.5% DMSO
	R3F9	0.01-25µM	0.12% DMSO
	REH	0.1-100µM	0.5% DMSO
	TK6	0.1-100µM	0.5% DMSO
	PDX	0.001-100µM	0.5% DMSO
Ibrutinib	PreB 697	0.1-25µM	0.12% DMSO
	Nalm-6	0.1-25µM	0.12% DMSO
	R3F9	0.01-25µM	0.12% DMSO
	REH	0.1-25µM	0.12% DMSO
	TK6	0.1-25µM	0.12% DMSO
	PDX	0.001-50µM	0.25% DMSO
Fostamatinib R406	PreB 697	0.001-50µM	0.25% DMSO
	Nalm-6	0.001-50µM	0.25% DMSO
	R3F9	0.001-25µM	0.12% DMSO
	REH	0.001-50µM	0.25% DMSO
	TK6	0.001-50µM	0.25% DMSO
	PDX	0.001-25µM	0.12% DMSO
Dasatinib	PreB 697	0.005-20µM	0.1% DMSO
	Nalm-6	0.005-20µM	0.1% DMSO
	R3F9	0.01-25µM	0.12% DMSO
	REH	0.005-20µM	0.1% DMSO
	TK6	0.005-20µM	0.1% DMSO
	PDX	0.01-25µM	0.12% DMSO
Dexamethasone	PreB 697	0.01-40µM	0.2% ethanol
	Nalm-6	0.01-40µM	0.2% ethanol
	R3F9	0.01-25µM	0.12% ethanol
	REH	0.01-40µM	0.2% ethanol
	TK6	0.01-40µM	0.2% ethanol
	PDX	0.01-25µM	0.12% ethanol

Table 2.8: A list of single drugs used in this study and concentration ranges for each cell line and PDX. All drugs were prepared from stock solutions adjusted to 20mM and stored in -20 to -80 °C.

2.5.1 Procedure for testing drug sensitivity using single agents

Cells in mid-log phase were used to determine the growth effects of different single drugs (Table 2.8). The optimum seeding density for each cell line was previously shown by Irving lab members to be $3x10^5$ cells /ml, which allows three doubling times over a 4 day period and for PDX cells, was $4x10^6$ cells/ml as they don't divide in suspension culture. Wells were seeded with 100µl of medium-containing cells ($2x10^4$-$4x10^5$ cells per well) in a 96-well sterile plate. To each well, 100µl of drug dosings or control vehicle (CV) made up in relevant medium (RF10 for cell lines and RF15 for PDX cells) were added as outlined in table 2.8. The dilution media was prepared in control vehicle to ensure similar amount of CV across all drug dosings. Two hundred microliters of media were added to the surrounding empty wells to minimise the evaporation from the central wells. Cells were then incubated for approximately 96 hours (about 3 doublings for cell lines) before the addition of twenty microliters of Alamar blue to all the wells. Cells were left for 4 hours (cell lines) or 6 hours (PDXs) then the fluorescent absorbance was measured using a FLUOstar microplate reader (Section 2.1.1) and raw data were then analysed by MARS data analyses software. The fluorescent readings were averaged and expressed as a percentage of control vehicle treated cells. GraphPad Prism software (6.0) was used to analyse the data. The variable slope with sigmoidal shape was fitted to all the data, and the GI_{50} (the drug dose that decreases cells proliferation to 50% when compared to the control) was calculated manually from the curve.

2.5.2 Procedure for testing synergism using combination of single TKI with dexamethasone

To test the effect of combining TKI inhibitor with dexamethasone, the combination index (CI) value was calculated which determine whether this combination is synergistic, additive and antagonistic (Chou and Talalay, 1984). This assay was performed after defining the GI_{50}s of cells to single TKI inhibitors and dexamethasone. For each single agent, 0.25 0.5, 1, 2 and 4 times the GI_{50} concentrations was tested separately and then both drugs combined. The same number of cells were seeded as in section 2.5.1. To ensure equal amount of CV across all wells of drugs (TKI alone, dexamethasone alone and combined), the dilution media was prepared in a universal control vehicle made up from DMSO and ethanol (Tables 2.9 and 2.10). Apart from

control vehicle preparation and concentration ranges, the same steps outlined in section 2.5.1 were used to assess the effect of drug combination on cells viability.

After calculating the percentage of growth due to treating cells with fractions of GI_{50}s of single agents and combination, the fraction affected (FA) is calculated for each tested concentration using the following formula (Bijnsdorp *et al.*, 2011):

$$\mathrm{FA} = 1 - \left(\frac{\%\ \mathrm{growth}}{100}\right)$$

FA values were then entered for analysis by CalcuSyn software to calculate CI values.

Combination	Cells	TKI concentration range	Dexamethasone concentration range	Control Vehicle (CV)
CAL-101 + Dexamethasone	PreB 697	2.5-40µM	11-176nM	0.2% DMSO + 0.00088% EtOH
	Nalm-6	2.5-40µM	2.5-40µM	0.2% DMSO + 0.2% EtOH
	R3F9	2.5-40µM	2.5-40µM	0.2% DMSO + 0.2% EtOH
	REH	2.5-40µM	2.5-40µM	0.2% DMSO + 0.2% EtOH
Ibrutinib + Dexamethasone	PreB 697	2.5-40µM	11-176nM	0.2% DMSO + 0.00088% EtOH
	Nalm-6	2.5-40µM	2.5-40µM	0.2% DMSO + 0.2% EtOH
	R3F9	2.5-40µM	2.5-40µM	0.2% DMSO + 0.2% EtOH
	REH	2.5-40µM	2.5-40µM	0.2% DMSO + 0.2% EtOH
Fostamatinib R406 + Dexamethasone	PreB 697	0.75-12µM	11-176nM	0.06% DMSO + 0.00088% EtOH
	Nalm-6	0.75-12µM	2.5-40µM	0.06% DMSO + 0.2% EtOH
	R3F9	1.5-24µM	2.5-40µM	0.12% DMSO + 0.2% EtOH
	REH	1.5-24µM	2.5-40µM	0.12% DMSO + 0.2% EtOH
Dasatinib + Dexamethasone	PreB 697	0.75-12µM	11-176nM	0.06% DMSO + 0.00088% EtOH
	Nalm-6	1.25-20µM	2.5-40µM	0.1% DMSO + 0.2% EtOH
	R3F9	0.625-10µM	2.5-40µM	0.05% DMSO + 0.2% EtOH
	REH	2.5-40µM	2.5-40µM	0.2% DMSO + 0.2% EtOH

Table 2.9: A list of drug combinations used in this study and concentration ranges for each cell line. All drugs were prepared from stock solutions adjusted to 20mM and stored in -20 to -80 °C.

Combination	Cells	TKI concentration range	Dexamethasone concentration range	Control Vehicle (CV)
CAL-101 + Dexamethasone	L910/AZ27	2.5-40µM	13.75-220nM	0.2% DMSO + 0.001% EtOH
	L4951/AZ26	1-16µM	2.5-40µM	0.08% DMSO + 0.2% EtOH
	L920/AZ24	2.5-40µM	9.25-148nM	0.2% DMSO + 0.0007% EtOH
	L824/AZ22	2.5-40µM	2.5-40µM	0.2% DMSO + 0.2% EtOH
	L707/AZ33	0.75-12µM	25-400nM	0.06% DMSO + 0.0002% EtOH
	L919/AZ19	2.5-40µM	2.5-40µM	0.2% DMSO + 0.2% EtOH
Ibrutinib + Dexamethasone	L910/AZ27	2.5-40µM	13.75-220nM	0.2% DMSO + 0.001% EtOH
	L4951/AZ26	1.87-30µM	2.5-40µM	0.15% DMSO + 0.2% EtOH
	L920/AZ24	2.5-40µM	9.25-148nM	0.2% DMSO + 0.0007% EtOH
	L824/AZ22	1.62-26µM	2.5-40µM	0.13% DMSO + 0.2% EtOH
	L707/AZ33	0.75-12µM	25-400nM	0.06% DMSO + 0.0002% EtOH
	L919/AZ19	2.5-40µM	2.5-40µM	0.2% DMSO + 0.2% EtOH
Fostamatinib R406 + Dexamethasone	L910/AZ27	0.437-7µM	13.75-220nM	0.037% DMSO + 0.001% EtOH
	L4951/AZ26	2.5-40µM	2.5-40µM	0.2% DMSO + 0.2% EtOH
	L920/AZ24	2.5-40µM	9.25-148nM	0.2% DMSO + 0.0007% EtOH
	L824/AZ22	0.75-12µM	2.5-40µM	0.06% DMSO + 0.2% EtOH
	L707/AZ33	0.75-12µM	25-400nM	0.06% DMSO + 0.0002% EtOH
	L919/AZ19	2.5-40µM	2.5-40µM	0.2% DMSO + 0.2% EtOH
Dasatinib + Dexamethasone	L910/AZ27	37.5-600nM	13.75-220nM	0.003% DMSO + 0.001% EtOH
	L4951/AZ26	2.5-40nM	2.5-40µM	0.0002% DMSO + 0.2% EtOH
	L920/AZ24	2.5-40µM	9.25-148nM	0.2% DMSO + 0.0007% EtOH
	L824/AZ22	25-400nM	2.5-40µM	0.002% DMSO + 0.2% EtOH
	L707/AZ33	0.75-12µM	25-400nM	0.06% DMSO + 0.0002% EtOH
	L919/AZ19	2.5-40µM	2.5-40µM	0.2% DMSO + 0.2% EtOH

Table 2.10: A list of drug combinations used and concentration ranges for some PDXs used in this study. All drugs were prepared from stock solutions adjusted to 20mM and stored in -20 to -80 °C.

2.6 Protein analysis

2.6.1 Western blotting

Background

This technique involves separation of proteins depending on their molecular weight using a polyacrylamide gel, and antibodies to visualise specific target proteins. Western blotting method involves 5 major stages:

1. Protein sample preparation
2. Protein concentration estimation
3. Gel electrophoresis
4. Electroblotting
5. Immunodetection

2.6.1.1 Protein samples preparation for Western Blotting

Background

Before proteins are separated on polyacrylamide gel, cells need to be lysed to release proteins. Depending on the phosphorylation status of the target protein, two cell lysis buffers were used. 1x cell lysis buffer for non-phosphorylated protein and PhosphoSafe reagent for cytosolic proteins in which the phosphorylation state need to be preserved. PhosphoSafe contains four phosphatase inhibitors, sodium vanadate, sodium fluoride, sodium pyrophosphate and β-glycerophosphate. After lysing the cells, proteins were denatured into their individual polypeptide units. Sodium dodecyl sulphate (SDS), an anionic detergent, was used as a denaturing agent. Samples were heated at 100°C in the presence of SDS and thiol reagent 2-mercaptoethanol which cleaves the S-S bonds to allow solubilisation and denaturation of protein mixtures. Also, the overall charge of polypeptides becomes negative after binding with SDS which enables separation of proteins based on their sizes after being placed in an electric field. To monitor samples whilst running on the gel, bromophenol blue was used as a dye front.

Reagents

- 25x Cocktail of protease inhibitors: 1 tablet of cOmplete, EDTA- free protease inhibitor cocktail tablet is dissolved in 2ml ddH_2O (Roche, Welwyn Garden City, UK).
- 1x cell lysis buffer: 10% v/v of 10x Cell lysis buffer (Cell Signalling, USA); 86% v/v ddH_2O; 4% v/v 25x cocktail of protease inhibitors.
- PhosphoSafe™ Extraction Reagent (Merck Millipore, USA)
- Laemmli Buffer: 4% SDS; 62.5mM Tris-HCl, pH 6.8; 20% (v/v) glycerol; 5% 2-mercaptoethanol; 0.005% bromophenol blue

Procedure

Before adding the appropriate lysis buffer, cells were washed in PBS (Section 2.2.5). Between 25-100 microliters of chilled 1x lysis buffer were added depending on the cell number. Cells were then vortexed and incubated with the lysis buffer. For non-phospho proteins, cell were incubated with 1x lysis buffer for 20 minute on ice with intermittent vortexing. While for phospho proteins, cells were vortexed well and then incubated with PhosphoSafe (containing 4% v/v of 25x cocktail of protease inhibitors) for 10 minutes at room temperature. After exposing cells to the appropriate lysis buffer, samples were centrifuged at 12000 RPM for five minutes at 4°C to pellet debris. The supernatant containing the protein extract was then transferred into a new, chilled eppendorf tube. Bicinchoninic acid (BCA) assay was then used to assess protein concentration of the lysate. Appropriate volumes of protein samples were made up to 0.5-1mg/ml using Laemmli buffer before heating at 100°C for 5 minutes to allow protein denaturation. Samples were either loaded in the gel or stored at -20°C for use at a later date.

2.6.1.2 Samples protein estimation

Background

It's necessary to measure the protein concentration of a lysate before performing any protein study by electrophoresis. The protein concentration of all samples studied by western blotting was evaluated by Pierce™ BCA Protein reagents (Thermo Fisher Scientific, Cramlington, UK) which is based on BCA. In this assay, proteins reduce Cu^{2+} to Cu^{+} in an alkaline medium (biuret

reaction). The cuprous cation (Cu^{+}) is then reacted with BCA to form a purple complex which enables colorimetric evaluation of total proteins by measuring absorbance at 540-590nm wavelength on a FLUOStar omega microplate reader (Smith *et al.*, 1985). A standard protein samples were then used to quantify the protein concentration of unknown samples.

Reagents

- BCA Reagent A (Thermo Fisher Scientific, Cramlington, UK): contains sodium bicarbonate, sodium carbonate, bicinchoninic acid and sodium tartrate in 0.1M NaOH
- BCA Reagent B (Thermo Fisher Scientific, Cramlington, UK): contains 4% cupric sulphate
- Pierce™ Bovine Serum Albumin Standard (Thermo Fisher Scientific, Cramlington, UK): 2mg/ml bovine serum albumin in 0.9% NaCl solution containing sodium azide

Procedure

The Pierce™ BCA Protein assay was performed according to the manufacturer's instructions. Ten microliters of diluted bovine serum albumin standards in dH_2O (0.2-1.2mg/ml) were plated out in quadruplicates to a 96 well plate. Following that, 10µl of 1:10 diluted protein samples were added in quadruplicate before addition of 190µl of BCA working solution (50 parts of BCA reagent A mixed with 1 part of BCA reagent B) to all wells being tested. The wells were then sealed and incubated for 30 minutes at 37°C before measuring absorbance at 562nm using FLUOStar omega microplate reader (Section 2.1.1). The unknown protein concentration of samples was then extrapolated from a standard curve generated by MARS Data Analysis Software after multiplying concentrations by the dilution factor.

2.6.1.3 Polyacrylamide gel electrophoresis

Background

The scientific principle of this method is the migration of charged molecules through a matrix after application of an electric current. Polyacrylamide is a suitable electrophoresis gel as it is electrically neutral, chemically inert, transparent and hydrophilic. Proteins separation by this method is size dependent, with smaller proteins migrating quicker than larger proteins. Polyacrylamide gel is formed after acrylamide monomers are polymerised into long chains by

N,N-methylene-bisacrylamide reaction. The rate of proteins transfer in polyacrylamide gel varies depending on the pore size of the gel and therefore the protein size range of the gel is determined according to the target protein. In this project, 4-20% gradient polyacrylamide gels were used to resolve small and large sized proteins on the same gel.

Reagents

- Electrode Buffer – 41.2nM Tris, 192mM glycine, 0.1% (w/v) SDS
- Precision Plus Protein™ Dual Color Standards (Bio-Rad Laboratories, Perth, UK)
- 4–20% Mini-PROTEAN® TGX™ Precast Protein Gels (Bio-Rad Laboratories, Perth, UK)

Procedure

Electrophoresis was performed using mini-gel equipment (Bio-Rad, UK) according to Laemmli`s method (Laemmli, 1970). Five microliters of protein marker was loaded in the first and last wells to flank the samples wells. Also, 15µl of samples prepared in Laemmli buffer (0.5-1mg/ml) were then loaded into the precast gel. Constant voltage of 220V was then applied for 25-35 minutes to separate the proteins of interest.

2.6.1.4 Electroblotting

Background

Following gel electrophoresis, proteins were transferred from the polyacrylamide gel to a polyvinylidine difluoride (PVDF) membrane (Bio-Rad Laboratories, USA) which has a high affinity to proteins to allow Immunodetection of target proteins (Burnette, 1981). This was achieved by placing the PVDF membrane upon the gel to ensure mirror image proteins transfer. After applying electrical field perpendicular to the gel surface, proteins were transferred from the gel to the membrane while immersed in the electrode buffer. This buffered solution contained methanol which increases PVDF membranes capacity for protein binding and counteracts acrylamide gel swelling.

Reagents

- Transfer Buffer – 10mM CAPS, 10% (v/v) methanol

Procedure

Mini-blot equipment (Bio-Rad, UK) was used to perform electroblotting. Sponges (Bio-Rad, UK), pre-soaked PVDF membrane in absolute methanol and 3mm Whatman filter card (GE Healthcare Life Sciences, UK) were soaked in a freshly prepared transfer buffer before sandwiching. Within electroblotting cassette, the sandwich was constructed as in the following sequence:

1. Sponge
2. Two filter cards
3. SDS gel
4. PVDF membrane
5. Two filter cards
6. Sponge

Any air bubbles formed were removed by rolling a 5ml tip over the sandwich. One hundred volts was then applied to the transfer tank and an icepack was added to prevent overheating.

2.6.1.5 Immunodetection

Background

After electroblotting, PVDF membranes were probed with specific antibodies (mono or polyclonal) to detect the target protein. Before probing with antibodies, PVDF membranes were incubated with a blocking buffer (buffer containing fat-free milk or Superblock) (Thermo Fisher Scientific, Cramlington, UK) to prevent non-specific binding of antibodies. The primary antibodies were also diluted in the same blocking buffer. Tween 20 is the detergent used to make up all buffers involved in Immunodetection procedure due to its ability to reduce the background formed from binding of non-specific proteins to the PVDF membrane. Following blocking, PVDF membranes were incubated with a primary antibody specific for the protein of interest. Before probing with the secondary antibody, membranes were washed to get rid of unbound antibodies. The membrane was then incubated with a secondary antibody produced in a different animal species against primary antibody Immunoglobulins (Ig). Secondary antibodies used in this project were linked to a horseradish peroxidase (HRP)

reporter enzyme which catalyses cyclic diacylhydrazide (luminol) oxidation to form acrinidium ester intermediates. High intensity chemiluminescence (430nm emission) was then produced after reaction of intermediates with peroxide in the presence of slight alkaline conditions. This luminescence is then detected by exposing the PVDF membrane to x-ray film and then developed by Automatic X-ray Film Processor (Section 2.1).

Reagents

- Tris-Buffered Saline (TBS) supplemented with Tween-20 (TBS-Tween or TBST) – 0.154M NaCl, 0.05M Tris, 0.5% (v/v) Tween-20
- Blocking buffers
    - 5% (w/v) dried skimmed milk powder prepared in TBST
    - SuperBlock™ T20 (TBS) Blocking Buffer (Thermo Fisher Scientific, Cramlington, UK)
- Amersham ECL Prime Western Blotting Detection Reagent (GE Healthcare Life Sciences, UK)
    - Solution A, Luminol enhancer
    - Solution B, Peroxide solution
- Primary and secondary antibodies (Table 2.11)

Procedure

After electroblotting, the PVDF membrane was immersed in a blocking buffer for 45 minutes on a rocking platform at room temperature. The PVDF membrane was then cut and incubated overnight with the relevant primary antibody at the appropriate dilution (Table 2.11) on a rocking platform at 4°C. Before probing with the HRP conjugated secondary antibody, the PVDF membrane was rinsed 3 times and then washed in TBST buffer for twelve minutes on a rocking platform to remove any unbound primary antibody. The PVDF membranes were then incubated for 30-60 minutes at room temperature. Membranes were then washed for 5 minutes in TBST on a rocking platform, and same washing conditions were repeated for further 3 times using fresh TBST. ECL reagents were then used to detect chemiluminescence from membrane bound HRP. Based on the manufacturer instructions, one part of solution A (Luminol enhancer) was mixed with one part of solution B (Peroxide solution) and then pipetted onto the membrane and left for 5 minutes at room temperature. The PVDF membranes were then drained and wrapped in SaranWrap (Thermo Fisher Scientific,

Cramlington, UK) and then put in an autoradiography cassette (Genetic Research Instrumentation Ltd., Dunmow, UK) for detection of chemiluminescence. Automatic X-ray Film Processor (JPI Healthcare, Korea) was then used in a dark room to develop the x-ray film after being exposed to the PVDF membrane for a definite amount of time to allow visualisation of the protein. Chemiluminescence was also detected by BioRad imaging system (Section 2.1.1) and images were analysed by Image Lab™ Software 6.0 with a computer connected to the machine.

Target protein	Molecular wt (kDa)	Species and clone	Dilution used	Diluting buffer	Dilution of secondary Ab	Supplier	Catalogue number	
BIM	12, 15, 23	Rabbit monoclonal	1:3000	5% BSA	1:2000	Cell Signaling	2933	Primary
GR	94.91	Rabbit monoclonal	1:2000	5% Milk	1:4000	Cell Signaling	3660	
pGR^{S211}	95	Rabbit polyclonal	1:2000	5% Milk	1:2500	Cell Signaling	4161s	
PARP	116	Rabbit polyclonal	1:2000	5% Milk	1:5000	Santa Cruz	sc-7150	
$pAKT^{s473}$	60	Rabbit monoclonal	1:2000	Super block	1:2000	Cell Signaling	4060	
Total AKT	60	Rabbit monoclonal	1:80 000	Super block	1:2000	Cell Signaling	4691	
Alpha tubulin	45	Mouse monoclonal	1:500 000	5% Milk	1:8000	Sigma-Aldrich	T6074	
Rabbit-Ig	–	Goat	–	TBST	–	Dako, Glosturp, Denmark	P0448	Secondary
Mouse-Ig	–	Goat	–	TBST	–	Dako, Glosturp, Denmark	P0447	

Table 2.11: List of antibodies used in western blotting with their relevant dilutions.

Procedure for stripping proteins from PVDF membrane

In order to re-probe a given blot with several different antibodies, Re-blot Plus (Merck Millipore, UK) stripping solution was used in this project. According to the manufacturer instructions, blots were submerged in 1x antibody stripping solution (one part 10x antibody stripping solution diluted in 9 parts distilled water) and incubated for 15 minutes with mild mixing on a rocking platform at room temperature. PVDF membranes were then blocked in an appropriate blocking solution for 30 minutes before washing twice in TBST buffer, for 5 minutes. Following that, the PVDF membrane was ready for re-probing with a different antibody.

2.6.2 Extraction of cytoplasmic and nuclear proteins

Background

In order to investigate the presence or absence of a target protein in cytosolic or nuclear compartments of the cells, subcellular fractionation was used to extract proteins from these two compartments. A stepwise separation of cytosolic and nuclear extract from cultured cell lines was performed according to a protocol developed by Schreiber *(Schreiber et al., 1989)*. The cytoplasmic contents were released from pelleted cells after addition of buffer A which acts by disrupting the plasma membrane. Intact nuclei were recovered by centrifugation after removal of the cytosolic extract. Nuclear proteins were then extracted from nuclei after addition of buffer B with vigorous rocking. Protease inhibitors were added immediately before use to maintain function and integrity. This method used to extract proteins from the two cellular compartments to investigate glucocorticoid receptor translocation from the cytoplasm to the nucleus.

Reagents

- 25x Cocktail of protease inhibitors: 1 tablet of cOmplete, EDTA- free protease inhibitor cocktail was dissolved in 2ml ddH_2O (Roche, Welwyn Garden City, UK).
- Buffer A: 10 mM HEPES; pH 7.5, 10mM KCl, 0.1mM EDTA, 1mM dithiothreitol (DTT), 0.5% IGEPAL CA-630, 0.5mM PMSF and 4% v/v 25x protease inhibitor cocktail

- Buffer B: 20mM HEPES (pH 7.5), 400mM NaCl, 1mM EDTA, 1mM DTT, 1mM PMSF and 4% v/v of 25x protease inhibitor cocktail

A. Procedure for extracting cytosolic proteins using buffer A

A suspension of 10 million cells growing in exponential phase were collected and washed in 10ml of PBS (Section 2.2.5). The pelleted cells were then resuspended in 1ml of cold PBS and transferred into 1.5ml eppendorf tube and centrifuged at 450g for 5 minutes in a cold centrifuge at 4°C. Following that, the supernatant was removed and pelleted cells were resuspended in 150µl of cold buffer A for 15 minutes on ice. During this incubation time, tubes were vortexed for 10 seconds every 7 minutes to disrupt the cell membrane. Tubes were then centrifuged at 12,000g for 10 minutes at 4°C and the supernatant was stored at -80°C for use at a later time. An aliquot (10µl) of this cytoplasmic extract was diluted in 40µl of distilled water for protein concentration quantification (Section 2.6.1.2).

B. Procedure for extracting nuclear proteins using buffer B

One ml of buffer A was then used to gently resuspend the remaining nuclei pellet and then was centrifuged for 450g for 5 minutes at 4°C. After decanting the supernatant, the pelleted nuclei were resuspended in 60-75µl of buffer B and the tubes were vigorously rocked by thermomixer (Section 2.1.1) at 1300 RPM for 30 minutes at 4°C. The eppendorf tubes were then centrifuged at 12,000g for 15 minutes at 4°C. Ten microliters of the nuclear extract were diluted in 40µl of distilled water for protein concentration quantification (Section 2.6.1.2) and the remaining supernatant was stored at -80°C for use at a later date as nuclear extract.

2.6.3 GR transcription factor binding

This assay involves 3 stages:

1. Protein extraction from the cells
2. Quantification of protein using Bradford assay
3. Investigating GRE binding by an ELISA method

2.6.3.1 Extraction of nuclear proteins

Reagents

- Buffer A: 10mM HEPES; pH 7.5, 10mM KCl, 0.1mM EDTA, 1mM dithiothreitol (DTT), 0.5% IGEPAL CA-630, 0.5mM PMSF and 4% v/v 25x protease inhibitor cocktail
- Complete Lysis Buffer: 0.1% (v/v) of 1M DTT, 1% (v/v) protease inhibitor cocktail in 1 ml Lysis buffer AM2 (Provided with GRE ELISA kit) (Active Motif Europe, La Hulpe, Belgium)

A. Procedure for extracting cytosolic proteins using buffer A

Please see section 2.6.2.A

B. Procedure for extracting nuclear proteins using Active Motif`s lysis buffer

One ml of buffer A was then used to gently resuspend the resulting nuclei pellet and then centrifuged for 450g for 5 minutes at 4°C. After decanting the supernatant, the pelleted nuclei were resuspended in 50µl of freshly prepared Complete Lysis Buffer and the tubes were vigorously rocked by thermomixer (Section 2.1.1) at 1300 RPM for 30 minutes at 4°C. The eppendorf tubes were then centrifuged at 14,000g for 10 minutes at 4°C. Ten microliters of the nuclear extract were diluted in 40µl of distilled water for protein concentration quantification and the remaining supernatant was stored at -80°C for use at a later date as nuclear extract.

2.6.3.2 Quantification of protein using Bradford assay

Background

In this study, the protein was quantified using Bradford based assay. Briefly, the proteins were measured by microplate reader at 595nm after adding an acidic dye to a protein extract solution. In this dye-binding assay, the change of dye colour is relative to the protein concentration present in the solution (Bradford, 1976). Upon binding of dye-protein, the absorbance maximum of acidic solution of Coomassie Brilliant Blue G-250 Dye will shift from 465 nm to 595 nm.

Unlike BCA protein quantification method (Section 2.6.1.2), this reagent showed no interference with Complete Lysis buffer and therefore this method was employed in the GRE binding study.

Reagents

- Bio-Rad Protein Assay Dye Reagent Concentrate (Bio-Rad Laboratories GmbH, Munchen, Germany)
- Pierce™ Bovine Serum Albumin Standard (Thermo Fisher Scientific, Cramlington, UK): 2mg/ml bovine serum albumin in 0.9% NaCl solution containing sodium azide

Procedure

The Bradford protein assay was performed according to the manufacturer's instructions. Ten microliters of diluted bovine serum albumin standards in dH_2O (0.2-1.2mg/ml) were plated out in quadruplicates to a 96 well plate. Following that, 10µl of 1:5 diluted protein samples were added in quadruplicate before addition of 190µl of Bradford working solution (One part Dye Reagent Concentrate with four parts distilled water) to all wells being tested and pipette up and down to allow thorough mixing. Following that, incubation was performed for 5 minutes at room temperature before measuring the absorbance at 595nm using FLUOStar omega microplate reader (Section 2.1.1). The unknown protein concentration of samples was then extrapolated from a standard curve generated by MARS Data Analysis Software after multiplying concentrations by the dilution factor.

2.6.3.3 ELISA method for measuring GR transcriptional activity

Background

It has been established that activated GR transcription factor regulates target gene expression level after binding to consensus sequences of the promoter region of genes. These palindromic sequences which are located at the regulatory region of target genes are called glucocorticoid response elements (GREs) (Oakley and Cidlowski, 2013b).

In this study, the GR activation level was detected and quantified by using the commercially available kit purchased from Active Motif which utilises the ELISA based colorimetric method as outlined in figure 2.2. At the bottom of each well of the ELISA plate, a consensus

oligonucleotides sequence (GRE) has been immobilised. Hence, any GR molecule contained in the nuclear extract will bind to the GRE oligonucleotide sequence specifically which can then detected by primary antibody against GR. Secondary HRP labelled antibody specific to the primary antibody is then added before developing and quantification of GRE activity by spectrophotometer.

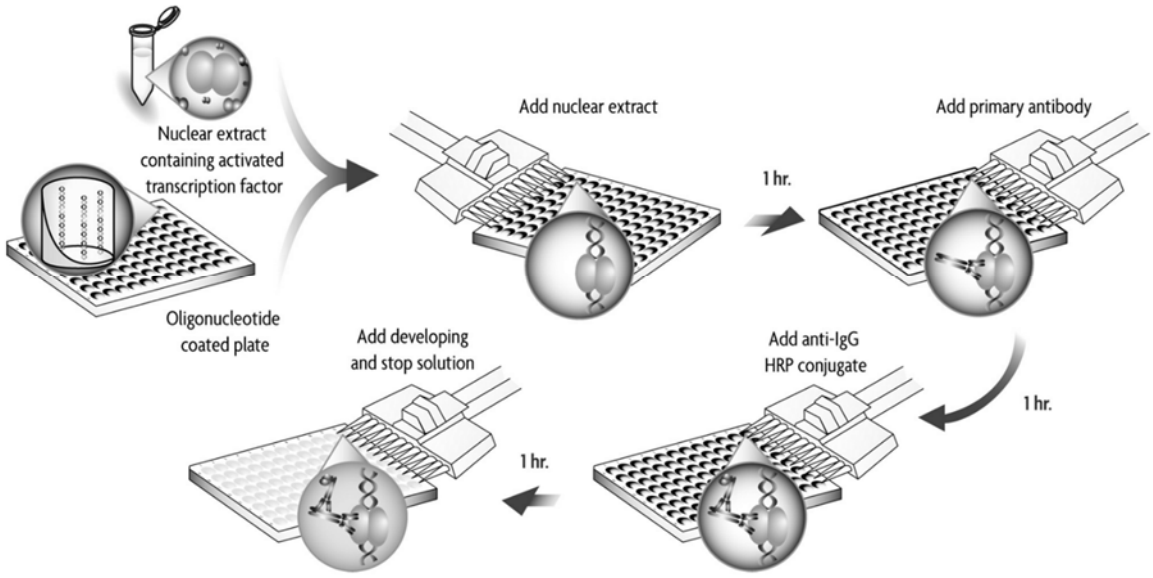

Figure 2.2: Flow chart of ELISA based assay for measuring GRE transcription factor activity.

Active GRE transcription factor contained in the nuclear extract binds to the consensus sequence immobilised on the oligonucleotide coated well. The amount of GRE is then quantified after incubation with primary and secondary antibodies. Flow chart reproduced from www.activemotif.com/documents/59.pdf.

Reagents

- TransAM™ GR Transcription Factor Assay Kit (Active Motif, Belgium; Cat# 45496)

Procedure

According to the manufacturer`s instructions, GR-DNA binding activity was assessed. Briefly, for each well to be used, 30µl of freshly made complete lysis buffer was added (Table 2.12). 10µl of nuclear protein extract was prepared (Section 2.6.3.1) and then quantified using the Bradford assay (Section 2.6.3.2), and was diluted in complete lysis buffer (Table 2.12) to 0.5µg/µl. Twenty µl of each sample were then added in single replicates for 60 minutes with

mild agitation at rocking platform. Twenty µl of complete lysis buffer was used as a blank, and also, the same volume of nuclear protein extracted from HeLa cells treated with dexamethasone was used as positive control. Two hundred µl of 1x washing buffer was used to wash each well and this was repeated 3 times. 100µl of diluted GR primary antibody (diluted to 1:1000 with Antibody Dilution Buffer) provided with the kit was then added for each well without agitation. Following 60 minutes incubation at room temperature, wells were washed as before and 100 microliters of secondary HRP-conjugated antibody (diluted to 1:1000 with Antibody Dilution Buffer) was added for each well and incubated for one hour. Wells were then washed as mentioned above before addition of one hundred microliter of Developing Solution for 7 minutes. 100µl of Stop Solution was then added and absorbance was measured using a FLUOstar omega microplate reader (Section 2.1.1) at 450 nm with a reference wavelength of 655 nm.

Reagent	Component	Volume (µl)/well
Complete Lysis Buffer	DTT	0.02
	Protease Inhibitor Cocktail	0.23
	Lysis Buffer AM2	22.25
Complete Binding Buffer	DTT	0.03
	Herring Sperm DNA	0.34
	Binding Buffer AM2	33.4

Table 2.12: Preparation of buffers for use in GR transcription factor activity, buffers were provided with the kit.

2.7 Xenotransplantation of ALL samples

Background

In order to perform various downstream assays using clinical material, such as drug sensitivity testing of numerous drugs, a large number of cells are often required. During the last few decades, it has become possible to xenotransplant primary haematopoietic cells into mice with impaired immune system to serve as a preclinical bridge between human and mouse (Cox *et al.*, 2004; Shultz *et al.*, 2007). These pre-clinical models also maintain the genetic diversity of patient samples and this may justify their usage in testing potential compounds and studying biology of diseases (Scott *et al.*, 2013; Wang *et al.*, 2017). It has been found that the genotypic and phenotypic properties and MRD markers of the original patient ALL cells are retained in the non-obese diabetic/severe combined immunodeficiency [(NOD/SCID), IL-2R common gamma chain null (NSG)] ALL mouse model (Cox *et al.*, 2004; Woiterski *et al.*, 2013). Leukaemic blast engraftment can be monitored in peripheral blood by flow cytometry at frequent intervals. Enlarged spleens taken from highly engrafted mice are made up of high percentage of human blast cells which can be utilised in the downstream *ex vivo* analyses or reinjected into new NSG mice to amplify the patient material. However, this technique is time consuming and the time elapsed for spleen engraftment is unpredictable as is deciding on when to harvest mouse spleen before the disease impacts on mouse health. Spleen engraftment does not necessarily correlate with peripheral blood leukaemia monitoring.

2.7.1 Cells preparation for xenotransplantation

The primary patient samples were randomly selected from high risk and relapse patients, however, two known Pre-BCR$^+$ cases, one with a t(1;19) and another with a t(17;19) were also included. Cryopreserved primary patient ALL or PDX cells (Table 2.13) were allowed to thaw at 37°C and then washed twice in warm RF10. Cells were then resuspended in RF10 and adjusted to $5x10^7$/ml ($1x10^6$ in 20µl) as the final concentration. Home office licence was obtained before embarking animal work and all patient samples were obtained from the Haematology biobank following project ethical approval. Dr Helen Blair, as staff member of the NICR kindly performed the intrafemoral procedure (Sections 2.7.2).

Patient ID	Gender	Age at presentation (years)	Cytogenetics	Oncogene	Mice implanted
L825 Presentation	Female	14	Normal	CBL	L825/JM 158
					L825/JM 157
					L825/AZ12
					L825/AZ10
					L825/AZ17
					L825/AZ18
L897 Presentation	Male	16	Failed	RAS	L897/JM 234
					L897/JM 233
L779 Presentation	Male	5	High Hyperdiploidy	RAS	L779/JM 151
					L779/JM 150
					L779/JM 152
					L779/AZ14
					L779/AZ13
L578 Relapse	Female	3	relapse 2 46XX[20]FISH:MLL,BCR/ABL,TEL/AML-ve Gain of AML1	NRAS	L578/JM 162
					L578/AZ7
					L578/AZ9
					L578/AZ8
L829 Presentation	Female	3	High Hyperdiploidy	NRAS, KRAS	L829/AZ3
					L829/AZ2
					L829/AZ1
L829 Relapse	Female	3	High Hyperdiploidy	KRAS	L829/JM 254
					L829/AZ16
					L829/AZ15
L914 Presentation	Female	7	High Hyperdiploidy	CBL, FLT3	L914/AZ6
					L914/AZ4
					L914/AZ5
L910 Presentation	Female	2	46,XX,**t(1;19)**(q23;p13)[9]/46,XX[1]	*TCF3-PBX1*	L910/AZ28
					L910/AZ27

Patient ID	Gender	Age at presentation (years)	Cytogenetics	Oncogene	Mice implanted
L4951 Presentation	No info	15	t(9;22)	*BCR-ABL1*	L4951/AZ25
					L4951/AZ26
LK196 2nd relapse	Male	15	At diagnosis 46,XY[20].arr[hg19](9p21.3)x0, (14q32.33)x1 So the g-banding is normal.	biallelic lost of 9p21.3 (CDKN2A/B) and a monoallelic lost of 14q32.33 (IGH).	LK196/JM272
L920 Presentation	Female	4	Failed	N/A	L920/AZ23
					L920/AZ24
L919 2nd Relapse	Male	2	No info	N/A	L919/AZ20
					L919/AZ19
L824 Presentation	Female	16	Failed	*PDGFR*	L824/AZ21
					L824/AZ22
L919 1st Relapse	Male	2	No info	N/A	L919/JM267
L881 2nd Relapse	Male	6	No info	N/A	L881/JM276
					L881/JM275
L707 Presentation	Female	16	46,XX,der(19)t(17;19)(q2?2;p13)[12]/ 46,idem,fra(10)(q25)[17]/ 46,XX[1].ish der(19)**t(17;19)**(19ptel-,wcp17+,wcp19+,19qtel+)	*TCF3-HLF*	L707/AZ33
L523 Rel	Female	15	Presentation 46,XX,t (1;9)(q2?5;q34) [7]	N/A	L523/AZ29

Table 2.13: Details of patient samples used in this project to generate PDX samples. All mice labelled with JM were kindly given from Liz Matheson or Marian Case, L4951 patient cells was kindly donated from Alex Elder.

2.7.2 Intrafemoral transplantation protocol

In order to perform intrafemoral transplantation, NSG mice were subject to general anaesthesia. Mice were placed in an anaesthesia chamber which is connected to oxygen and an isoflurane vaporiser. Five percent v/v of Isoflurane was applied in a constant flow of oxygen (1500-2000 ml/minute) until the animal lost consciousness inside the anaesthesia chamber. To maintain the anaesthesia outside the chamber, a face mask supplied with Isoflurane (~3%) was fitted. A pain stimulus was then applied to the mouse foot to ensure the appropriate amount of anaesthesia was utilised before embarking on the procedure. At the start of the procedure, mice were weighed before injecting them with analgesic (5mg/kg Carprofen) subcutaneously. The leg fur was then shaved and sterilised with Hydrex Derma spray before drilling the kneecap and femur with a 29G insulin needle. One million patient or PDX cells were suspended in 20µl of RF10 and injected into the femur using a new needle. After completion of the procedure, mice were put back in their cages and observed for full recovery and signs of prolonged bleeding. Highly aseptic conditions were ensured throughout anaesthesia and intrafemoral procedures.

2.7.3 NSG mice husbandry

After injecting the mice with human leukaemic cells, mice were weighed weekly and checked for signs of sickness. According to the home office license, the end point is defined as more than 10% weight loss maintained for 3 days or more than 20% weight loss (compared to the heaviest weight). Further to the defined end points, the general health of the mice are also considered and signs of illness are monitored such as:

1. Enlarged spleen
2. Paleness of the ears, feet or the tail may indicate poor circulation or anaemia
3. Loss of skin tone
4. Laboured breathing
5. Reduced movement or hind limb paralysis
6. Inability to maintain upright position
7. A starry coat with porphyrin staining around eyes or nose

Mice were sacrificed humanly according to schedule one method (cervical dislocation).

Protocol for mouse tail bleeding

A tiny amount of mouse blood (50µl) was taken from the tail by venepuncture to assess the percentage of leukaemic cells. Mice were restrained in a plastic tube and then the tail vein was nicked by a sterile scalpel blade. The droplet of blood formed on the tail was then collected in heparin coated tubes (Sarstedt Ltd, Leicester, UK) by capillary action. After blood collection, the bleeding was stopped by applying pressure above the cut and the mouse was released from the restraining tube and put back in the cage. Mice were observed for several minutes to make sure that the bleeding had stopped. Blood samples were then taken to the lab for analysis as described in section (2.3.4.2).

2.7.4 Processing of harvested xenograft mouse spleen

Once mice were sacrificed after detection of a high percentage of leukaemic cells in the peripheral blood (>40%) or after showing signs of illness (section 2.7.3), their spleens were removed for analysis. Mice spleens were then weighed before homogenisation using a 1ml syringe plunger. In order to get single cell suspension, the homogenate was passed through cell sieve using sterile RF15 medium. After two washes in the same medium and centrifugation at 1000 RPM for 5 minutes, cells were counted using trypan blue (Section 2.2.6). Cells were then used for downstream assays or frozen at -150°C for use at a later date.

2.8 Statistical analysis

Unpaired student`s t-test was used to determine statistical significance using GraphPad Prism software, $p<0.05$ were considered significant. CalcuSyn software was used to calculate the combination index of 2 drugs based on Chou and Talalay method (Chou and Talalay, 1984).

Chapter 3 (Results 1): Characterisation of BCP-ALL cells

Chapter 3: Characterisation of BCP-ALL cells

3.1 Introduction

As described earlier, Pre-BCR signalling plays an important role in the survival and differentiation of normal B cells through key signalling pathways, however, recurrent genetic aberrations in ALL, including chromosomal translocations and gene deletions or mutations, interfere with normal Pre-BCR signalling to enhance leukaemogenesis (Herzog *et al.*, 2009; Eswaran *et al.*, 2015). Therefore, characterising BCP-ALL cells for Pre-BCR signalling is informative for therapeutic exploitation. In order to assess a potential target(s) for small molecule inhibitor TKIs, Pre-BCR expression, activation status, and function were comprehensively investigated in ALL cells.

The aim of this chapter was to:

- Assess cell surface expression of Pre-BCR molecules (µHC, VPREB and λ5) in ALL cell lines and PDX cells.
- Measure Ca^{2+} mobilisation due to stimulation with F(ab)2 anti-µHC antibody to assess Pre-BCR function.
- Measure the baseline phosphorylation of key signalling intracellular proteins associated with the Pre-BCR signalling pathways (i.e. pBTK, pAKT, pSYK, pBLNK, pERK, and pPLC-Y2) and their activation due to stimulation with anti-µHC antibody.

3.2 Cell surface expression of Pre-BCR molecules

It is well established that the cell surface of most BCP-ALL cells do not express Pre-BCR (Kuwahara *et al.*, 1996; Geng *et al.*, 2015) but it is a key parameter which must be characterised in the ALL cells used in this study. Therefore, to evaluate expression of Pre-BCR, the Immunoglobulin μ heavy chain (μHC) and the surrogate light chain fragments (VPREB and λ5) were measured by Flow cytometry (Section 2.3.4.1) in a series of cell lines from different developmental stages (n=7) and 31 PDX samples derived from 15 primary patient samples (Figures 3.1 and 3.2).

Only cell lines at the precursor B cell stage (PreB 697, R3F9, Nalm-6) expressed surrogate light chains, whereas μHC was expressed on the surface of all cell lines (Pre-B, immature and mature B cells) except REH cells (pro-B cells). However, the Ig heavy chain was more abundant on the Burkitt's lymphoma cell lines (Daudi and Ramos; immature and mature B cell, respectively) (Figure 3.1). TK6 cells are considered immature B cells as they express μHC and lack surrogate light chain molecules, however μHC expression is less abundant than immature and mature B cells.

In addition to cell lines, PDX samples used in this study were evaluated for Pre-BCR expression and only 7 PDX samples derived from 3 patient samples expressed Pre-BCR molecules. Two harboured the chromosomal translocations t(1;19) *TCF3-PBX1*; t(17;19)(q22;p13) *TCF3-HLF*, while the third had normal cytogenetics (Figure 3.2, top 3 panels, table 2.13). However, the remaining 24 PDX samples (derived from 12 patient samples) were shown to be Pre-BCR negative as they lack expression of μHC and surrogate light chain molecules. They did not bear classic Pre-BCR-associated cytogenetics. (Figure 3.2, bottom 12 panels, table 2.13).

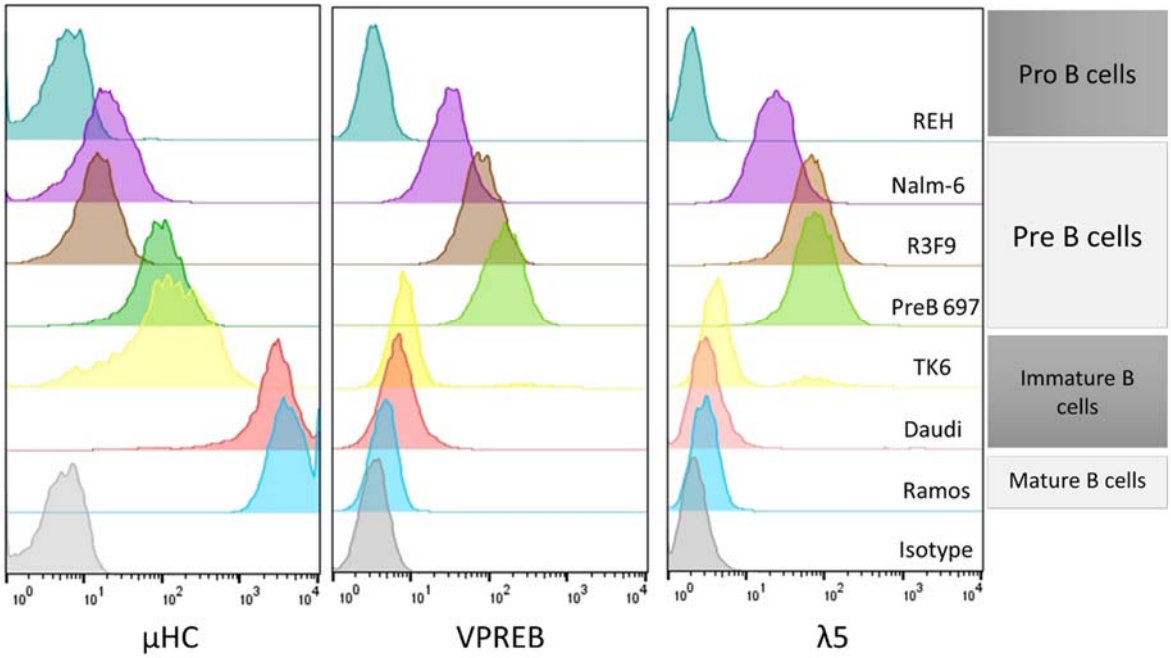

Figure 3.1: Flow cytometry analysis of Pre-BCR expression in a subset of B lineage cell lines from different developmental stages.

Cells at the logarithmic growth phase were harvested and analysed by flow cytometry for surface binding of anti-μHC, anti-VPREB and anti-λ5. Each cell line was also stained with an isotype control (grey histogram), a representative trace is shown. Histogram overlays were generated by Flowjo software.

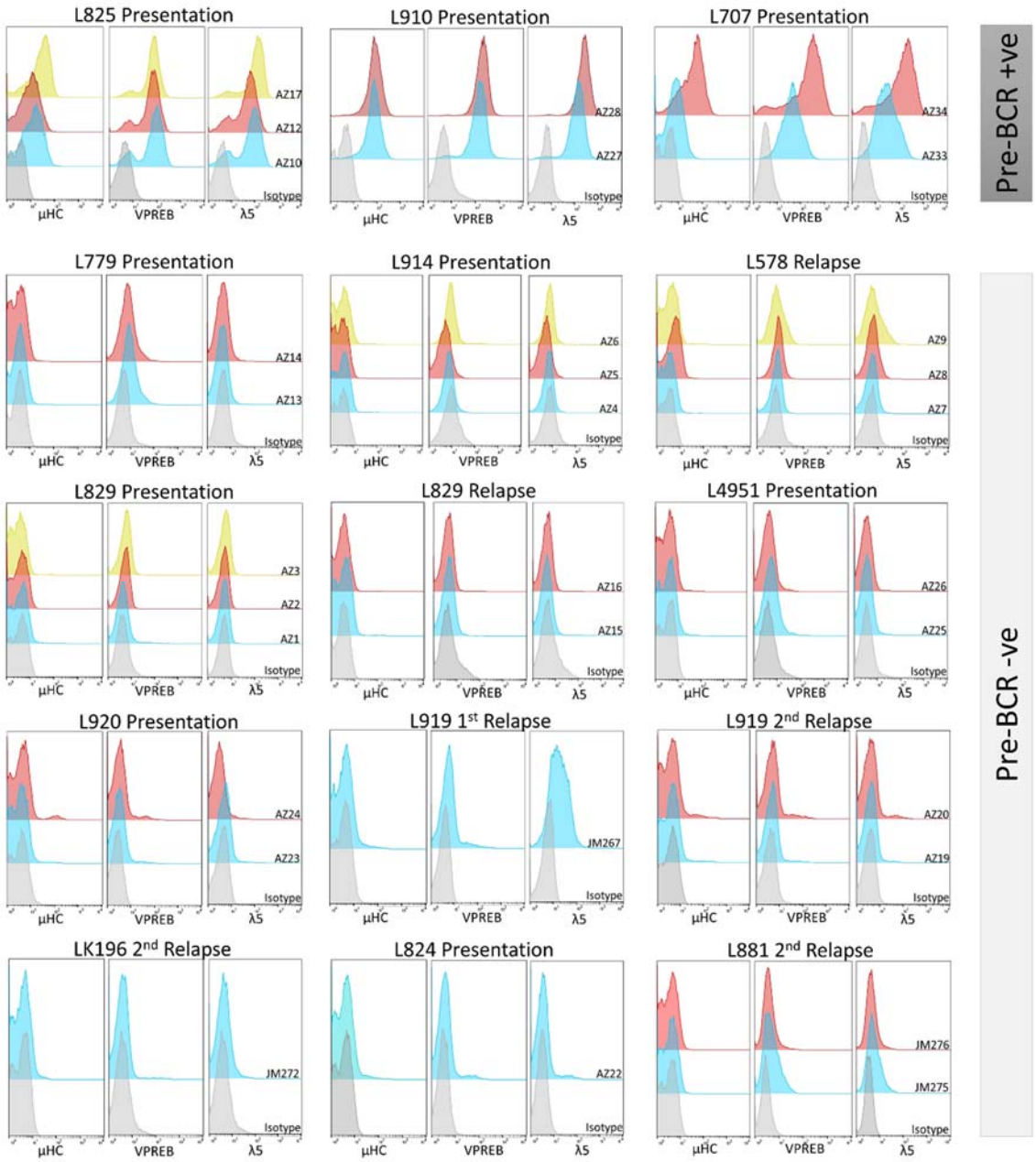

Figure 3.2: Flow cytometry analysis of Pre-BCR expression in PDX samples.

PDX cells harvested from mice spleens were analysed by flow cytometry for surface binding of anti-µHC, anti-VPREB and anti-λ5. Each PDX sample was also stained with isotype control (grey histogram) that matches the isotype and concentration of fluorescent labelled primary antibody. 1-3 PDX samples were used for each primary patient sample. Histogram overlays were generated by Flowjo software.

3.3 Measurement of Ca^{2+} mobilisation

As reviewed in chapter one, intracellular Ca^{2+} mobilisation is a process induced after activation of Pre-BCR mediated downstream signalling (Kuwahara *et al.*, 1996; Scharenberg *et al.*, 2007b). To confirm the expression and functionality of Pre-BCR in cell lines and PDX samples, Ca^{2+} flux was measured by flow cytometry after stimulation with anti-µHC antibody using Flou-4 dye imaging assay (Section 2.3.1). Immature and mature B cells (Daudi and Ramos) were used as a positive controls due to their known positive response to anti-µHC antibody cross-linkage (Kuwahara *et al.*, 1996; Schneider *et al.*, 2015). Ionomycin treatment was also used as an internal control which induces Ca^{2+} release and thereby confirms successful loading of the Fluo-4 dye in the cells (Kauffman *et al.*, 1980). Ca^{2+} release was assessed in all cell lines during the log phase of growth (Figure 3.3) and a transient increase in FITC signal was seen after anti-µHC addition to the BCR^{+} (Ramos and Daudi) and Pre-BCR^{+} cell lines (PreB 697 and Nalm-6), however, TK6 (BCR^{+}), R3F9 (Pre-BCR^{+}) and REH (Pre-BCR^{-}) showed no increase in calcium mobilisation. Also, all cell lines showed a prominent increase in FITC fluorescence after ionomycin treatment (Figure 3.3). Surprisingly, late and weak calcium flux was only observed in one out of 3 Pre-BCR^{+} ALLs (L910 presentation) but was similar in duplicate PDX derived from this sample. Consistent with Pre-BCR lacking REH cell line, all Pre-BCR^{-} PDX samples (24 PDX derived originally from 10 patient samples) showed no flux of calcium after anti-µHC antibody addition. Nevertheless, an increase in FITC fluorescent was observed after addition of ionomycin in all PDX samples but it was generally less potent than in cell lines and this might suggest a lower calcium content in the cytosolic stores of PDX cells (Figure 3.4) compared to cell lines (Figure 3.3).

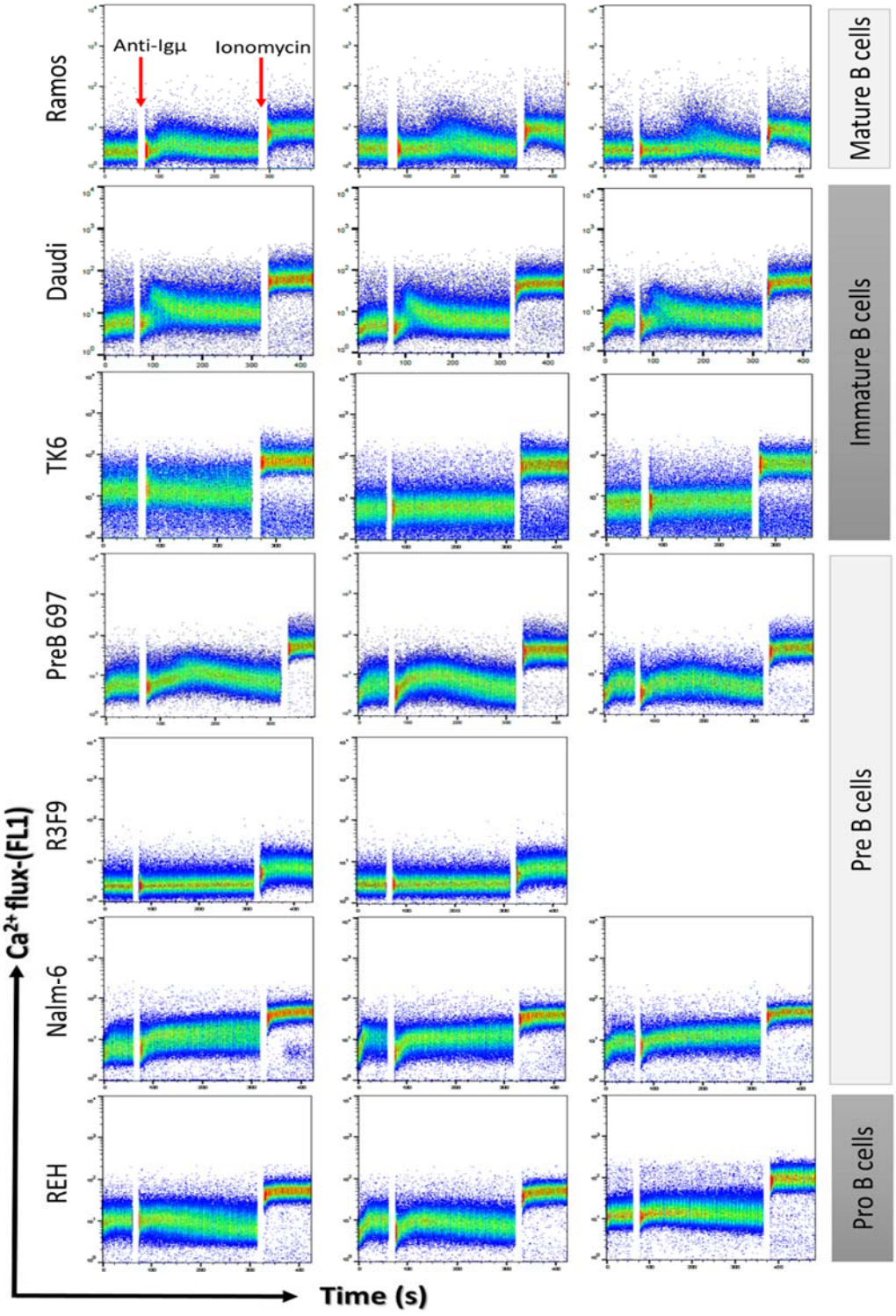

Figure 3.3: Ca^{2+} mobilisation measurement in human B-lineage cell lines by Flow cytometry.

Ca^{2+} flux measurement in mature-B, immature-B, Pre-B and Pro-B cell lines (2-3 replicates each) after engagement of the Pre-B or B cell receptor. Cells were loaded with Fluo-4, AM imaging kit and analysed on a FACSCalibur. FITC Fluorescence was recorded for 60 seconds of baseline Ca^{2+} mobilisation, followed by addition of 20µg/ml of F(ab)2 goat anti-µHC antibody for Pre-B/BCR stimulation. Ionomycin (10µg/ml) was then added to the remaining sample as a positive control to achieve a maximum cytosolic Ca^{2+} concentration. Flowjo software was used to analyse the data. Red arrows denote the additions of anti-µHC and ionomycin which were applied for all samples.

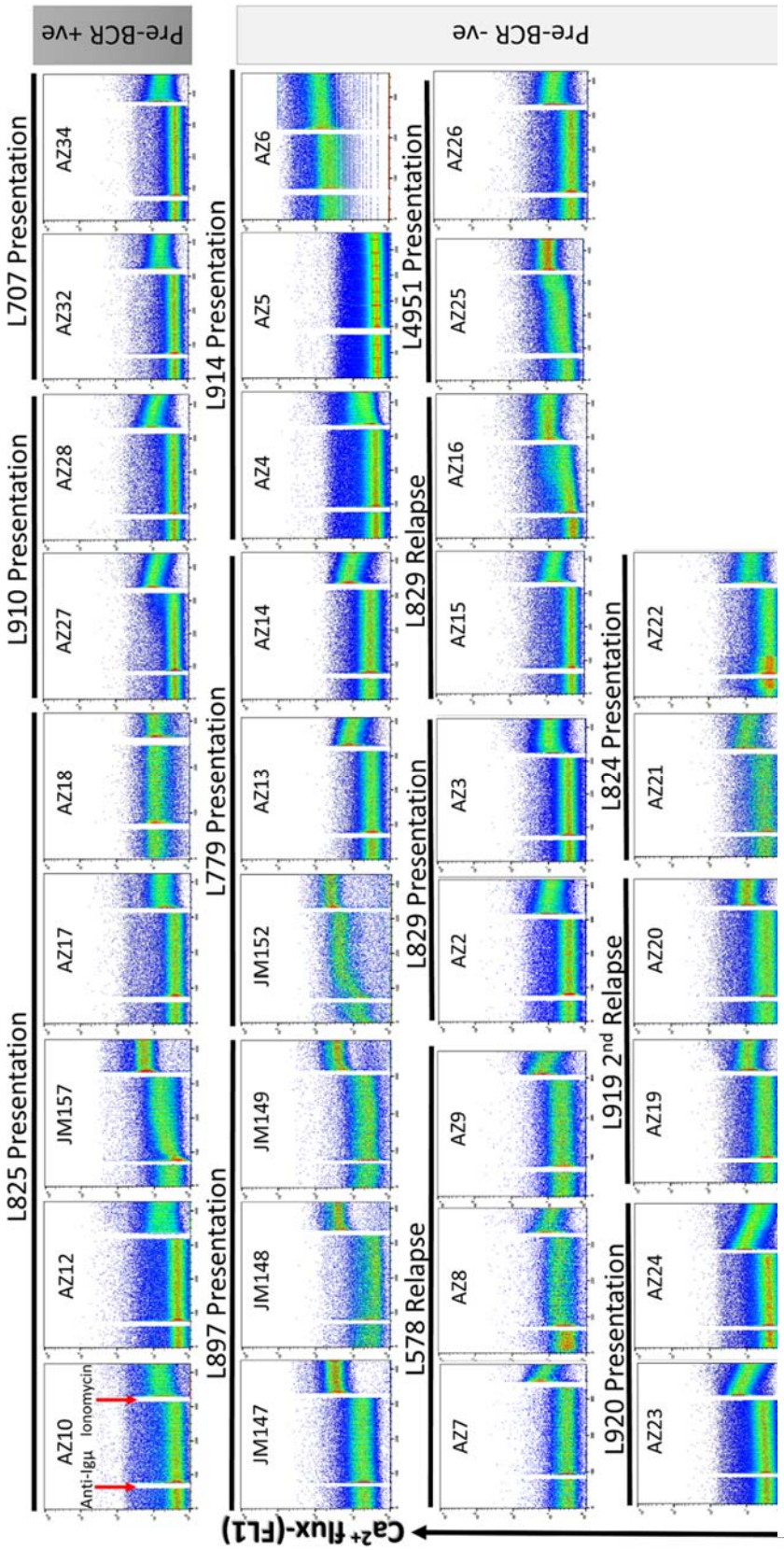

Figure 3.4: Ca^{2+} mobilisation measurement in PDX cells by Flow cytometry.

Freshly harvested PDX cells from mice spleens were loaded with Fluo-4, AM imaging kit and analysed on FACScalibur. FITC fluorescence was recorded for 60 seconds of baseline Ca^{2+} mobilisation, followed by addition of 20µg/ml of F(ab)2 goat anti-µHC for Pre-BCR stimulation. Ionomycin (10µg/ml) was then added to the remaining sample as a positive control to achieve a maximum cytosolic Ca^{2+} concentration. 2-5 PDX replicates for each patient sample were used. Flowjo software was used to analyse the data. Red arrows denote the additions of anti-µHC and Ionomycin which were applied for all samples.

3.4 Phospho-profiling of key proteins associated with Pre-BCR signalling pathways

ALL cells may have driver mutations activating key signaling cascades downstream of the Pre-BCR, granting survival of malignant cells (Feldhahn *et al.*, 2005; Herzog *et al.*, 2009; Knight and Irving, 2014). To identify the basal and anti-µHC induced activation of key tyrosine kinases, phospho-flow cytometry staining was conducted to assess the phosphorylation status of pBTK(Y223), pAKT(S473), pSYK(Y348), pSYK(Y352), pBLNK(Y84), pERK1-2(T202-Y204) and pPLC-γ2(Y759) (Section 2.3.5) in a series of cell lines and PDX samples (Figures 3.5-3.11). The phosphorylation threshold was defined by using an isotype-matched control for all signals. Basal MFI ratio was calculated by dividing basal MFI/ isotype control MFI (Table 3.1), Ramos cells stimulation with anti-µHC antibody served as a positive control for all studied phospho kinases (Figures 3.5-3.11).

Analysis by Flow cytometry for both cell lines and PDX cells demonstrated apparent constitutive basal activity of pBTK(Y223) (Figure 3.5), pAKT(S473) (Figure 3.6), pSYK(Y352) (Figure 3.8), and pERK1-2(T202-Y204) (Figure 3.10). However pSYK(Y348) (Figure 3.7) and pPLC-γ2(Y759) (Figure 3.11) were also activated but to a lesser extent in both cell lines and PDX cells. In addition, phospho-flow cytometry data demonstrated low constitutive activity of pBLNK(Y84) (Figure 3.9) in both cell lines and PDX samples.

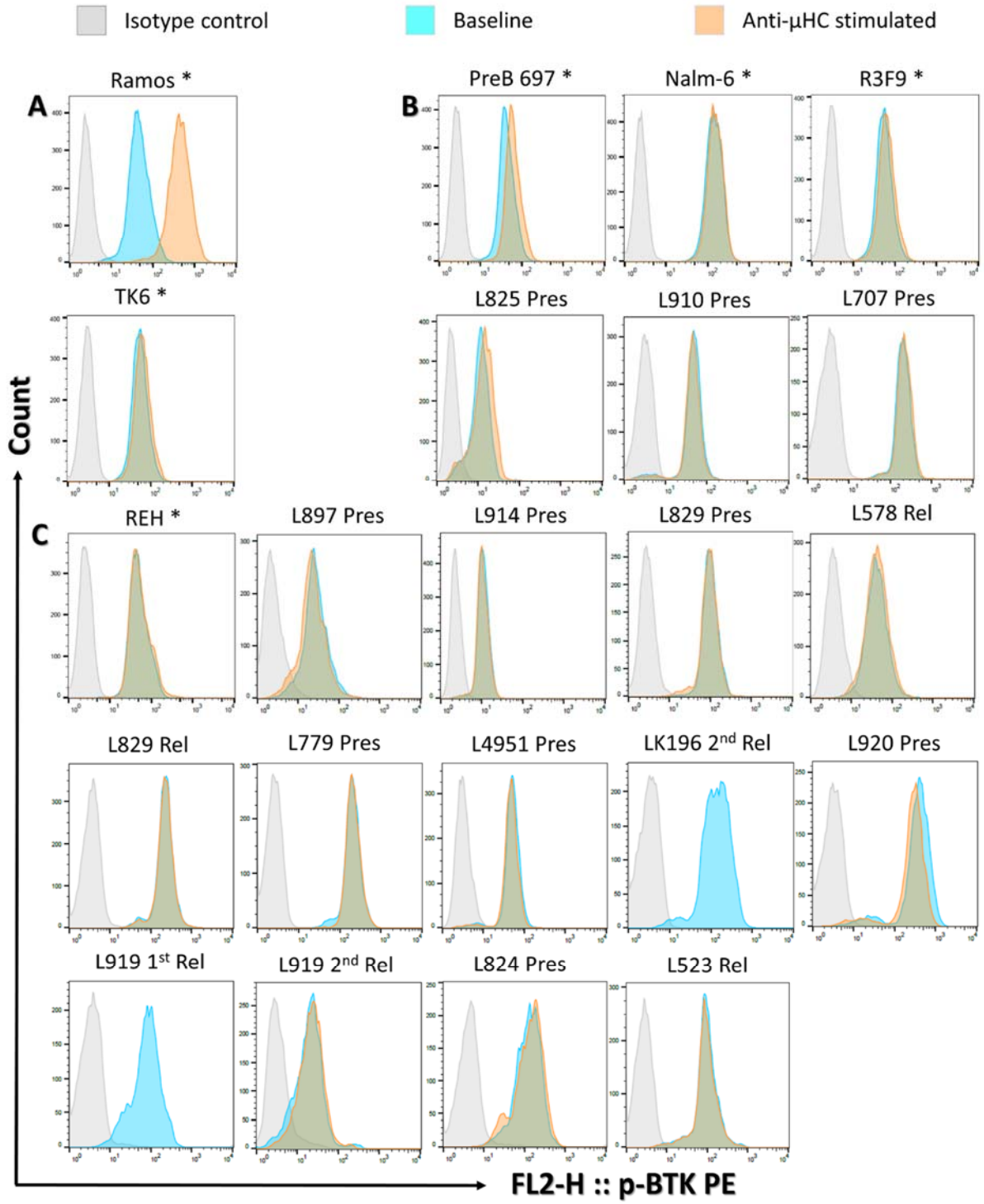

Figure 3.5: Intracellular phospho flow cytometry of pBTK(Y223) in BCP-ALL cells.

Baseline and anti-µHC stimulated phosphorylation levels of BTK were measured in **(A)** BCR^+ cells, Ramos cells served as positive control **(B)** Pre-BCR^+ cells and **(C)** Pre-BCR^- cells. One representative histogram overlay for 6 cell lines (of 1 to 3 replicates) and 16 patient-derived samples (1-4 individual PDXs) are shown. Intracellular phospho-flow staining by flow cytometry was used to analyse the samples in this study. 25µg/ml of F(ab`)2 anti-µHC antibody was added for 4 minutes at 37°C to induce stimulation before fixation. Flow cytometry data were analysed by Flowjo software. Cell lines denoted with asterisk.

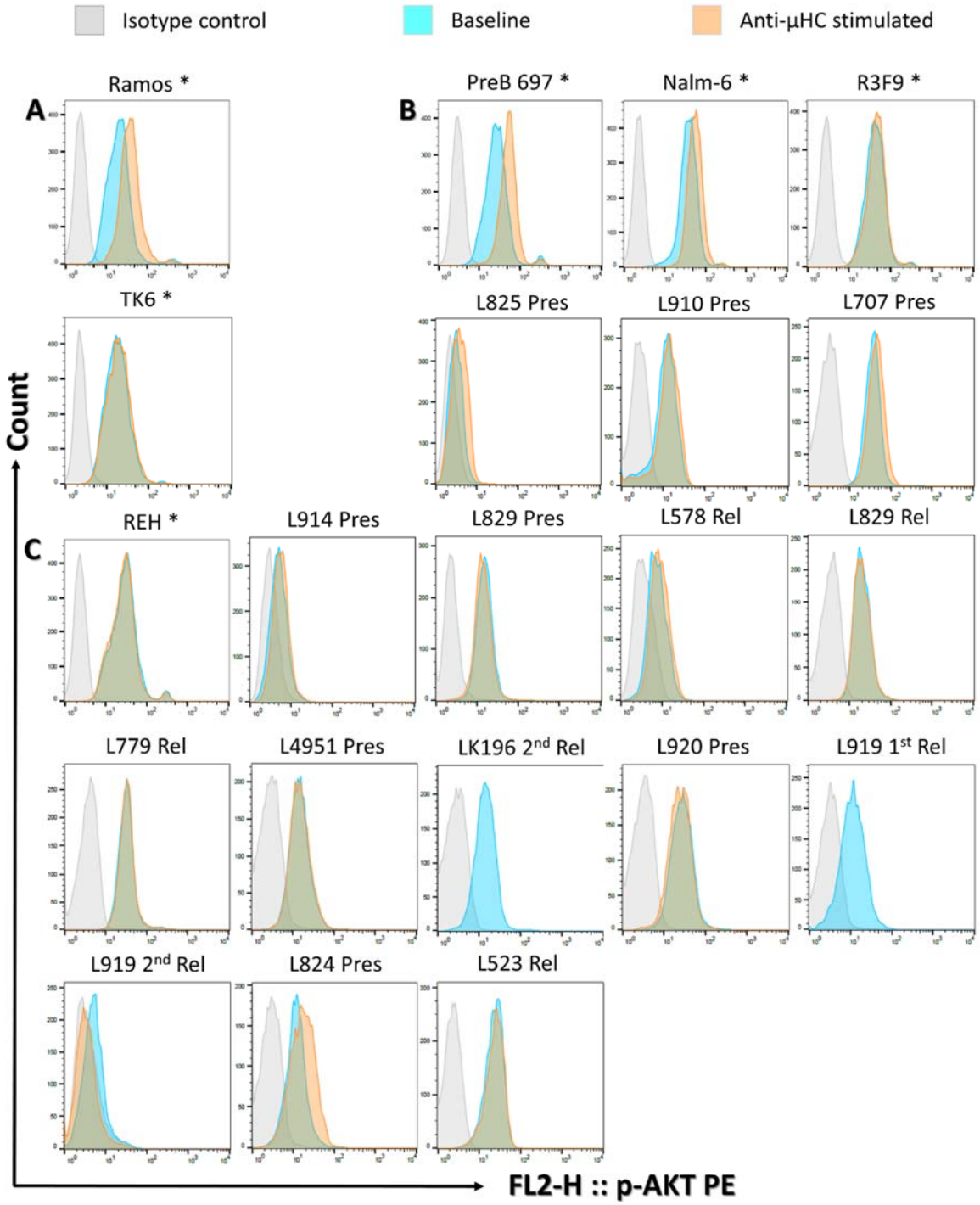

Figure 3.6: Intracellular phospho flow cytometry of pAKT(S473) in BCP-ALL cells.

Baseline and anti-µHC stimulated phosphorylation levels of AKT were measured in **(A)** BCR^+ cell lines, Ramos cells served as positive control **(B)** Pre-BCR^+ cells and **(C)** Pre-BCR^- cells. One representative histogram overlay for 6 cell lines (representative of 1 to 3 replicates) and 15 patient-derived samples (representative of 1-4 individual PDXs) are shown. Intracellular phospho-flow staining by flow cytometry was used to analyse the samples in this study. 25µg/ml of F(ab`)2 anti-µHC antibody was added for 4 minutes at 37°C to induce stimulation before fixation. Flow cytometry data were analysed by Flowjo software. Cell lines denoted with asterisk.

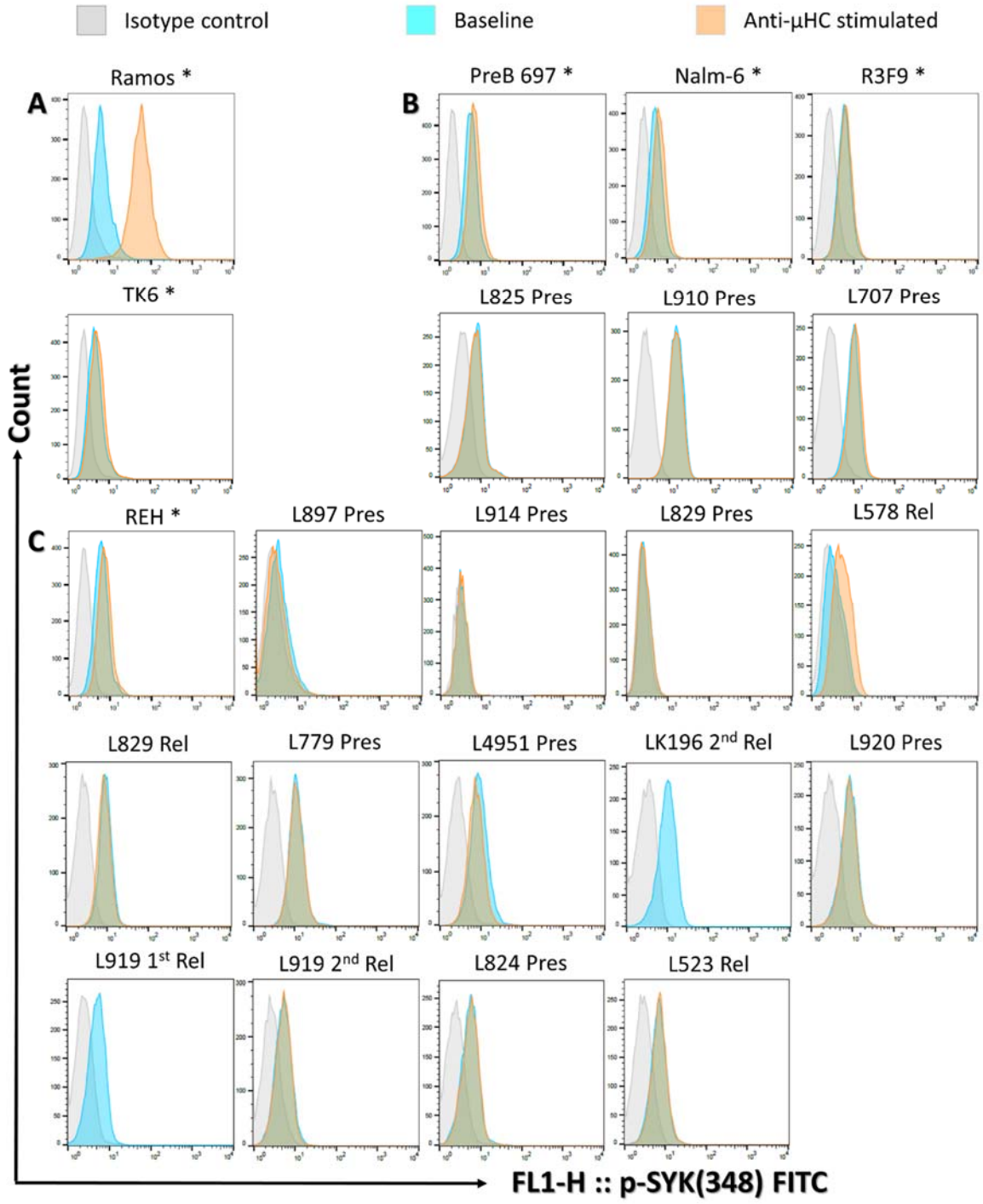

Figure 3.7: Intracellular phospho flow cytometry of pSYK(Y348) in BCP-ALL cells.

Baseline and anti-µHC stimulated phosphorylation levels of SYK were measured in **(A)** BCR^+ cell lines, Ramos cells served as positive control **(B)** Pre-BCR^+ cells and **(C)** Pre-BCR^- cells. One representative histogram overlay for 6 cell lines (representative of 1 to 3 replicates) and 16 patient-derived samples (representative of 1-4 individual PDXs) are shown. Intracellular phospho-flow staining by flow cytometry was used to analyse the samples in this study. 25µg/ml of F(ab`)2 anti-µHC antibody was added for 4 minutes at 37°C to induce stimulation before fixation. Flow cytometry data were analysed by Flowjo software. Cell lines denoted with asterisk.

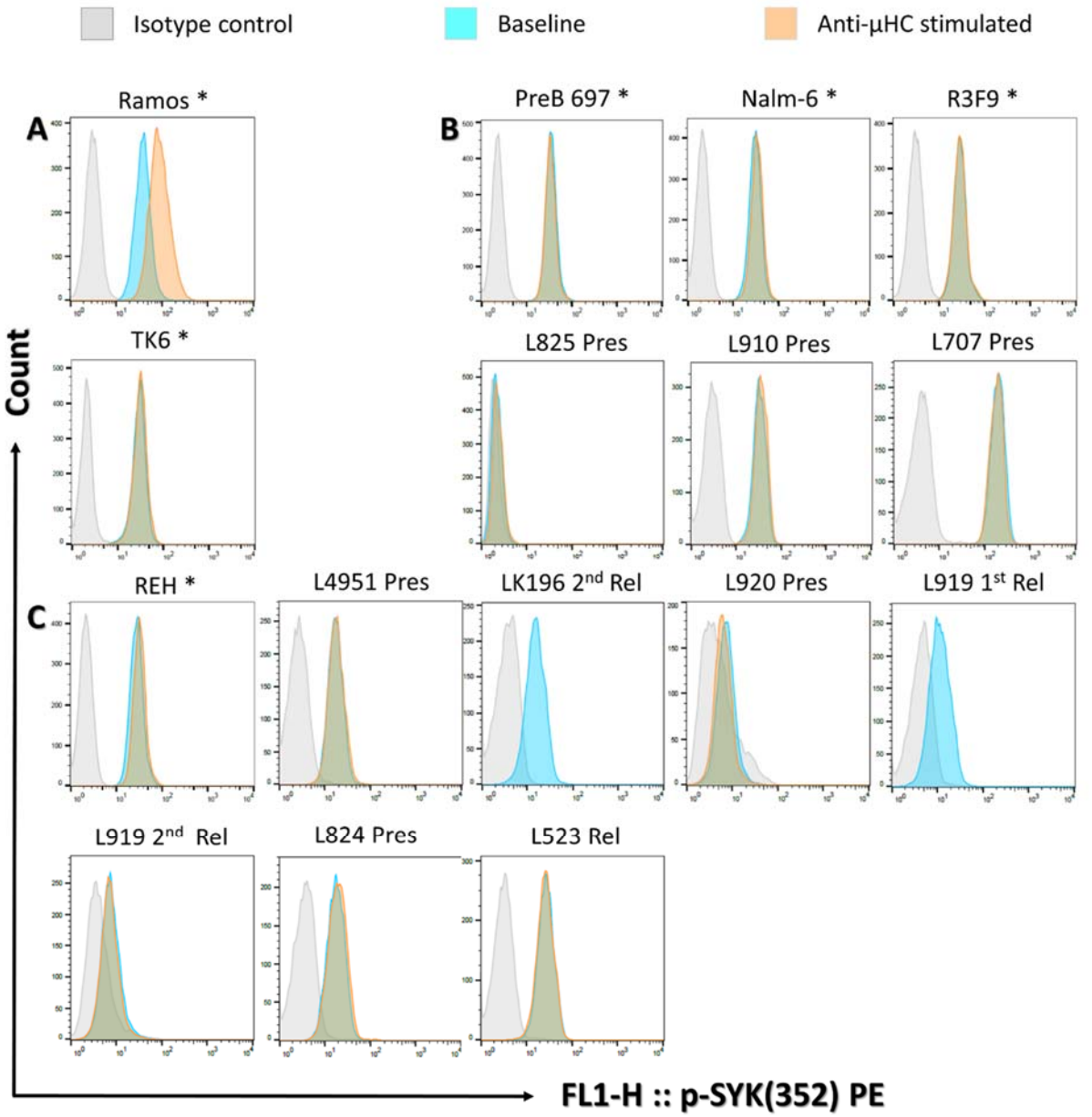

Figure 3.8: Intracellular phospho flow cytometry of pSYK(Y352) in BCP-ALL cells.

Baseline and anti-µHC stimulated phosphorylation levels of SYK were measured in **(A)** BCR^+ cell lines, Ramos cells served as positive control **(B)** Pre-BCR^+ cells and **(C)** Pre-BCR^- cells. One representative histogram overlay for 6 cell lines (representative of 1 to 3 replicates) and 10 patient-derived samples (representative of 1-4 individual PDXs) are shown. Intracellular phospho-flow staining by flow cytometry was used to analyse the samples in this study. 25µg/ml of F(ab`)2 anti-µHC antibody was added for 4 minutes at 37°C to induce stimulation before fixation. Flow cytometry data were analysed by Flowjo software. Cell lines denoted with asterisk.

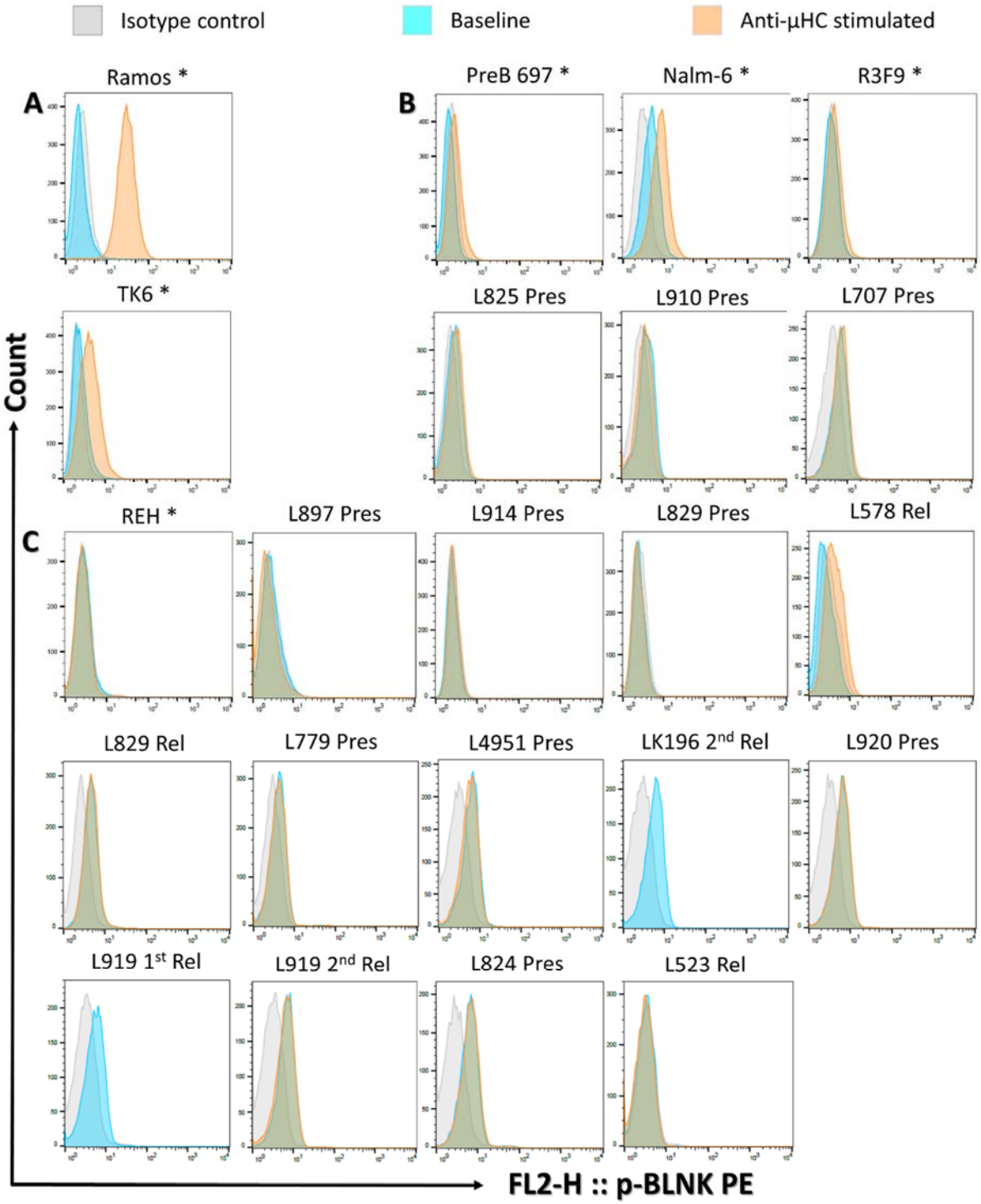

Figure 3.9: Intracellular phospho flow cytometry of pBLNK(Y84) in BCP-ALL cells.

Baseline and anti-µHC stimulated phosphorylation levels of BLNK were measured in **(A)** BCR^+ cell lines, Ramos cells served as positive control **(B)** Pre-BCR^+ cells and **(C)** Pre-BCR^- cells. One representative histogram overlay for 6 cell lines (representative of 1 to 3 replicates) and 16 patient-derived samples (representative of 1-4 individual PDXs) are shown. Intracellular phospho-flow staining by flow cytometry was used to analyse the samples in this study. 25µg/ml of F(ab`)2 anti-µHC antibody was added for 4 minutes at 37°C to induce stimulation before fixation. Flow cytometry data were analysed by Flowjo software. Cell lines denoted with asterisk.

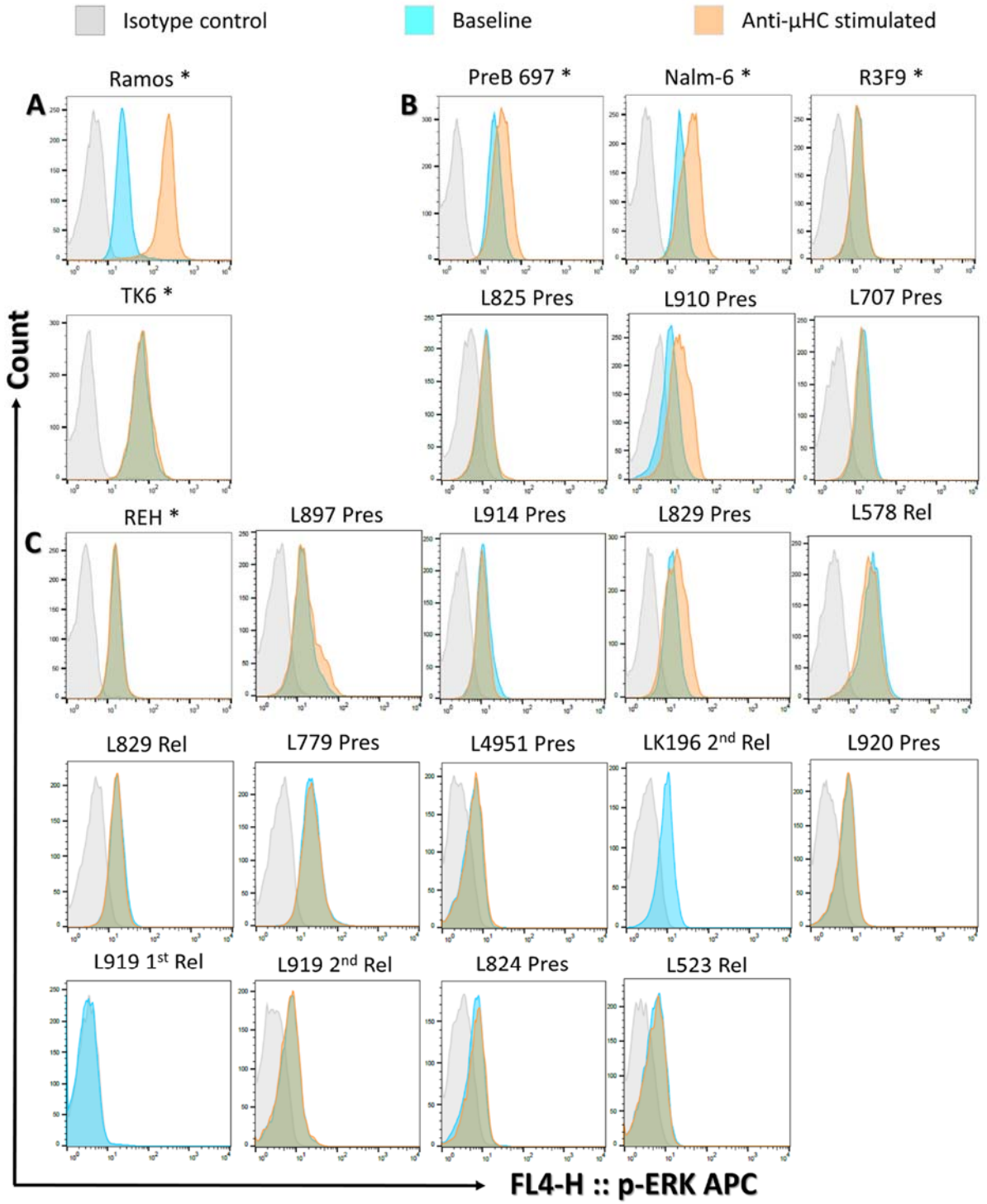

Figure 3.10: Intracellular phospho flow cytometry of pERK1-2 (T202-Y204) in BCP-ALL cells.

Baseline and anti-µHC stimulated phosphorylation levels of ERK were measured in **(A)** BCR^+ cell lines, Ramos cells served as positive control **(B)** Pre-BCR^+ cells and **(C)** Pre-BCR^- cells. One representative histogram overlay for 6 cell lines (representative of 1 to 3 replicates) and 16 patient-derived samples (representative of 1-4 individual PDXs) are shown. Intracellular phospho-flow staining by flow cytometry was used to analyse the samples in this study. 25µg/ml of F(ab`)2 anti-µHC antibody was added for 4 minutes at 37°C to induce stimulation before fixation. Flow cytometry data were analysed by Flowjo software. Cell lines denoted with asterisk.

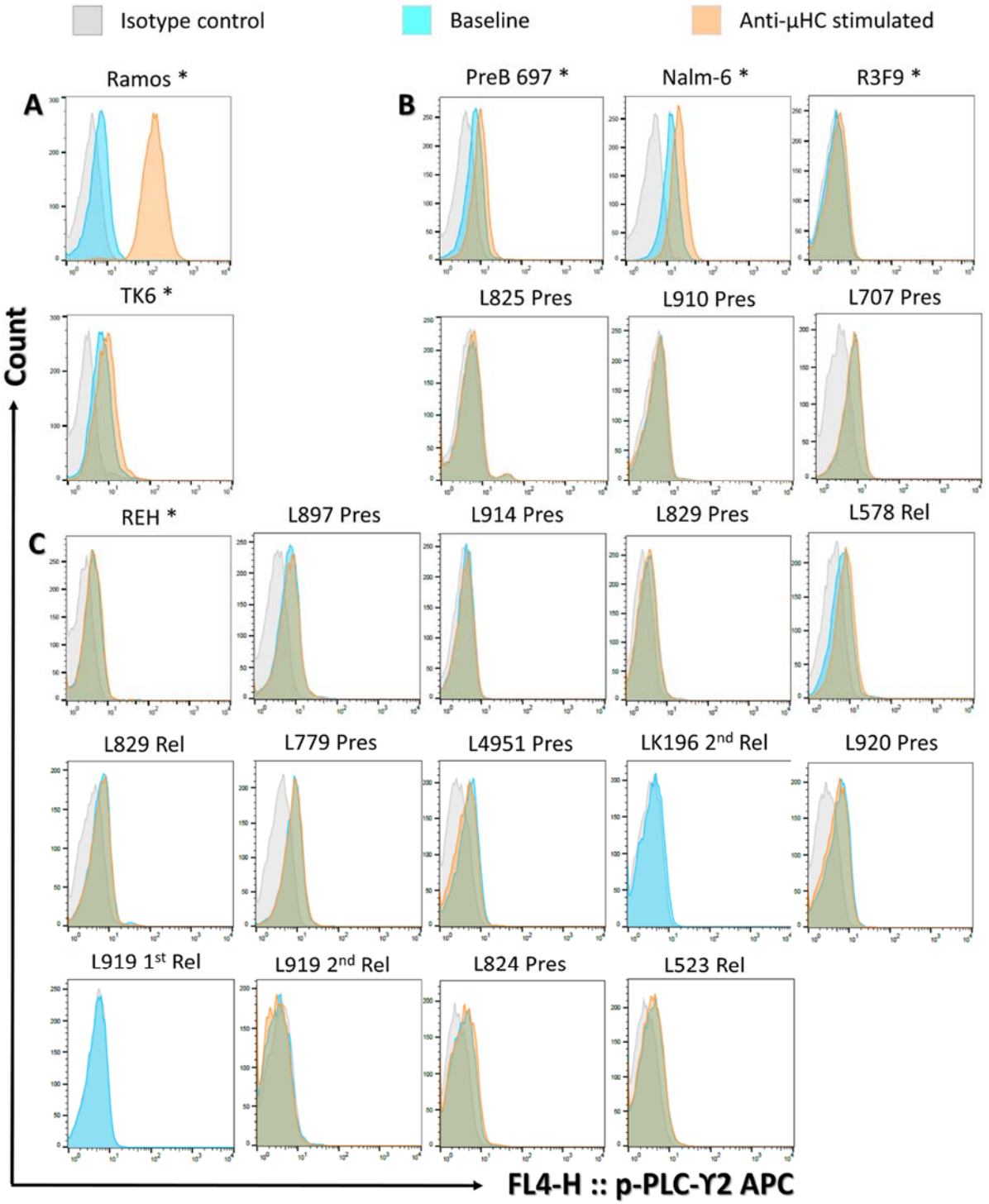

Figure 3.11: Intracellular phospho flow cytometry of pPLC-ϒ2 (Y759) in BCP-ALL cells.

Baseline and anti-µHC stimulated phosphorylation levels of PLC-ϒ2 were measured in **(A)** BCR^+ cell lines, Ramos cells served as positive control **(B)** Pre-BCR^+ cells and **(C)** Pre-BCR^- cells. One representative histogram overlay for 6 cell lines (representative of 1 to 3 replicates) and 16 patient-derived samples (representative of 1-4 individual PDXs) are shown. Intracellular phospho-flow staining by flow cytometry was used to analyse the samples in this study. 25µg/ml of F(ab`)2 anti-µHC antibody was added for 4 minutes at 37°C to induce stimulation before fixation. Flow cytometry data were analysed by Flowjo software. Cell lines denoted with asterisk.

Regarding induced phosphorylation after anti-μHC stimulation, Ramos cells which express mature B cell receptor showed significant increase in phosphorylation levels of all proteins studied (Figures 3.5-3.15). Therefore, it`s stimulation was considered as positive control to validate different phospho-proteins and was run side by side with all phospho-flow cytometry experiments. However, TK6 (Immature B cell) also showed statistically significant increased phosphorylation but only in AKT, ERK and PLC-Ɣ2 (Figures 3.12B, 3.14B and 3.15 respectively).

There was, an increased phosphorylation which reached statistical significance in some Pre-BCR^{+} cell lines and PDX samples for pAKT(S473), pBLNK(Y84), pERK1-2(T202-Y204) and pPLC-Ɣ2(Y759) on stimulation with anti-μHC antibody. Upregulation was also seen in pSYK(Y348) but did not reach statistical significance. On the other hand, both Pre-BCR negative cell line and PDX cells did not demonstrate increased phosphorylation of these proteins [pAKT(S473) (Figure 3.12B); pSYK(Y348) (Figure 3.13A); pSYK(Y352) (Figure 3.13B); pBLNK(Y84) (Figure 3.14A) and pPLC-Ɣ2(Y759) (Figure 3.15)], an exception being L829 presentation in pERK1-2(T202-Y204) and L824 presentation in pBTK(Y223). In addition, no increased phosphorylation of pBTK(Y223) was seen despite a 10 fold increase in Ramos cells (Figure 3.12A).

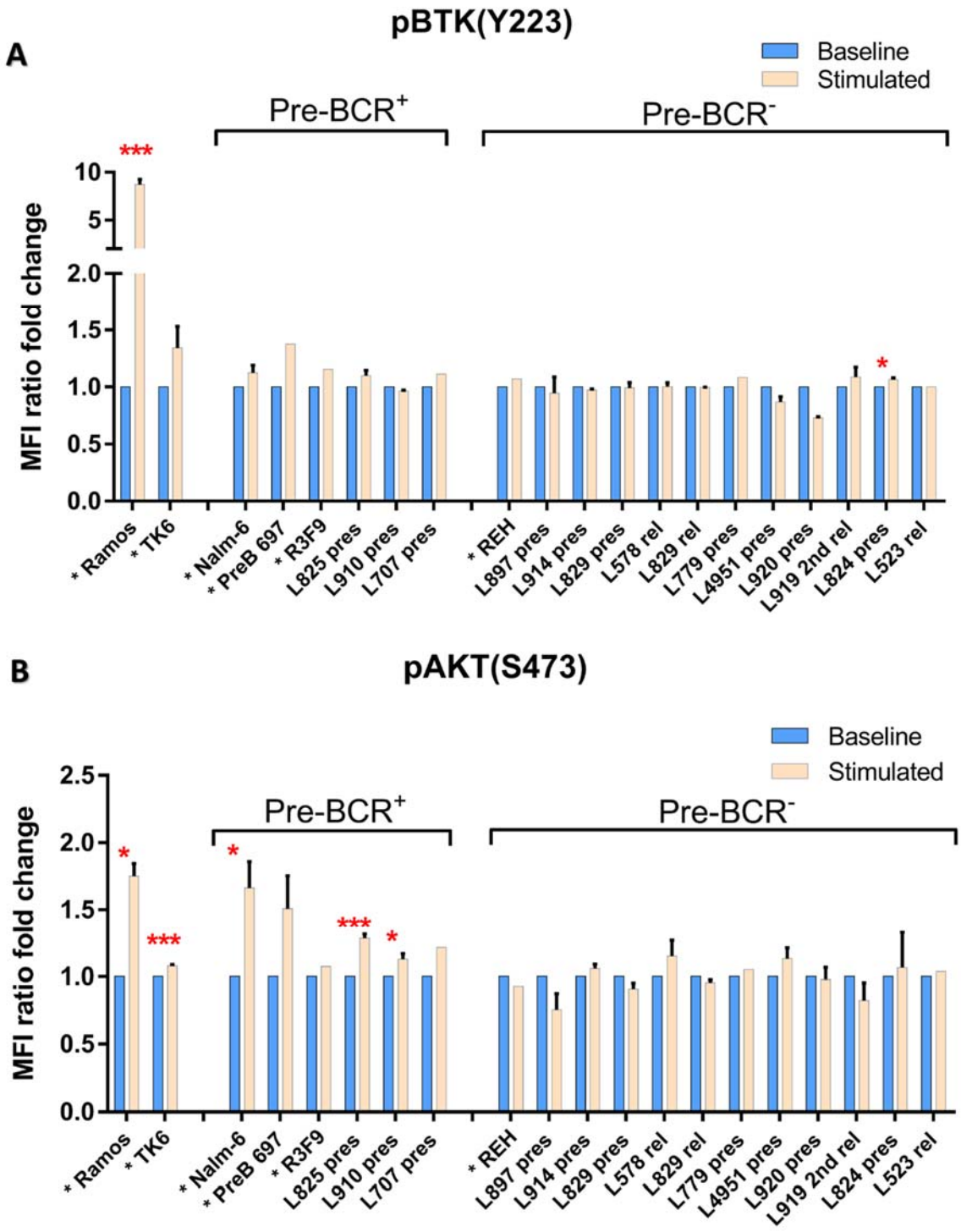

Figure 3.12: Fold change increase of basal phosphorylation of pBTK(Y223) and pAKT(S473) in BCP-ALL cells due to stimulation with anti-µHC antibody.

Intracellular phospho-flow staining by flow cytometry was used to measure anti-µHC stimulated levels of **(A)** pBTK(Y223) and **(B)** pAKT(S473) in BCP-ALL cells. 25µg/ml of F(ab`)2 anti-µHC antibody was added for 4 minutes at 37°C to induce stimulation before fixation. Each stimulated bar (brown) denote the mean ratio ± SEM of stimulated MFI/basal MFI and all basal phosphorylation signals were normalised to one. 1-3 replicates for cell lines (black asterisks) and in patient derived cells represent 1-3 individual PDX samples. MFIs were analysed by BD CellQuest software. Student`s t-test was used to calculate p values. *p<0.05, ****p<0.0001.

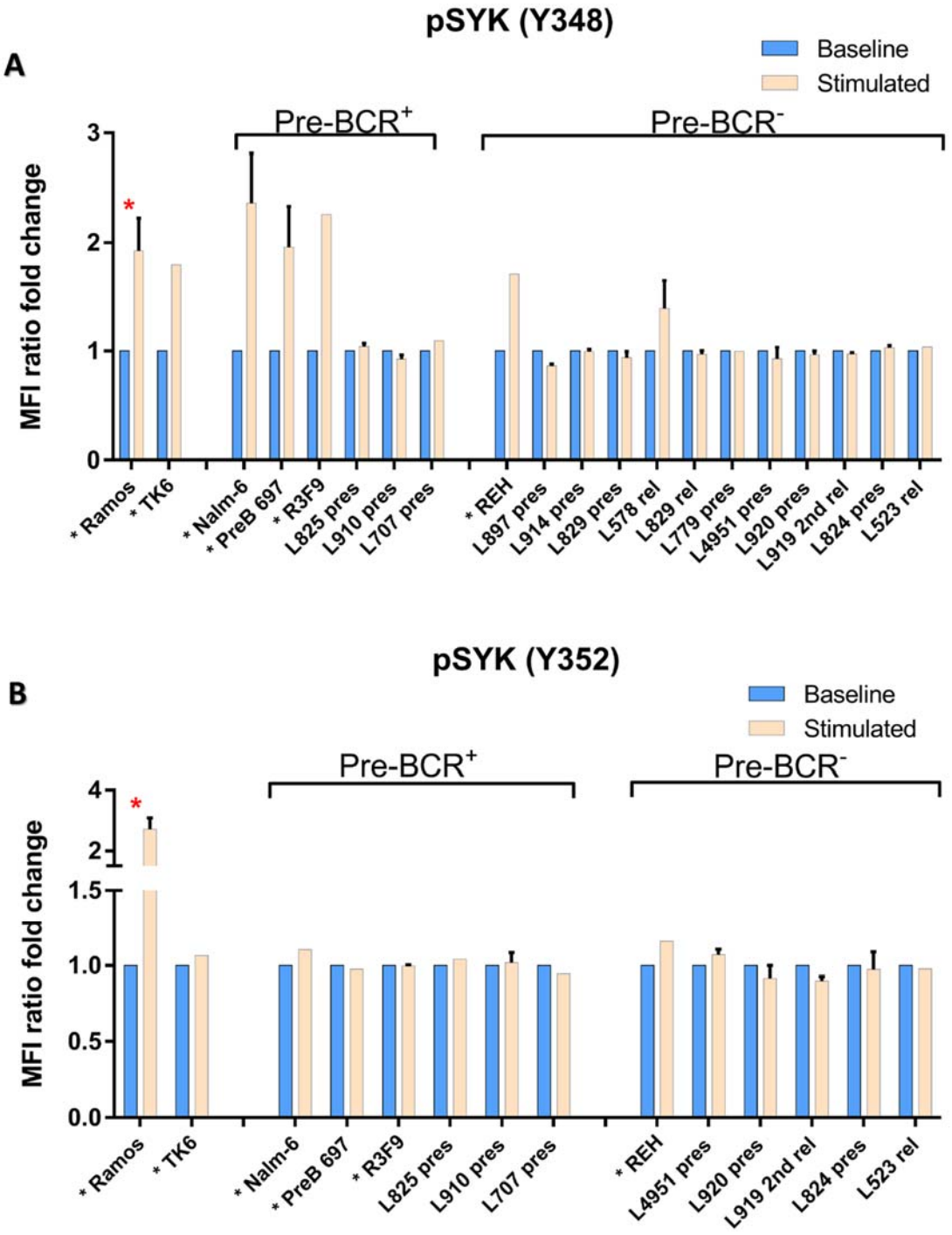

Figure 3.13: Fold change increase of basal phosphorylation of pSYK(Y348) and pSYK(Y352) in BCP-ALL cells due to stimulation with anti-µHC antibody.

Intracellular phospho-flow staining by flow cytometry was used to analyse anti-µHC stimulated levels of **(A)** pSYK(Y348) and **(B)** pSYK(Y352) in samples used in this study. 25µg/ml of F(ab`)2 anti-µHC antibody was added for 4 minutes at 37°C to induce stimulation before fixation. Each stimulated bar (brown) denote the mean ratio ± SEM of stimulated MFI/basal MFI and all basal phosphorylation signals were normalised to one. 1-3 replicates for cell lines (black asterisks) and in patient derived cells represent 1-3 individual PDX samples. MFIs were analysed by BD CellQuest software. Bar chart showing the mean ± SEM. Student`s t-test was used to calculate p values. *$p<0.05$.

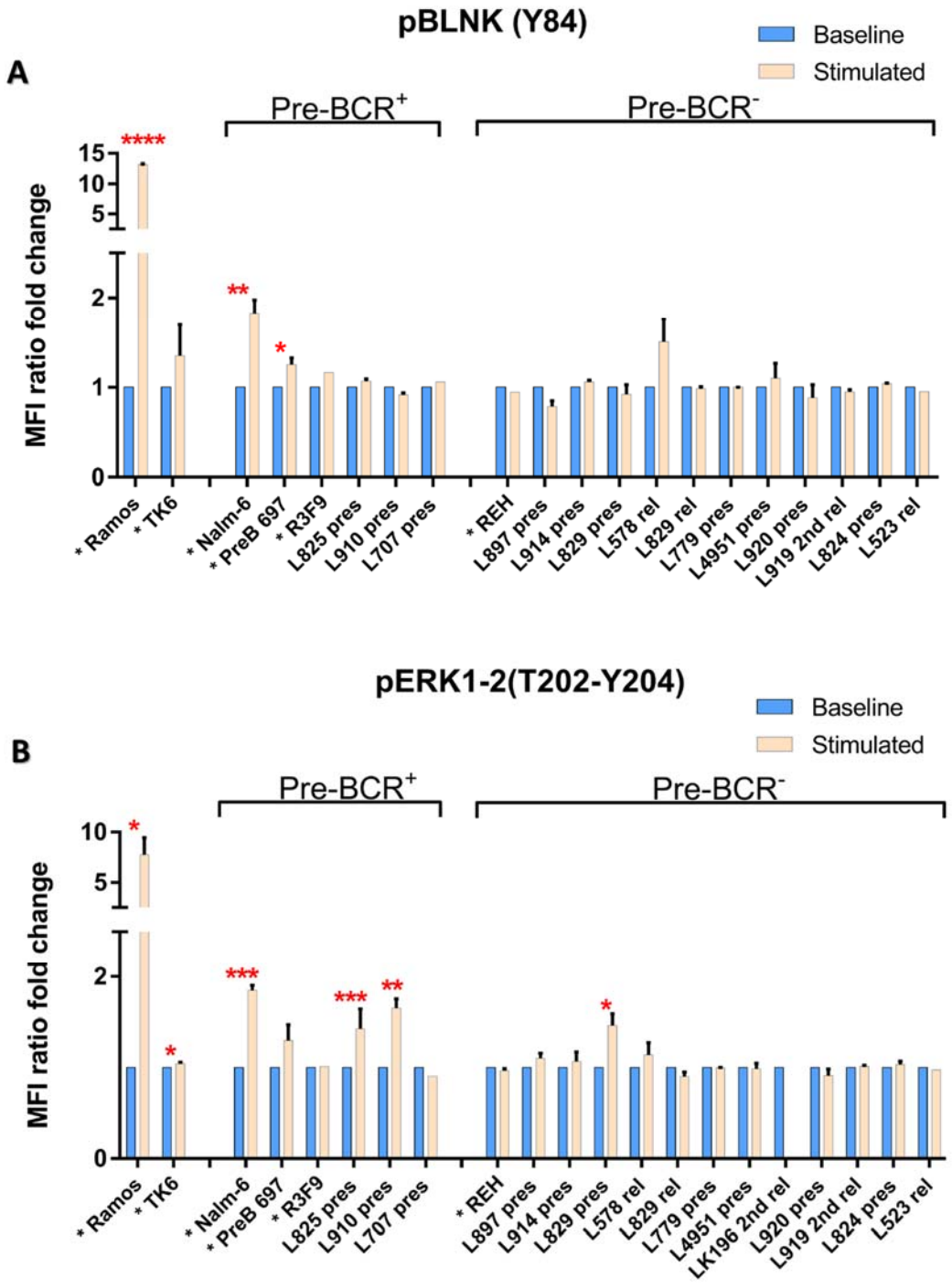

Figure 3.14: Fold change increase of basal phosphorylation of pBLNK(Y84) and pERK1-2(T202-Y204) in BCP-ALL cells due to stimulation with anti-µHC antibody.

Intracellular phospho-flow staining by flow cytometry was used to analyse the anti-µHC stimulated levels of **(A)** pBLNK(Y84) and **(B)** pERK1-2(T202-Y204) in BCP-ALL cells. 25µg/ml of F(ab`)2 anti-µHC antibody was added for 4 minutes at 37°C to induce stimulation before fixation. Each stimulated bar (brown bars) denote the mean ratio ± SEM of stimulated MFI/basal MFI and all basal phosphorylation signals (blue bars) were normalised to one. 1-3 replicates for cell lines (black asterisks) and in patient derived cells represent 1-3 individual PDX samples. MFIs were analysed by BD CellQuest software. Bar chart showing the mean ± SEM. Student`s t-test was used to calculate p values. *p<0.05, **p<0.01, ***p<0.001, ****p<0.0001.

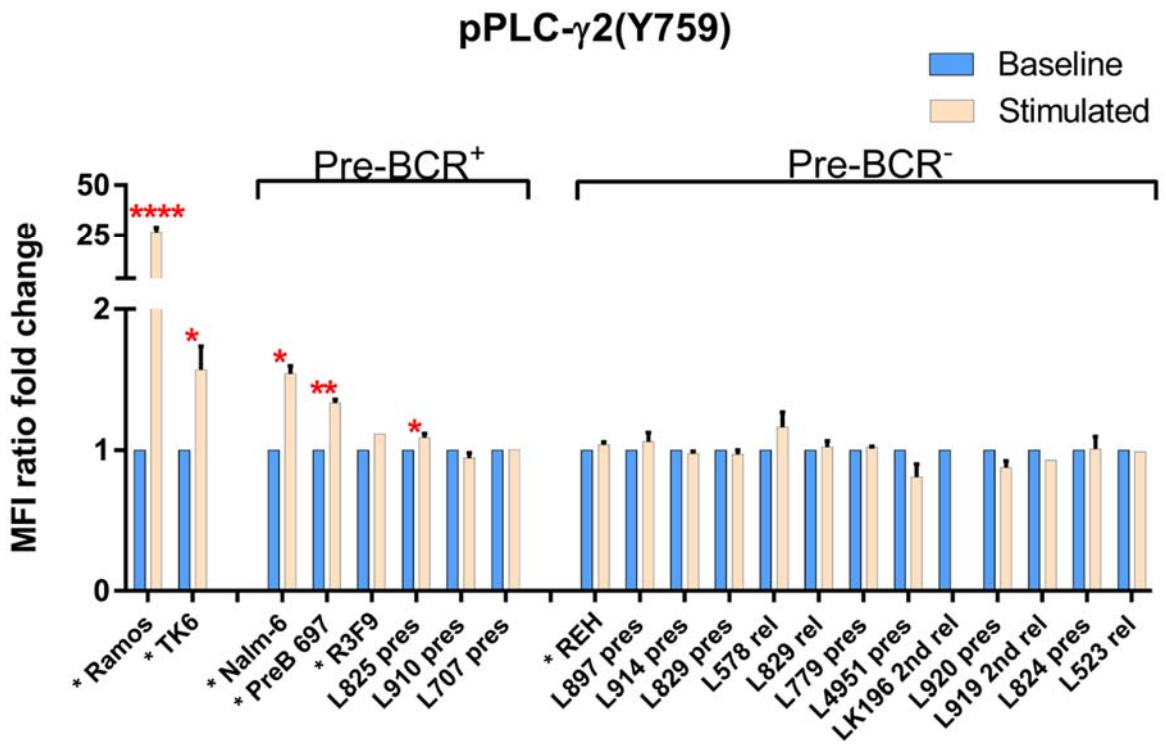

Figure 3.15: Fold change increase of basal phosphorylation of pPLC-ϒ2(Y759) in BCP-ALL cells due to stimulation with anti-µHC antibody.

Intracellular phospho-flow staining by flow cytometry was used to analyse the pPLC-ϒ2(Y759) levels after stimulation of BCP-ALL cells with anti-µHC antibody. 25µg/ml of F(ab`)2 anti-µHC antibody was added for 4 minutes at 37°C to induce stimulation before fixation. Each stimulated bar (brown bars) denote the mean ratio ± SEM of stimulated MFI/basal MFI and all basal phosphorylation signals (blue bars) were normalised to one. 1-3 replicates for cell lines (black asterisks) and in patient derived cells represent 1-3 individual PDX samples. MFIs were analysed by BD CellQuest software. Bar chart showing the mean ± SEM. Student`s t-test was used to calculate p values. *p<0.05, **p<0.01, ****p<0.0001.

Cells	Mean basal phosphorylation (basal MFI/Isotype control MFI ratio)							Receptor expression
	p-AKT (S473)	p-BTK (Y223)	p-BLNK (Y84)	p-SYK (Y348)	p-ERK1-2 (T202-Y204)	p-PLCγ2 (Y759)	p-SYK (Y352)	
* Ramos	6.36	6.35	0.93	1.93	6.70	1.67	16.01	BCR$^+$
* TK6	8.19	9.56	0.93	2.49	21.73	2.37	13.55	
* PreB 697	9.07	8.62	0.90	1.96	8.94	1.52	14.83	Pre-BCR$^+$
* Nalm-6	13.39	28.67	1.40	2.36	8.81	3.08	14.17	
* R3F9	14.43	17.68	1.03	2.26	3.48	1.06	11.04	
L825 pres	2.53	9.32	0.94	1.48	3.32	1.17		
L910 pres	21.79	16.84	4.98	3.52	3.00	1.56	7.16	
L707 pres	11.93	57.48	1.58	3.65	4.47	2.08	47.86	
* REH	11.90	18.89	0.92	2.12	6.14	1.71	12.81	Pre-BCR$^-$
L897 pres	2.99	12.06	0.87	1.50	4.80	1.71		
L914 pres	1.38	3.78	0.80	1.14	2.98	1.08		
L829 pres	3.80	16.80	0.97	1.45	4.68	1.30		
L578 rel	3.44	13.71	0.90	1.35	7.56	1.48		
L829 rel	6.37	54.81	1.40	2.22	8.70	2.20		
L779 pres	7.60	70.18	1.35	2.46	6.23	1.82		
L4951 pres	3.78	20.20	1.68	3.23	2.45	1.82	4.60	
LK196 2nd rel	5.45	47.38	2.08	3.33	2.93	1.11	4.31	
L920 pres	5.21	60.18	1.58	2.77	2.37	1.81	5.25	
L919 1st rel	3.56	19.38	1.64	2.04	1.47	1.00	2.40	
L919 2nd rel	3.11	14.72	1.65	2.23	2.10	0.95	3.52	
L824 pres	2.99	30.56	1.96	2.34	2.15	1.76	6.00	
L523 rel	9.76	31.61	0.92	2.60	2.06	1.35	7.93	

Table 3.1: Basal phosphorylation of key signals downstream of Pre-BCR checkpoint in BCP-ALL cells.

Intracellular phospho-flow staining by flow cytometry was used to analyse the samples in this study. Basal MFI ratio for each replicate was calculated by dividing basal MFI/ isotype control MFI. Mean of basal MFI ratios of 1-4 replicates of 6 cell lines (asterisks) and 1-4 PDX replicates of 16 patient samples were shown and were classified into BCR$^+$, Pre-BCR$^+$ and Pre-BCR$^-$.

To investigate the difference between Pre-BCR$^+$ and Pre-BCR$^-$ PDX samples, the basal phosphorylation of two groups was interrogated. Phospho-flow cytometry analysis revealed that Pre-BCR harbouring ALL samples exhibited significantly higher phosphorylation levels (about 2 fold increase) of pAKT(S473) (Pre-BCR$^+$: 7.798 ± 2.027 versus Pre-BCR$^-$: 4.567 ± 0.5685; $p<0.05$) and pSYK(Y352) (Pre-BCR$^+$: 10.90 ± 1.893 versus Pre-BCR$^-$: 5.514 ± 0.9913; $p<0.05$). Interestingly, there was no difference in basal levels of the alternative tyrosine site phosphorylation for pSYK(348) (Pre-BCR$^+$: 2.143 ± 0.3194 versus Pre-BCR$^-$: 2.073 ± 0.1578; $p>0.05$) (Table 3.2 and Figure 3.16).

Phospho protein	Mean basal phosphorylation ± SEM		p-value
	Pre-BCR$^+$	Pre-BCR$^-$	
pBTK (Y223)	23.09 ± 6.585	28.58 ± 4.575	0.542
pAKT (S473)	7.798 ± 2.027	4.567 ± 0.5685	0.0384 (*)
pSYK (Y348)	2.143 ± 0.3194	2.073 ± 0.1578	0.84
pSYK (Y352)	10.90 ± 1.893	5.514 ± 0.9913	0.0129 (*)
pBLNK (Y84)	1.111 ± 0.09793	1.280 ± 0.08851	0.341
pERK1-2 (T202-Y204)	4.822 ± 0.9556	3.888 ± 0.3800	0.2814
pPLCγ2 (Y759)	1.608 ± 0.2048	1.453 ± 0.06234	0.3361

Table 3.2: Constitutive phosphorylation of key signals downstream of Pre-BCR checkpoint in Pre-BCR$^+$ versus Pre-BCR$^-$ PDX cells.

Intracellular phospho-flow staining by flow cytometry was used to analyse the samples in this study. Basal MFI ratio is calculated by dividing basal MFI/ isotype control MFI. Mean of basal MFIs ratios ± SEM of all Pre-BCR$^+$ versus Pre-BCR$^-$ PDX samples were shown. Student`s t-test was used to calculate p values, *$p<0.05$.

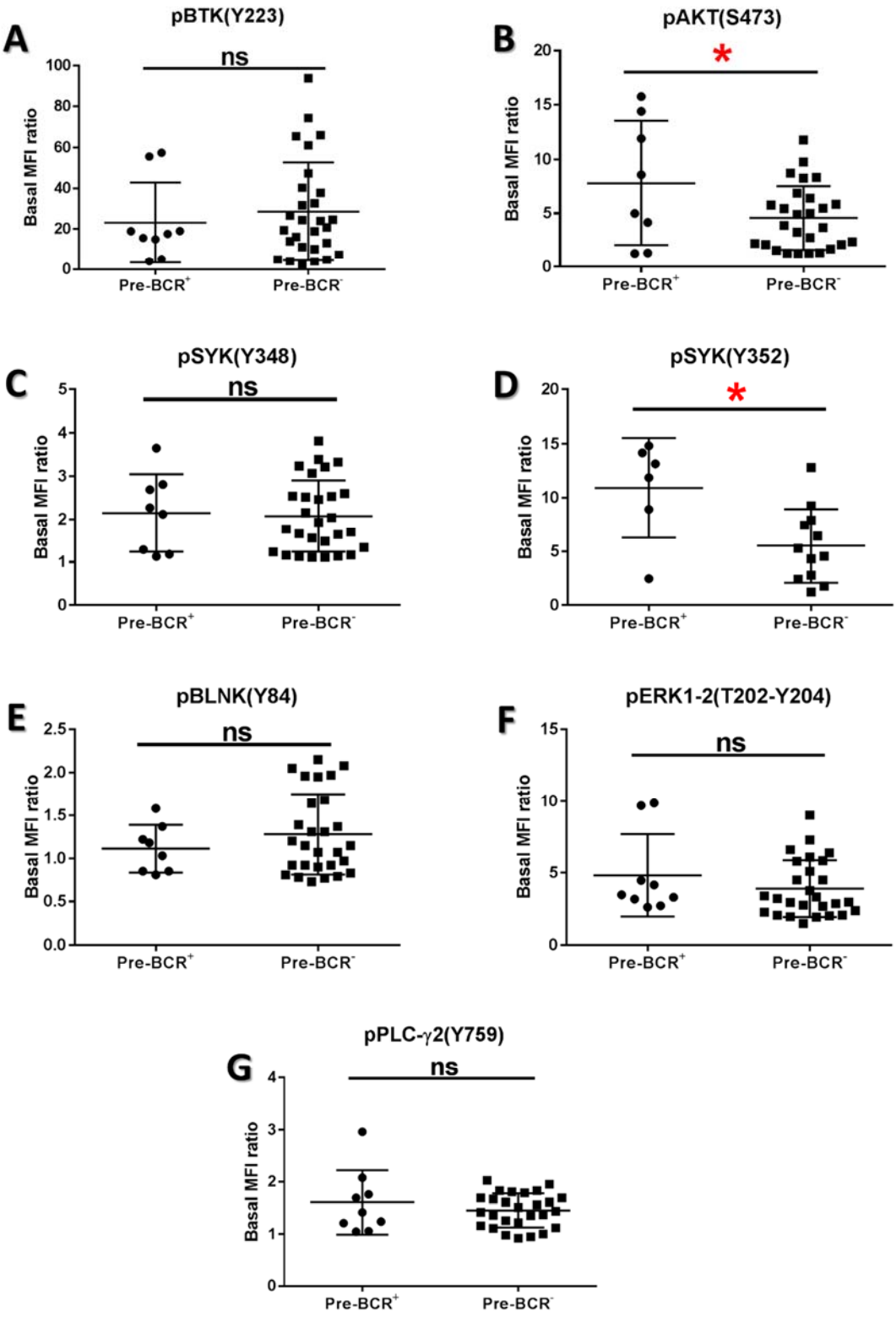

Figure 3.16: Basal phosphorylation levels in Pre-BCR$^+$ versus Pre-BCR$^-$ PDX samples.

Constitutive activation of **(A)** pBTK(Y223), **(B)** pAKT(S473), **(C)** pSYK(Y348), **(D)** pSYK(Y352), **(E)** pBLNK(Y84), **(F)** pERK1-2(T202-Y204) and **(G)** pPLC-Y2(Y759) was presented in Pre-BCR$^+$ versus Pre-BCR$^-$ PDX samples. Y axis shows ratio of Basal MFI relative to isotype-matched control MFI. Bar graphs showing the mean ± SEM. p values were calculated by Student`s t-test. p>0.05 not significant, *p<0.05.

3.5 Discussion

The aim of this chapter was to characterise BCP-ALL cells for Pre-BCR expression, function and to assess Pre-BCR mediated downstream signalling using cell lines and PDX cells derived from high risk and relapsed childhood ALL patient samples. These studies were performed to investigate whether Pre-BCR expression/function and key signalling pathways predict sensitivity to certain drug(s) treatment (as will be shown in the following chapters).

Pre-BCR expression in normal cells is responsible for orchestrating cell fate of B cells through activating and shutting down relevant Pre-BCR mediated pathways (Niiro and Clark, 2002; Clark *et al.*, 2014; Eswaran *et al.*, 2015). However, in BCP-ALL the majority of cases lack surface expression of Pre-BCR but have the capability of unlimited reproduction (Trageser *et al.*, 2009; Geng *et al.*, 2015). Recent studies have shown that the surface expression of Pre-BCR is a predictive biomarker of sensitivity to key TKI and therefore could be exploited therapeutically, for example ibrutinib has been shown to be a potential therapy for Pre-BCR$^+$ ALL patients with *TCF3-PBX1* genetic lesion (Geng *et al.*, 2015; Kim *et al.*, 2017). Data presented in this chapter showed that only 3 of 15 randomly selected PDX samples harboured surface expression of Pre-BCR giving an incidence of 20%, which is in keeping with previous reports (Trageser *et al.*, 2009; Geng *et al.*, 2015). Two of these belonged to the expected cytogenetic group i.e. t(1;19) (*TCF3-PBX1*) and t(17;19) (*TCF3-HLF*), while the third had normal cytogenetics (Fischer *et al.*, 2015; Geng *et al.*, 2015; Chen *et al.*, 2016). Notably, there was less abundant expression of µHC molecules on the surface of the PDX cells with normal cytogenetics. As evidenced before and confirmed in this project, only immature and mature cell lines expressed the µHC molecule (Mielenz *et al.*, 2005; Liu *et al.*, 2013), also, data presented here also identified Pre-BCR components (µHC and surrogate light chain molecules) in Pre-B cell lines while REH, a Pro-B line, was negative (Wang *et al.*, 2002a; Taguchi *et al.*, 2004; Geng *et al.*, 2015). In addition, TK6, a normal lymphoblastoid line, was shown to be derived from immature B cells, as they expressed only µHC molecules, and stimulation with anti-µHC increased the phosphorylation of many downstream kinases.

It has been documented that Pre-BCR cross linkage and subsequent phosphorylation of SYK is followed by activation of PLC-ϒ2 which then triggers calcium mobilisation (Su and Jumaa, 2003; Scharenberg *et al.*, 2007b), therefore, a Ca^{2+} flux assay was employed as an assessment of Pre-BCR function. Data in this chapter showed that Ca^{2+} mobilisation was only observed in

Pre- or B cell receptor harbouring cell lines. Daudi or Ramos and REH were selected as positive and negative controls for anti-µHC stimulation (Kuwahara *et al.*, 1996). The assay clearly showed a transient Ca^{2+} flux from intracellular stores in response to anti-µHC stimulation in Daudi and Ramos cells whereas, REH did not show a Ca^{2+} mobilisation, as expected, since they are µHC-negative pro-B cells (Wang *et al.*, 2002a). PreB 697 and Nalm-6 were responsive to Pre-BCR cross linkage, however, R3F9 cells were not. Ca^{2+} mobilisation in the Pre-B cells was less notable than in the more mature cells and could be attributed to the lesser amount of µHC surface expression. In keeping with these data, increased kinase activity of PLC-ϒ2 was also observed in PreB 697 and Nalm-6 after anti-µHC stimulation (Su and Jumaa, 2003). Some authors have reported that both Nalm-6 and PreB 697 showed a detectable Ca^{2+} flux upon anti-µHC cross linkage (Genevier and Callard, 1997; Geng *et al.*, 2015) while others have shown no mobilisation of calcium in both cell lines (Kuwahara *et al.*, 1996). The reason for this discrepancy may be due to differences in assays and/or immunoglobulin amounts. Interestingly there was no detectable Ca^{2+} flux in TK6 cells which are presumed to have normal B cell characteristics (Levy *et al.*, 1968; Skopek *et al.*, 1978). However, it is possible they require stromal and other co-stimulatory molecules from the normal microenvironment niche to induce a partial signal transduction (Kuwahara *et al.*, 1996) and also they express less µHC molecules than Daudi and Ramos cells. Among Pre-BCR^+ PDX samples, only L910 derived PDX cells showed weak and late Ca^{2+} mobilisation and may be due to the higher expression of µHC molecules compared to the other Pre-BCR^+ PDX samples. Ionophore stimulation level in PDX cells was generally less than cell lines and this may indicate depletion of Ca^{2+} from endoplasmic reticulum stores. Hence, the difficulty in obtaining detectable Ca^{2+} flux in Pre-BCR^+ PDXs after Pre-BCR cross linkage (King and Freedman, 2009).

Several reports have shown that quantification of tyrosine kinases could be employed as a predictive biomarker in several malignancies (De Luca and Normanno, 2010; Li *et al.*, 2015; Maude *et al.*, 2015). In BCP-ALL for example, constitutive activation of RAS pathway as measured by pERK levels is predictive of response to MEK inhibitors (Irving *et al.*, 2014). Therefore, identification of the key signalling pathways required for proliferation and survival of BCP-ALL cells is crucial for targeted therapies development. To this end, this chapter phospho-profiles key signalling pathways downstream of the Pre-BCR checkpoint in BCP-ALL cells, using Ramos cells as a positive control. In addition, increased phosphorylation after anti-µHC stimulation confirmed the Pre-BCR functionality in Pre-BCR expressing cells. Importantly,

the basal phosphorylation determined with intracellular flow cytometry method wasn't necessarily reflect the actual basal phosphorylation levels of different phospho-proteins and this issue was also experienced by our group as the isotype matched concentrations wasn't always consistent due to the batch to batch variations. In agreement with our findings, it has been found that most of Pre-BCR downstream kinases were constitutively activated even in the absence of Pre-BCR expression and their activation could be exploited therapeutically (Kim *et al.*, 2012; Perova *et al.*, 2014; Geng *et al.*, 2015; Dolai *et al.*, 2016) and similar trend of sustained signalling was also found previously in BCR malignancies (Chen *et al.*, 2002; Petlickovski *et al.*, 2005; Muzio *et al.*, 2008; Scupoli and Pizzolo, 2012).

Interestingly, constitutive activation of pAKT(S473) and pSYK(Y352) was significantly higher in Pre-BCR$^+$ than in Pre-BCR$^-$ PDX samples. Relatively similar to what have been observed in our findings, a recent study utilized reverse phase protein array (RPPA) to analyse a cohort of Pre-BCR$^+$ and Pre-BCR$^-$ ALL cells showed that Pre-BCR$^+$ are phenotypically defined by constitutive activation of PI3K-AKT and SRC signaling (Geng *et al.*, 2015). Also, BTK expression was significantly higher in Pre-BCR$^+$ than Pre-BCR$^-$ as shown by others (Kim *et al.*, 2017). However, no significant difference was observed in pERK1-2(T202-Y204) as it was relatively high in 5 out of 12 Pre-BCR$^-$ patient samples as they were RAS pathway mutants and this generally upregulate the ERK phosphorylation level and therefore potentially skew the results when compared with Pre-BCR$^+$ PDX samples (Irving *et al.*, 2014). In addition, we noticed that SYK basal phosphorylation was higher in Pre-BCR$^+$ than Pre-BCR$^-$ but only at Y352 phosphorylation site. This could be attributed to the conformational structure of SYK domain which make the SYK tyrosine at position Y348 not available for phosphorylation and this what is called `auto-inhibitory structure of SYK` (Huse and Kuriyan, 2002; Kulathu *et al.*, 2009).

Taken together, the induced phosphorylation of Pre-BCR signalling and/or calcium flux seen in Pre-BCR$^+$ PDX ALL cells, suggest that Pre-BCR is functional in Pre-BCR$^+$ cells. The higher level of basal phosphorylation in pSYK and pAKT may suggest that SYK inhibitors and /or PI3K/AKT inhibitors may have activity in these ALLs.

Chapter 4 (Results 2): Effect of Single TKIs on BCP-ALL cells

Chapter 4: Effect of Single TKIs on BCP-ALL cells

4.1 Introduction

As shown in the previous chapter, several phospho-proteins were activated in both Pre-BCR$^+$ and Pre-BCR$^-$ cells. Therefore, harnessing of Pre-BCR signalling by ALL cells may be subject to therapeutic exploitation using small molecule inhibitors that target key components of the signalling cascade (Muschen, 2015; Trimarchi and Aifantis, 2015). During the last decade, several small molecule tyrosine kinase inhibitors have been introduced in haemato-oncology targeting abnormal signalling cascades, in order to enhance the effectiveness of therapy and ideally, reduce toxic side effects. Tyrosine kinases are key elements in signal transduction of cellular pathways, which transmit information from extracellular or cytoplasmic domains to the nucleus. As many malignant cells show aberrant activity of particular tyrosine kinases, this could be exploited using tyrosine kinases inhibitors in cases where kinases are therapeutic targets (Krause and Van Etten, 2005; Rebecca and Smalley, 2014; Sun and Bernards, 2014). For example, the combination of imatinib mesylate, a tyrosine-kinase inhibitor, with conventional chemotherapy, has revolutionised the therapy for ALL patients harbouring the Philadelphia chromosome and survival has increased from 30-70% compared to historical controls. Importantly, there was no increase in toxicity and its usage may reduce the need for stem cell transplantation (Ottmann and Pfeifer, 2009; Schultz *et al.*, 2009).

In this chapter, the effects of single TKIs inhibitors [CAL-101 (PI3K-δ inhibitor); Ibrutinib (BTK inhibitor); Fostamatinib R406 (SYK inhibitor); Dasatinib (multi-kinase inhibitor)] were tested on ALL cells and the aim was to:

- Investigate cell viability in ALL cell lines and PDX cells after exposure to the candidate small molecules TKI inhibitors
- Test the effects of TKIs on cell cycle and apoptosis in BCP-ALL cell lines
- Study the pharmacodynamic effect of TKIs inhibitors on the phosphorylation level of the target molecule(s) in cell lines and PDX cells

4.2 Effect of idelalisib or CAL-101 (PI3K-δ inhibitor) on BCP-ALL cells

4.2.1 Effect of CAL-101 on BCP-ALL cells viability

CAL-101 (Idelalisib) is a selective inhibitor of phosphatidylinositol 3-kinase-δ (PI3K-δ) and has shown promising preclinical activity in relapsed *TCF3-PBX1* positive ALL cells *in vitro.* In the clinic*,* it was effective and well tolerated in patients with NHL and relapsed CLL (Meadows *et al.*, 2012; Jabbour *et al.*, 2014; Do *et al.*, 2016; Eldfors *et al.*, 2017; Slinger *et al.*, 2017).

To evaluate the *in vitro* activity of CAL-101 on BCP-ALL cells, Alamar blue assay (Section 2.5.1) was used after incubating the cells with increasing concentrations (Table 2.8) of CAL-101 to assess the viability in 5 cell lines and 33 PDX cells derived from 14 patient samples. The most obvious finding to emerge from this drug was that it decreased the growth of cell lines but only at high doses (>20µM) (Figure 4.1 A, figure 4.2 and table 4.1). R3F9 and Nalm-6 cells were more sensitive to CAL-101 than PreB 697 and REH cells (Mean GI_{50} 52.08µM, range 22.16µM -75.3µM). Moreover, TK6 cells were almost resistant to the PI3K-δ inhibitor even at the highest dose (100µM) (Figure 4.1A and table 4.1). Interestingly, 2 out of 14 patient samples (Table 4.1 and figure 4.2) were sensitive to CAL-101 (Mean GI_{50} 607nM, range 115nM – 1100nM) and were Pre-BCR^+ (L825 presentation) (Figure 4.1B) and Pre-BCR^- (L914 presentation) (Figure 4.1C) and both harboured *c-CBL* mutations. Similar to GI_{50}s obtained in cell lines, the remaining 27 PDX samples (derived from 12 patient samples) were resistant to CAL-101 (Figure 4.1B, C, figure 4.2 and table 4.1) and had various genetic alterations. Moreover, consistent GI_{50} values were observed across different PDX replicates derived originally from the same patient ALL cells.

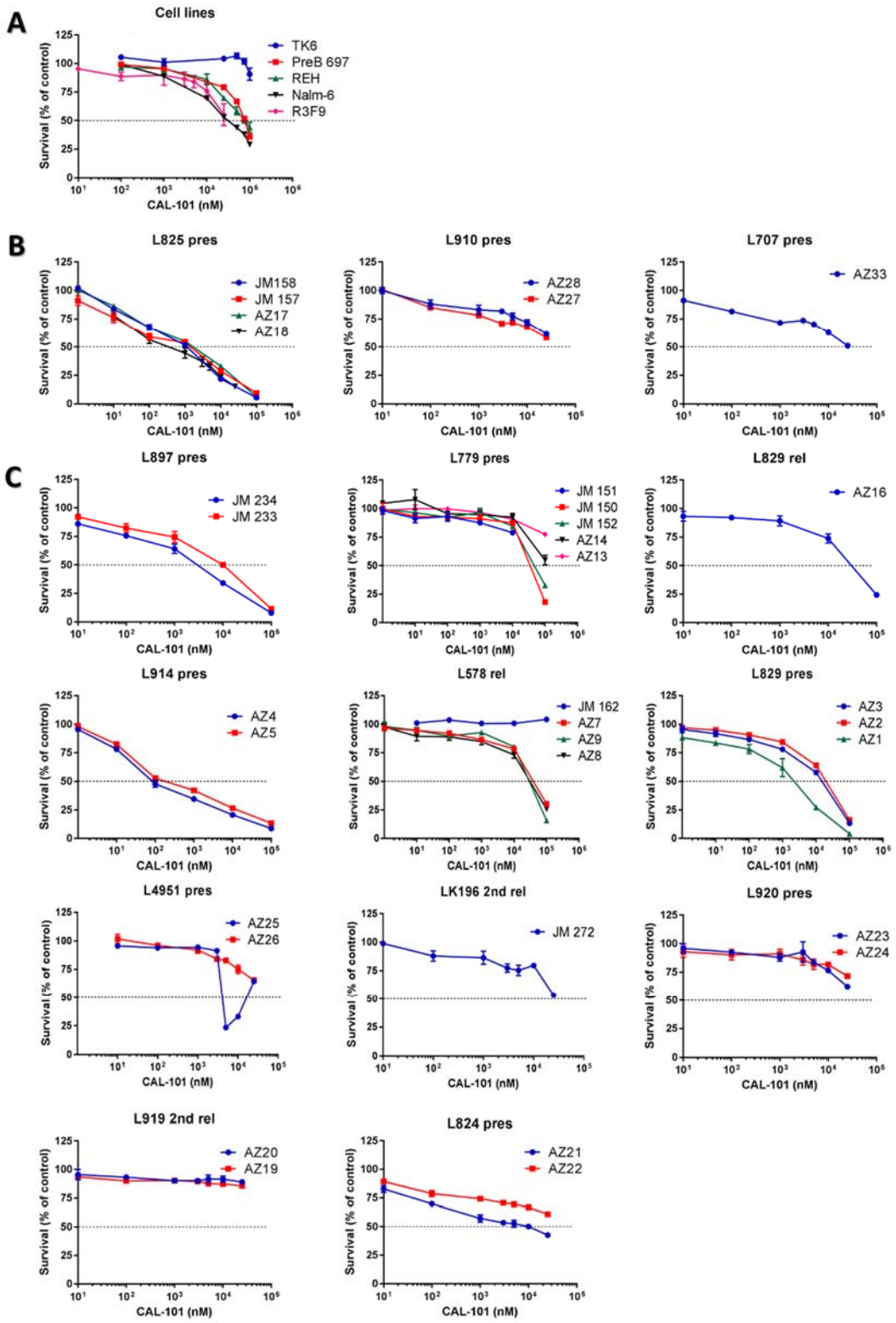

Figure 4.1: The survival curves of BCP-ALL cells treated with CAL-101 for 96 hours.

Five cell lines **(A)**, 3 Pre-BCR$^+$ and 11 Pre-BCR$^-$ patient samples **(B and C)** were cultured in the presence of escalating doses of CAL-101 for 96 hours before measuring viability by Alamar blue assay. Curve points of cell lines graph **(A)** represent the mean of 3 independent experiments ± SEM, whereas only one test was achievable in each individual PDX material and error bars represent the mean of 3 different wells ± SEM **(B and C)**. Each patient sample was amplified into 1-5 PDX replicates. Data were analysed by GraphPad prism software.

Cells	GI_{50} Mean ± SEM (CAL-101 µM)	Number of replicates
* TK6	> 100	3
* PreB 697	75.3 ± 2.05	3
* Nalm-6	31.22 ± 1.03	3
* R3F9	22.16 ± 2.83	3
L825 pres	1.10 ± 0.29	4
L910 pres	> 25	2
L707 pres	> 25	1
* REH	79.2 ± 11	3
L897 pres	6.37 ± 3.56	2
L779 Pres	56.34 ± 18.82	5
L578 rel	49.28 ± 16.98	4
L829 rel	29.10	1
L914 pres	0.115 ± 0.039	2
L829 pres	12.14 ± 5.16	3
L4951 pres	14.55 ± 10.45	2
LK196 2nd rel	> 25	1
L920 pres	> 25	2
L919 2nd rel	> 25	2
L824 pres	17.25 ± 7.75	2

Table 4.1: A list of mean GI_{50}s for BCP-ALL cells treated with CAL-101 for 96 hours.

Cells were incubated with dose escalation of CAL-101 for 96 hours before measurement of viability by Alamar blue assay. Mean GI_{50}s were calculated from 3 independent replicates of 5 cell lines (asterisks) or 33 PDX replicates derived from 14 patient samples ± SEM.

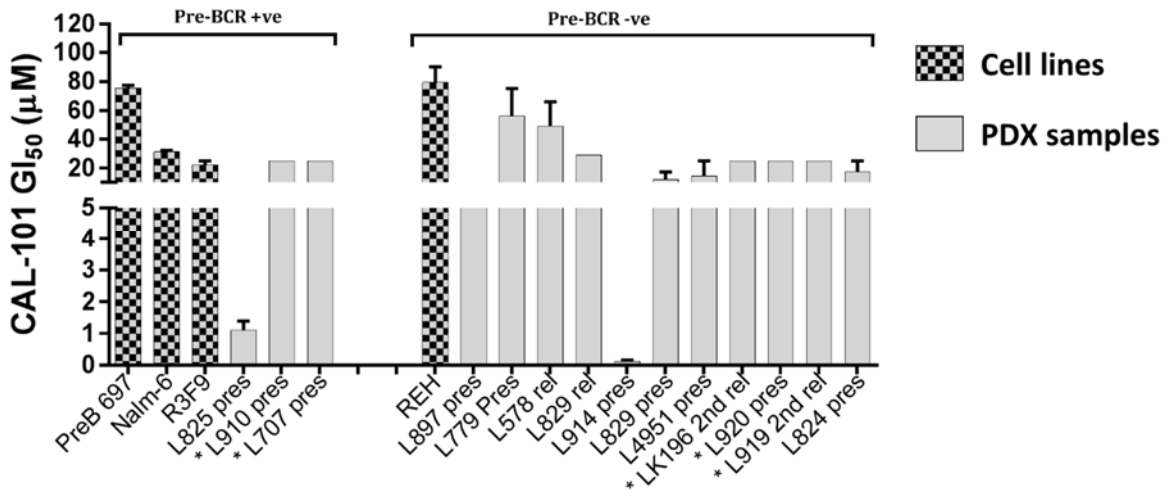

Figure 4.2: Mean GI_{50}s of cell lines and PDX cells incubated with CAL-101 for 96 hours.

Cell lines and PDX cells were exposed to a concentration range of CAL-101 for 96 hours. Alamar blue assay was subsequently performed to assess cells viability. The bar chart shows the mean of GI_{50}s of cell lines (4) and PDX samples (14). Three independent replicates were used to calculate the mean GI_{50} ± SEM. However, each patient sample was amplified into 1-5 PDX sample and hence mean GI_{50}s were calculated ± SEM. Asterisks denote samples for which the GI_{50} was not reached. GraphPad prism software was used to calculate the GI_{50}s.

4.2.2 Effect of CAL-101 on cell cycle profile of BCP-ALL cell lines

To evaluate the mechanism by which CAL-101 inhibits ALL cells viability, propidium iodide staining was carried out to measure cell cycle distribution by flow cytometry (Section 2.3.3) using 3 cell lines. Nalm-6, PreB 697 and REH cell lines were incubated with their relevant GI_{50}s (35µM, 75µM and 75µM respectively) for 24 and 48 hours (Figure 4.3). The analyses showed a significant increase in the percentage of Nalm-6 cells arrested at G1-phase after 24 hours incubation with the PI3K-δ inhibitor (% of cells in G1, CV: 33.1 ± 0.75% versus CAL-101: 37.2 ± 1.25%; $p<0.05$) (Figure 4.3A and table 4.2). Similarly, after 48 hours exposure to CAL-101, G1 arrest was also induced (% of cells in G1, CV: 37.63 ± 1.92% versus CAL-101: 46.43 ± 0.86%; $p<0.05$) and a concomitant reduction in the percentage of cells at G2-phase (% of cells in G2, CV: 17.4 ± 0.45% versus CAL-101: 11.73 ± 0.34%; $p<0.001$), however, no significant change was gained across the S phase at both time points (Figure 4.3A and table 4.2).

For PreB 697 cells, a G1 arrest phase was also observed after 24 hours (% of cells at G1, CV: 31.8% versus CAL-101: 38.9%), however, no change in cell cycle phases was observed after 48 hours apart from mild arrest at S-phase (CV: 47% versus CAL-101: 53.3%) as shown in figure

4.3B. A similar trend of G1 arrest was observed in REH cells incubated with CAL-101 for 24 hours (% of cells in G1, CV: 44.2% versus CAL-101: 63.3%), in addition to a sub-G1 peak (CV: 2.21% versus CAL-101: 7.17%) (Figure 4.3C) and these increases were associated with reduction in the ratio of cells arrested at S-phase (CV: 46.5% versus CAL-101: 26.8%). Similarly, G1 arrest persisted at 48 hours and there was evidence of a sub-G1 peak at this point too (Figure 4.3C). Taken together, these data suggest that CAL-101 induces G1 arrest in ALL cell lines.

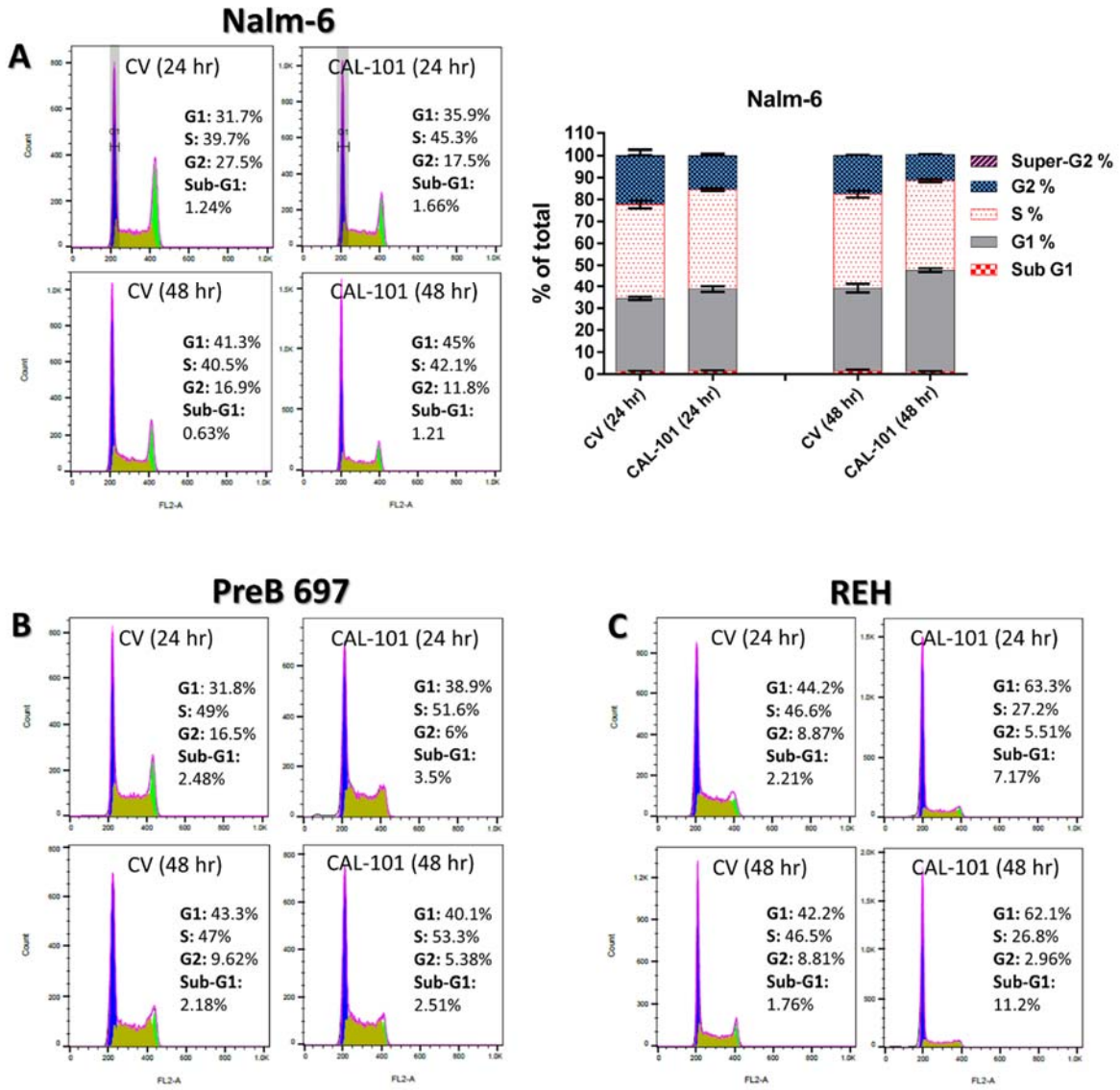

Figure 4.3: CAL-101 treatment induces G1- arrest in BCP-ALL cell lines.

Cell cycle phases were assessed by flow cytometry using propidium iodide staining after exposing Nalm-6 cells to 35µM **(A)**, PreB 697 and REH to 75µM **(B and C)** of CAL-101 for 24 and 48 hours. Histograms of one representative cell cycle run of 3 independent experiments were presented for Nalm-6 **(A)** or 1 experiment for both PreB 697 **(B)** and REH **(C).** The bar graph shows the mean percentage of Nalm-6 cells distributed at different phases of the cell cycle ± SEM (n=3) **(A).** FlowJo software was used to analyse cell cycle data.

Cell cycle phase	Mean ± SEM (n=3)		p-value	Time point
	CV	CAL-101		
Sub-G1 %	1.36 ± 0.188	1.51 ± 0.16	0.5698	**24 hours**
G1 %	33.1 ± 0.75	37.2 ± 1.25	0.0486 *	
S %	43.23 ± 1.79	45.73 ± 0.64	0.2591	
G2 %	22.1 ± 2.73	15.33 ± 1.11	0.084	
Super-G2 %	0.22 ± 0.14	0.21 ± 0.1	0.9583	
Sub-G1 %	1.45 ± 0.65	1.3 ± 0.11	0.8355	**48 hours**
G1 %	37.63 ± 1.92	46.43 ± 0.86	0.014 *	
S %	43.37 ± 1.54	40.83 ± 0.67	0.2073	
G2 %	17.4 ± 0.45	11.73 ± 0.34	0.0006 ***	
Super-G2 %	0.19 ± 0.19	0.15 ± 0.1	0.852	

Table 4.2: Percentages of Nalm-6 cells distributed at different cell cycle phases after treatment with CAL-101.

Cell cycle phases were assessed by flow cytometry using propidium iodide staining after exposing Nalm-6 cells to 35µM of CAL-101 or DMSO (CV) for 24 and 48 hours. Mean percentages of different cell cycle phases were calculated from 3 independent experiments ± SEM. FlowJo software was used to analyse cell cycle data. Student`s t-test was carried out to calculate p values. p> 0.05 not significant, *p<0.05, ***p<0.001.

4.2.3 The apoptotic effect of CAL-101 on BCP-ALL cell lines

To explore the mechanism behind the cytotoxic effect of CAL-101, Annexin V-FITC staining (Section 2.3.2) was carried out to measure programmed cell death in Nalm-6 cells by flow cytometry. Nalm-6 cells were treated with the GI_{50} concentration of CAL-101 (35µM) and apoptosis was measured after 48 and 72 hours. At both time points, no significant increase in the percentage of apoptotic cells was observed. Surprisingly, a decrease in the percentage of cell death was obtained in cells incubated with CAL-101 (3.92 ± 0.3%) when compared to CV treatment (1.51 ± 0.17%) (Figure 4.4). These data indicate that CAL-101 does not induce cell death in ALL cells and is cytostatic and parallels the cell cycle data shown above.

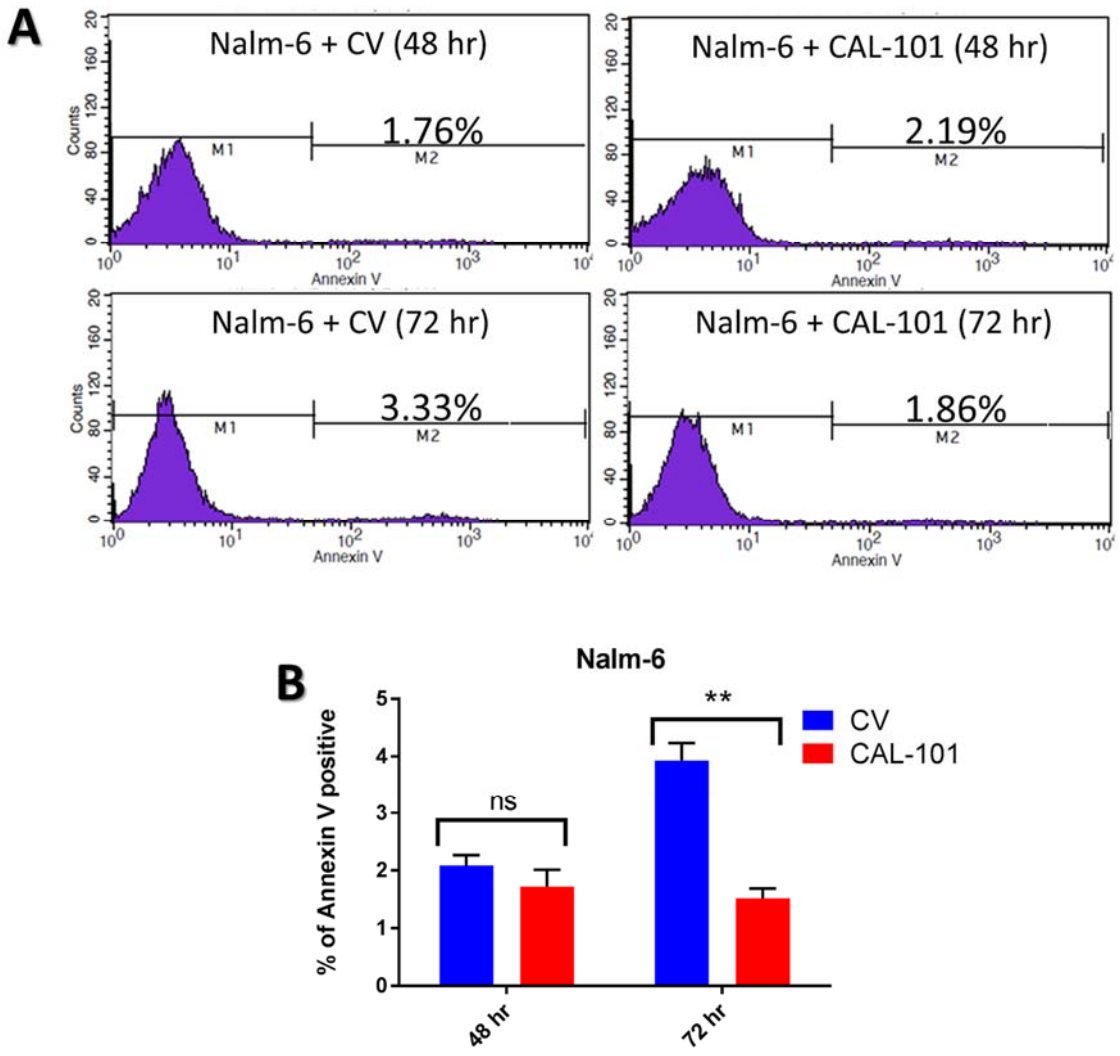

Figure 4.4: CAL-101 does not induce apoptosis in Nalm-6 cell line.

Nalm-6 cells were cultured for 48, 72 hours with the control vehicle or CAL-101 (35µM) before Annexin V-FITC staining and assessment by flow cytometry. **(A)** Representative histograms of Annexin V staining are shown for the two time points. **(B)** Bar graph chart denoting the mean ± SEM (n=3). CellQuest software was used to analyse Annexin V data. Student`s t-test was carried out to calculate p values. p> 0.05 not significant, **p<0.01.

4.2.4 The pharmacodynamic effect of CAL-101 on BCP-ALL cells

To confirm that CAL-101 abrogated the key target of PI3K pathway, $pAKT^{pS473}$ inhibition was investigated by western blotting (Section 2.6.1). Total AKT was used as a loading control and Ramos stimulation with anti-μHC (20μg/ml for 5 minutes) was used as positive control for pAKT activation (Figure 4.5). Both PreB 697 and Nalm-6 cell lines were co-cultured with their relevant GI_{50} concentrations of CAL-101 (75μM and 35μM respectively) for 90 minutes and 17 hours. Basal activation of the pathways was apparent in both cell lines and inhibition of pAKT was strong in both PreB 697 and Nalm-6 cells at the one and half hour time point. However, after 17 hours incubation, persistent de-phosphorylation was only observed in PreB 697 cells (Figure 4.5A).

In addition to cell lines, pharmacodynamics were also investigated in the most sensitive PDX cells to CAL-101 taken from newly harvested spleens. PDXs were incubated with the pre-defined GI_{50} concentrations of previously harvested PDX replicate(s) injected with the same patient cells. L825/AZ18 and L914/AZ4 were incubated with their relevant GI_{50} concentrations (316nM and 76nM respectively) for 90 minutes. In both PDX samples, no inhibition in pAKT activation was observed as shown in figure 4.5B.

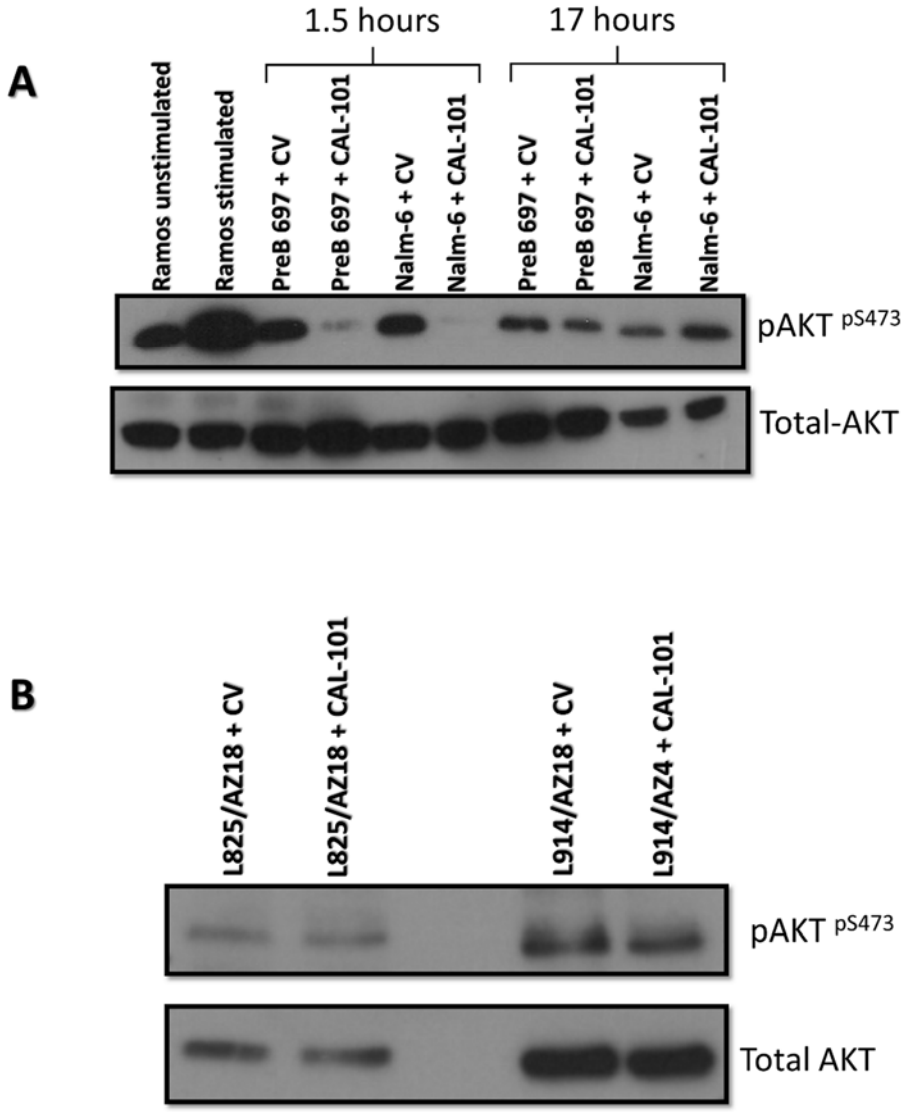

Figure 4.5: Effects of CAL-101 on the phosphorylation level of AKT after exposing BCP-ALL cells to the drug.

(A) Western blot analysis for Pre B697 and Nalm-6 cell lines co-cultured with CAL-101 (75µM and 35µM respectively) for 90 minutes and 17 hours. **(B)** Western blot analysis for L825/AZ18 and L914/AZ4 PDXs exposed to CAL-101 (316nM and 76nM respectively) for 90 minutes. Ramos cells were stimulated with 20µg/ml of anti-µHC antibody for 5 minutes. 20µg of protein was loaded to each lane and total AKT was used as a loading control. Only one experiment was performed for both **A** and **B**.

4.3 Effect of ibrutinib (BTK inhibitor) on BCP-ALL cells

4.3.1 Effect of ibrutinib on BCP-ALL cells viability

Ibrutinib (PCI-32765) is a selective BTK-Inhibitor approved by FDA for patients with waldenström macroglobulinemia, CLL and MCL for its ability to block B-cell receptor signalling. Most recently, ibrutinib was preclinically tested on *TCF3*-rearranged ALL and was proposed as a potential therapy for Pre-BCR$^+$ ALL patients (Advani *et al.*, 2013; van der Veer *et al.*, 2014; Geng *et al.*, 2015; Raedler, 2016).

To investigate its effect on high risk ALL, ibrutinib was tested in a panel of cell lines (n=5), Pre-BCR$^+$ samples (n=3) and Pre-BCR$^-$ PDXs (n=11) (Figure 4.6). Cells were incubated with increasing drug doses of ibrutinib (Table 2.8) for 96 hours and then viability examined by Alamar blue assay (Section 2.5.1). Figure 4.6 A shows that R3F9, REH, PreB 697 and Nalm-6 cells revealed a dose dependent decrease in cell viability. However, the GI_{50}s of cell lines to ibrutinib ranged between 11.43-18.3µM with a mean of 15.91µM (Figure 4.7 and table 4.3). Moreover, TK6 cells were shown to be resistant to this drug, even at the highest concentration (50µM) (Figure 4.6A and table 4.3). Interestingly, 8 PDX samples (derived from 3 patient samples) were sensitive to the BTK inhibitor as defined a GI_{50} of less than 5µM (Mean GI_{50} 2.53µM, range 0.8-4.55µM). They belonged to both Pre-BCR$^+$ (L825 presentation) and Pre-BCR$^-$ PDX cells (L897 presentation and L914 presentation) as shown in figure 4.6 (B and C), figure 4.7 and table 4.3. These sensitive samples harboured a CBL mutation (L825 presentation), RAS mutation (L897 presentation) and a high hyperdiploidy sample which was also associated with CBL and FLT3 mutations in L914 presentation. Furthermore, the remaining 25 PDXs (derived from 11 patient samples, table 2.13) were highly resistant to ibrutinib (Figure 4.6 and table 4.3) (Table 2.13). Importantly, comparable GI_{50} values were obtained from the replicates PDX materials which were derived originally from the same patient ALL cells, however, L578/JM162 was an exception (Figure 4.6 C).

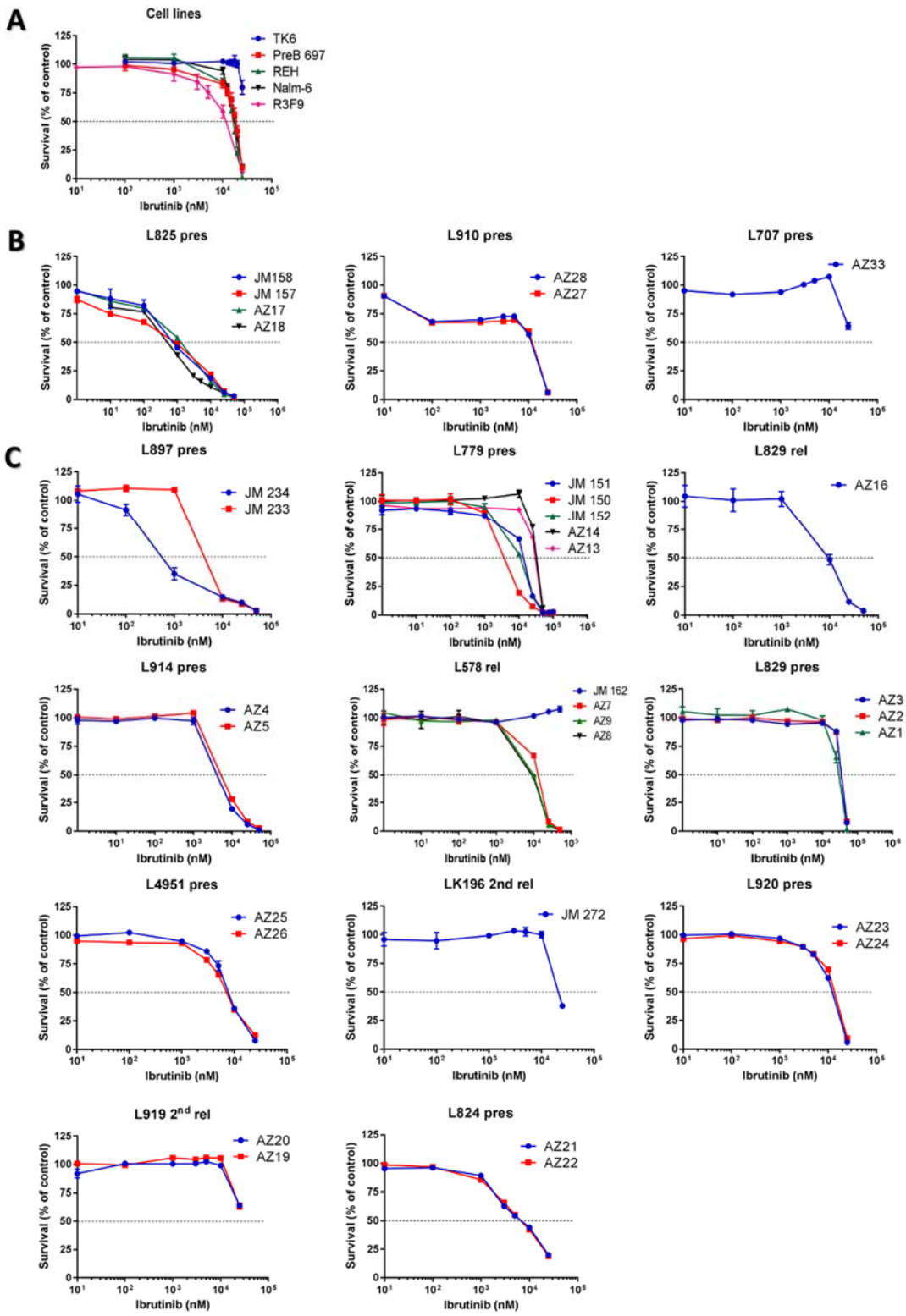

Figure 4.6: The survival curves of BCP-ALL cells treated with Ibrutinib for 96 hours.

Five cell lines **(A)**, 3 Pre-BCR$^+$ and 11 Pre-BCR$^-$ patient samples **(B and C)** were cultured in the presence of increasing doses of ibrutinib for 96 hours before measuring viability by Alamar blue assay. Curve points of cell lines graph **(A)** represent the mean of 3 independent experiments ± SEM, whereas only one test was achievable in each individual PDX material and error bars represent the mean of 3 different wells ± SEM **(B and C)**. Each patient sample was amplified into 1-5 PDX replicates. Data were analysed by GraphPad prism software.

Cells	GI_{50} Mean ± SEM (Ibrutinib µM)	Number of replicates
* TK6	> 25	3
* PreB 697	18.3 ± 0.61	3
* Nalm-6	17.83 ± 0.36	3
* R3F9	11.48 ± 0.916	3
L825 pres	0.80 ± 0.16	4
L910 pres	11.65 ± 0.25	2
L707 pres	> 25	1
* REH	16.03 ± 0.218	3
L897 pres	2.26 ± 1.73	2
L779 Pres	19.01 ± 5.5	5
L578 rel	10.48 ± 1.24	4
L829 rel	8.98	1
L914 pres	4.55 ± 0.55	2
L829 pres	33.33 ± 1.56	3
L4951 pres	7.39 ± 0.31	2
LK196 2nd rel	20.80	1
L920 pres	12.77 ± 0.47	2
L919 2nd rel	> 25	2
L824 pres	6.55 ± 0.085	2

Table 4.3: A list of mean GI_{50}s for BCP-ALL cells treated with ibrutinib.

Cells were incubated with escalating doses of Ibrutinib for 96 hours before measurement of viability by Alamar blue assay. Mean GI_{50} concentrations were calculated from 3 independent replicates of 5 cell lines (asterisks) or 33 PDX replicates derived from 14 patient samples ± SEM.

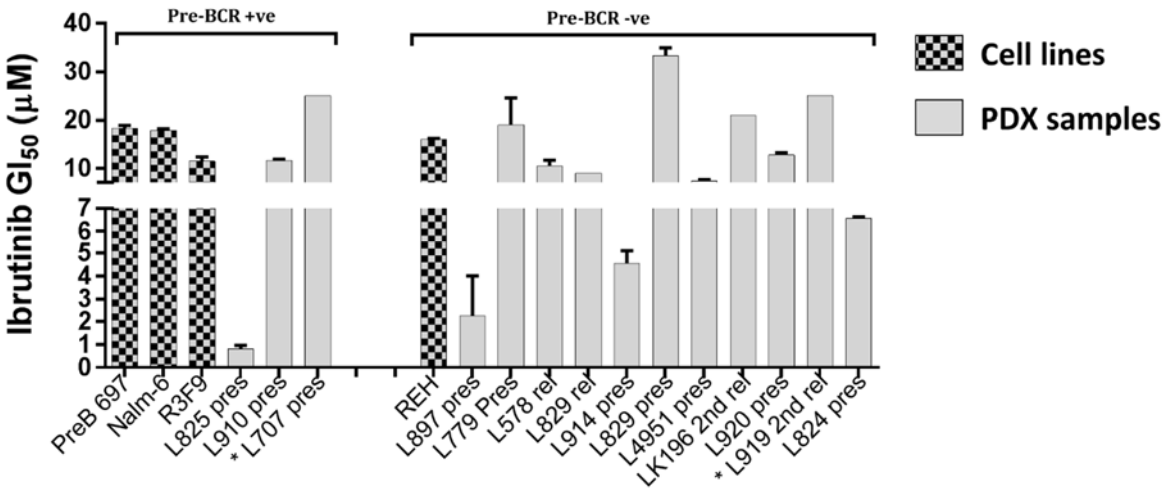

Figure 4.7: Mean GI_{50}s of cell lines and PDX cells incubated with ibrutinib for 96 hours.

Cell lines and PDX cells were exposed to a concentration range of ibrutinib for 96 hours. Alamar blue assay was subsequently performed to assess cells viability. The bar chart shows the mean of GI_{50}s of cell lines (4) and PDX samples (14). Three independent replicates were used to calculate the mean GI_{50} ± SEM. However, each patient sample was amplified into 1-5 PDX sample and hence mean GI_{50}s were calculated ± SEM. Asterisks denote samples for which the GI_{50} was not reached. GraphPad prism software was used to calculate the GI_{50}s.

4.3.2 Effect of ibrutinib on cell cycle profile of BCP-ALL cell lines

To further understand the inhibitory mechanism of ibrutinib on BCP-ALL cells, propidium iodide staining was performed to measure the distribution of cell cycle phases by flow cytometry (Section 2.3.3). To this end, Nalm-6 (n=3), PreB 697 (n=1) and REH (n=1) were co-cultured with 18μM ibrutinib for 24 and 48 hours. After 24 hours incubation with the GI_{50} concentration of ibrutinib, cell cycle analyses showed a significant increase in the percentage of Nalm-6 cells in the G1-phase (% of cells in G1, CV: 34.53 ± 2.7% versus ibrutinib: 44.47 ± 1.1%; $p<0.05$) and an associated reduction in cells in the G2-phase (% of cells in G2, CV: 20.6 ± 3.1% versus ibrutinib: 9.29 ± 0.46%; $p<0.05$) (Figure 4.8A and table 4.4). Moreover, a small but significant proportion ($p<0.05$) of Nalm-6 cells showed a sub-G1 peak (% of cells in sub-G1, CV: 1.57 ± 0.34% versus ibrutinib: 4.88 ± 0.71%) at the same time point (Figure 4.6A and table 4.4). By 48 hours, there was a significant sub-G1 peak (% of cells in sub-G1, CV: 1.16 ± 0.39% versus ibrutinib: 4.85 ± 0.91%; $p<0.05$) (Figure 4.8A and table 4.4).

For PreB 697, there was also evidence of a G1 arrest phase after 24 hours exposure to ibrutinib (% of cells in G1, CV: 36.4% versus ibrutinib: 60.8%) with a concomitant increase in sub-G1 (% of cells in sub-G1, CV: 3.29% versus ibrutinib: 11.1%), a 2 fold decrease in both S-phase (% of

cells in S, CV: 46.6% versus ibrutinib: 22.8%) and G2 phase (% of cells in G2, CV: 17.2% versus ibrutinib: 8.02%). Consistently with Nalm-6 cells, the effect on cell cycle phases was less potent at 48 hours (Figure 4.8B).

For REH cells also, 24 hours incubation with ibrutinib also induced G1 arrest (% of cells in G1, CV: 39% versus Ibrutinib: 50.3%) with a concomitant decrease in cells at S-phase (% of cells in S, CV: 17.2% versus ibrutinib: 8.02%), and an increase in the % of cells with a sub-G1 was observed after 48 hours (CV: 2.93% versus Ibrutinib: 12%) (Figure 4.8C).

Taken together, these data suggests that ibrutinib induces G1-phase arrest and modest apoptosis.

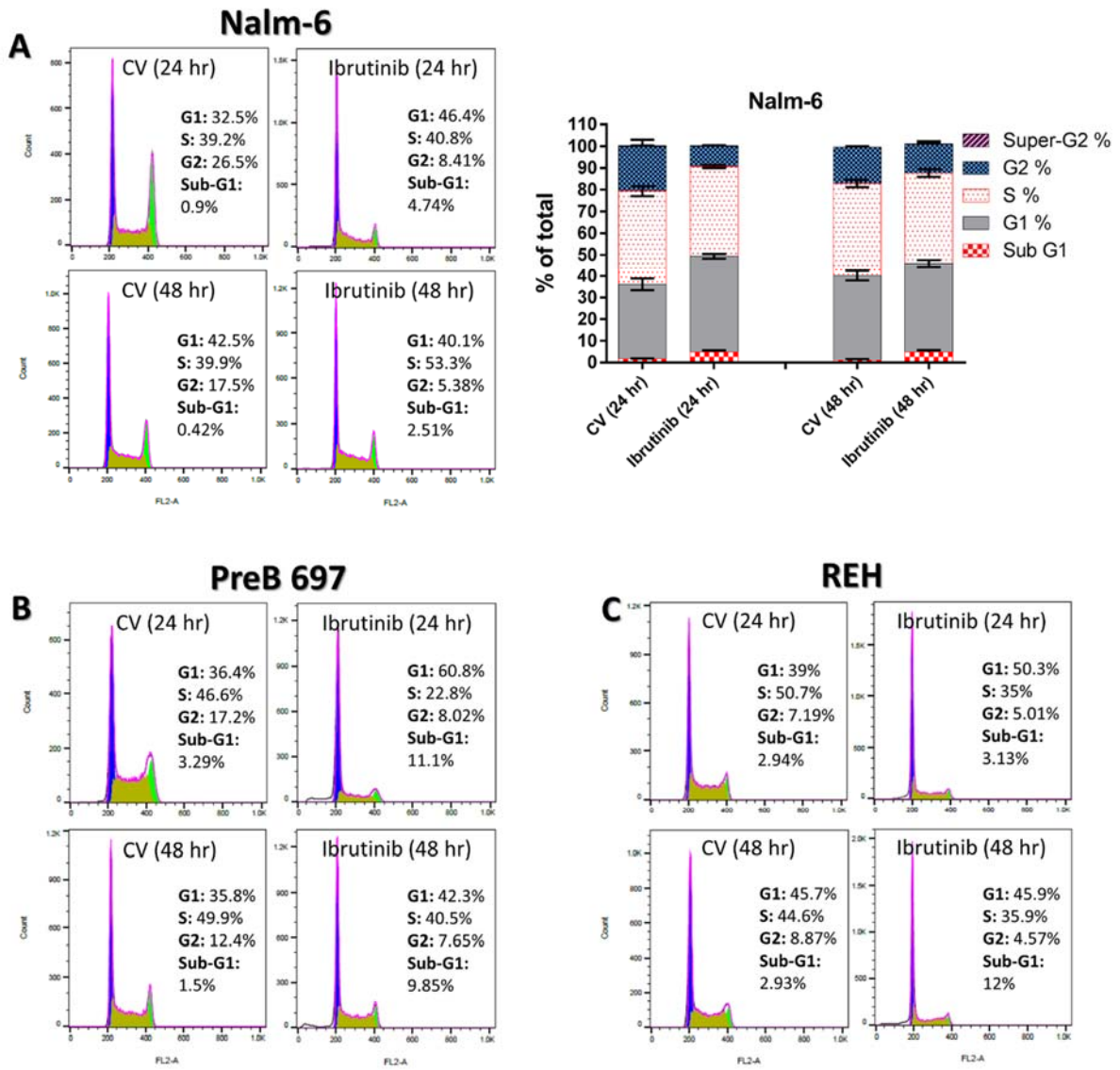

Figure 4.8: Ibrutinib treatment induces G1- arrest in BCP-ALL cell lines.

Cell cycle phases were assessed by flow cytometry using propidium iodide staining after exposing **(A)** Nalm-6, **(B)** PreB 697 and **(C)** REH cell lines to 18µM ibrutinib for 24 and 48 hours. Histograms of one representative cell cycle run of 3 independent experiments were presented for Nalm-6 **(A)** or 1 experiment for both PreB 697 **(B)** and REH **(C).** The bar graph shows the mean percentage of Nalm-6 cells distributed at different phases of the cell cycle ± SEM (n=3) **(A).** FlowJo software was used to analyse cell cycle data.

Cell cycle phase	Mean ± SEM (n=3)		p-value	Time point
	CV	Ibrutinib		
Sub-G1 %	1.57 ± 0.34	4.88 ± 0.7	0.0136 *	**24 hours**
G1 %	34.53 ± 2.7	44.47 ± 1.09	0.0273 *	
S %	43.2 ± 2.22	41.3 ± 0.65	0.4592	
G2 %	20.6 ± 3.05	9.29 ± 0.46	0.0215 *	
Super-G2 %	0.29 ± 0.16	0.24 ± 0.06	0.8062	
Sub-G1 %	1.16 ± 0.39	4.85 ± 0.91	0.0208 *	**48 hours**
G1 %	38.97 ± 2.24	41.23 ± 1.54	0.4522	
S %	42.73 ± 1.7	41.6 ± 1.71	0.664	
G2 %	16.73 ± 0.38	13.13 ± 1.43	0.072	
Super-G2 %	0.03 ± 0.03	0.22 ± 0.11	0.1929	

Table 4.4: Percentages of Nalm-6 cells distributed at different cell cycle phases after treatment with ibrutinib.

Cell cycle phases were assessed by flow cytometry using propidium iodide staining after exposing Nalm-6 cells to 18µM of ibrutinib or DMSO (CV) for 24 and 48 hours. Mean percentages of different cell cycle phases were calculated from 3 independent experiments ± SEM. FlowJo software was used to analyse cell cycle data. Student`s t-test was carried out to calculate p values. p> 0.05 not significant, *p<0.05.

4.3.3 The apoptotic effect of ibrutinib on BCP-ALL cell lines

To confirm the apparent apoptotic effect of ibrutinib in reducing cell viability, Annexin V-FITC staining (Section 2.3.2) was used to measure programmed cell death in Nalm-6 cells by flow cytometry. Nalm-6 cells were incubated with the GI_{50} concentration of ibrutinib (18µM) for 48 and 72 hours and showed a significant increase in the percentage of apoptotic cells at both time points when compared to the CV (Figure 4.9A). The percentage of cell death after 48 hours was 9.67±1.86% compared to 2.06±0.27% for CV ($p<0.05$) and after 72 hours was 16.82±1.46% compared to CV treated, 3.59±0.88 %, p-value was 0.0015 (Figure 4.9B). These data indicate that ibrutinib significantly induced cell death at the GI_{50} concentrations in Nalm-6 cells and is consistent with cell cycle data described above.

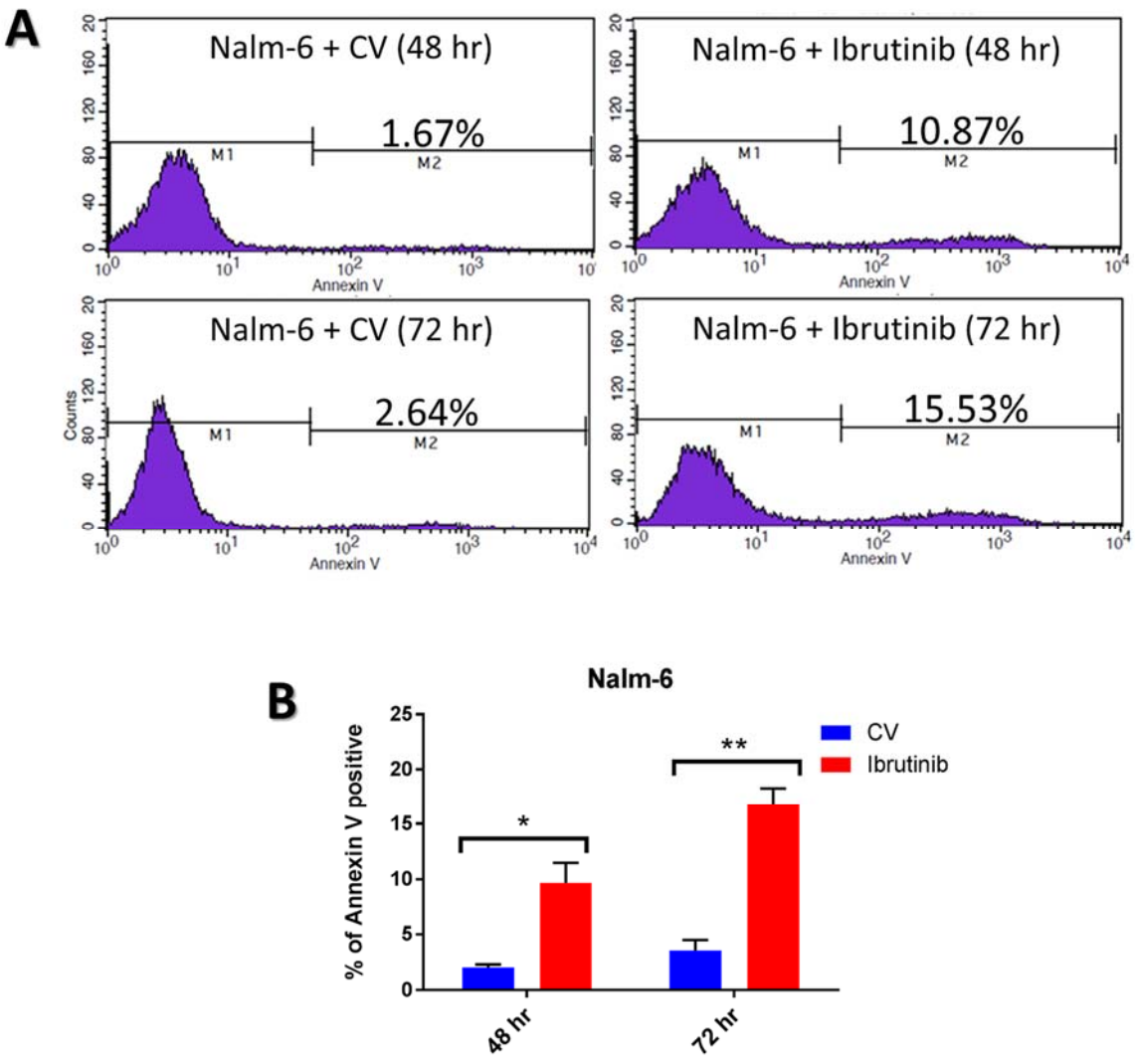

Figure 4.9: Ibrutinib treatment induces significant programmed cell death in Nalm-6 cell line.

Nalm-6 cells were cultured for 48, 72 hours with the control vehicle or ibrutinib (18µM) before Annexin V-FITC staining and assessment by flow cytometry. **(A)** Representative histograms of Annexin V staining are shown for the two time points. **(B)** Bar graph chart denoting the mean ± SEM (n=3). CellQuest software was used to analyse Annexin V data. Student`s t-test was carried out to calculate p values. *p< 0.05, **p<0.01.

4.3.4 The pharmacodynamic effect of ibrutinib on BCP-ALL cells

To confirm that the effect of Ibrutinib on cell cycle arrest and apoptosis was associated with BTK inhibition, the phosphorylation of BTK was analysed by intracellular phospho-staining followed by detection by flow cytometry (Section 2.3.5). Ramos stimulation with anti-µHC (20µg/ml for 4 minutes) was used as a positive control for pBTK activation (Figure 4.10A) which was run side by side with all experiments. Nalm-6 cells were exposed to their pre-defined GI_{50} value (18µM) of ibrutinib at three different time points (1, 6 and 24 hours). Interestingly, a reduction in the level of pBTK was observed in all time points, however, inhibition was more potent at 6 and 24 hours than at 1 hour (Figure 4.10 B).

The pharmacodynamic effect of ibrutinib was also investigated in PDX samples. PDX samples, previously shown to be sensitive to ibrutinib, were incubated with pre-defined GI_{50} concentrations. L825/AZ16 and L914/AZ4 were incubated respectively with 490nM and 4µM of ibrutinib for 6 hours. A mild reduction in pBTK was seen in both PDX samples but the inhibition was less marked than Nalm-6 cell line (Figure 4.10 C).

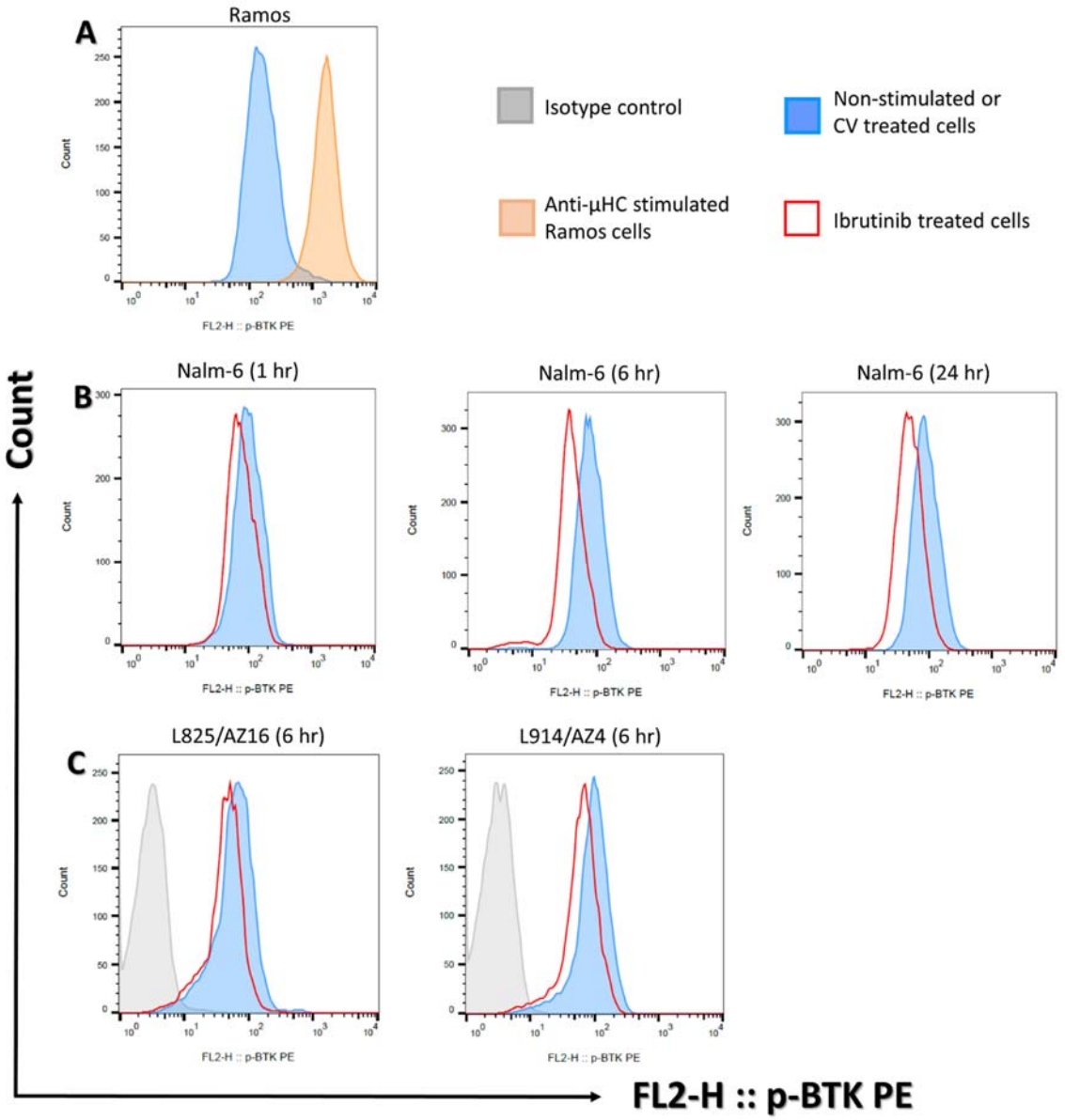

Figure 4.10: Pharmacodynamic effect of ibrutinib on BCP-ALL cells.

Intracellular staining with anti-pBTK(pY233) antibody-PE and acquisition on a FACSCalibur were carried out following incubation of Pre-B cells with their relevant ibrutinib GI_{50} concentrations. **(A)** Overlay histogram shows Ramos cells stimulation by F(ab)2 anti-µHC antibody which was used as a positive control. **(B)** Histograms show pBTK inhibition in Nalm-6 cells treated with DMSO (CV) or 18µM ibrutinib for 1, 6 and 24 hours. **(C)** Histograms depict pBTK inhibition in L825/AZ16 and L914/AZ4 which were incubated with 490nM and 4µM of ibrutinib respectively for 6 hours. Only one replicate was performed for all experiments. FlowJo software was used to make histograms overlays.

4.4 Effect of fostamatinib R406 (SYK inhibitor) on BCP-ALL cells

4.4.1 Effect of R406 on BCP-ALL cells viability

Fostamatinib R788, the pro-drug form of the SYK inhibitor, has shown activity in clinical trials performed in patients with Rheumatoid Arthritis, Lymphoma and CLL (Friedberg *et al.*, 2010; Morales-Torres, 2012). In addition, preclinical data evidenced that fostamatinib decreased tumour burden in mice transplanted with high risk and relapsed BCP-ALL cells (Perova *et al.*, 2014).

To determine the effect of fostamatinib R406, the active form of this drug, on high risk ALL, five cell lines and 30 PDX samples (derived from 15 ALL patient samples) were exposed to increasing doses of R406 (Table 2.8) for 96 hours followed by Alamar blue assay (Section 2.5.1). R406 treatment decreased the viability of both Pre-BCR$^+$ (PreB 697, Nalm-6 and R3F9) and Pre-BCR$^-$ (REH) cell lines (Mean GI_{50} 4.32µM, range 2.88 – 5.83µM), however, the highest R406 concentration (50µM) didn't reduce the viability of TK6 cells (Figure 4.11 A, Figure 4.12 and table 4.5). Interestingly, remarkable sensitivity was seen in 2 out of 3 Pre-BCR$^+$ samples (L825 presentation and L910 presentation) (Mean GI_{50} 0.947µM, range 150nM -1.74µM) - defined as GI_{50} less than 2µM - as shown in figure 4.9B and table 4.5 and also, 4 from 12 Pre-BCR$^-$ samples (L914 presentation, L829 presentation, L824 presentation and L881 2nd relapse) (Mean GI_{50} 3.06µM, range 125nM -4.2µM) (Figure 4.11 B, C, figure 4.12 and table 4.5). The sensitive samples harboured different genetic mutations such as c-*CBL* (L825 presentation), *TCF3-PBX1* (L910 presentation), *NRAS* mutation (L829 presentation), *CBL* and *FLT3* (L914 presentation) and *PDGFR* (L824 presentation). (Table 2.13). Again, consistent GI_{50} values were obtained in all replicates PDXs apart from L578/JM162.

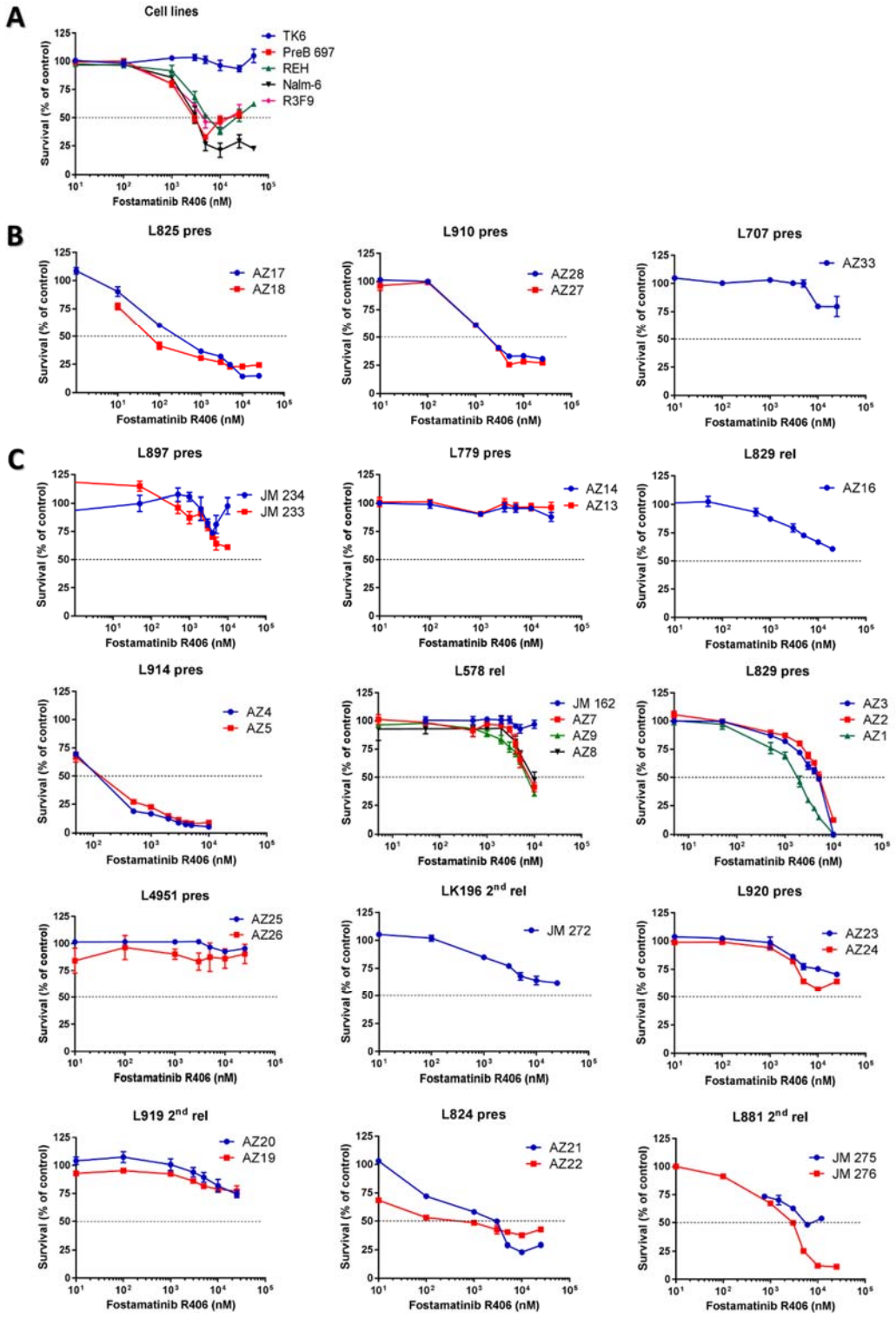

Figure 4.11: The survival curves of BCP-ALL cells treated with R406 for 96 hours.

Five cell lines **(A)**, 3 Pre-BCR^{+} and 12 Pre-BCR^{-} patient derived samples **(B and C)** were cultured in the presence of escalating doses of R406 for 96 hours before measuring viability by Alamar blue assay. Curve points of cell lines in graph **(A)** represent the mean of 3 independent experiments ± SEM, whereas only one test was achievable in each individual PDX material and error bars represent the mean of 3 different wells ± SEM **(B and C)**. Each patient sample was amplified into 1-5 PDX replicates. Data were analysed by GraphPad prism software.

Cells	GI_{50} Mean ± SEM (R406 µM)	Number of replicates
* TK6	> 25	6
* PreB 697	2.88 ± 0.27	3
* Nalm-6	2.97 ± 0.37	4
* R3F9	5.83 ± 2.08	3
L825 pres	0.15 ± 0.09	2
L910 pres	1.745 ± 0.005	2
L707 pres	> 25	1
* REH	5.63 ± 0.269	3
L897 pres	10.00	2
L779 Pres	> 25	2
L578 rel	8.525 ± 0.668	4
L829 rel	20.00	1
L914 pres	0.125 ± 0.005	2
L829 pres	3.89 ± 1.06	3
L4951 pres	> 25	2
LK196 2nd rel	> 25	1
L920 pres	> 25	2
L919 2nd rel	> 25	2
L824 pres	1.695 ± 1.195	2
L881 2nd rel	4.205 ± 1.295	2

Table 4.5: A list of mean GI_{50} concentrations for BCP-ALL cells treated with R406 for 96 hours.

Cells were incubated with dose escalation of R406 for 96 hours before measurement of viability by Alamar blue assay. Mean GI_{50}s were calculated from 3-6 independent replicates of 5 cell lines (asterisks) or 30 PDX replicates derived from 15 patient samples ± SEM.

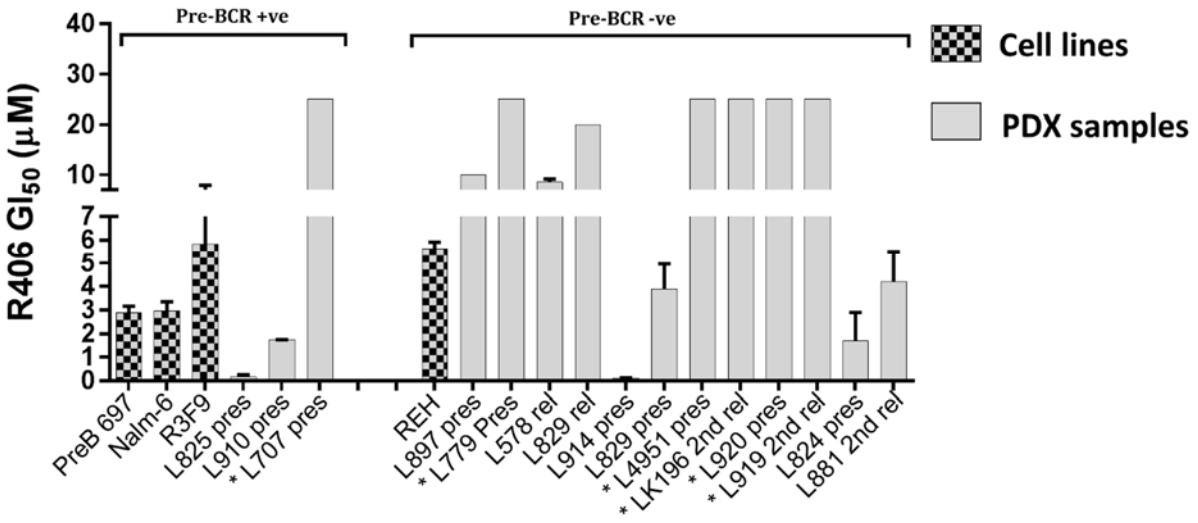

Figure 4.12: Mean GI_{50}s of cell lines and PDX cells incubated with R406 for 96 hours.

Cell lines and PDX cells were exposed to a concentration range of R406 for 96 hours. Alamar blue assay was subsequently performed to assess cells viability. The bar chart shows the mean of GI_{50}s of cell lines (4) and PDX samples (15). Three independent replicates were used to calculate the mean GI_{50} ± SEM. However, each patient sample was amplified into 1-5 PDX sample and hence mean GI_{50}s were calculated ± SEM. Asterisks denote samples for which the GI_{50} was not reached. GraphPad prism software was used to calculate the GI_{50}s.

4.4.2 Effects of R406 on cell cycle profile of BCP-ALL cell lines

To evaluate the mechanism by which fostamatinib R406 inhibits ALL cells viability, propidium iodide staining was carried out to measure cell cycle distribution by flow cytometry (Section 2.3.3) using 3 cell lines. Nalm-6, PreB 697 and REH cell lines were incubated with their relevant GI_{50}s (3µM, 3µM and 6µM respectively) for 24 and 48 hours (Figures 4.13, 4.14 and tables 4.6-4.8). The cell cycle profile analyses after 24 hours incubation with the SYK inhibitor showed an increase in the percentage of Nalm-6 cells arrested at G2 (% of cells in G2, CV: 22.47 ± 0.49% versus R406: 36.13 ± 1.75%; $p<0.01$) and a 19 fold increase in the ratio of cells present in a super-G2 peak (% of cells in super-G2, CV: 0.65 ± 0.07% versus R406: 19 ± 1.37%; $p<0.001$) (Figure 4.13 A and table 4.6). In addition, a reduction in the ratio of Nalm-6 cells arrested at G1 and S phases was apparent (% of cells in G1, CV: 32.57 ± 0.81% versus R406: 11.77 ± 0.75%; $p<0.0001$), (% of cells in S, CV: 43.07 ± 1.29% versus R406: 30.2 ± 0.87%; $p<0.01$) respectively. After 48 hours, there was a 7 fold increase in cells present in the sub-G1 peak (% of cells in sub-G1, CV: 1.34 ± 0.15% versus R406: 11.9 ± 0.45%) (Figure 4.13A and table 4.6).

For PreB 697, there was a small decrease in the percentage of cells in the G2-phase after 24 hours incubation (% of cells in G2, CV: 14.93 ± 0.47% versus R406: 11.87 ± 0.4%; $p<0.01$). There was a small decrease in the ratio of cells arrested at the G1 phase after 48 hours (% of cells in G1, CV: 41.27 ± 1.36% versus R406: 33.97 ± 0.69%; $p<0.01$) which was associated with very small but significant increase cells within sub-G1 (% of cells in sub-G1, CV: 1.36 ± 0.19% versus R406: 2.2 ± 0.05%; $p<0.05$) and super-G2 (% of cells in super-G2, CV: 0.01 ± 0.01% versus R406: 0.36 ± 0.08%; $p<0.05$) (Figure 4.13 B and table 4.7).

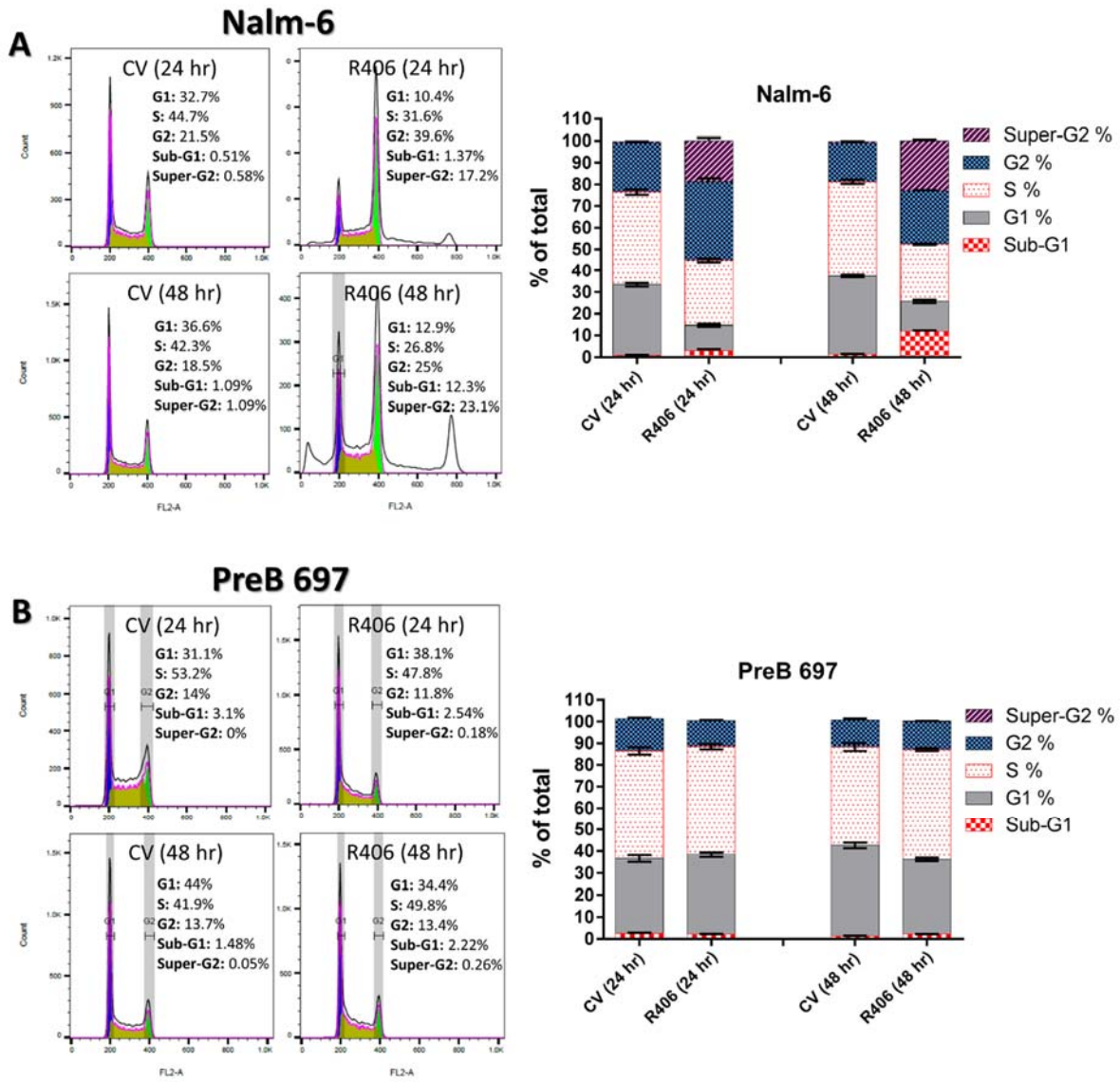

Figure 4.13: The effect of R406 treatment on cell cycle distribution of BCP-ALL cell lines.

Cell cycle phases were assessed by flow cytometry using propidium iodide staining after exposing **(A)** Nalm-6, **(B)** PreB 697 cell lines to 3µM R406 for 24 and 48 hours. Histograms of one representative cell cycle run of 3 independent experiments were presented. The bar graphs show the mean percentage of cells distributed at different phases of the cell cycle ± SEM (n=3) **(A).** FlowJo software was used to analyse cell cycle data.

Cell cycle phase	Mean ± SEM (n=3)		p-value	Time point
	CV	Fostamatinib R406		
Sub-G1 %	0.84 ± 0.28	2.96 ± 0.79	0.0669	**24 hours**
G1 %	32.57 ± 0.81	11.77 ± 0.75	< 0.0001 ****	
S %	43.07 ± 1.29	30.2 ± 0.87	0.0012 **	
G2 %	22.47 ± 0.49	36.13 ± 1.75	0.0017 **	
Super-G2 %	0.65 ± 0.07	19 ± 1.37	0.0002 ***	
Sub-G1 %	1.34 ± 0.15	11.9 ± 0.45	< 0.0001 ****	**48 hours**
G1 %	36.07 ± 0.48	13.8 ± 0.75	< 0.0001 ****	
S %	43.8 ± 0.96	26.73 ± 0.29	< 0.0001 ****	
G2 %	17.63 ± 0.81	24.63 ± 0.23	0.0012 **	
Super-G2 %	0.82 ± 0.14	22.87 ± 0.67	< 0.0001 ****	

Table 4.6: Percentages of Nalm-6 cells distributed at different cell cycle phases after treatment with R406.

Cell cycle phases were assessed by flow cytometry using propidium iodide staining after exposing Nalm-6 cells to 3µM of R406 or DMSO (CV) for 24 and 48 hours. Mean percentages of different cell cycle phases were calculated from 3 independent experiments ± SEM. FlowJo software was used to analyse cell cycle data. Student`s t-test was carried out to calculate p values. p> 0.05 not significant, **p<0.01, ***p<0.001 and ****p<0.0001.

Cell cycle phase	Mean ± SEM (n=3)		p-value	Time point
	CV	Fostamatinib R406		
Sub-G1 %	2.53 ± 0.34	2.17 ± 0.2	0.4146	24 hours
G1 %	34.1 ± 1.51	36.17 ± 0.96	0.3134	
S %	49.8 ± 1.71	50.1 ± 1.27	0.8951	
G2 %	14.93 ± 0.47	11.87 ± 0.4	0.0078 **	
Super-G2 %	0.0 ± 0.0	0.09 ± 0.05	0.1388	
Sub-G1 %	1.36 ± 0.19	2.2 ± 0.05	0.0140 *	48 hours
G1 %	41.27 ± 1.36	33.97 ± 0.69	0.0089 **	
S %	45.6 ± 1.86	50.83 ± 0.63	0.0564	
G2 %	12.5 ± 0.6	12.83 ± 0.29	0.6457	
Super-G2 %	0.01 ± 0.01	0.36 ± 0.08	0.0185 *	

Table 4.7: Percentages of PreB 697 cells distributed at different cell cycle phases after treatment with R406.

Cell cycle phases were assessed by flow cytometry using propidium iodide staining after exposing PreB 697 cells to 3µM of R406 or DMSO (CV) for 24 and 48 hours. Mean percentages of different cell cycle phases were calculated from 3 independent experiments ± SEM. FlowJo software was used to analyse cell cycle data. Student`s t-test was carried out to calculate p values. p> 0.05 not significant, *p<0.05 and **p<0.01.

Consistent with Nalm-6 cells, a substantial increase (fivefold) in the proportion of cells arrested at G2 was observed in REH cells incubated with R406 for 24 hours (% of cells in G2, CV: 10.32 ± 0.49% versus R406: 47.97 ± 1.29%; p<0.0001), in addition to a significant increase in the % of cells in the sub-G1 peak (CV: 1.18 ± 0.14% versus R406: 2.62 ± 0.46%; p<0.05) and super-G2 peaks (% of cells in super-G2, CV: 1.22 ± 0.2% versus R406: 7.81 ± 0.63%; p<0.001). There was a concomitant decrease in the proportion of cells in the G1 phase (% of cells in G1, CV: 35.47 ± 1.61% versus R406: 5.75 ± 0.23%; p<0.0001) and S-phase (% of cells in S, CV: 51.43 ± 1.51% versus R406: 35.77 ± 0.92%; p<0.001) after 24 hours (Figure 4.14 and table 4.8). Similarly, the % of cells were also significantly increased at G2, S, sub-G1 and super-G2 phases after 48 hours and were associated with highly significant decrease in the ratio of cells in the % of cells in the G1 phase as shown in figure 4.14 and table 4.8. Taken together, these data suggest that R406 induces a G2 arrest and apoptosis in two cell lines out of three.

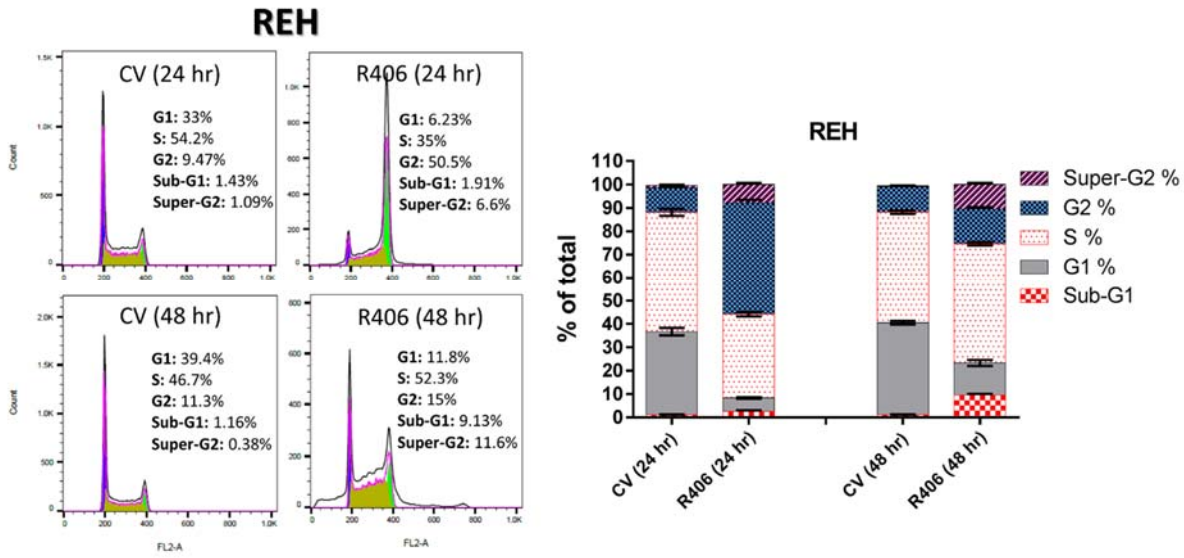

Figure 4.14: The effect of R406 treatment on cell cycle distribution of REH cell line.

Cell cycle phases were assessed by flow cytometry using propidium iodide staining after exposing REH cells to 6µM R406 for 24 and 48 hours. Histograms of one representative cell cycle run of 3 independent experiments are presented. The bar graphs show the mean percentage of cells distributed at different phases of the cell cycle ± SEM (n=3). FlowJo software was used to analyse cell cycle data.

Cell cycle phase	Mean ± SEM (n=3)		p-value	Time point
	CV	Fostamatinib R406		
Sub-G1 %	1.18 ± 0.14	2.62 ± 0.46	0.0425 *	**24 hours**
G1 %	35.47 ± 1.61	5.75 ± 0.23	< 0.0001 ****	
S %	51.43 ± 1.51	35.77 ± 0.92	0.0009 ***	
G2 %	10.32 ± 0.49	47.97 ± 1.29	< 0.0001 ****	
Super-G2 %	1.22 ± 0.2	7.81 ± 0.63	0.0006 ***	
Sub-G1 %	1.17 ± 0.13	9.58 ± 0.55	0.0001 ***	**48 hours**
G1 %	39.33 ± 0.8	13.73 ± 1.29	< 0.0001 ****	
S %	47.67 ± 0.73	51.3 ± 0.68	0.0220 *	
G2 %	10.93 ± 0.2	14.87 ± 0.75	0.0073 **	
Super-G2 %	0.28 ± 0.14	10.44 ± 0.65	0.0001 ***	

Table 4.8: Percentages of REH cells distributed at different cell cycle phases after treatment with R406.

Cell cycle phases were assessed by flow cytometry using propidium iodide staining after exposing REH cells to 6µM of R406 or DMSO (CV) for 24 and 48 hours. Mean percentages of different cell cycle phases were calculated from 3 independent experiments ± SEM. FlowJo software was used to analyse cell cycle data. Student`s t-test was carried out to calculate p values. *p<0.05, **p<0.01, ***p<0.001 and ****p<0.0001.

4.4.3 The apoptotic effect of R406 on BCP-ALL cell lines

To further understand the cytotoxic effect of R406, Annexin V-FITC staining (Section 2.3.2) was used to measure the percentage of apoptotic BCP-ALL cells by flow cytometry. Nalm-6, PreB 697 and REH cells were treated with their relevant GI_{50} concentrations of R406 (3µM, 3µM and 6µM respectively) followed by Annexin V staining at 48 and 72 hours (Figure 4.15).

In Nalm-6, an increase in the percentage of apoptosis was seen at both time points, however, it was only significant at 72 hours incubation (CV: 7.9 ± 1.52% versus R406: 31.34 ± 1.55%; $p<0.01$) (Figure 4.15 A). In addition, induction of programmed cell death was apparent in PreB 697 cells at 72 hours (CV: 4.7 ± 0.38% versus R406: 20.92 ± 0.34%; $p<0.0001$) (Figure 4.15 B). Moreover, a significant induction of apoptosis was seen in REH cells after 48 hours (CV: 4.21 ± 0.05% versus R406: 27.34 ± 1.59%; $p<0.001$) and 72 hours (CV: 3.15 ± 0.32% versus R406: 26.86 ± 1.9%; $p<0.001$) (Figure 4.15C). Taken together, these data indicate that R406 is associated with the formation of a super G2 peak and induced significant apoptosis at the GI_{50} concentrations in all 3 cell lines.

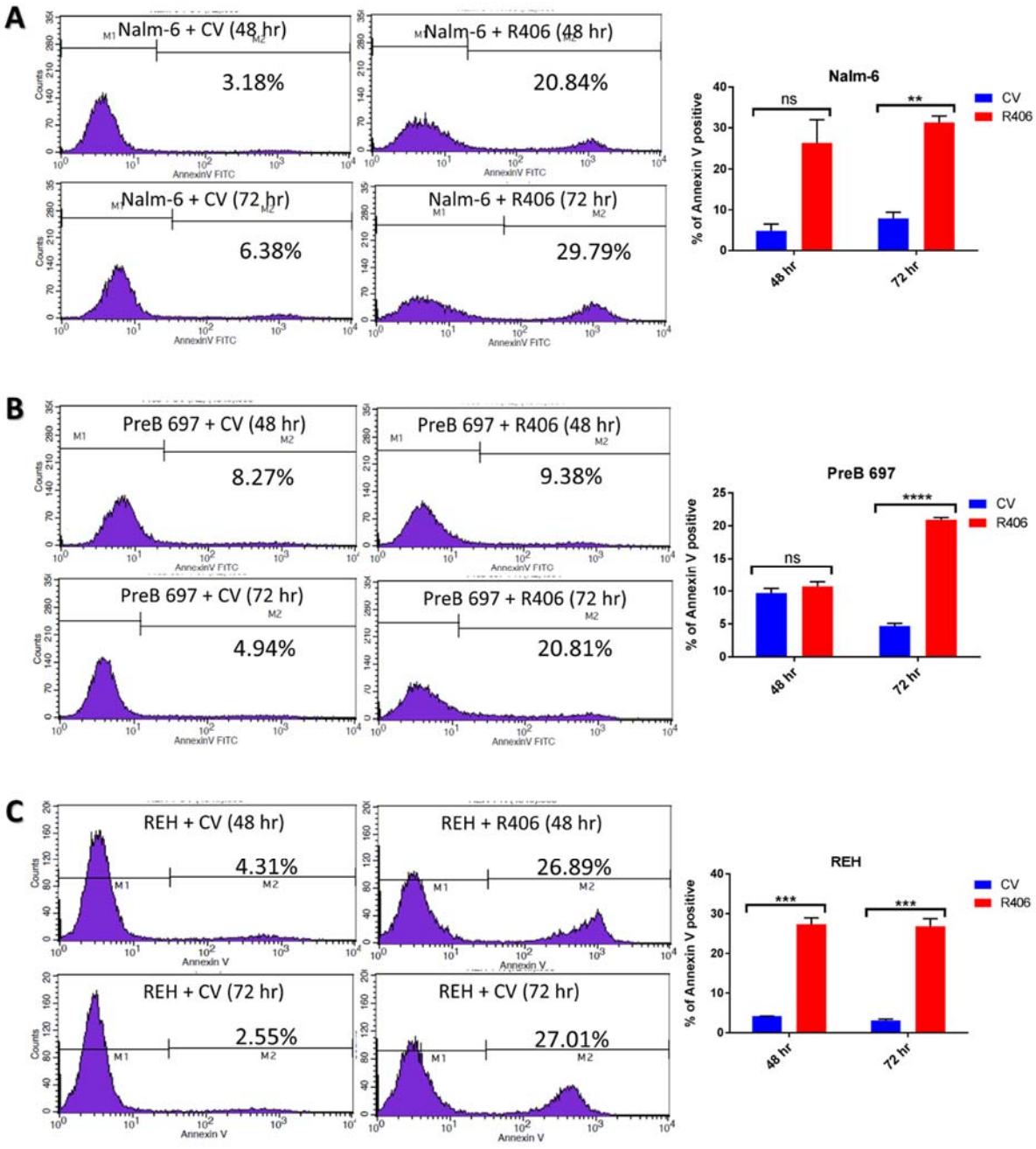

Figure 4.15: The effect of R406 treatment on apoptosis induction in BCP-ALL cell lines.

Apoptosis was assessed by flow cytometry using Annexin V-FITC staining after exposing **(A)** Nalm-6, **(B)** PreB 697 and **(C)** REH cell lines to their relevant GI_{50} values of R406 (3µM, 3µM and 6µM respectively) for 48 and 72 hours. One representative histogram of 2-3 independent experiments were presented. The bar graphs show the mean percentage of cells distributed at different phases of the cell cycle ± SEM**.** CellQuest software was used to analyse Annexin V data. Student`s t-test was carried out to calculate p values. p>0.05 not significant (ns), *p< 0.05, **p<0.01, ***p<0.001 and ****p<0.0001.

4.4.4 Pharmacodynamic effects of R406 on BCP-ALL cells

To confirm the mechanism of action of the fostamatinib R406 cytotoxicity, the inhibition of several potential targets [pSYK(Y352), pSYK(Y348) and pAKT(S473)] were investigated by intracellular phospho-flow cytometry (Section 2.3.5). Ramos stimulation with anti-µHC (20µg/ml for 4 minutes) was used as positive control for target activation (Figure 4.16 A). Ramos cells were run side by side with all experiments of cell lines and R406-sensitive PDX samples (Figures 4.16 and 4.17).

Nalm-6 and R3F9 cell lines were exposed to their relevant GI_{50} concentrations of R406 (3µM and 6µM respectively) for 2 hours. Measurement by flow cytometry showed a modest small inhibition in all targets, but was only significant for pSYK(Y348) in both cell lines (Figure 4.16 B and C). Interestingly, about 10 % inhibition in pSYK(Y348) was obtained in R406-treated Nalm-6 and R3F9 cells compared to DMSO treated cells (Figure 4.16 D and E).

In addition to cell lines, similar experiments were also performed in PDX samples. The R406 sensitive PDX samples taken from newly harvested spleens were incubated with the pre-defined GI_{50} concentration of previously harvested PDX replicates injected with the same patient cells. L825/AZ18, L910/AZ28, L914/AZ4, L829/AZ2, and L824/AZ22 were incubated with their relevant GI_{50} concentrations of R406 (56nM, 1.75µM, 120nM, 5.12µM and 500nM respectively). Surprisingly, no inhibition was observed in all targets studied in all PDX samples (Figure 4.17) apart from mild inhibition of pAKT in L914/AZ4 (Figure 4.17 C).

Therefore, these results indicate that a very modest inhibition of pSYK(Y348) was only seen in cell lines.

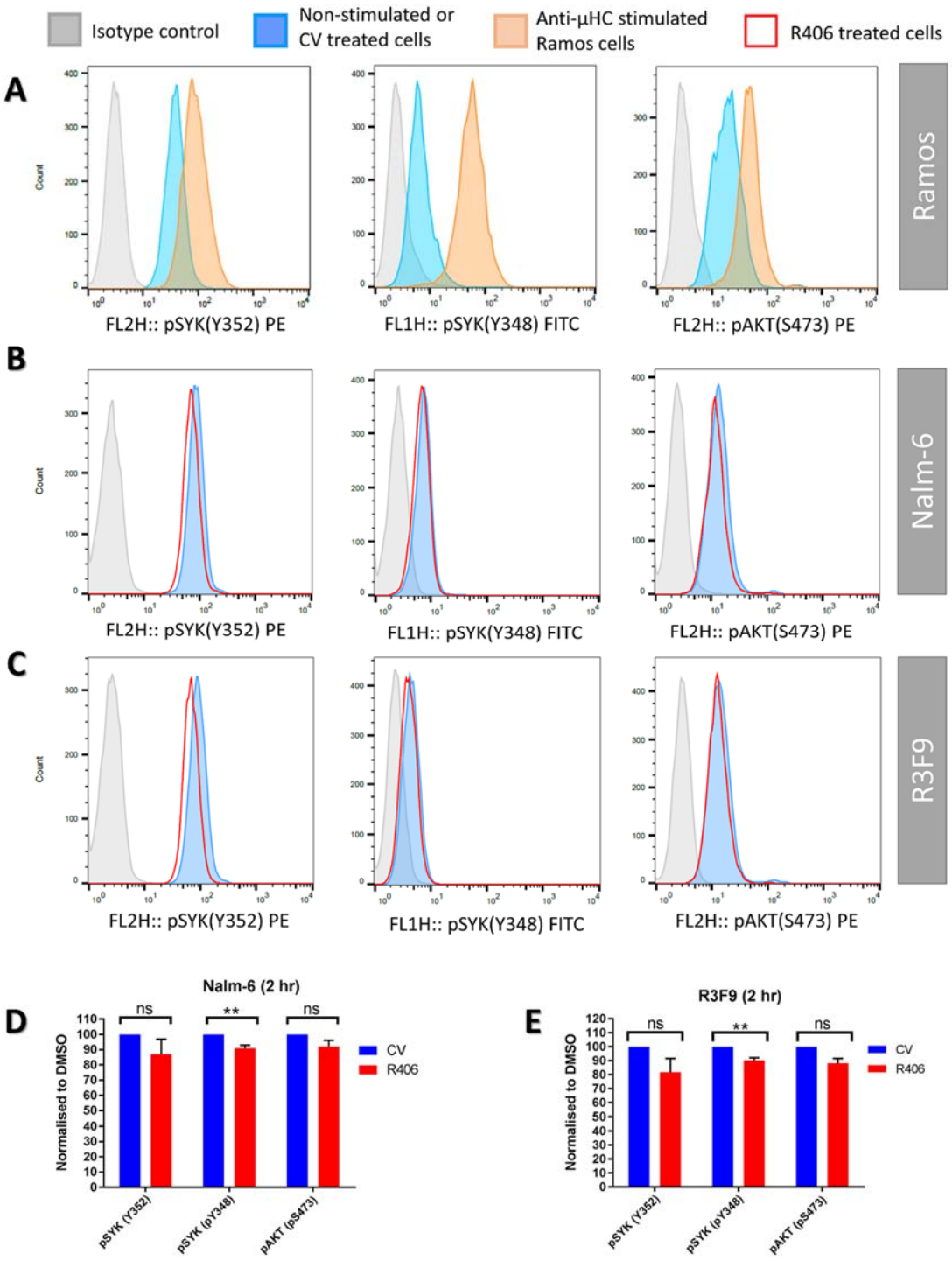

Figure 4.16: The pharmacodynamic effects of R406 on BCP-ALL cell lines.

Intracellular staining [pSYK (Y352), pSYK (Y348) and pAKT(S473)] and acquisition on a FACSCalibur were carried out following incubation of Nalm-6 and R3F9 with their relevant R406 GI_{50} concentrations. **(A)** Overlay histograms showing Ramos cells stimulation by F(ab)2 anti-μHC antibody for all targets and were used as positive controls. **(B)** Histograms show targets inhibition in Nalm-6 cells treated with DMSO (CV) or 3μM R406 for 2 hours. **(C)** Histograms depict pharmacological targets inhibition in R3F9 cells incubated with CV or 6μM R406 for 2 hours. Bar charts represent the mean ± SEM (n=2-4) of Nalm-6 **(D)** and R3F9 **(E)**. FlowJo software was used to perform histograms overlays. Student`s t-test was carried out to calculate p values. p>0.05 not significant (ns), **p<0.01.

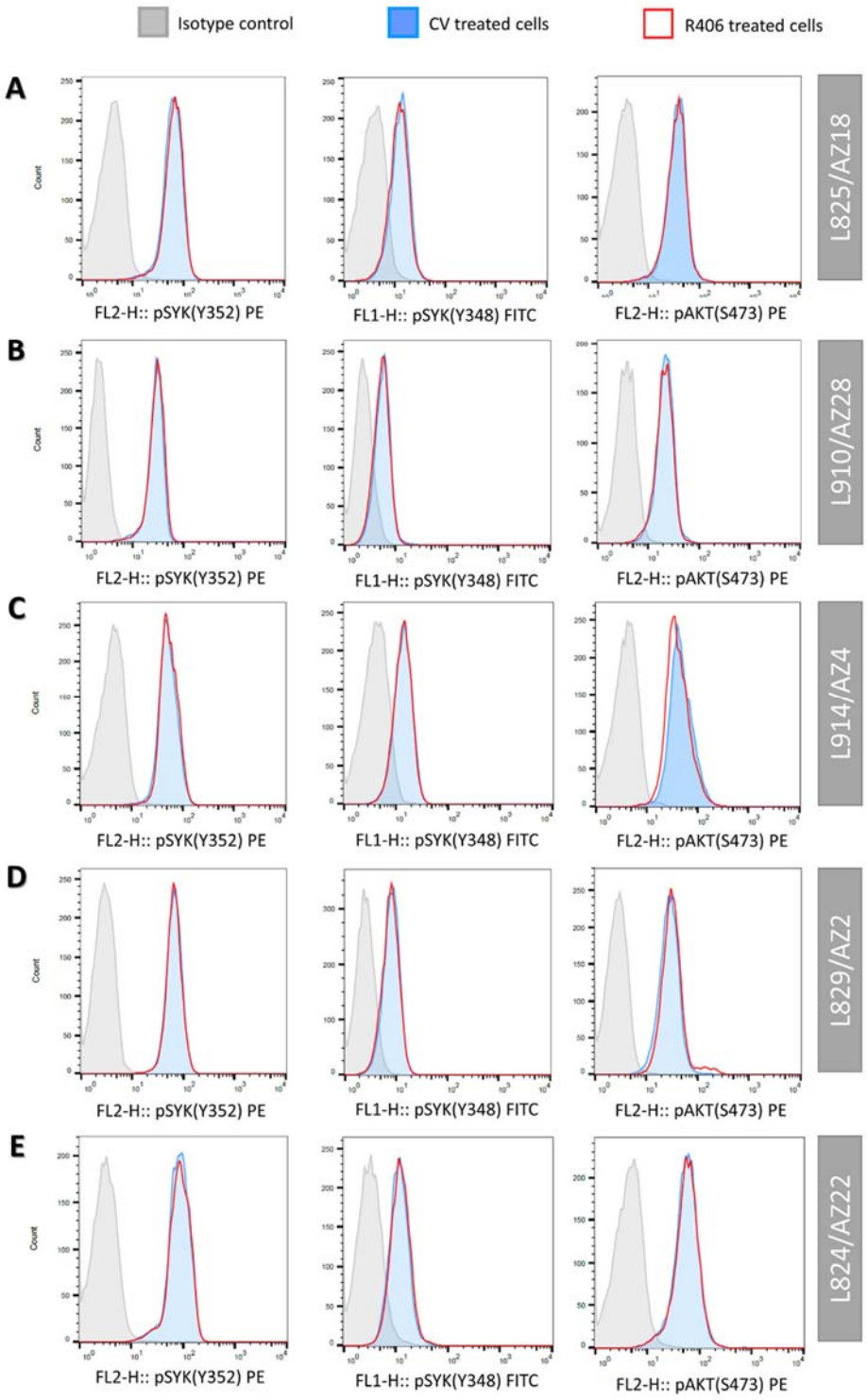

Figure 4.17: The pharmacodynamic effects of R406 on BCP-ALL PDX cells.

Intracellular staining [pSYK (Y352), pSYK (Y348) and pAKT(S473)] and acquisition on a FACSCalibur were carried out following incubation of PDX cells with their relevant R406 GI_{50} concentrations. Histogram overlays of **(A)** L825/AZ18 (56nM), **(B)** L910/AZ28 (1.75µM), **(C)** L914/AZ4 (120nM), **(D)** L829/AZ2 (5.12µM) and **(E)** L824/AZ22 (500nM) cells exposed to R406 for 2 hours. FlowJo software was used to perform histograms overlays. Ramos cells stimulation by F(ab)2 anti-µHC antibody of all targets were used as positive controls.

4.5 Effect of dasatinib (BCR-ABL/SRC inhibitor) on BCP-ALL cells

4.5.1 Effect of dasatinib on BCP-ALL cells viability

Recently, dasatinib, the multi-kinase inhibitor, was approved by FDA for the treatment of CML and Ph positive adult ALL (Kantarjian *et al.*, 2010a; Foa *et al.*, 2011). Moreover, preclinical and clinical data evidenced that dasatinib was also effective in Ph-like and t(1;19) ALL (Bicocca *et al.*, 2012; Kobayashi *et al.*, 2015; Welsh *et al.*, 2017). To this end, the viability effect of dasatinib on high risk BCP-ALL cells which had different genetic alterations were investigated *in vitro*. Five cell lines and 29 PDX samples (derived from cells of 15 ALL patients) were exposed to a dose range of dasatinib (Table 2.9) for 96 hours followed by Alamar blue assay (Section 2.5.1). Pre-BCR harbouring cell lines (PreB 697, Nalm-6 and R3F9) showed sensitivity to dasatinib treatment (Mean GI_{50} 2.95µM, range 2.45 -3.81µM) which was greater than Pre-BCR^- cells (REH) or TK6 (Mean GI_{50} 15.31µM, range 12.49-18.13µM) (Figure 4.18 A, figure 4.19 and table 4.9). Consistent with the cell lines, 2 out of 3 Pre-BCR^+ PDX samples (L825 presentation and L910 presentation) were remarkably sensitive to dasatinib (Mean GI_{50} 159nM, range 147-171nM), furthermore, the Ph positive and Ph-like (PDGFR) Pre-BCR^- samples (L4951 presentation and L824 presentation respectively) were very sensitive to dasatinib treatment (Mean GI_{50} 53.7nM, range 8.9-98.5nM) among 12 Pre-BCR^- samples (Figure 4.18 B, C, figure 4.19 and table 4.9). The sensitive Pre-BCR^+ samples had different genetic alterations including *c-CBL* (L825 presentation) and *TCF3-PBX1* (L910 presentation) (Table 2.13). Again consistent GI_{50} values were obtained in all replicates PDXs of all patient materials.

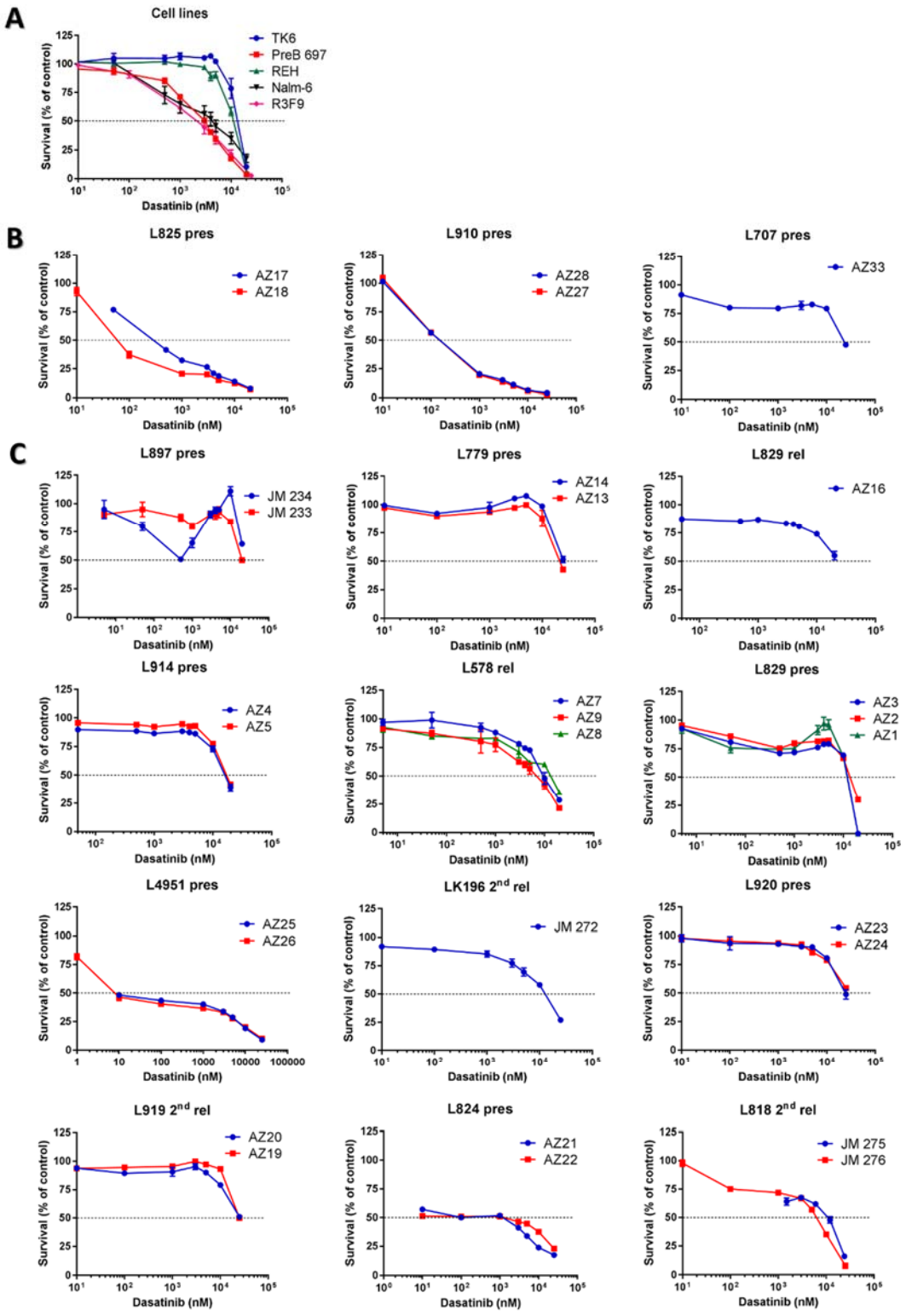

Figure 4.18: The survival curves of BCP-ALL cells treated with dasatinib for 4 days.

Five cell lines **(A)**, 3 Pre-BCR$^+$ and 12 Pre-BCR$^-$ patient samples **(B and C)** were cultured in the existence of dose escalation of dasatinib for 96 hours before measuring viability by Alamar blue assay. Curve points of cell lines graph **(A)** represent the mean of 3 independent experiments ± SEM, whereas only one test was achievable in each individual PDX material and error bars represent the mean of 3 different wells ± SEM **(B and C)**. Each patient sample was amplified into 1-3 PDX replicates. Data were analysed by GraphPad prism software.

Cells	GI_{50} Mean ± SEM (Dasatinib µM)	Number of replicates
* TK6	18.13 ± 3.56	3
* PreB 697	2.59 ± 0.35	3
* Nalm-6	3.81 ± 1.98	3
* R3F9	2.45 ± 0.86	3
L825 pres	0.171 ± 0.113	2
L910 pres	0.147 ± 0.003	2
L707 pres	22.80	1
* REH	12.49 ± 0.73	3
L897 pres	> 20	2
L779 Pres	24.9 ± 0.1	2
L578 rel	9.87 ± 1.92	3
L829 rel	20.00	1
L914 pres	16.4 ± 0.5	2
L829 pres	12.80 ± 0.65	3
L4951 pres	0.0089 ± 0.0011	2
LK196 2nd rel	12.58	1
L920 pres	24.65 ± 0.35	2
L919 2nd rel	24.7 ± 0.2	2
L824 pres	0.0985 ± 0.0015	2
L881 2nd rel	8.51 ± 2.29	2

Table 4.9: A list of mean GI_{50} concentrations for BCP-ALL cells treated with dasatinib.

Cells were incubated with dose escalation of dasatinib for 96 hours before measurement of viability by Alamar blue assay. Mean GI_{50}s were calculated from 3 independent replicates of 5 cell lines (asterisks) or 30 PDX replicates derived from 15 patient samples ± SEM.

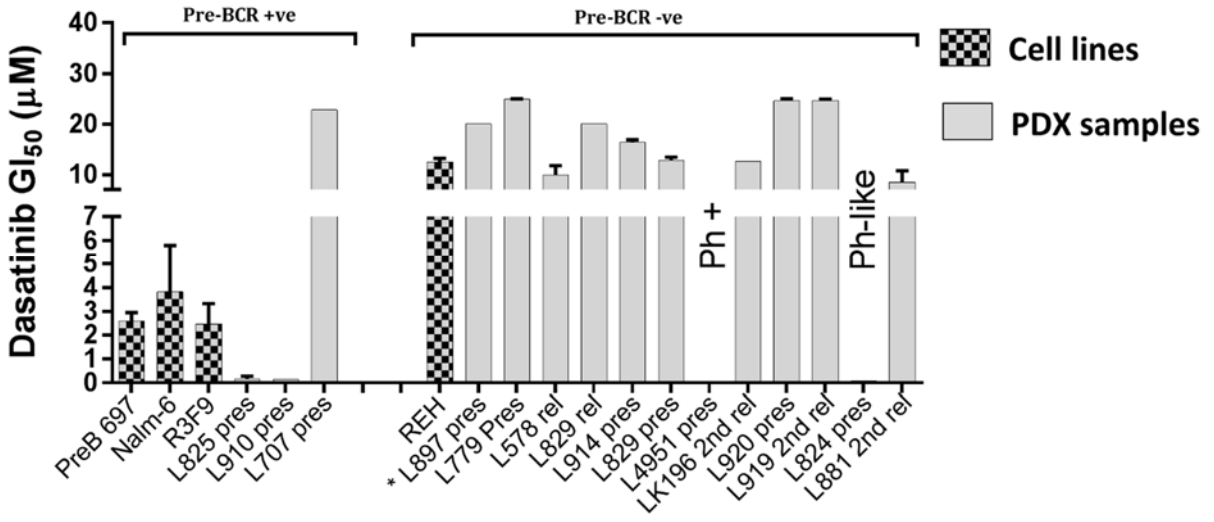

Figure 4.19: Mean GI_{50}s of cell lines and PDX cells incubated with dasatinib for 96 hours.

Cell lines and PDX cells were exposed to a concentration range of dasatinib for 96 hours. Alamar blue assay was subsequently performed to assess cell viability. The bar chart shows the mean of GI_{50}s of cell lines (n=4) and PDX samples (n=15). Three independent replicates were used to calculate the mean GI_{50} ± SEM. However, each patient sample was amplified into 1-5 PDX sample and hence mean GI_{50}s were calculated ± SEM. Asterisk denotes sample for which the GI_{50} was not reached. GraphPad prism software was used to calculate the GI_{50}s.

4.5.2 Effect of dasatinib on cell cycle profile of BCP-ALL cell lines

To further understand the inhibitory mechanism of dasatinib on BCP-ALL cells, propidium iodide staining was performed to measure the distribution of cell cycle phases by flow cytometry (Section 2.3.3). To this end, PreB 697 (n=3), Nalm-6 (n=3), R3F9 (n=2) and REH (n=1) were co-cultured with their relevant GI_{50} concentrations (3µM, 5µM, 2.5µM and 13µM respectively) for 24 and 48 hours (Figures 4.20, 4.21 and tables 4.10-4.12).

The cell cycle analyses in PreB 697 cells showed a mild but significant increase in the percentage of cells arrested at G1-phase at 24 hour time point (% of cells in G1, CV: 35.53 ± 0.75% versus dasatinib: 40.17 ± 1.22%; $p<0.05$) and a concomitant 3 fold reduction in ratio of cells arrested at the G2-phase (% of cells in G2, CV: 14.9 ± 0.15% versus dasatinib: 5.12 ± 1.08%; $p<0.001$) (Figure 4.20 A and table 4.10). Similarly, a G1 arrest was maintained in cells dosed with dasatinib for 48 hours (% of cells in G1, CV: 36.83 ± 0.42% versus dasatinib: 48.73 ± 1.27%; $p<0.001$) which was associated with significant reduction in the ratio of cells at S-phase (% of cells in S, CV: 49.43 ± 0.31% versus dasatinib: 41.3 ± 1.2%; $p<0.01$) and the G2-phase (% of

cells in G2, CV: 18.63 ± 0.48% versus dasatinib: 6.043 ± 0.67%; $p<0.01$) (Figure 4.20 A and table 4.10).

In Nalm-6 cells, dasatinib treatment for 24 hours induced arrest at S-phase (% of cells in S, CV: 42.73 ± 1.3% versus dasatinib: 47.03 ± 0.38%; $p<0.05$) with concomitant decrease in the percentage of cells at G2-phase (% of cells in G2, CV: 18.63 ± 0.48% versus dasatinib: 11.67 ± 1.02%; $p<0.01$). However, only G1 arrest was observed in Nalm-6 cells left with dasatinib for 48 hours (% of cells in G1, CV: 33.6 ± 1.85% versus dasatinib: 47.20 ± 0.56%; $p<0.01$) (Figure 4.20 B and table 4.11).

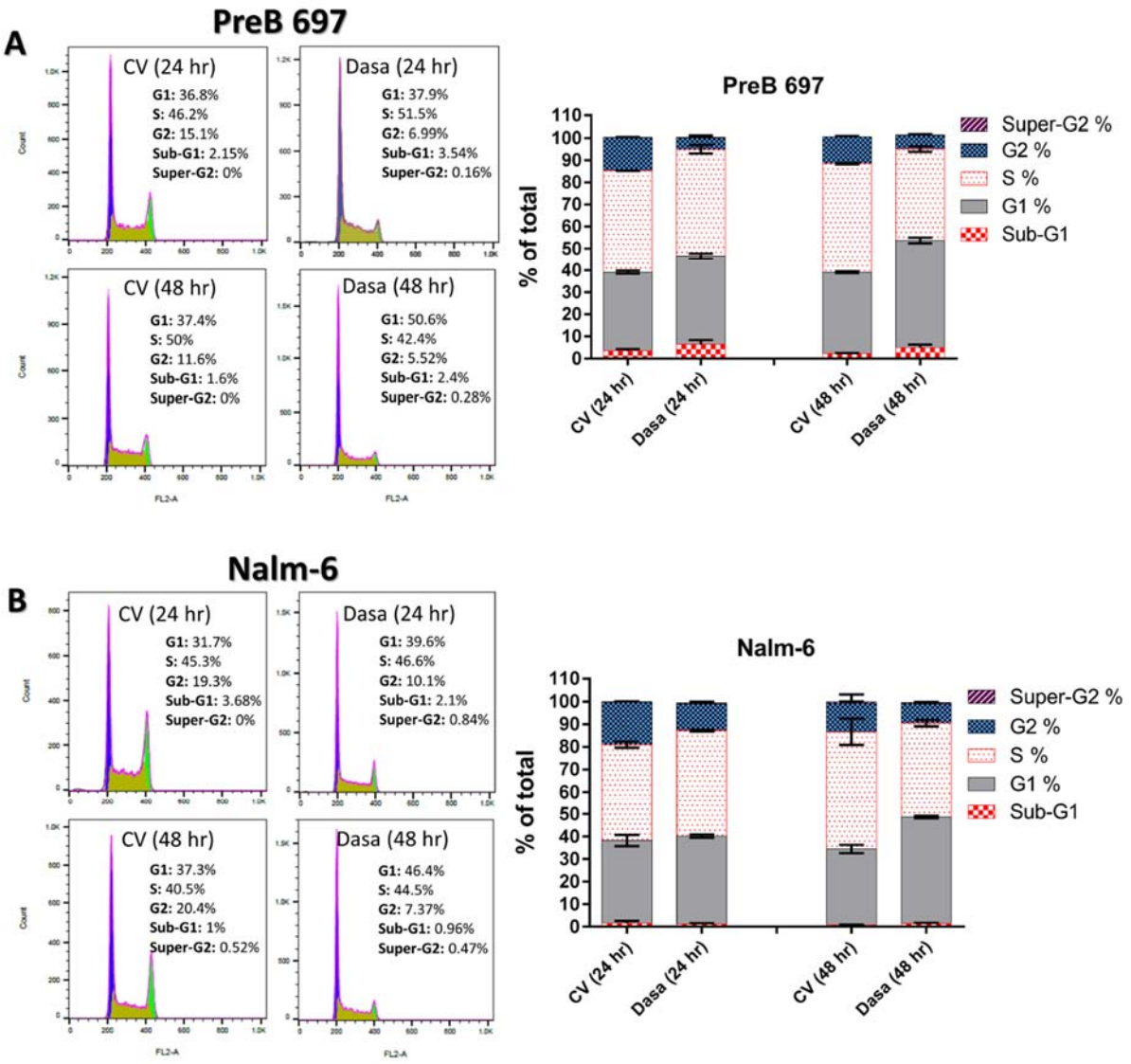

Figure 4.20: The effect of dasatinib treatment on cell cycle distribution of PreB 697 and Nalm-6 cell lines.

Cell cycle phases were assessed by flow cytometry using propidium iodide staining after exposing **(A)** PreB 697, **(B)** Nalm-6 cell lines to their relevant dasatinib GI_{50}s (3µM and 5µM respectively) for 24 and 48 hours. Histograms of one representative cell cycle run of 3 independent experiments were presented. The bar graphs show the mean percentage of cells distributed at different phases of the cell cycle ± SEM (n=3) **(A).** FlowJo software was used to analyse cell cycle data.

Cell cycle phase	Mean ± SEM (n=3)		p-value	Time point
	CV	Dasatinib		
Sub-G1 %	3.55 ± 0.78	6.42 ± 1.93	0.2422	24 hours
G1 %	35.53 ± 0.75	40.17 ± 1.22	0.0321 *	
S %	46.17 ± 0.03	48.33 ± 1.91	0.3201	
G2 %	14.9 ± 0.15	5.12 ± 1.08	0.0009 ***	
Super-G2 %	0.19 ± 0.11	0.31 ± 0.08	0.4421	
Sub-G1 %	2.2 ± 0.32	5.02 ± 1.32	0.1075	48 hours
G1 %	36.83 ± 0.42	48.73 ± 1.27	0.0009 ***	
S %	49.43 ± 0.31	41.3 ± 1.2	0.0028 **	
G2 %	12.13 ± 0.31	6.043 ± 0.67	0.0012 **	
Super-G2 %	0.0 ± 0.0	0.21 ± 0.11	0.1237	

Table 4.10: Percentages of PreB 697 cells distributed at different cell cycle phases after treatment with dasatinib.

Cell cycle phases were assessed by flow cytometry using propidium iodide staining after exposing PreB 697 cells to 3µM of dasatinib or DMSO (CV) for 24 and 48 hours. Mean percentages of different cell cycle phases were calculated from 3 independent experiments ± SEM. FlowJo software was used to analyse cell cycle data. Student`s t-test was carried out to calculate p values. P>0.05 not significant, *p< 0.05, **p<0.01, ***p<0.001.

Cell cycle phase	Mean ± SEM (n=3)		p-value	Time point
	CV	Dasatinib		
Sub-G1 %	1.57 ± 1.05	1.19 ± 0.45	0.7558	24 hours
G1 %	36.63 ± 2.46	38.93 ± 0.66	0.4191	
S %	42.73 ± 1.3	47.03 ± 0.38	0.0345 *	
G2 %	18.63 ± 0.48	11.67 ± 1.02	0.0036 **	
Super-G2 %	0.29 ± 0.13	0.46 ± 0.19	0.5194	
Sub-G1 %	0.84 ± 0.08	1.45 ± 0.31	0.1366	48 hours
G1 %	33.6 ± 1.85	47.20 ± 0.56	0.0022 **	
S %	52.17 ± 5.83	41.83 ± 1.41	0.1604	
G2 %	12.5 ± 3.94	8.45 ± 0.6	0.3684	
Super-G2 %	0.63 ± 0.26	0.59 ± 0.17	0.9049	

Table 4.11: Percentages of Nalm-6 cells distributed at different cell cycle phases after treatment with dasatinib.

Cell cycle phases were assessed by flow cytometry using Propidium iodide staining after exposing Nalm-6 cells to 5µM of dasatinib or DMSO (CV) for 24 and 48 hours. Mean percentages of different cell cycle phases were calculated from 3 independent experiments ± SEM. FlowJo software was used to analyse cell cycle data. Student`s t-test was carried out to calculate p values. p>0.05 not significant, *p< 0.05, **p<0.01.

Concerning R3F9 cells, no statistically significant changes in cell cycle profile were observed after 24 hours incubation with dasatinib. However, G1 arrest was induced after 48 hours (% of cells in G1, CV: 38.20 ± 1.4% versus dasatinib: 46.05 ± 0.85%; $p<0.05$) which was associated with a decrease in the ratio of cells arrested at S-phase (% of cells in S, CV: 50.05 ± 0.05% versus dasatinib: 46.10 ± 0.2%; $p<0.01$) and at sub-G1 phase (% of cells in sub-G1, CV: 0.57 ± 0.01% versus dasatinib: 1.08 ± 0.08%; $p<0.05$) (Figure 4.21 A and table 4.12).

As shown in figure (4.21 B), G1-arrest was induced in REH cells following 24 hours (% of cells in G1, CV: 37.1% versus dasatinib: 44.5%) in addition to relatively high ratio of cells at sub-G1 (% of cells in sub-G1, CV: 1.94% versus dasatinib: 11%) and this was associated with reduction in S and G2 phases. At 48 hours, the ratio of cells at sub-G1 was maintained (% of cells in sub-G1, CV: 0.59% versus dasatinib: 11.7%) which was associated with a reduction in S (% of cells in S, CV: 44.1% versus Dasatinib: 36.4%) and G2 (% of cells in G2, CV: 10.1% versus dasatinib: 5.93%) phases (Figure 4.21 B). Taken together, dasatinib treatment induced significant G1 arrest in both Pre-BCR$^+$ and Pre-BCR$^-$ cell lines.

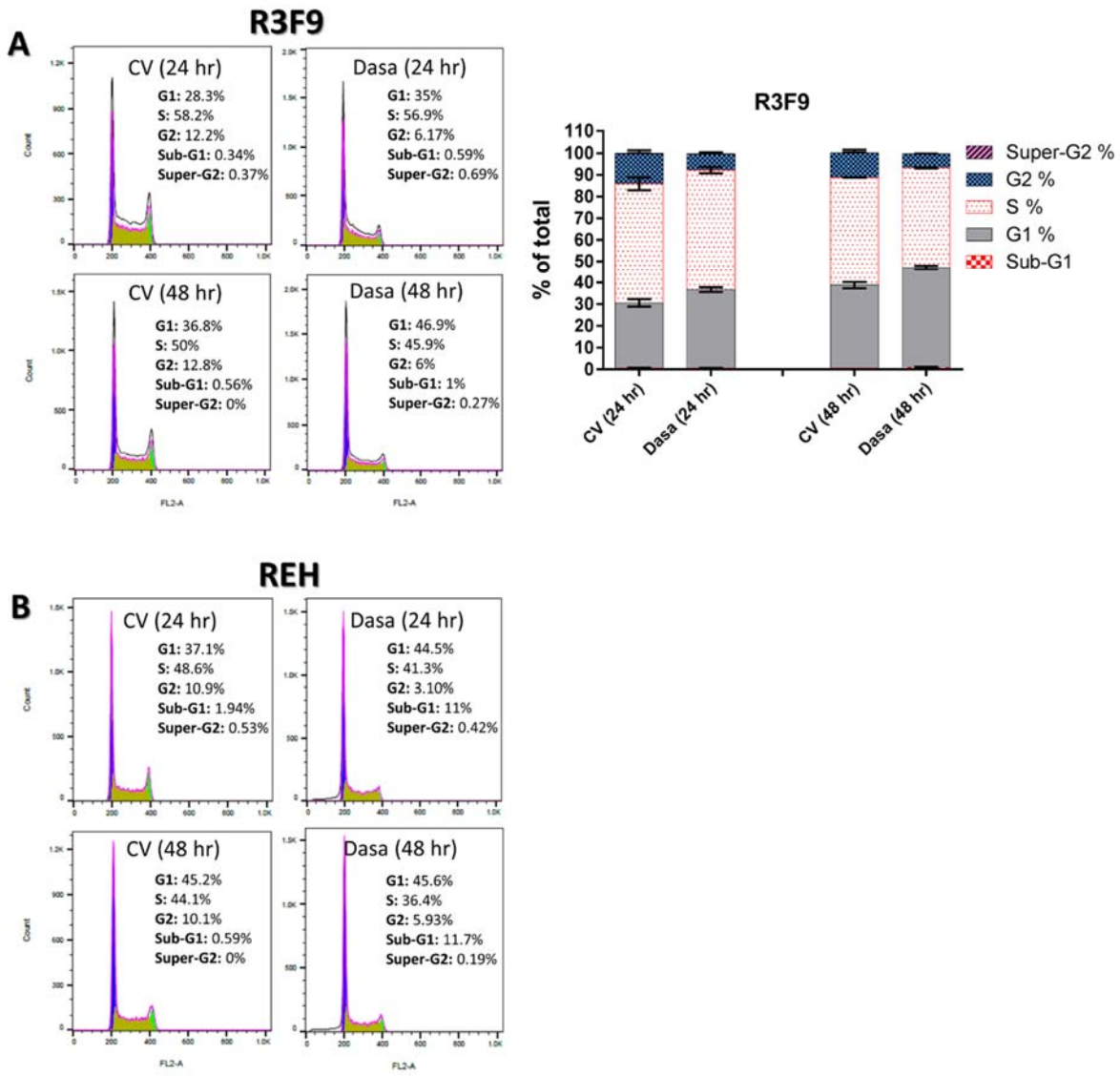

Figure 4.21: The effect of dasatinib treatment on cell cycle distribution of R3F9 and REH cell lines.

Cell cycle phases were assessed by flow cytometry using propidium iodide staining after exposing **(A)** R3F9, **(B)** REH cell lines to their relevant dasatinib GI_{50}s (2.5µM and 13µM respectively) for 24 and 48 hours. Histograms of one representative cell cycle run of 3 independent experiments were presented. The bar graph shows the mean percentage of cells distributed at different phases of the cell cycle ± SEM (n=3). FlowJo software was used to analyse cell cycle data.

Cell cycle phase	Mean ± SEM (n=2)		p-value	Time point
	CV	Dasatinib		
Sub-G1 %	0.58 ± 0.24	0.62 ± 0.03	0.8839	**24 hours**
G1 %	30 ± 1.7	36.1 ± 1.1	0.0948	
S %	55.3 ± 3	55.45 ± 1.45	0.9682	
G2 %	13.85 ± 1.65	7.15 ± 0.98	0.0732	
Super-G2 %	0.18 ± 0.18	0.36 ± 0.32	0.6755	
Sub-G1 %	0.57 ± 0.01	1.08 ± 0.08	0.0241 *	**48 hours**
G1 %	38.20 ± 1.4	46.05 ± 0.85	0.0409 *	
S %	50.05 ± 0.05	46.10 ± 0.2	0.0027 **	
G2 %	11.22 ± 1.58	6.27 ± 0.27	0.0917	
Super-G2 %	0.12 ± 0.09	0.25 ± 0.01	0.3118	

Table 4.12: Percentages of R3F9 cells distributed at different cell cycle phases after treatment with dasatinib.

Cell cycle phases were assessed by flow cytometry using propidium iodide staining after exposing R3F9 cells to 13µM of dasatinib or DMSO (CV) for 24 and 48 hours. Mean percentages of different cell cycle phases were calculated from 2 independent experiments ± SEM. FlowJo software was used to analyse cell cycle data. Student`s t-test was carried out to calculate p values. *p< 0.05, **p<0.01.

4.5.3 The apoptotic effect of dasatinib on BCP-ALL cell lines

To further evaluate the effect of dasatinib on cell growth, Annexin V-FITC staining (Section 2.3.2) was performed to measure programmed cell death in PreB 697 cells by flow cytometry. PreB 697 cells were co-cultured in the presence of the GI_{50} concentration of dasatinib (3µM) and apoptosis was measured after 48 and 72 hours (Figure 4.22). At both time points, a small increase in the percentage of apoptotic cells was observed and was only significant at 72 hours (CV: 1.65 ± 0.21% versus dasatinib: 2.96 ± 0.19%; p<0.05) (Figure 4.22 B). These data indicate that dasatinib does not induce cell death in PreB 697 cell line at the GI_{50} concentration of dasatinib and therefore cytostatic which confirms the cell cycle data described above.

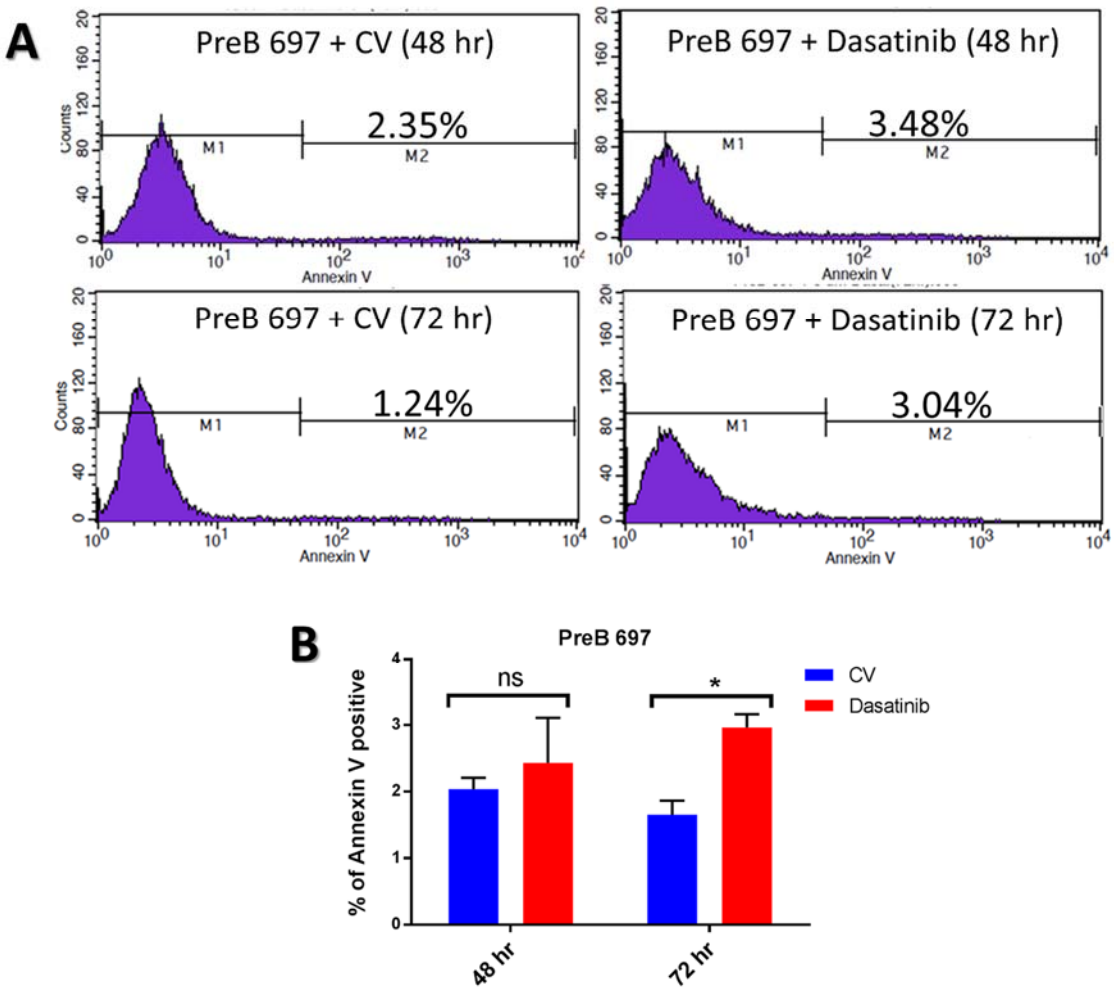

Figure 4.22: Dasatinib does not induce apoptosis in PreB 697 cell line.

PreB 697 cells were cultured for 48, 72 hours with the control vehicle or dasatinib (3µM) followed by Annexin V-FITC staining and assessment by flow cytometry. **(A)** Representative histograms are shown for the two time points. **(B)** Bar graph chart denoting the mean ± SEM (n=3). CellQuest software was used to analyse Annexin V data. Student`s t-test was carried out to calculate p values. p> 0.05 not significant, *p<0.05.

4.5.4 Pharmacodynamic effects of dasatinib on BCP-ALL cells

In order to understand the mechanism of action of dasatinib seen in BCP-ALL cells, the potential pharmacological targets [pBTK(Y223), pSYK(Y348), pBLNK(Y84) and pPLC-γ2(Y759)] were investigated by intracellular phospho-flow cytometry (Section 2.3.5). Stimulation of Ramos cells with anti-μHC (20μg/ml for 4 minutes) was used as positive control for targets activation (Figure 4.23 A). Ramos cells were run side by side with all experiments of cell lines and dasatinib-sensitive PDX samples (Figures 4.23 and 4.24).

PreB 697 and Nalm-6 cells were co-cultured in the presence of dasatinib using their relevant GI_{50} concentrations (3μM and 5μM respectively). Interestingly, all investigated phospho-proteins were significantly inhibited after 24 hours incubation of both cell lines (Figure 4.23) with the multi-kinase inhibitor. Basal phosphorylation levels of dasatinib-treated PreB 697 were reduced to 28.02 ± 2.3% for pBTK, 57.58 ± 2.32% for pSYK(Y348), 61.69 ± 3.18% for pBLNK(Y84) and 57.87 ± 3.61 for pPLC-γ2(Y759) when compared to CV treated cells (100 % basal phosphorylation) and p values ranged between $p<0.01$ to $p<0.0001$ (Figure 4.23 B and D). Moreover, the degree of phosphorylation inhibition in Nalm-6 cells was similar to that in PreB 697 in different phospho targets [27.87 ± 2.39% in pBTK(Y223), 58.54 ± 4.72% in pSYK(Y348), 68.73 ± 3.85 in pBLNK(Y84) and 66.48 ± 0.61 in pPLC-γ2(Y759) and p values ranged between $p<0.05$ to $p<0.0001$] (Figure 4.23 C and E).

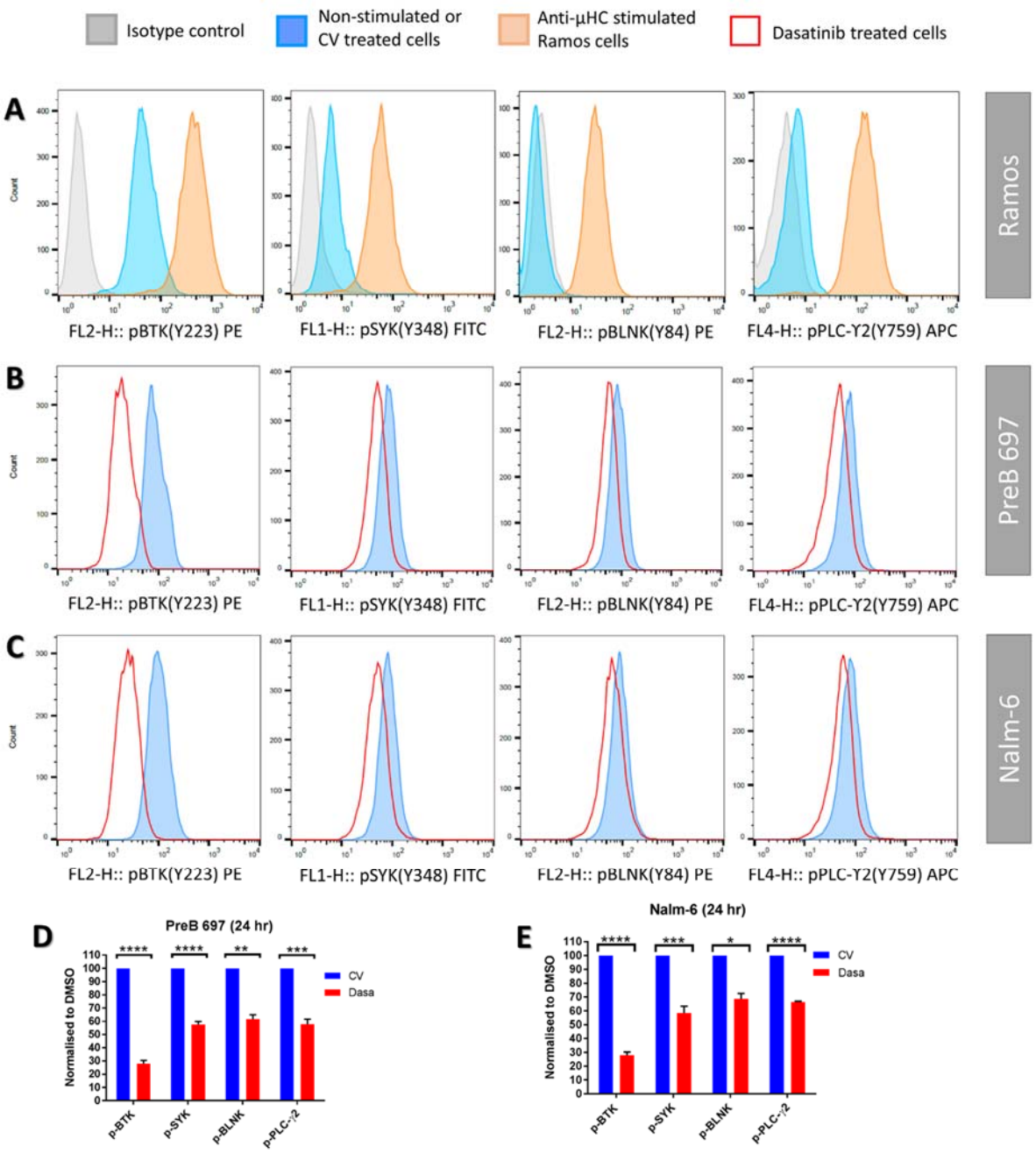

Figure 4.23: The pharmacodynamic effects of dasatinib on BCP-ALL cell lines.

Intracellular staining [pBTK (Y223), pSYK (Y348), pBLNK (Y84) and pPLC-γ2(Y759)] and acquisition on a FACSCalibur were carried out following incubation of PreB 697 and Nalm-6 with their relevant dasatinib GI_{50} concentrations for 24 hours. **(A)** Overlay histograms showing Ramos cells stimulation by F(ab)2 anti-µHC antibody of all targets which were used as positive controls. **(B)** Histograms show target inhibition in PreB 697 cells treated with DMSO (CV) or 3µM dasatinib. **(C)** Histograms depict pharmacological targets inhibition in Nalm-6 cells incubated with CV or 5µM dasatinib. Bar charts represent the mean ± SEM (n=2-3) of PreB 697 **(D)** and Nalm-6 **(E)**. FlowJo software was used to make histograms overlays. Student`s t-test was used to calculate p values. *p< 0.05, **p<0.01, ***p<0.001 and ****p<0.0001.

The pharmacodynamic effects of dasatinib were also investigated in PDX cells. The dasatinib-sensitive PDX samples taken from newly harvested spleens were incubated with the pre-defined GI_{50} concentrations of previously harvested PDX replicate(s) injected with the same patient cells. L825/AZ18, L910/AZ28, L4951/AZ25 and L824/AZ22 were co-cultured with the pre-defined GI_{50} concentrations of dasatinib (58nM, 150nM, 120nM, 10nM and 100nM respectively) for 24 hours (Figure 4.24). Generally, a similar trend of inhibition of multiple phospho protein targets was seen in PDX cells. The percentage reduction in pBTK was comparable to that in cell lines (Mean: 51 %, range: 32 -71%), however, less inhibition was observed in pSYK(Y348) (Mean: 82%, range: 57-97%) and pPLC-γ2(Y759) (Mean: 73%, range: 43-90%) (Figure 4.24 A-D and table 4.13). In addition, a minimal inhibition was observed in BLNK, L910/AZ28 (92%) and L4951/AZ25 (81%) (Figure 4.24 B, C and table 4.13).

In summary, dasatinib inhibits several phospho-proteins downstream of Pre-BCR signalling in both Pre-BCR^+ and Pre-BCR^- cells.

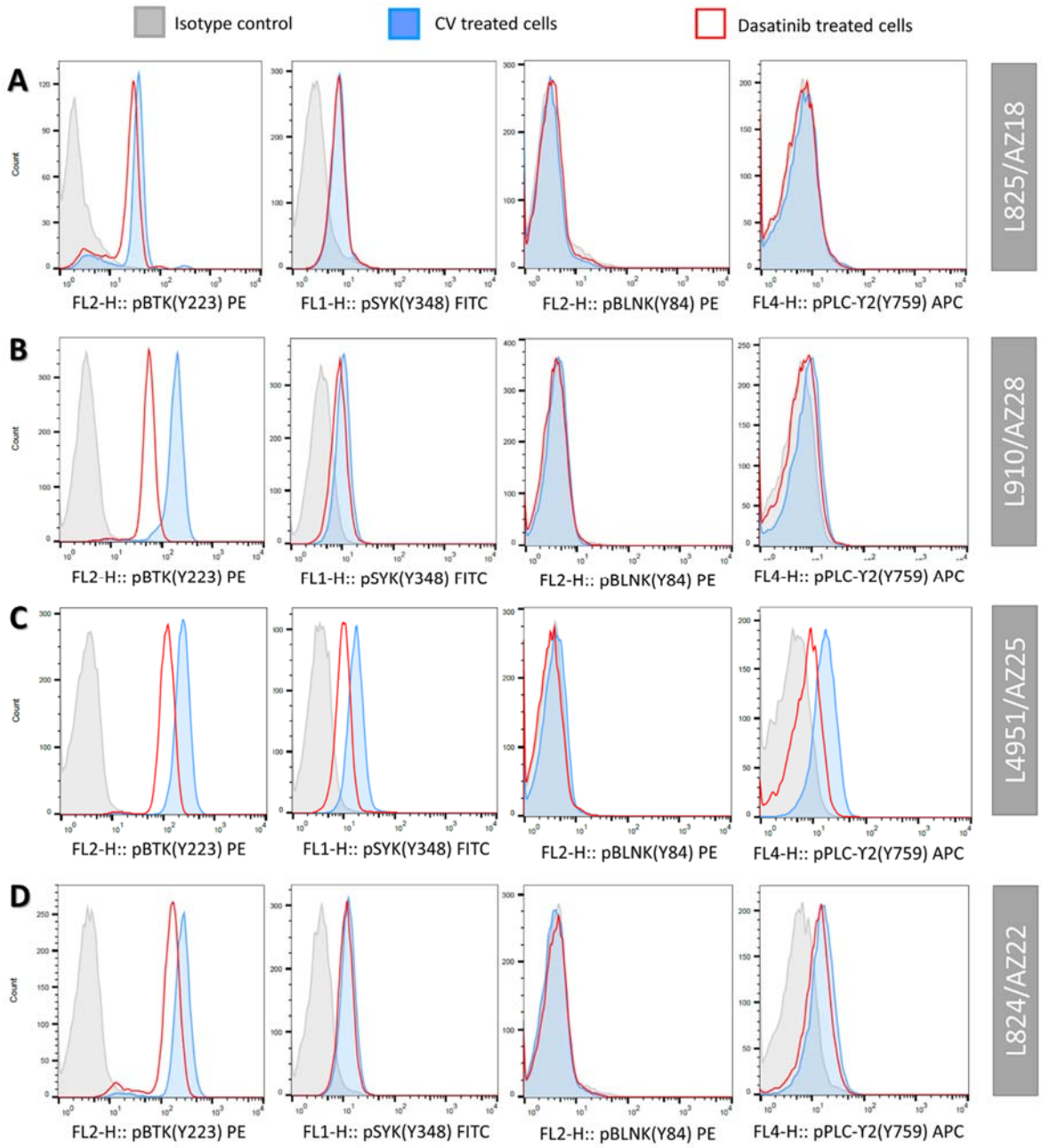

Figure 4.24: The pharmacodynamic effects of dasatinib on BCP-ALL PDX cells.

Intracellular staining [pBTK (Y223), pSYK (Y348), pBLNK (Y84) and pPLC-γ2(Y759)] and acquisition on a FACSCalibur were performed following incubation of PDX cells with their relevant dasatinib GI_{50} concentrations. Histogram overlays of **(A)** L825/AZ18 (58nM), **(B)** L910/AZ28 (150nM), **(C)** L4951/AZ25 (10nM) and **(D)** L824/AZ22 (100nM) PDX cells exposed to dasatinib for 24 hours. FlowJo software was used to generate histograms overlays. Ramos cells stimulation by F(ab)2 anti-μHC antibody of all targets were considered as positive controls.

PDX sample	(Dasatinib treated MFI/CV treated MFI) *100%			
	pBTK %	pSYK %	pBLNK %	pPLC-ϒ2 %
L825/AZ18	71.02	97.95	110.13	90.83
L910/AZ28	32.04	83.43	92.56	80.00
L4951/AZ25	49.78	57.06	81.38	43.25
L824/AZ22	51.46	91.27	106.42	79.87

Table 4.13: The percentages of pharmacological targets inhibition in PDX cells following co-culture with dasatinib.

The percentage of pBTK (Y223), pSYK (Y348), pBLNK (Y84) and pPLC-ϒ2(Y759) inhibition following incubation of PDX cells with their relevant dasatinib GI_{50} concentrations or CV for 24 hours. FlowJo software was used to calculate mean fluorescent intensities (MFIs). The MFI ratio for each phospho-protein was calculated (MFI of dasatinib treated cells/MFI of CV treated cells) and then multiplied by 100% to represent the percentage of signal inhibition.

4.6 Discussion

Sustained activation of kinase signalling in cancer cells has led to the development of TKI inhibitors, and tyrosine kinases activation is used as a predictive biomarker of response to different TKIs (De Luca and Normanno, 2010; Li *et al.*, 2015; Maude *et al.*, 2015). Some TKI inhibitors have demonstrated efficacy in certain haematological malignancies and were associated with less toxicity than traditional chemotherapies (Young and Staudt, 2013; Buchner and Muschen, 2014; Muschen, 2015; Trimarchi and Aifantis, 2015). Previous data from our laboratory has shown that the RAS pathway was constitutively activated in a high proportion of ALL, as measured by pERK levels, and was predictive of response to selumetinib (MEK inhibitor) both *in vitro* and *in vivo* (Irving *et al.*, 2014). This robust data set has prompted phase I/II clinical trials of selumetinib in multiple relapsed/ refractory ALL and lends credence to the experimental approach used in the study presented here.

The aim of this chapter was to investigate the effect of four TKI inhibitors, already used in the clinic, with some being FDA approved, in BCP-ALL cell lines and PDX samples from relapse or high risk groups. PDX samples were generated to bulk up the amount of cells available for experiments and have been shown by other groups to recapitulate the genotype and phenotype of the primary leukaemias from which they were derived and importantly for this project, drug response (Lee *et al.*, 2007; Samuels *et al.*, 2010; Wong *et al.*, 2014; Wang *et al.*, 2017). The PDX model also enables drugs that show promising *in vitro* activity to undergo *in vivo* efficacy studies (Tentler *et al.*, 2012; Siolas and Hannon, 2013; Hidalgo *et al.*, 2014). Therefore, this study addressed the effects of each TKI inhibitor (CAL-101, ibrutinib, R406 and dasatinib) on viability, cell cycle, apoptosis and pharmacodynamic action.

CAL-101 or idelalisib has shown clinical activity in patients with relapsed CLL and NHL and was well tolerated. Recently, promising preclinical *in vitro* activity of CAL-101 was seen in relapsed *TCF3-PBX1* ALL cells (Meadows *et al.*, 2012; Jabbour *et al.*, 2014; Do *et al.*, 2016; Eldfors *et al.*, 2017; Slinger *et al.*, 2017). In the data presented here, the *in vitro* sensitivity results revealed that all cell lines were resistant to CAL-101. Moreover, The GI_{50}s of one Pre-BCR^+ and Pre-BCR^- PDX samples were within the clinically bioavailable concentration [C_{max} = 5180nM (Liston and Davis, 2017)]. Interestingly, both samples housed *c-CBL* mutation which is an ubiquitin ligase that regulates several signalling pathways including JAK-STAT, RAS and PI3K and has been reported to be mutated in ALL (Nicholson *et al.*, 2012). Mutations of this gene are more

commonly found in chronic myelomonocytic leukaemia and mutated cells show sensitivity to CAL-101 both *in vitro* and in a mouse model (Nakata *et al.*, 2017). While basal phosphorylation of AKT was significantly higher in Pre-BCR$^+$ than Pre-BCR$^-$ PDX cells, this did not confer sensitivity to CAL-101 and conflicts with preclinical data from other laboratories suggested that CAL-101 was effective in *TCF3-PBX1* positive BCP-ALL cells which express Pre-BCR on their surfaces (Geng *et al.*, 2015; Eldfors *et al.*, 2017). In cell lines, CAL-101 led to cell cycle arrest at the G1 phase which has been observed by others in BCP-ALL Nalm-6 cell line (Safaroghli-Azar *et al.*, 2017), however, CAL-101 appeared cytostatic in this cell lines and did not lead to the induction programmed cell death unlike what has been observed in cell lines from more differentiated B cell tumors (Herman *et al.*, 2010; Lannutti *et al.*, 2011). Surprisingly, the pharmacodynamics data indicated inhibition of pAKT only at high CAL-101 doses (doses applied for cell lines), while the more sensitive PDX cells incubated with low inhibitor doses (GI_{50}s) were not associated with target inhibition and may suggest an off target effect in these cells (Table 4.14).

PI3K Kinase	IC_{50} at 5-10000 nM
p110α	820
p110β	565
p110δ	2.5
p110ɣ	89

Table 4.14: A list of PI3K kinases inhibited by CAL-101 using an *in vitro* kinase assay.

Kinase binding experiments were performed in the existence of 5-10000nM of CAL-101 followed by determination of the maximal inhibitory concentration (IC_{50}). Data adapted from (Lannutti *et al.*, 2011).

It has been proven that ibrutinib interferes with the replication of BCR positive malignant cells both preclinically and clinically (Herman *et al.*, 2014a; Herman *et al.*, 2014b; Burger *et al.*, 2017). Interestingly, three PDX samples (one Pre-BCR$^+$ and 2 Pre-BCR$^-$) were sensitive to the BTK inhibitor and were more sensitive than cell lines, and challenged two recent studies suggesting that only Pre-BCR$^+$ cells can benefit from ibrutinib treatment *in vitro* (Geng *et al.*, 2015; Kim *et al.*, 2017). Among the three sensitive samples, only Pre-BCR$^+$ PDX cells were within the clinical range of ibrutinib [C_{max} =277nM (Liston and Davis, 2017)], and were notably

more sensitive than reports in primary CLL cells (Herman *et al.*, 2011; Ponader *et al.*, 2012). In cell lines, the effects on cell viability were associated with cell cycle arrest at G1 and significant induction of programmed cell death. This cytotoxic action of ibrutinib paralleled early studies in CLL (Herman *et al.*, 2011; Ponader *et al.*, 2012; Cheng *et al.*, 2014) and ALL (Kim *et al.*, 2012) and G1 arrest and an induction of apoptosis associated with ibrutinib cytotoxicity was also reported in Hairy cell leukemia (HCL) and CLL patient cells (Cheng *et al.*, 2014; Sivina *et al.*, 2014). Ponader and colleagues also showed that DNA replication in cells of CLL was inhibited by ibrutinib (Ponader *et al.*, 2012). Furthermore, an *in vivo* study carried out by Herman and co-workers found that proliferation of CLL xenograft cells was reduced by more than 80% by ibrutinib with a 12% increase in cell death (Herman *et al.*, 2013). In the data presented here ibrutinib clearly decreased the constitutive phosphorylation of BTK in Nalm-6 cells and in sensitive PDX cells at concentrations that were associated with cytotoxicity (GI_{50}). Again, constitutive activation of pBTK in all cell lines and PDX cells was not necessarily predictive of sensitivity to ibrutinib. BTK was significantly inhibited in dasatinib-sensitive PDX cells, but not all these samples were sensitive to ibrutinib suggesting that BTK inhibition alone was not sufficient to reduce cell viability and that other pharmacodynamic target such as SRCs may need to be inhibited (Table 4.15) (Honigberg *et al.*, 2010; Lanning *et al.*, 2014; Kim *et al.*, 2017).

Kinase	% Activity remaining at 100 nM ± SD	% Activity remaining at 1000 nM ± SD
BRK	10 ± 3	4 ± 1
YES1	20 ± 0	16 ± 0
LCK	22 ± 1	14 ± 2
CSK	25 ± 6	15 ± 13
SRC	37 ± 4	13 ± 1
BTK	55 ± 3	55 ± 1
ERK1	83 ± 8	93 ± 21
ABL	87 ± 13	80 ± 1
Aurora A	92 ± 0	57 ± 2
Aurora B	96 ± 13	61 ± 7

Table 4.15: A list of selected kinases inhibited by ibrutinib using an *in vitro* kinase assay.

Kinase binding experiments were performed in the existence of 100 and 1000nM of ibrutinib followed by determination of the percentage of remaining activity. Data adapted from (Honigberg *et al.*, 2010).

Several reports evidenced that the SYK inhibitor, fostamatinib R406, showed interesting preclinical activity in several haematological malignancies including BCP-ALL (Gobessi *et al.*, 2009; Quiroga *et al.*, 2009; Perova *et al.*, 2014; Koerber *et al.*, 2015; Kuiatse *et al.*, 2015; Kohrer *et al.*, 2016). Furthermore, fostamatinib R788, the pro-drug form of the SYK inhibitor, showed clinical activity in patients with lymphoma, rheumatoid arthritis and CLL (Friedberg *et al.*, 2010; Morales-Torres, 2012). The data presented in this chapter evidenced that fostamatinib R406 significantly attenuated the growth of some cell lines and some PDX samples. In the Nalm-6 cell line, the effect on viability was associated with a significant G2 arrest and the presence of super-G2 and sub-G1 peaks in addition to significant induction of apoptosis. However, the pharmacological target inhibition was modest in ALL cell lines, as noted by a previous study (Perova *et al.*, 2014). Among 15 PDX samples, 6 samples (2 Pre-BCR$^+$ and 4 Pre-BCR$^-$) were sensitive to R406 treatment and 4 of them (2 Pre-BCR$^+$ and 2 Pre-BCR$^-$) were within the achievable clinical range [C_{max} = 2100nM (Baluom *et al.*, 2013)]. In addition, kinase assay studies performed at the National Centre for Protein Kinase Profiling to measure the half maximal inhibitory concentration (IC_{50}) (http://www.kinase-screen.mrc.ac.uk/) of R406 showed several kinases that are inhibited at similar concentration to SYK (Table 4.16). Other inhibited tyrosine kinases important for growth and survival include FLT3, Aurora B, LCK, PDGFR and JAK2 (Table 4.16) (Braselmann *et al.*, 2006; Davis *et al.*, 2010b; Davis *et al.*, 2011; Maude *et al.*, 2012; Roberts *et al.*, 2012; Roberts *et al.*, 2014; Rolf *et al.*, 2015). These 'off target' effects may contribute to the cytotoxicity obtained in both Pre-BCR harbouring and Pre-BCR negative cell lines and PDX cells with varied genetic alterations. Perova and co-workers found that the primary reason for fostamatinib sensitivity was SYK inhibition, even when it was mild, rather than FLT3 and SRC family kinases (SFKs) in standard and high risk BCP-ALL samples (Perova *et al.*, 2014). In this study, however, the induction of super-G2 arrest and apoptosis in Nalm-6 cells may suggest inhibition of Aurora B, a key kinase that play a role in maintaining a functional mitotic spindle, and if inhibited leads to super G2 peaks indicative of polyploidy (Girdler *et al.*, 2006; Carpinelli and Moll, 2008; Bavetsias and Linardopoulos, 2015) and this notion supports the assumption that off targets may influence R406 activity. Interestingly, fostamatinib treatment induced G1 arrest with induction of apoptosis in WM cell lines (Kuiatse *et al.*, 2015). Above all, our R406 findings challenges two recent papers suggested that only Pre-BCR$^+$ BCP-ALL cells could benefit from SYK inhibitors (Duque-Afonso *et al.*, 2016; Kohrer *et al.*, 2016).

Kinase	% Activity remaining at 100 nM ± SD	% Activity remaining at 1000 nM ± SD
JAK2	50 ± 6	3 ± 8
Aurora B	60 ± 3	23 ± 2
BTK	67 ± 3	29 ± 1
Aurora A	75 ± 42	29 ± 32
SYK	79 ± 0	73 ± 9
SRC	80 ± 0	41 ± 5
YES1	87 ± 4	64 ± 2
ZAP70	97 ± 3	51 ± 0
ERK8	107 ± 2	86 ± 6
LCK	107 ± 2	61 ± 1

Table 4.16: A list of selected kinases inhibited by fostamatinib R406 using an *in vitro* kinase assay.

Kinase binding experiments were performed in the existence of 100 and 1000nM of fostamatinib R406 followed by determination of the percentage of remaining activity. Data adapted from the data base of National Centre for Protein Kinase Profiling (http://www.kinase-screen.mrc.ac.uk/).

Dasatinib, the multi-kinase inhibitor (Table 4.17), was approved by FDA for ALL and AML Philadelphia chromosome positive patients (Brave *et al.*, 2008) and recent preclinical data evidenced that it could be effective in Pre-BCR$^+$ and Ph-like ALL (Bicocca *et al.*, 2012; Roberts *et al.*, 2014; Geng *et al.*, 2015). This study showed that Pre-BCR$^+$ cell lines (3 lines) and PDX (2 samples) cells were sensitive to dasatinib. In addition, two Pre-BCR$^-$ PDX samples (Ph$^+$ and Ph-like cytogenetics) as expected were highly sensitive to dasatinib, and therefore served as positive controls. Importantly, most of GI_{50} values (both Pre-BCR$^+$ and Pre-BCR$^-$) were within clinically achievable concentrations [Cmax = 264nM (Liston and Davis, 2017)]. Two of dasatinib-sensitive Pre-BCR$^+$ cells (L910 PDX samples and PreB 697 cell line) harboured the t(1;19) translocation in keeping to what has been found before in terms of the sensitivity of *TCF3-PBX1* positive ALL cells to dasatinib *in vitro* (Bicocca *et al.*, 2012; Geng *et al.*, 2015). Although, Bicocca and co-authors (Bicocca *et al.*, 2012) found that *TCF3-HLF* positive ALL cells were also sensitive to dasatinib, however, the Pre-BCR$^+$ PDX sample L707 [t(17;19)] was totally resistant to dasatinib. The cytotoxic effect of dasatinib was associated with decreased phosphorylation of multiple pharmacological targets downstream of the Pre-BCR checkpoint (e.g. SYK, BTK, PLC-γ2 and BLNK) in cell lines and PDX samples. In cell lines, cell cycle profile changes (G1-arrest) was observed at GI_{50} doses of the drug but no significant apoptosis

induction was observed. However, other reports revealed that dasatinib induced significant apoptosis and cell cycle arrest at S-phase in Ph^+ ALL cells incubated on a stromal layer (Fei *et al.*, 2010). Taken together, the dasatinib findings presented in this chapter evidenced that Pre-BCR^+ cells which harbour *TCF3-PBX1* (but not *TCF3-HLF* positive) were sensitive to dasatinib treatment which is in agreement with others (Bicocca *et al.*, 2012; Fischer *et al.*, 2015; Geng *et al.*, 2015). In addition, a Pre-BCR^+ PDX sample bearing normal cytogenetics but harboured a *c-CBL* mutation was also sensitive to dasatinib, within a clinical drug concentration range.

Kinase	% Activity remaining at 100 nM ± SD	% Activity remaining at 1000 nM ± SD
ABL	0 ± 0	0 ± 0
SRC	1 ± 0	2 ± 0
LCK	1 ± 0	1 ± 0
YES1	1 ± 0	1 ± 0
BTK	1 ± 0	1 ± 0
PDGFRA	6 ± 1	3 ± 1
MAP4K5	22 ± 1	3 ± 1
p38 alpha MAPK	79 ± 15	29 ± 2
ERK5	87 ± 2	91 ± 4
JAK2	94 ± 2	42 ± 1
SYK	97 ± 1	90 ± 0

Table 4.17: A list of selected kinases inhibited by dasatinib using an *in vitro* kinase assay.

Kinase binding experiments were performed in the existence of 100 and 1000nM of dasatinib followed by determination of the percentage of remaining activity. Data adapted from (Kantarjian *et al.*, 2010b).

The Pre-BCR^+ PDX cells L707 which harboured the poor prognostic translocation (*TCF3-HLF*) was highly resistant to dasatinib and all other TKIs tested and may be due to the higher levels of basal phosphorylation of most Pre-BCR downstream signalling compared to other PDX cells (Table 3.1). Similar findings of *TCF3-HLF* positive resistance to dasatinib but sensitivity to dexamethasone has also been reported previously (Fischer *et al.*, 2015).

Generally, the findings shown here match those of other authors (Geng *et al.*, 2015) who screened the effects of SYK (PRT062607), SRC (Dasatinib), BTK (Ibrutinib) and PI3K-δ (CAL-101) inhibitors on a subsets of Pre-BCR^+ and Pre-BCR^- cells both *in vitro* and *in vivo* and they found

that inhibitors showed efficacy in Pre-BCR$^+$ samples, with dasatinib being the most effective. Similarly, the classification of BCP-ALL cells in our study into Pre-BCR$^+$ and Pre-BCR$^-$ showed similar patterns of sensitivity associated with a Pre-BCR phenotype. Fostamatinib R406 and dasatinib (the most effective single inhibitors in this study) were effective in Pre-BCR harbouring PDX samples [apart from *TCF3-HLF* positive PDX cells] and cell lines. Furthermore, unexpected sensitivity was also observed in some Pre-BCR$^-$ PDX cells incubated with fostamatinib R406, CAL-101 and ibrutinib, however, the least number of sensitive PDX cells was seen in both Pre-BCR$^+$ and Pre-BCR$^-$ treated with CAL-101 or Ibrutinib. Although basal phosphorylation levels of AKT and SYK were higher in Pre-BCR$^+$ compared to Pre-BCR$^-$ PDX cells, this increased activity did not seem to be the principal reason underlying the sensitivity seen in some Pre-BCR$^+$ PDX cells to CAL-101 and R406, as evidenced by the pharmacodynamic data .

In this study, the cytotoxicity associated with most TKIs was correlated with the inhibition of the potential pharmacological targets in PDX cells when treated with GI_{50} concentrations and this may indicate that effective doses could be reproducible *in vivo* (Tables 4.15 and 4.17). However, no relationship was observed between the response of PDX cells to all inhibitors and genetic lesions apart from the dasatinib-sensitive Pre-BCR$^-$ PDX samples (L4951 and L824) which were Ph$^+$ and PDGFR translocation positive, respectively and therefore served as useful positive controls. This heterogeneous activity was similarly noticed by others (Pemovska *et al.*, 2013; Tyner *et al.*, 2013; Perova *et al.*, 2014; Frismantas *et al.*, 2017).

Interestingly, the trend of increased sensitivity in primary or PDX cells compared to cell lines has also been reported for MEK inhibitors (Irving *et al.*, 2014; Ryan *et al.*, 2016) where cell lines showed resistance even when they have the druggable lesion and this may be due to adoption of cell lines to immortalisation (Garnett *et al.*, 2012). The NSG orthotopic model enables drugs that show promising *in vitro* activity to undergo *in vivo* efficacy studies with accompanying pharmacodynamic assessments. Interestingly, our data evidenced that an *in vitro* response was seen in Ph$^+$ and PDGFR positive PDX samples and other groups have shown this translates in an *in vivo* mouse model and in patients (Lock *et al.*, 2002; Liem *et al.*, 2004; Houghton *et al.*, 2007; Irving *et al.*, 2014).

Initial drug screening in PDX cells *in vitro* is not ideal as the cells are not dividing. However, response to some drugs such as glucocorticoids and other small molecule inhibitors does not

rely on cell division (Kaspers *et al.*, 1994; Irving *et al.*, 2014). For drugs such as CAL-101, stromal interactions may play a role in determining sensitivity and cell lines in this study are grown in suspension in the initial drug screen (McMillin *et al.*, 2013). Moreover, others have reported that PDX cells may undergo clonal evolution and this may occur during cells proliferation in the mouse and, therefore, PDXs are not identical to the primary sample (Meyer and Debatin, 2011; Williams *et al.*, 2013). This may justify the resistance seen in L578/JM162 to CAL-101, ibrutinib and R406 unlike the remaining PDX replicates (L578/AZ7, L578/AZ8 and L578/AZ9) which showed a consistent response to the same inhibitors. Moreover, the small samples size may partly contribute to the difficulty in finding a correlation between genotype and drug response.

Taken together, significant sensitivity was seen in all TKIs targeting effectors of Pre-BCR checkpoint signalling at clinically relevant concentrations. The Pre-BCR phenotype was associated with sensitivity to dasatinib and fostamatinib R406. Sensitivity was also seen in some Pre-BCR$^-$ PDX ALL samples but a predictive biomarker could not be identified. Also, sensitivity in some PDX cells was seen to all drugs, with PDX cells being more sensitive to inhibitors than cell lines. For drugs where the drug target is unclear, knockdown of potential candidates using siRNA methodologies may aid in identifying the relevant kinase that is associated with cell death. This is definitely worthwhile for fostamatinib R406, but may also be valid in confirming ibrutinib and dasatinib drug targets. Since most paediatric ALL trials favour drug combination studies, based on the observations presented here, the prioritisation of dasatinib and fostamatinib with candidate drug combinations was an obvious next step, and the synthetic glucocorticoid dexamethasone, was selected as a suitable candidate.

Chapter 5 (Results 3): Effect of TKIs Combinations with Dexamethasone on BCP-ALL cells

Chapter 5: Effect of TKIs Combinations with Dexamethasone on BCP-ALL Cells

5.1 Introduction

As shown in the previous chapters, multiple tyrosine kinases were highly activated in BCP-ALL cells and some cell lines and PDX samples were sensitive to single TKI inhibitors. Historically, GCs such as dexamethasone, have been used for decades in the treatment of ALL and other lymphoid malignancies due to their specific effect of inducing cell death in lymphoid cells, an effect mediated by GR (Inaba and Pui, 2010; Pui *et al.*, 2012b). The response to GCs is used as prognostic indicator and some trials used a GC monotherapy window to inform on risk stratification. At relapse, most patients show resistance to GCs (Hongo *et al.*, 1997; Kaspers *et al.*, 1998; Choi *et al.*, 2007). To improve outcome and/or overcome GC resistance, a combination of dexamethasone with a TKI inhibitor targeting unconventional effector(s) downstream of the Pre-BCR checkpoint which are independent of the GR pathway, may be useful.

In this chapter, the effects of combining dexamethasone with single TKI inhibitor (CAL-101, ibrutinib, fostamatinib R406 and dasatinib) were investigated and the aim was to:

- Define the combination indices in ALL cell lines and PDX cells after exposure to the candidate TKIs plus dexamethasone using the Chou and Toulalay median effect (Chou, 2010)
- Test the effects of TKI plus dexamethasone on cell cycle and apoptosis in BCP-ALL cell lines
- Investigate the synergistic mechanisms of the most promising drug combinations

5.2 Effect of dexamethasone (glucocorticoid) as a single drug on BCP-ALL cells viability

Dexamethasone is used as an essential therapy for childhood ALL, however, resistance to GCs is an adverse prognostic factor in BCP-ALL (Inaba and Pui, 2010). The sensitivity of ALL cells to dexamethasone was first investigated using the Alamar blue assay (Section 2.5.1). Cells were incubated with increasing concentrations of dexamethasone (Table 2.8) and the growth inhibitory effect was assessed in 5 cell lines and 12 PDX cells derived from 9 patient samples (Figure 5.1 and table 5.1). Among all cell lines tested, only PreB 697 cells were very sensitive to dexamethasone treatment (Mean GI_{50}: 43.3nM) and the remaining cell lines (R3F9, Nalm-6, REH and TK6) were highly resistant to dexamethasone (Mean GI_{50} > 10µM) (Figure 5.1A and table 5.1). Moreover, 5 patient samples (amplified in 7 PDXs) were sensitive to dexamethasone out of 8 (L910 presentation, L707 presentation, LK196 2nd relapse, L920 presentation and L881 2nd relapse) (Mean GI_{50}: 50.78nM, range 6-125nM). Similar to the GI_{50}s obtained in cell lines, the remaining 3 patient samples (transplanted into 6 mice) were resistant to dexamethasone (GI_{50} values> 12µM) (Figure 5.1 B and table 5.1). Interestingly, consistent GI_{50} values were observed in the majority of PDX replicates which were derived originally from the same patient ALL cells.

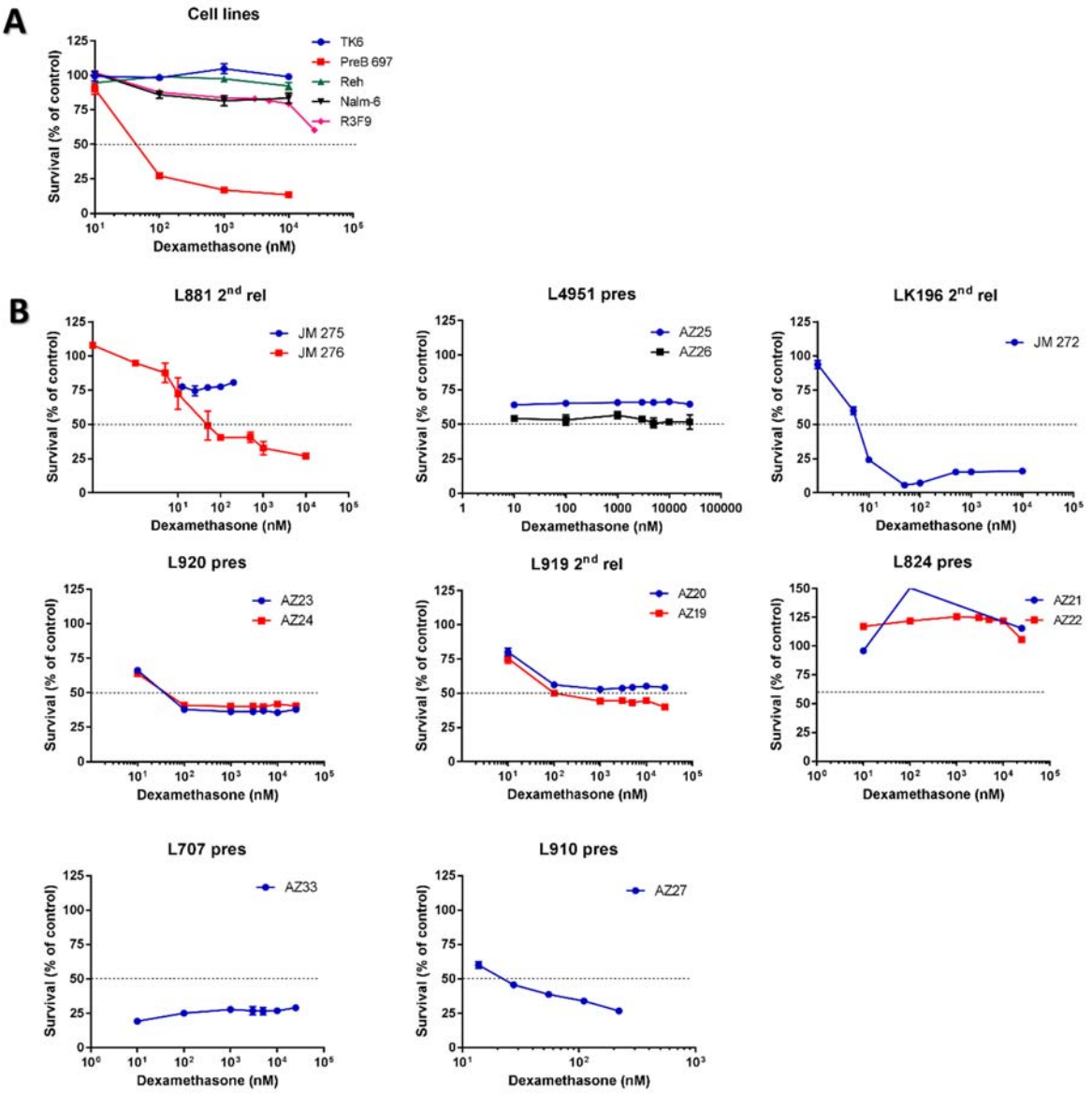

Figure 5.1: The survival curves of BCP-ALL cells treated with dexamethasone.

5 Cell lines **(A)**, 8 Pre-BCR$^+$ and Pre-BCR$^-$ patient samples **(B)** were cultured in the presence of escalating doses of dexamethasone for 96 hours before measuring cell viability by Alamar blue assay. Curve points of cell lines in graph **(A)** represent the mean of 3 independent experiments ± SEM, whereas only one test was achievable in each individual PDX material and error bars represent the mean of 3 different wells ± SEM **(B)**. Each patient sample was amplified into 1-2 PDX replicates. Data were analysed by Graphpad Prism software.

Cells	GI_{50} Mean ± SEM (Dex µM)	Number of replicates
* TK6	> 10	3
* PreB 697	0.0433 ± 0.0047	3
* Nalm-6	> 40	3
* R3F9	> 25	3
L910 pres	0.0550	1
L707 pres	0.0300	1
* REH	> 10	3
L4951 pres	> 25	2
LK196 2nd rel	0.0060	1
L920 pres	0.0379 ± 0.0009	2
L919 2nd rel	12.556 ± 12.44	2
L824 pres	> 25	2
L881 2nd rel	0.125 ± 0.075	2

Table 5.1: A list of mean GI_{50}s for BCP-ALL cells treated with dexamethasone alone.

Cells were incubated with dose escalation of dexamethasone for 96 hours before measurement of viability by Alamar blue assay. Mean GI_{50}s were calculated from 3 independent replicates of 5 cell lines (asterisks) or 13 PDX replicates (derived from 8 patient samples) ± SEM.

5.3 Effect of CAL-101 combination with dexamethasone on BCP-ALL cells

5.3.1 Effect of CAL-101 plus dexamethasone using the Chou and Toulalay median effect on BCP-ALL cells viability

It has been recently shown that inhibition of PI3K/AKT may enhance sensitivity or reverse resistance to glucocorticoids in B and T-ALL cells (Piovan *et al.*, 2013; Hall *et al.*, 2016; Kruth *et al.*, 2017). In addition, the sensitivity seen in some PDX samples as shown in the previous chapter provided the rationale to investigate the effect of CAL-101 plus dexamethasone on the viability of BCP-ALL cells using the Chou and Toulalay median effect analyses at ED50, ED75 and ED90 (Section 2.5.2). Based on that, CalcuSyn software was then used to calculate CI values.

To measure the *in vitro* cytotoxicity of CAL-101 plus dexamethasone combination on BCP-ALL cells, the Alamar blue assay (Section 2.5.1) was utilized after cells were incubated with 0.25x, 0.5x, 1.0x, 2.0x and 4.0x of GI_{50} concentrations of each drug alone and in combination (Table 2.9 for cell lines and table 2.10 for PDX cells). Four cell lines (Figure 5.2) and 6 PDX samples derived from 6 ALL patients (Figure 5.3) were tested in this study and combination indices were calculated to evaluate the combination indices.

Interestingly, the CAL-101 plus dexamethasone combination viability data showed very strong to strong synergism in GC-resistant R3F9 cells at ED50 [CI (mean ± SEM): 0.36 ± 0.02] and at ED75 [CI (mean ± SEM): 0.72 ± 0.12] respectively, however, the CI value at ED90 [CI (mean ± SEM): 2.13 ± 0.62] suggested antagonism (Figure 5.2 B and E). Moreover, the same combination was very synergistic with consistent CI values in Nalm-6 cells [CI (mean ± SEM) range: 0.05 ± 0.02 to 0.21 ± 0.01] (Figure 5.2 C and E) which were also resistant to dexamethasone monotherapy (Section 5.2). However, no enhanced sensitivity was seen in the GC-resistant REH cell line, which is GR null and thus serves as useful negative control, nor GC-sensitive PreB 697 cells with all CI values being consistently above 1.1 therefore suggesting no/antagonistic effects (Figure 5.2 A, D and E).

Similar experiments were also performed in 5 PDX samples and CI values at ED50 were considered. The strength of synergy was strong in L919/AZ19 (CI range: 0.15 – 0.03), synergistic in L910/AZ27 (CI range: 0.32 – 0.06) and L4951/AZ26 but only at ED50 (CI range:

0.55-2.17), nearly additive in L920/AZ24 (CI range: 0.96 – 0.25). Moreover, the CI values at ED50 suggested an antagonistic effect in L707/AZ33 (CI = 2) although the CI value at ED90 (CI = 0.48) was indicative of synergistic effect. Interestingly, synergy was seen in one of 2 Pre-BCR^{+} and all Pre-BCR^{-} PDX cells (Figure 5.3).

Taken together, CAL-101 and dexamethasone combination was synergistic in both GC-resistant and GC- sensitive ALL cells regardless of Pre-BCR expression status.

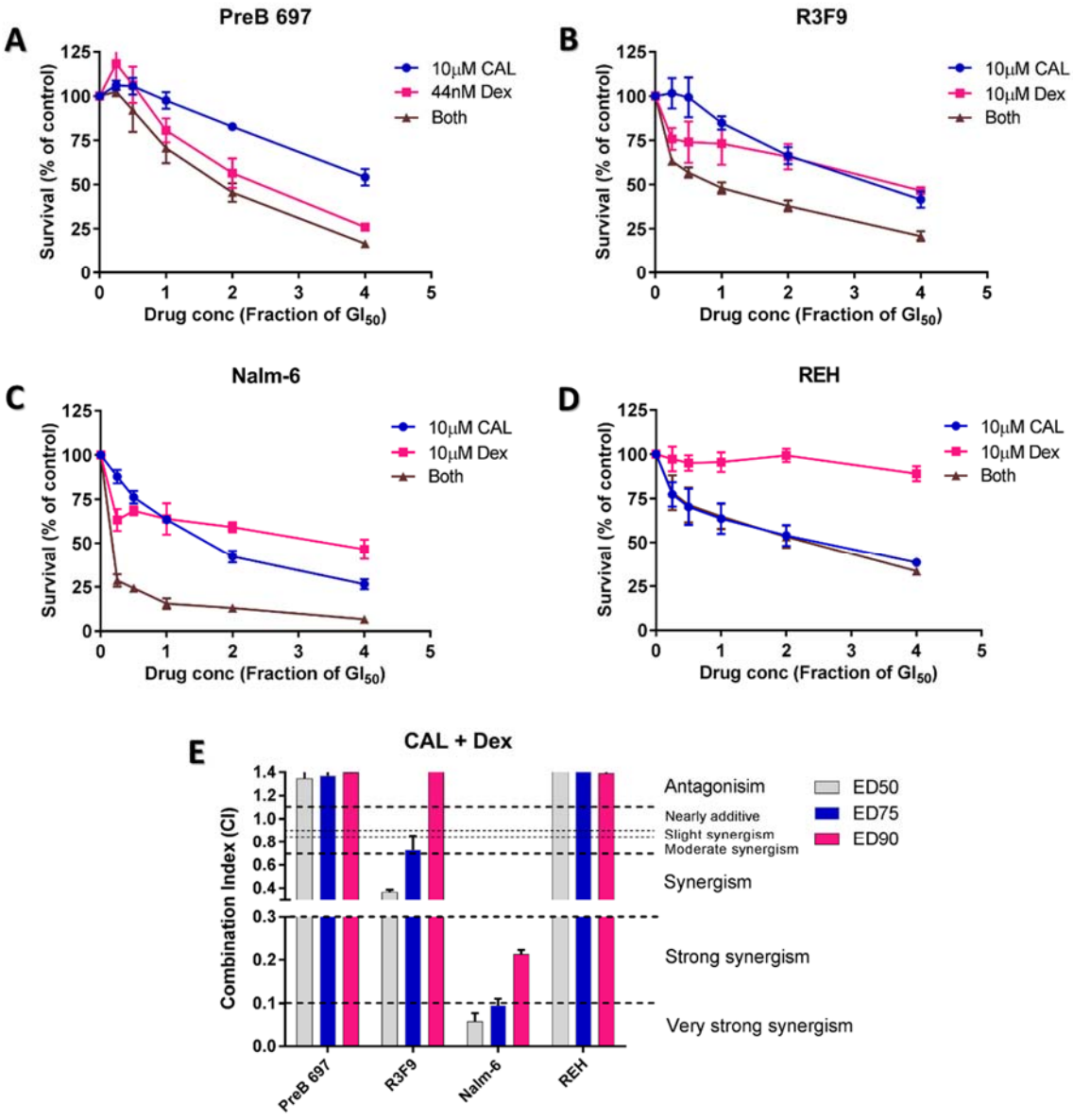

Figure 5.2: CAL-101 enhances the cytotoxic effect of dexamethasone in some BCP-ALL cell lines.

Dose response curves of **(A)** PreB 697, **(B)** R3F9, **(C)** Nalm-6 and **(D)** REH cell lines exposed to GI_{50} fractions of CAL-101 (CAL), dexamethasone (Dex) alone or their combination for 96 hours followed by Alamar blue assay. **(E)** Bar chart represent the mean combination indices calculated using CalcuSyn software at the effective doses (ED) 50, 75 and 90. The viability curves and CI values represent the mean ± SEM of 3 independent experiments. GI_{50} concentrations are indicated for each cell line.

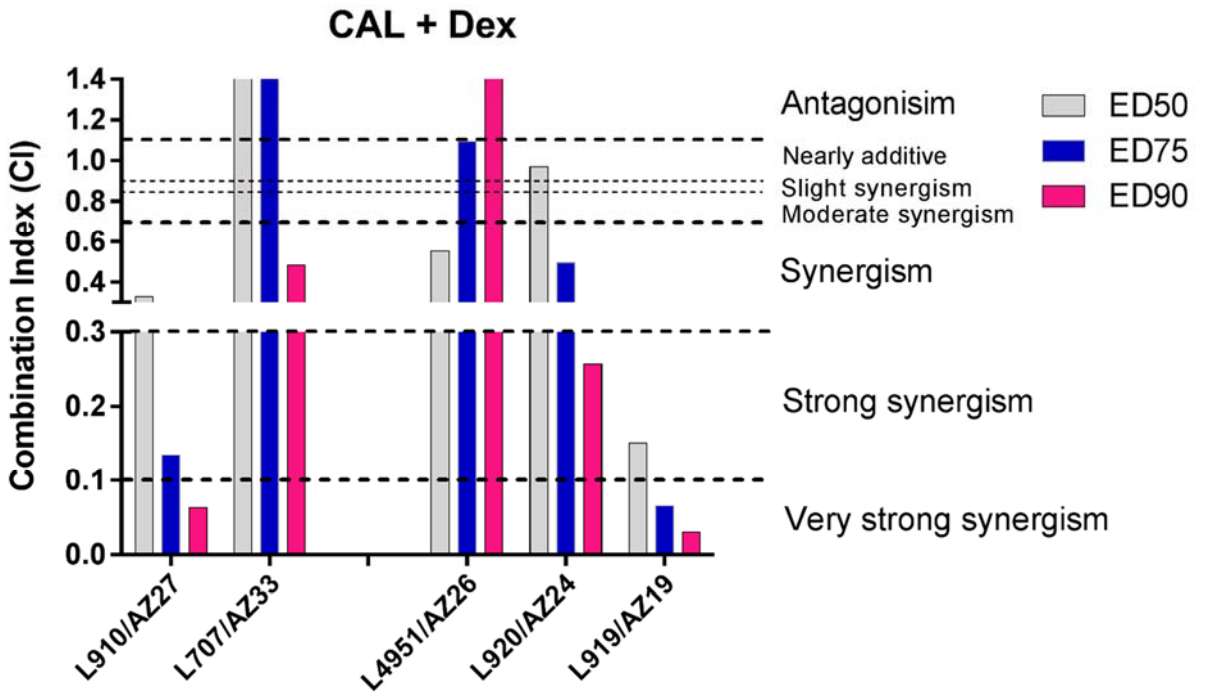

Figure 5.3: CAL-101 enhances the cytotoxic effect of dexamethasone in some PDX samples.

Histogram representing the CI calculated at 50, 75 and 90% effective doses (ED50, ED75 and ED90, respectively) using CalcuSyn software after PDX cells were exposed to GI_{50} fractions of CAL-101 (CAL), dexamethasone (Dex) alone and their mixture. CI values were calculated from one replicate PDX sample.

5.4 Effect of ibrutinib combination with dexamethasone on BCP-ALL cells

5.4.1 Effect of ibrutinib plus dexamethasone mixture on BCP-ALL cells viability using the Chou and Toulalay median effect

In the previous chapter, some PDX samples were sensitive to ibrutinib alone and GI_{50}s were within clinical ranges (as shown in chapter 4, section 4.3.1), therefore, assessing synergism with dexamethasone was a tempting aim. Using the Chou and Toulalay median effect analyses (Section 2.5.1), CIs were calculated after cells were incubated with the GI_{50} fractions of ibrutinib, dexamethasone, separately and in combination (Table 2.9 for cell lines and table 2.10 for PDX cells) for 96 hours (Section 2.5.1). In this assay, four cell lines and similar number of PDX samples were investigated and hence CI values were then calculated at ED50, ED75 and ED90 (Section 2.5.2).

The viability data of ibrutinib plus dexamethasone suggested synergistic effects in GC-resistant lines, Nalm-6 [CI (mean ± SEM) range: 0.41 ± 0.02 to 0.42 ± 0.02] and R3F9 [CI (mean ± SEM) range: 0.65 ± 0.03 to 0.69 ± 0.05]. In addition, the CI value at ED50 [CI (mean ± SEM): 0.97 ± 0.002] and at ED75 [CI (mean ± SEM): 1.06 ± 0.005] suggested additive effects in the GC-sensitive line, PreB 697, whereas, the CI value at ED90 displayed antagonistic or no effect [CI (mean ± SEM): 1.16 ± 0.01] (Figure 5.4). Moreover, no enhanced sensitivity was seen in REH (dexamethasone resistant) cells incubated with ibrutinib plus dexamethasone combination and all CI values were consistently above 1.1 (Figure 5.4 D and E).

PDX cells were also exposed to ibrutinib/dexamethasone combination and a Pre-BCR^+, GC-sensitive sample L910/AZ27 was found to be synergistic (CI range: 0.37-0.38). However, the CI values at ED50 consistently suggested antagonistic effect in all Pre-BCR^- PDX cells (L824/AZ22, L920/AZ24 and L4951/AZ26) with CI values were > 1.1 (Figure 5.5).

Taken together, ibrutinib enhanced sensitivity to dexamethasone in Pre-BCR^+ cell lines and PDX cells when cells were incubated with the drug combination.

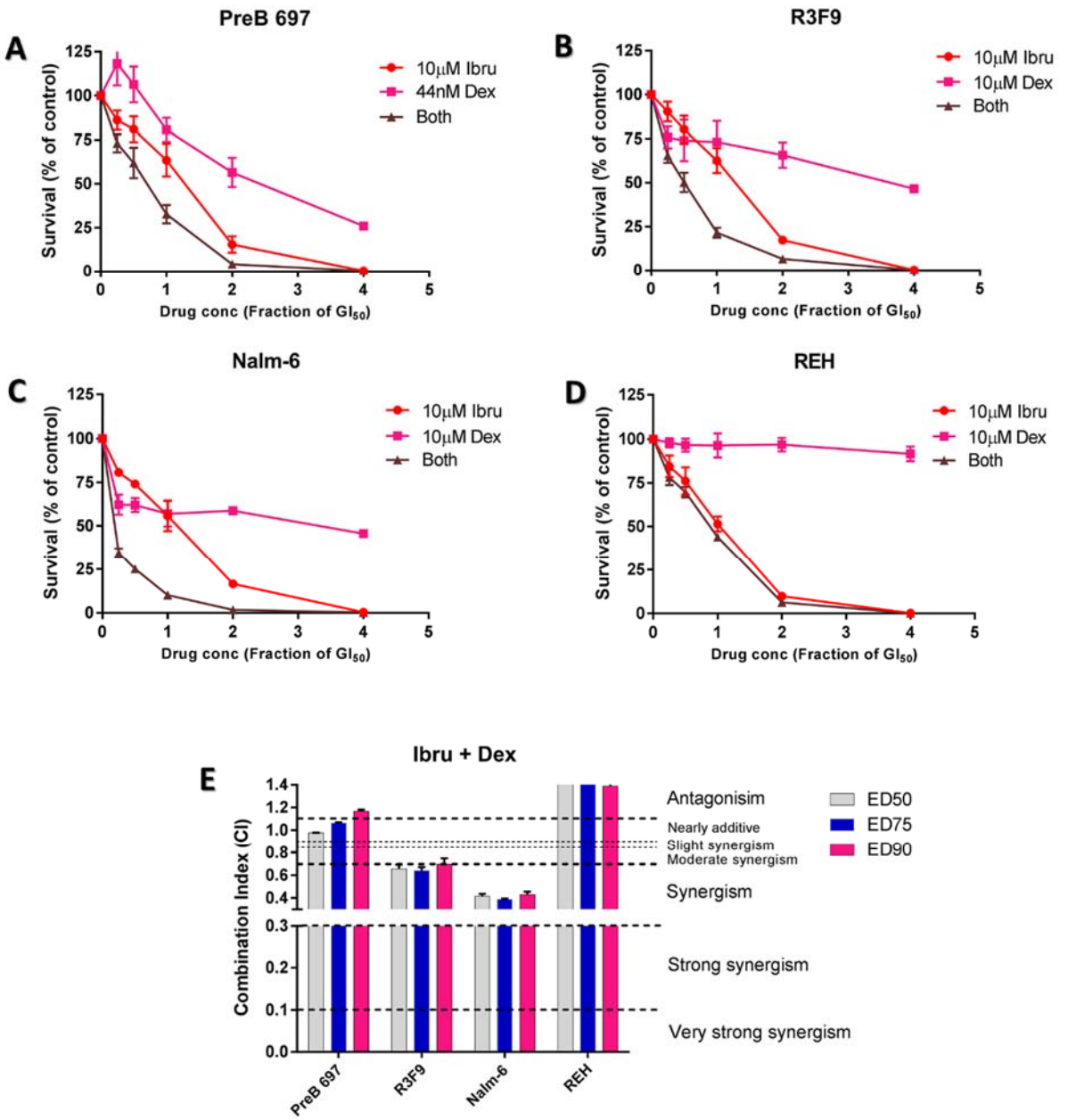

Figure 5.4: Ibrutinib enhances the cytotoxic effect of dexamethasone in Pre-BCR$^+$ BCP-ALL cell lines.

Dose response curves of **(A)** PreB 697, **(B)** R3F9, **(C)** Nalm-6 and **(D)** REH cell lines exposed to GI_{50} fractions of ibrutinib (Ibru), dexamethasone (Dex) or both for 96 hours followed by assessment using Alamar blue assay. **(E)** Bar chart represent the mean CI calculated using CalcuSyn software at the ED 50, 75 and 90. The viability curves points and CI values represent the mean ± SEM of 3 independent experiments. GI_{50} concentrations are indicated for each cell line.

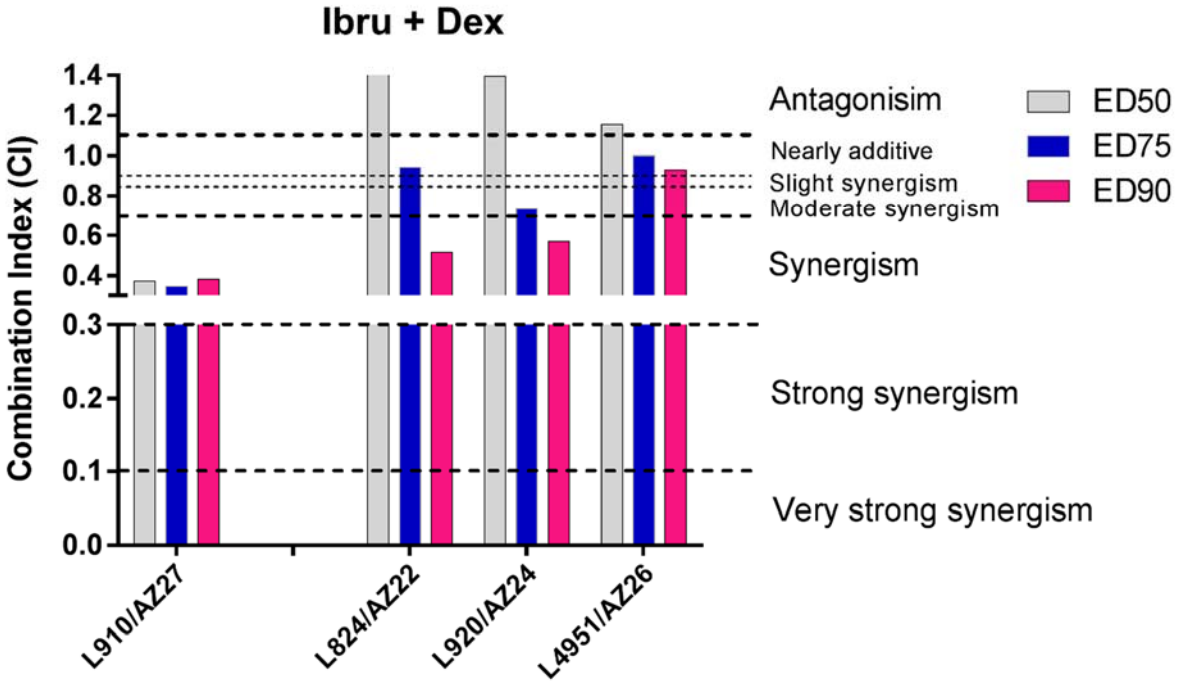

Figure 5.5: Ibrutinib synergizes with dexamethasone in Pre-BCR$^+$ PDX sample.

Histogram represent the combination indices calculated at 50, 75 and 90% effective doses (ED50, ED75 and ED90 respectively) using CalcuSyn software after PDX cells were exposed to GI_{50} fractions of ibrutinib (Ibru), dexamethasone (Dex) or both for 96 hours followed by Alamar blue assay. CI values were calculated from one replicate PDX.

5.4.2 Effect of ibrutinib plus dexamethasone on cell cycle phases of BCP-ALL cell line

To further understand the synergistic effect seen, cell cycle distribution was studied in R3F9 by flow cytometry (Section 2.3.3) after treatment with the drug combination for 24 and 48 hours. R3F9 cells were treated with ibrutinib (12µM), dexamethasone (25µM) and both together. As evidenced in chapter 4, treatment of BCP-ALL cells with ibrutinib alone induced G1 arrest (Figure 4.8), however, the effect of exposure to combination with dexamethasone was synergistic in R3F9 and therefore a higher percentage of cells were arrested at G1 (Figure 5.6).

R3F9 cells were found to be arrested at G1-phase after 24 hours co-exposure with ibrutinib plus dexamethasone (Mean ± SEM: 72.83 ± 1.95%) and the ratio was significantly higher than cells cultured with ibrutinib (Mean ± SEM: 50.97 ± 0.21%; p=0.0004) or dexamethasone (Mean ± SEM: 46.17 ± 1.67%; p=0.0005) alone. In addition, the enhanced G1 arrest was maintained

in cells exposed to the drug combination (Mean ± SEM: 69.43 ± 2.36%) for 48 hours compared to cells incubated with ibrutinib (Mean ± SEM: 43.20 ± 0.9%; p=0.0005) or dexamethasone (Mean ± SEM: 56.33 ± 1.04%; p=0.007) alone for the same period of time (Figure 5.6). In addition, a notable increase in the cells arrested at sub-G1 phase was observed in cells exposed to drug combination.

Taken together, enhanced G1 arrest was seen in R3F9 cells exposed to ibrutinib plus dexamethasone associated with accumulation of cells at sub-G1 phase.

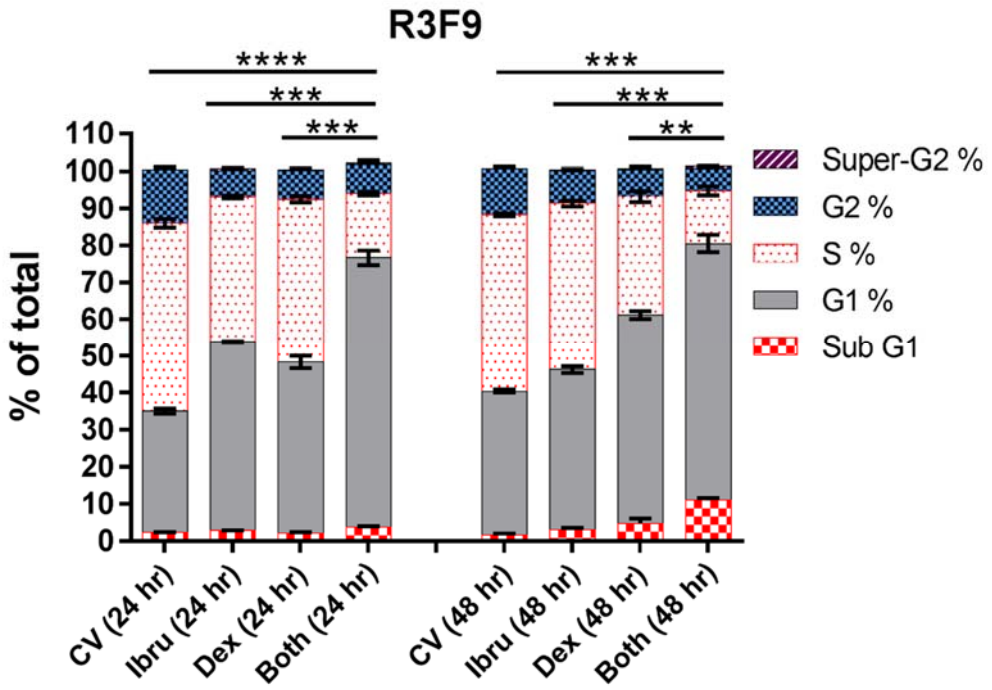

Figure 5.6: Ibrutinib co-exposure with dexamethasone increases G1- arrest in GC-resistant cell line.

Cell cycle phases were assessed by flow cytometry using propidium iodide staining after incubating R3F9 cells with 12µM ibrutinib (Ibru), 25µM dexamethasone (Dex) alone or with their combination for 24 and 48 hours. The bar graph shows the mean percentage of cells distributed at different phases of the cell cycle ± SEM (n=3). FlowJo software was used to analyse cell cycle data. Asterisks denote the student`s t-test statistical analysis of G1 phase only. **p<0.01, ***p<0.001, ****p<0.0001 and ns= not significant.

5.4.3 Apoptotic effect of ibrutinib plus dexamethasone on BCP-ALL cell lines

To further investigate the synergism seen after exposing cells to ibrutinib and dexamethasone combination, Annexin V-FITC staining (Section 2.3.2) was used to measure programmed cell death in R3F9 cells by flow cytometry. R3F9 cells were treated with ibrutinib (12µM), dexamethasone (25µM) and both together for 48 and 72 hours.

To confirm the previous findings (Section 5.4.1), R3F9 cells were exposed to the same combination for 48 hours and there was no significant change in the proportion of apoptotic cells in comparison with ibrutinib or dexamethasone. But, after 72 hours incubation, the percentage of Annexin V positive cells incubated with the drug combination (Mean ± SEM: 43.28 ± 2.52%) was 2 time higher than cells exposed to dexamethasone alone (Mean ± SEM: 22.0 ± 1.27%; p=0.0017) and 4 fold higher than ibrutinib alone (Mean ± SEM: 11.77 ± 0.86%; p=0.0003) (Figure 5.7).

Taken together, the addition of ibrutinib to dexamethasone greatly enhanced apoptosis in the GC-resistant line, R3F9.

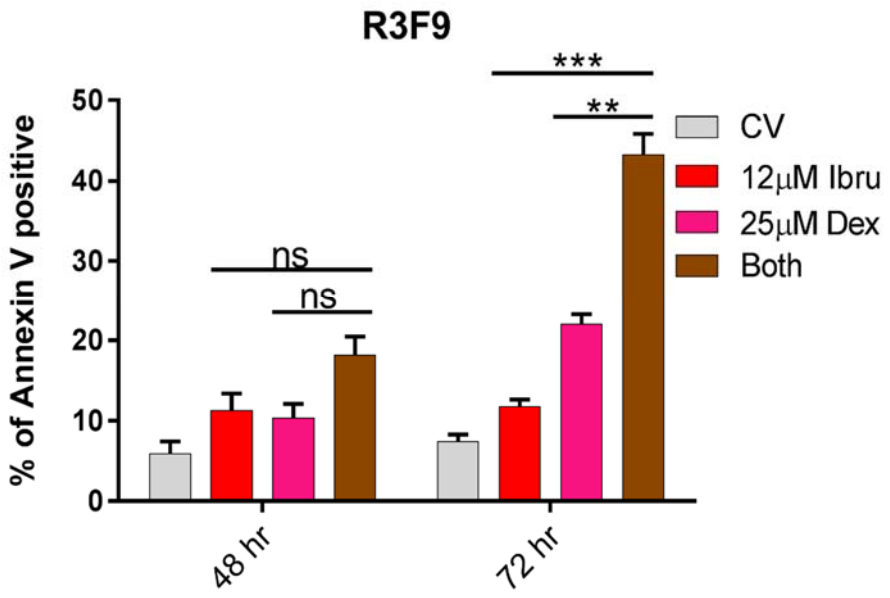

Figure 5.7: Ibrutinib plus dexamethasone mixture enhances apoptosis in R3F9 cell line.

R3F9 cells were exposed to 12µM ibrutinib (Ibru), 25µM dexamethasone (Dex) alone or their combination for 48, 72 hours before Annexin V-FITC staining and assessment by flow cytometry. Histograms denoting the mean ± SEM (n=3) of R3F9 cells. CellQuest software was used to analyse Annexin V data. Student`s t-test was carried out to calculate p-values. ns=not significant, **p<0.01, ***p<0.001.

5.5 Effect of fostamatinib R406 combination with dexamethasone on BCP-ALL cells

5.5.1 Effect of R406 plus dexamethasone using the Chou and Toulalay median effect on BCP-ALL cells viability

Fostamatinib and dexamethasone combination was found to be synergistic *in vitro* in WM (Kuiatse *et al.*, 2015). Moreover, R406 was found to inhibit multiple targets downstream of Pre-BCR signalling and their inhibition might play a role in re-sensitizing ALL cells to glucocorticoids (Rolf *et al.*, 2015; Kruth *et al.*, 2017). In addition, the sensitivity seen in some Pre-BCR^{+} and Pre-BCR^{-} PDX samples (Figure 4.12) was encouraging to go further and investigate the combination of R406 with dexamethasone *in vitro* in BCP-ALL cells. To this end, the Chou and Toulalay median effect analyses (Section 2.5.2) was studied after BCP-ALL cells were co-cultured with 0.25x, 0.5x, 1.0x, 2.0x and 4.0x of GI_{50} concentrations of R406, dexamethasone or their combination for 96 hours.

GC-resistant and GC-sensitive cell lines and PDXs were investigated in this study. Interestingly, the viability data of R406 plus dexamethasone combination suggested very strong to strong synergism in Nalm-6 [CI (mean ± SEM) range: 0.098 ± 0.03 to 0.049 ± 0.018] and R3F9 [CI (mean ± SEM) range: 0.15 ± 0.02 to 0.11 ± 0.006] cells respectively and CI values were consistent at different effective doses (Figure 5.8 B, C and E). In addition, the same combination was also synergistic in the GC-sensitive line PreB 697, however, only CI values at ED50 [CI (mean ± SEM): 0.6 ± 0.13] and ED75 [CI (mean ± SEM): 0.99 ± 0.0.21] suggested synergism. Consistent with other TKI combinations with dexamethasone, REH did not show synergy in the R406 with dexamethasone combination treatment (Figure 5.8 D, E).

In addition to cell lines, R406 combination was also investigated in PDX cells *ex vivo.* Interestingly, very strong synergism was observed in L919/AZ19 (CI range: 0.02 – 0.12) which lack Pre-BCR expression and was resistant to both drugs alone. In addition, the CI values obtained from the same combination (CI range: 0.29 – 0.11) suggested strong synergy in the Pre-BCR positive PDX sample, L910/AZ27 (Figure 5.9). Although the CI value at ED50 (CI = 0.43) suggested synergism in L824/AZ22, very strong synergism was apparent at ED75 (CI = 0.04) and ED90 (CI = 0.034). In L920/AZ24, R406 plus dexamethasone combination was also

synergistic (CI range: 0.68 – 0.31), however, this combination was antagonistic in L881/JM275 (CI values > 1.1) (Figure 5.9). Taken together, a strong synergism was seen in Pre-BCR$^+$ and Pre-BCR$^-$ cells and in some BCP-ALL cells resistant to dexamethasone alone.

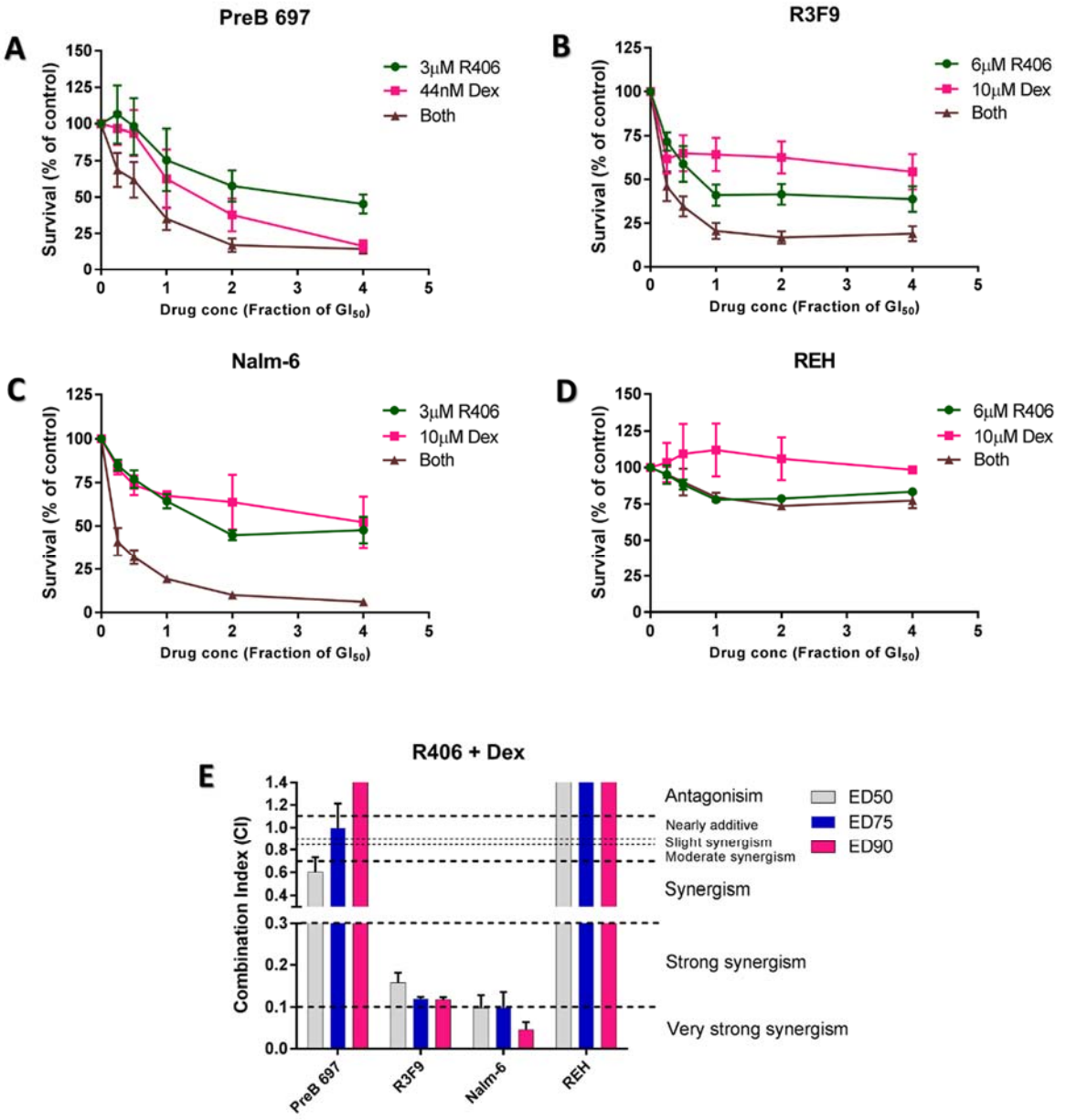

Figure 5.8: Fostamatinib R406 synergises with dexamethasone in Pre-BCR$^+$ BCP-ALL cell lines.

Dose response curves of **(A)** PreB 697, **(B)** R3F9, **(C)** Nalm-6 and **(D)** REH cell lines exposed to GI_{50} fractions of R406, dexamethasone (Dex) or both together for 96 hours followed by assessment by Alamar blue assay. **(E)** Histogram represent the mean CI calculated using CalcuSyn software at the ED 50, 75 and 90. The viability curves points and CI values represent the mean ± SEM of 3 independent experiments. GI_{50} concentrations were indicated for each cell line.

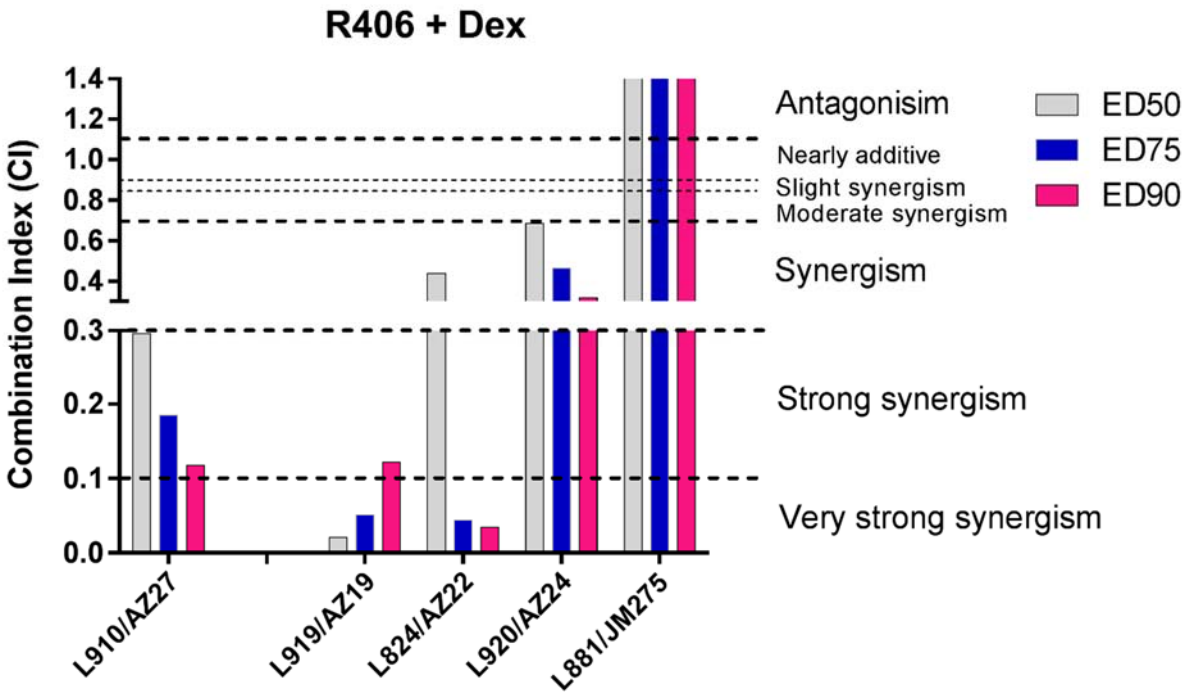

Figure 5.9: Fostamatinib R406 enhances sensitivity of Pre-BCR$^+$ and Pre-BCR$^-$ PDX samples to dexamethasone.

Histogram represent the combination indices calculated at 50, 75 and 90% effective doses (ED50, ED75 and ED90 respectively) using CalcuSyn software after PDX cells being exposed to GI_{50} fractions of R406, dexamethasone (Dex) or both together for 96 hours followed by Alamar blue assay. CI values were calculated from one replicate PDX.

5.5.2 Effect of R406 plus dexamethasone on cell cycle phases of BCP-ALL cell lines

To investigate the mechanism of synergy seen in BCP-ALL cells exposed to R406 and dexamethasone combination, propidium iodide staining was applied followed by cell cycle analysis by flow cytometry (Section 2.3.3). To this end, R3F9 and PreB 697 cell lines were co-cultured with R406 (6µM and 3µM respectively), dexamethasone (25µM and 44nM respectively) alone or the drug combination.

Interestingly, exposure of Nalm-6 or REH cells to R406 alone induced G2 and super-G2 arrest (Section 4.4.2), however, R406 treatment of R3F9 as a single agent was found to induce G1 arrest when compared to CV treated cells (Mean % of cells in G1 ± SEM, CV: 33.43 ± 0.52% versus R406: 38.90 ± 0.0%; $p<0.001$) (Figure 5.10 A). In addition, dexamethasone treatment also induced G1 arrest (Mean ± SEM: 48.17 ± 1.39%, $p=0.006$) but the mean percentage of R3F9 cells arrested at G1 phase was increased to 62.80 ± 1.6% in cells exposed to the drug combination for 24 hours (Figure 5.10 A). Consistently, after 48 hours, the percentage of cells

arrested at G1 was significantly higher in cells exposed to combination (Mean ± SEM: 59.60 ± 2.13%) compared to R406 treated cells (Mean ± SEM: 36.07 ± 10.36%, p=0.0073). However, no significant difference in the percentage of cells arrested at G1 was observed between combination and dexamethasone treated cells (Mean ± SEM: 57.50 ± 1.9%, p=0.5) (Figure 5.10 A).

The combination of R406 and dexamethasone was also investigated in PreB 697 cells. R406 treatment as a single agent did not show prominent significant change in any of cell cycle phases, however, G1 arrest was seen in cells incubated with dexamethasone alone (Mean % of cells in G1 ± SEM, CV: 32.27 ± 1.78% versus dexamethasone: 43.83 ± 3.06%; $p<0.05$). The combination of R406 plus dexamethasone significantly increased the percentage of cells arrested at G1 after 24 hours exposure (Mean ± SEM: 51.67 ± 0.49) compared to R406 treated cells (Mean ± SEM: 31.13 ± 0.52; p= 0.002) but no significant difference was registered when compared with dexamethasone treated cells (Mean ± SEM: 43.83 ± 3.06; p=0.19). At 48 hours, a similar trend was maintained in PreB 697 cells (Figure 5.10 B).

In summary, R406 in combination with dexamethasone was synergistic and enhanced G1 arrest in R3F9 and PreB 697 cells.

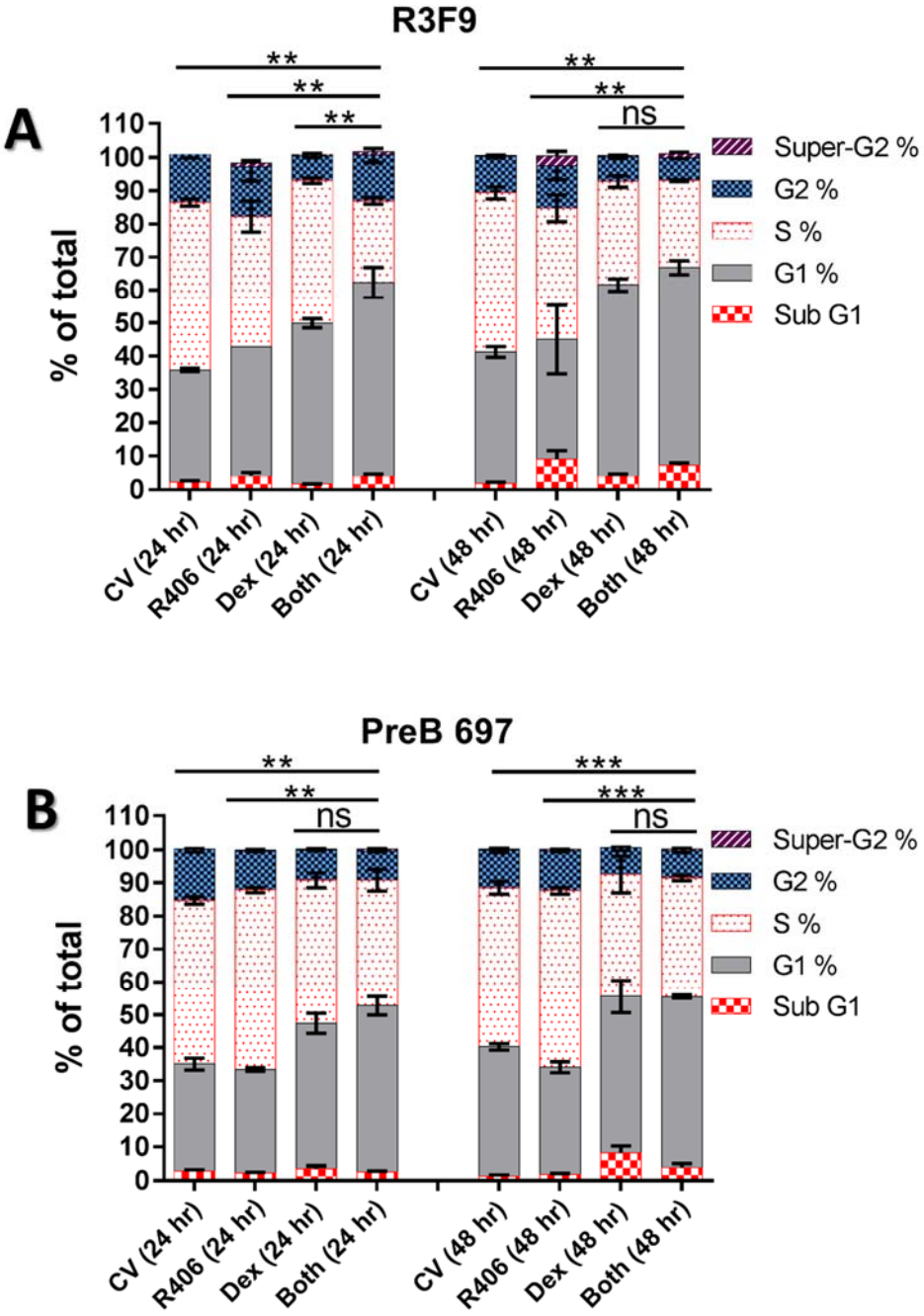

Figure 5.10: R406 co-exposure with dexamethasone enhances cell cycle arrest in BCP-ALL cell lines.

Cell cycle phases were assessed by flow cytometry using propidium iodide staining after incubating **(A)** R3F9 and **(B)** PreB 697 cells with R406, dexamethasone (Dex) alone or their combination. Cell lines were exposed to vehicle (CV), R406 (R3F9: 6µM and PreB 697: 3µM), dexamethasone (Dex) (R3F9: 25µM and PreB 697: 44nM) or both drugs for 24 and 48 hours. The bar graphs show the mean percentage of cells distributed at different phases of the cell cycle ± SEM (n=3). FlowJo software was used to analyse cell cycle data. Asterisks denote the student`s t-test statistical analysis of G1 phase. **p<0.01, ***p<0.001 and ns= not significant.

5.5.3 Apoptotic effect of R406 plus dexamethasone on BCP-ALL cell lines

To further understand the synergistic effect seen in multiple cell lines cultured with the R406 and dexamethasone combination (Section 5.5.1), Annexin V-FITC staining (Section 2.3.2) was used to measure the percentage of apoptotic BCP-ALL cells by flow cytometry. R3F9 and PreB 697 cell lines were co-treated with R406 (6µM and 3µM respectively), dexamethasone (25µM and 44nM respectively) alone or with the both agents for two time points (48 and 72 hours).

Surprisingly, no significant change was detected in the percentage of Annexin V positive R3F9 cells exposed to combination compared with single agents (Figure 5.11 A).

PreB 697 cells were also cultured with R406 plus dexamethasone for 48 hours and there was no significant difference in the percentage of cells undergoing programmed cell death which were exposed to combination compared with cells incubated with single drugs. However, after 72 hours, the percentage of apoptotic cells was significantly higher in combination (Mean ± SEM: 21.83 ± 2.136%) than R406 alone (Mean ± SEM: 10.37 ± 0.68%; p=0.007) but surprisingly lower than dexamethasone treated cells (Mean ± SEM: 32.86 ± 0.33%; p=0.007) (Figure 5.11 B).

To summarise, the synergistic effect seen in cell viability was not reflected in enhanced apoptosis in cell lines treated with R406 combination with dexamethasone.

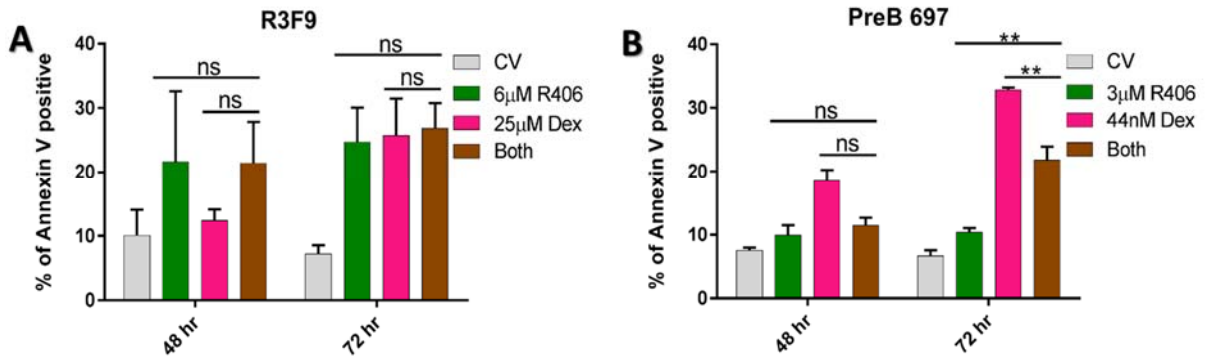

Figure 5.11: The effect of R406 plus dexamethasone mixture on apoptosis induction in BCP-ALL cell lines.

Cell lines were co-cultured with R406 (R3F9: 6µM and PreB 697: 3µM), dexamethasone (Dex) (R3F9: 25µM and PreB 697: 44nM) alone or their combination for 48, 72 hours before Annexin V-FITC staining and assessment by flow cytometry. Histograms denoting the mean ± SEM (n=3) of **(A)** R3F9 and **(B)** PreB 697. CellQuest software was used to analyse Annexin V data. Student`s t-test was carried out to calculate p values. ns=not significant, **p<0.01.

5.5.4 Pharmacodynamic effects of R406 plus dexamethasone on BCP-ALL cell lines

5.5.4.1 The effects of R406/dexamethasone combination on the inhibition of R406 pharmacological targets

To see if the synergistic effects seen in cell lines treated with R406 plus dexamethasone mixture (Section 5.5.1) were linked with enhanced inhibition of the target(s) phosphorylation, pSYK(Y352), pSYK(Y348) and pAKT(S473) levels were investigated by intracellular phospho flow cytometry (Section 2.3.5). Nalm-6 and R3F9 cell lines were exposed to R406 (3µM and 6µM respectively), dexamethasone (10µM for both cell lines) alone or using their mixture together for two hours. Similar to results in chapter 4 section 4.4.4, R406 treatment was associated with a modest inhibition in pSYK in both cell lines, but there was no additional inhibition observed in all phospho proteins in cells dosed with combination when compared with cells exposed to single drugs (Figure 5.12).

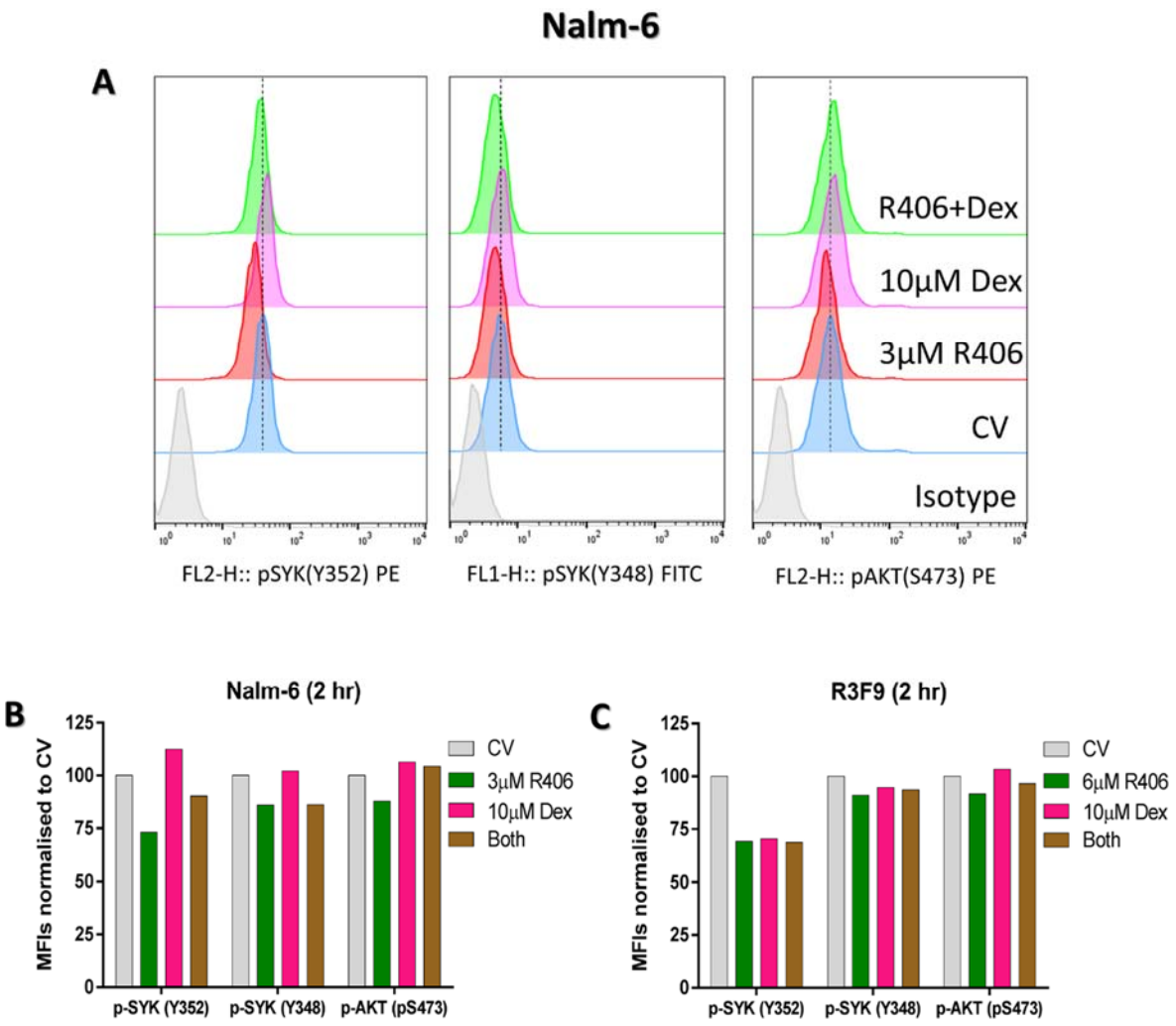

Figure 5.12: The pharmacodynamic effect of R406 plus dexamethasone on BCP-ALL cells.

Intracellular staining with anti-pSYK(Y352) PE, anti-pSYK(Y348) FITC and anti-pAKT(pS473) PE and acquisition on a FACSCalibur was carried out following incubation of cells with indicated concentrations of R406, dexamethasone (Dex) or both together for 2 hours. **(A)** One representative histogram overlay shows the phosphorylation levels of different proteins in Nalm-6 cells exposed to different treatments. Bar charts represent the mean fluorescent intensities (MFIs) of one biological replicate normalised to CV in Nalm-6 **(B)** and R3F9 **(C)**. FlowJo software was used to perform histograms overlays.

5.5.4.2 The effect of R406 plus dexamethasone on the Induction of GR target gene *GILZ*

To decipher the mechanism of synergy seen in BCP-ALL cells exposed to R406 and dexamethasone combination, the transcriptional level of GR target gene *GILZ* was investigated. R3F9 cells were treated with R406 (6µM), dexamethasone (25µM) or with their combination for 24 hours and expression of *GILZ* mRNA was then measured by QRT-PCR (Section 2.4). The $\Delta\Delta C_T$ method was then used to quantify the level of *GILZ* mRNA in relation to the endogenous control gene *TBP* (Section 2.4.4) and then *GILZ* transcript levels after different treatments were then normalised to CV. As shown in figure 5.13, dexamethasone significantly induced *GILZ* mRNA expression when compared with CV (~70 fold, p=0.0004), but surprisingly R406 also induced *GILZ* upregulation (~4.6 fold, p=0.03). Moreover, mRNA extracted from R3F9 cells exposed to the drug combination showed significantly higher level of *GILZ* transcription than cells treated with R406 (~58 fold, p=0.0001) or dexamethasone (~4 fold, p=0.0005) alone (Figure 5.13 A). Interestingly, *GILZ* upregulation in response to dexamethasone treatment was expected in GR^+ ALL cells and this finding also validates the stability of the reference gene *TBP.*

The same experiment was repeated with R3F9 and Nalm-6 cells using R406 (6µM and 3µM respectively), with a reduced dexamethasone concentration (10µM for both cell lines) or a mixture of both drugs. A similar trend of enhanced *GILZ* transcription was seen in R3F9 cells exposed to the drug combination compared to R406 (~32 fold) or dexamethasone (~ 2 fold) alone (Figure 5.13 B). In addition, the same trend of enhanced effect was also confirmed in Nalm-6 cells and the level of *GILZ* induction in cells treated with the drug combination was about 100 fold higher than R406 and 2 fold higher than dexamethasone treated cells (Figure 5.13 C)

As presented earlier in this chapter (Section 5.5.1), no synergism was seen in REH cells incubated with R406 plus dexamethasone (Figure 5.8 D, E) as REH cells lack GR expression (see later Figure 5.14). Therefore, to confirm these data, *GILZ* induction was also investigated in REH cells which served as negative control. REH cells were co-cultured with 6µM R406, 10µM dexamethasone or with their mixture together for 24 hours. There was no increase in *GILZ* mRNA levels in single agent of drug combination in comparison with CV (Figure 5.13 D).

In summary, R406 plus dexamethasone significantly enhanced the transcriptional activity of GR as measured by its target *GILZ* in cell lines that express GR protein.

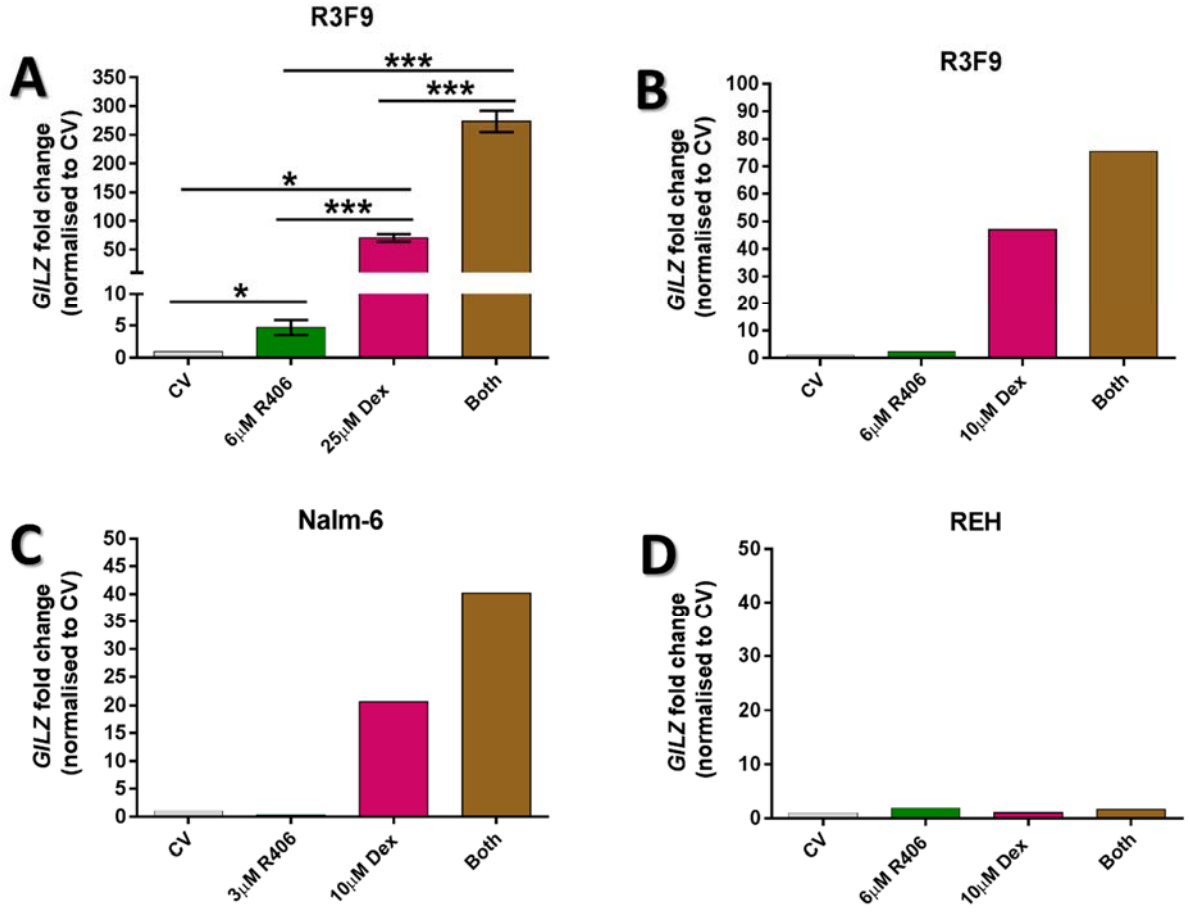

Figure 5.13: R406 and dexamethasone combination enhances the transcriptional activity of *GILZ.*

(A, B) R3F9, **(C)** Nalm-6 and **(D)** REH cells were co-cultured with the indicated concentrations of R406, dexamethasone (Dex) alone or in combination for 24 hours. The level of *GILZ* gene mRNA was measured in relation to the house keeping gene *TBP* by QRT-PCR, *GILZ* transcript levels with different treatments was then normalised to CV. Histogram **(A)** shows the mean fold change of *GILZ* ± SEM (n=3), Student`s t-test was used to calculate p values, *p<0.05, ***p<0.001. Histograms **(B, C and D)** show the mean fold change of *GILZ* of one replicate run.

5.5.5 Mechanistic study of the synergy seen in BCP-ALL cell lines treated with R406 plus dexamethasone combination at the GR level

In light of the significant synergy seen in some BCP-ALL cells (Sections 5.5.1 and 5.5.3) and the significant induction of the GR target gene *GILZ* (Section 5.5.4.2), the mechanism behind this synergy was investigated. To this end, the glucocorticoid receptor level, activation, cellular localisation and GRE binding were investigated in BCP-ALL cell lines which showed synergy.

5.5.5.1 Effect of R406 plus dexamethasone on GR expression and phosphorylation

It has been found that human GR is phosphorylated at multiple serine sites after exposure to hormone or synthetic glucocorticoid and mainly at S211. Interestingly, the amount of phosphorylation is reflective of GR transcriptional activity *in vivo* (Wang *et al.*, 2002b). To see if the combination treatment modulated the GR expression or phosphorylation at the S211 phosphorylation site, glucocorticoid resistant cell lines (Nalm-6 and R3F9) were co-cultured with R406 (Nalm-6: 3µM; R3F9: 6µM) or dexamethasone (10µM) individually or with both together for 4 hours before assessment of GR by western blotting (Section 2.6.1). REH cells which lack GR expression (Bachmann *et al.*, 2007) were used as negative control for both GR and pGR. In both cell lines, no change in the level of GR proteins extracted from whole cells lysates was observed across all treatments (Figure 5.14). In both cell lines, GR was phosphorylated after exposure to dexamethasone alone and a similar level of phosphorylation was exhibited in cells treated with R406 plus the dexamethasone combination (Figure 5.14). This indicates that levels of GR or its activation are not involved in the mechanism of synergy.

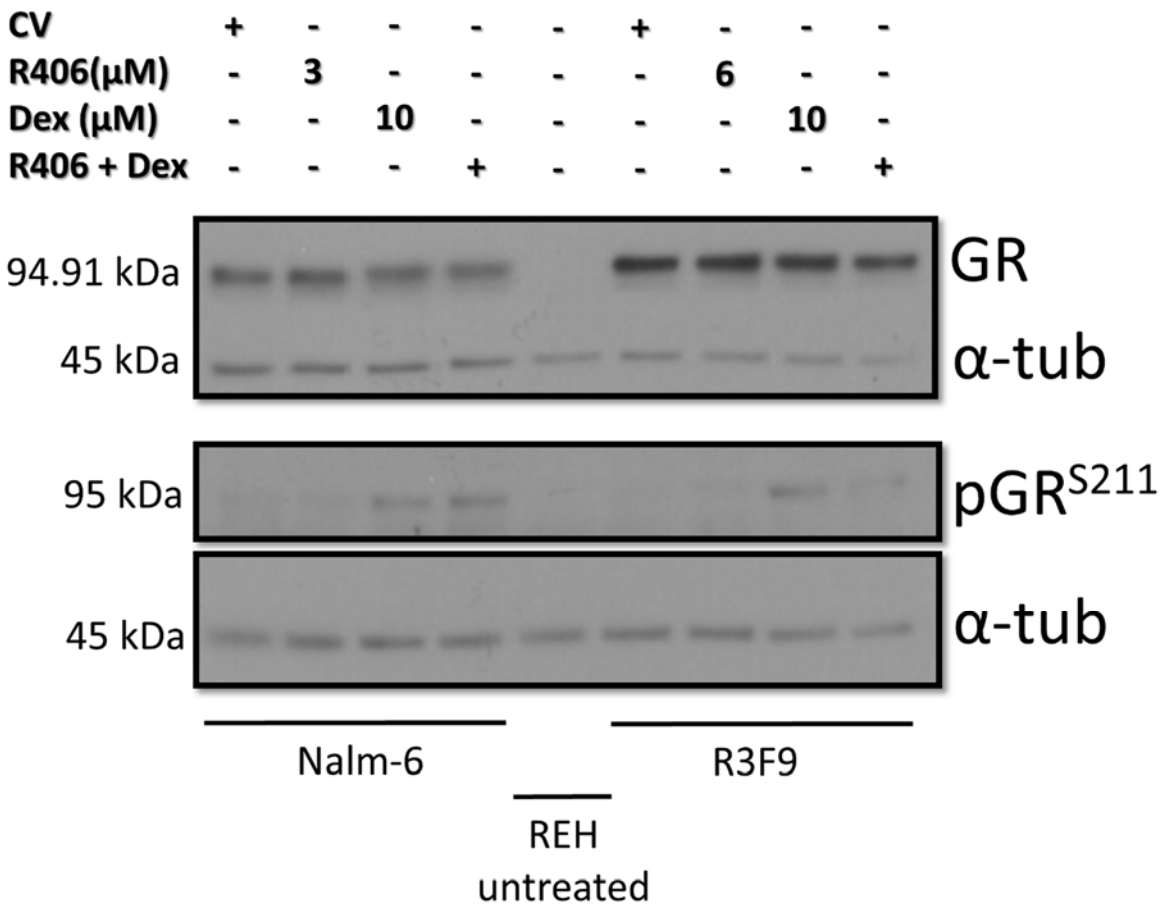

Figure 5.14: R406 plus dexamethasone combination does not enhance GR expression and phosphorylation at S211 in BCP-ALL cell lines.

Effects of R406 or dexamethasone alone or the drug combination using the indicated concentrations on GR expression and phosphorylation in Nalm-6 and R3F9 cells after 4 hours incubation. Total proteins were extracted from whole cell lysates before detection by western blotting, α-tubulin was used as a loading control. Untreated REH cells served as a negative control for both GR and pGR.

5.5.5.2 Effect of R406 plus dexamethasone on GR translocation from the cytosol to the nucleus

To further investigate the mechanism of synergy at the glucocorticoid receptor level, GR translocation from cytoplasm to the nucleus was evaluated. The GC-resistant cell line Nalm-6 was exposed to 3µM R406 or 10µM dexamethasone or to their mixture for 4 hours before fractionation of cytoplasmic and nuclear proteins (Section 2.6.2) and immunoblotting (Section 2.6.1). Whole cell lysates (Section 2.6.1.1) of untreated REH cells were used as negative control for GR protein. While dexamethasone treatment induced robust GR translocation to the

nucleus, there was no additional increase in levels of GR translocation in cells treated with the drug combination (Figure 5.15). These data suggest that enhanced GR translocation is not associated with the synergy and enhanced apoptosis observed after exposure to R406 plus dexamethasone. PARP (nuclear protein) and α-tubulin (cytoplasmic protein) were used as loading controls, they also validated the purity of protein extraction from cell compartments.

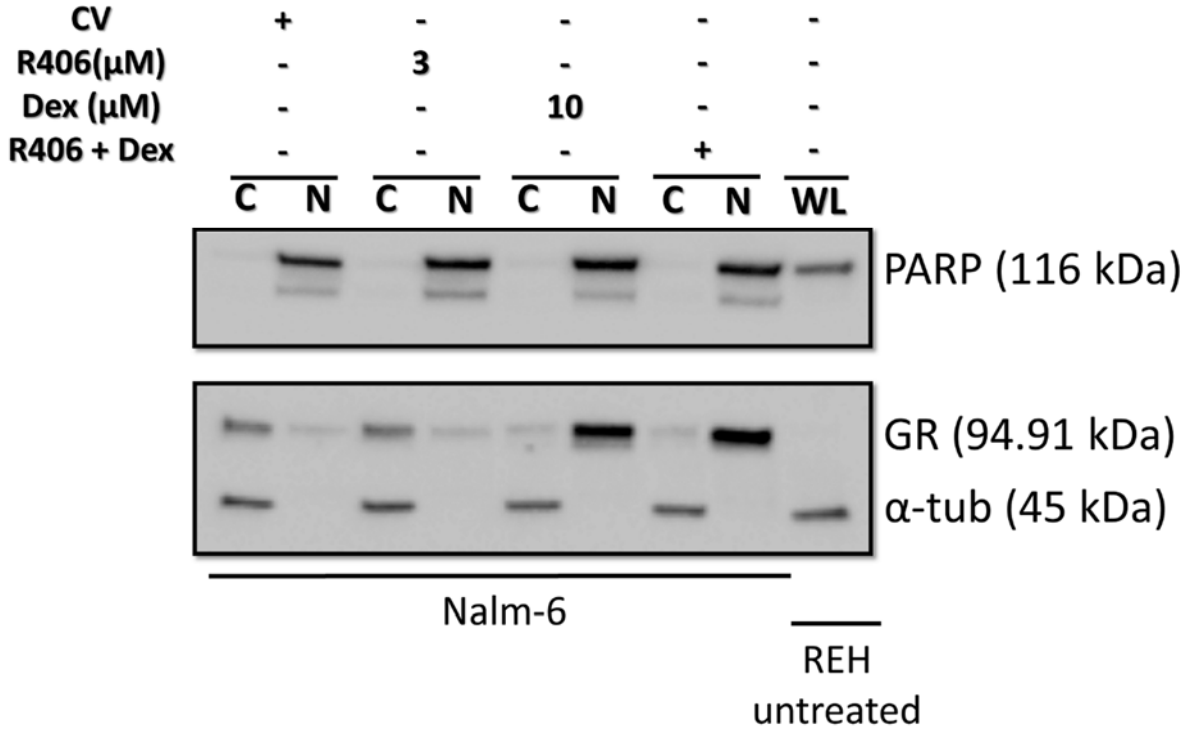

Figure 5.15: R406 plus dexamethasone combination has no effect on GR cellular localisation in Nalm-6 cells.

Nalm-6 cells were exposed to the indicated concentrations of R406, dexamethasone or their mixture together for 4 hours followed by cytoplasmic (C) and nuclear (N) proteins extraction to detect GR translocation by immunoblotting. Whole cell lysate (WL) extracted from untreated REH cells served as a negative control for GR protein. Cytoplasmic (α-tubulin) and nuclear (PARP) loading controls were used. One representative immunoblot of 2 replicates is presented.

5.5.5.3 Effect of R406 plus dexamethasone on GRE binding activity

As shown in the previous section (5.5.5.2), GR protein is translocated to the nucleus in Nalm-6 cells after exposure to dexamethasone or drug combination. To further characterise glucocorticoid receptor, the levels of GR binding to the consensus DNA sequence, 5'-GGTACAnnnTGTTCT-3' (Beato *et al.*, 1989), was measured. TransAM Transcription Factor ELISA kit (Active Motif) was used to assess the affinities of GRE-DNA binding for proteins extracted from nuclei by ELISA method (Section 2.6.3).

Briefly, Nalm-6 cells were incubated with 3µM R406 or 10µM dexamethasone or both together or the equivalent CV for 4 hours before harvesting. Nuclear proteins were extracted (Section 2.6.3.1) and then 10µg aliquots were used in the assay according to the manufacturer instructions (2.6.3.3). Nuclear extract of HeLa cells exposed to 100nM of dexamethasone for 60 minutes was provided with the kit and used as positive control and ran alongside test samples.

As shown in figure 5.16, cells treated with dexamethasone alone exhibited an increase in GRE binding activity (Abs. at 450nm: 0.606) as well as cells exposed to the drug combination but to a similar degree (Abs. at 450nm: 0.476). These data suggest that the synergism observed with R406 plus dexamethasone is not due to enhanced ligand-induced DNA binding activity.

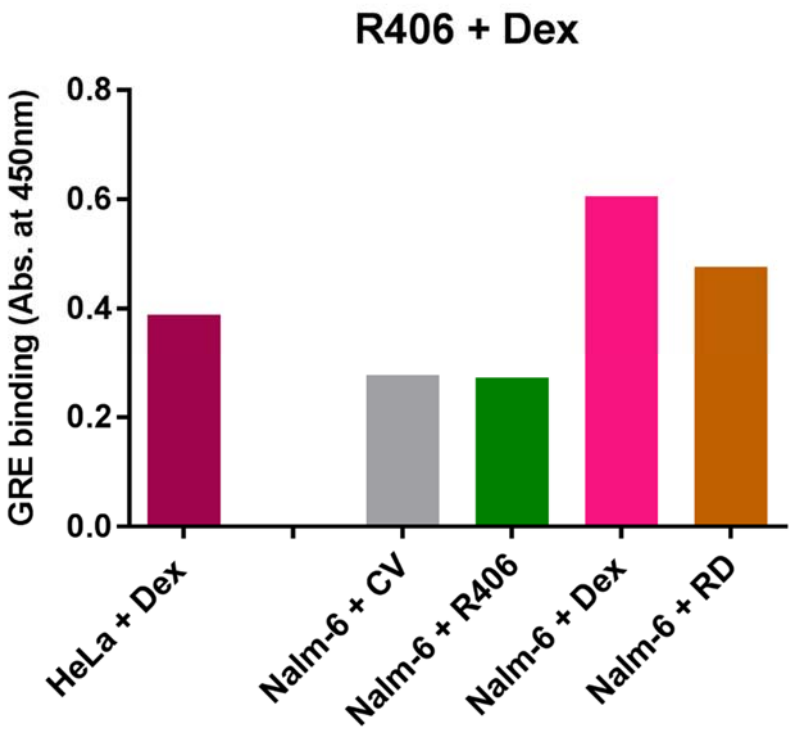

Figure 5.16: R406 plus dexamethasone mixture does not enhance GRE binding activity in Nalm-6 cells.

Nalm-6 cells were exposed to 3µM R406 or 10µM dexamethasone (Dex) or both (RD) for 4 hours before extracting nuclear protein to assess GRE binding activity by ELISA. Columns represent the absorbance at 450nm of one replicate experiment.

5.5.5.4 Effect of R406 plus dexamethasone on the Pro-apoptotic target BIM

Given the synergy seen in cells incubated with R406 plus dexamethasone (Sections 5.5.1 and 5.5.3), the mechanism of synergy was extended to investigate BIM, the indirect target of GC which plays a significant role in GC-induced apoptosis (Wang *et al.*, 2003; Bachmann *et al.*, 2005). Three isoforms of BIM (BIM_{EL}, BIM_L and BIM_S) differ from each other in cytotoxicity were characterised, and BIM_S is the most powerful (Marani *et al.*, 2002). R3F9 cells were treated with 6µM R406, 25µM dexamethasone or with their mixture together for 24 and 48 hours before assessment of BIM induction by western blotting (Section 2.6.1). While there was appeared to be induction of BIM_{EL} in the presence of dexamethasone at 48 hours, western blotting data from 3 independent runs did not show a significant increase in the levels of different BIM isoforms in R3F9 cells treated with combination compared to cells incubated with dexamethasone at both time points (24 and 48 hours) (Figure 5.17). Surprisingly, an

induction of BIM_L and BIM_S isoforms was seen in cells treated with R406 alone after 48 hours (Figure 5.17 B).

In summary, no enhanced induction of BIM isoforms was observed after dosing R406 and dexamethasone in R3F9 cells compared to single drugs.

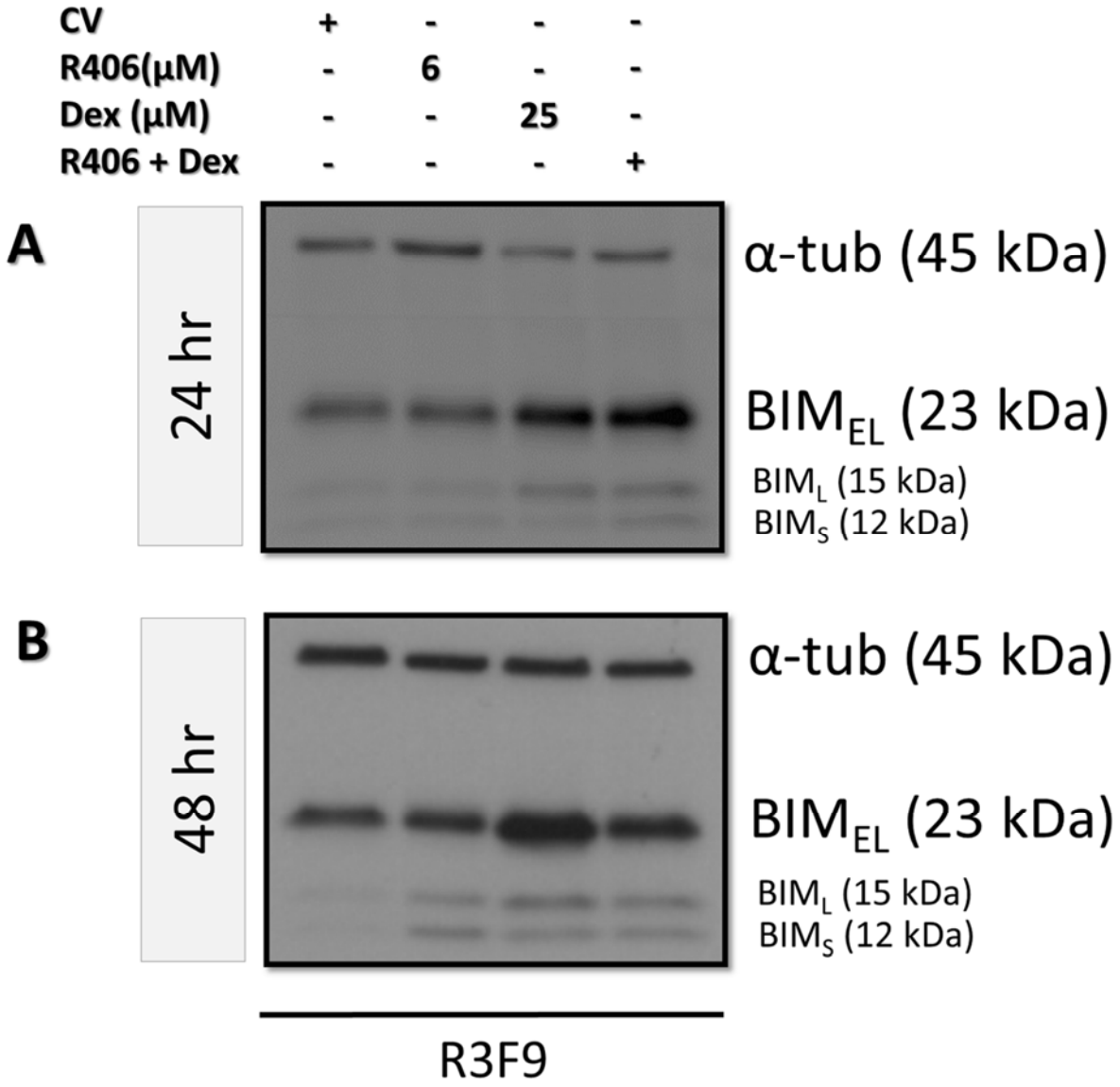

Figure 5.17: R406 and dexamethasone combination does not upregulate BIM protein.

R3F9 cells were co-cultured with the indicated concentrations of R406, dexamethasone (Dex) alone or with their mixture for **(A)** 24 and **(B)** 48 hours to investigate the effect on the pro-apoptotic factor BIM by western blotting. One representative blot of three experiments performed independently is depicted, α-tubulin served as a loading control.

5.6 Effect of dasatinib combination with dexamethasone on BCP-ALL cells

5.6.1 Effect of dasatinib plus dexamethasone using the Chou and Toulalay median effect on BCP-ALL cells viability

As shown in chapter 4, dasatinib as a single agent inhibited several targets downstream of Pre-BCR signalling and sensitivity was seen in multiple Pre-BCR$^+$ and Pre-BCR$^-$ ALL cells. Recently, it was shown that dasatinib could improve sensitivity of GC-resistant T-ALL cells to dexamethasone through inhibition of the dasatinib target, LCK (Serafin *et al.*, 2017). Therefore, the rationale to investigate dasatinib plus dexamethasone in BCP-ALL cells was tempting. To this end, BCP-ALL cells were exposed to 0.25x, 0.5x, 1.0x, 2.0x and 4.0x of GI_{50} concentrations of dasatinib, dexamethasone or their combination for 96 hours before viability assessment by Alamar blue assay (Section 2.5.1). CalcuSyn software was then used to calculate CI values based on Chou and Toulalay median effect at ED50, ED75 and ED90 (Section 2.5.2).

CI values calculated from dasatinib plus dexamethasone combination displayed strong synergism in Nalm-6 [CI (mean ± SEM) range: 0.144 ± 0.066 to 0.059 ± 0.013] and R3F9 [CI (mean ± SEM) range: 0.28 ± 0.059 to 0.148 ± 0.03] cells and CI values were consistent at different effective doses (Figure 5.18 B, C and E). In addition, the same combination was moderately synergistic in the GC-sensitive line PreB 697 at ED50 [CI (mean ± SEM): 0.82 ± 0.14], however, at higher doses (ED75 and ED90), the CI values were indicative of synergism [CI (mean ± SEM): 0.49 ± 0.0.01 and 0.32 ± 0.05 respectively] (Figure 5.18 A and E). Moreover, REH did not show synergy when cultured with dasatinib plus dexamethasone combination (Figure 5.18 D, E).

PDX cells harvested from mice spleens were also investigated *ex vivo* using dasatinib with the dexamethasone combination. Interestingly, very strong synergism was observed in a Ph$^+$ PDX sample, L4951/AZ26 (CI range: 0.02 – 0.16) which lack Pre-BCR expression and was resistant to dexamethasone alone. Moreover, strong synergy was obtained in the Pre-BCR$^+$ PDX sample L910/AZ27 (CI range: 0.224 – 0.229). Although the CI value at ED50 (CI = 0.78) suggested moderate synergism in L824/AZ22, very strong synergism and strong synergism at ED75 (CI = 0.36) and ED90 (CI = 0.17) was shown. However, this combination was antagonistic in L881/JM275 (CI values > 1.1) (Figure 5.19).

Taken together, dasatinib strongly synergised with dexamethasone in Pre-BCR$^+$ and Pre-BCR$^-$ BCP-ALL cells even in dexamethasone resistant cells.

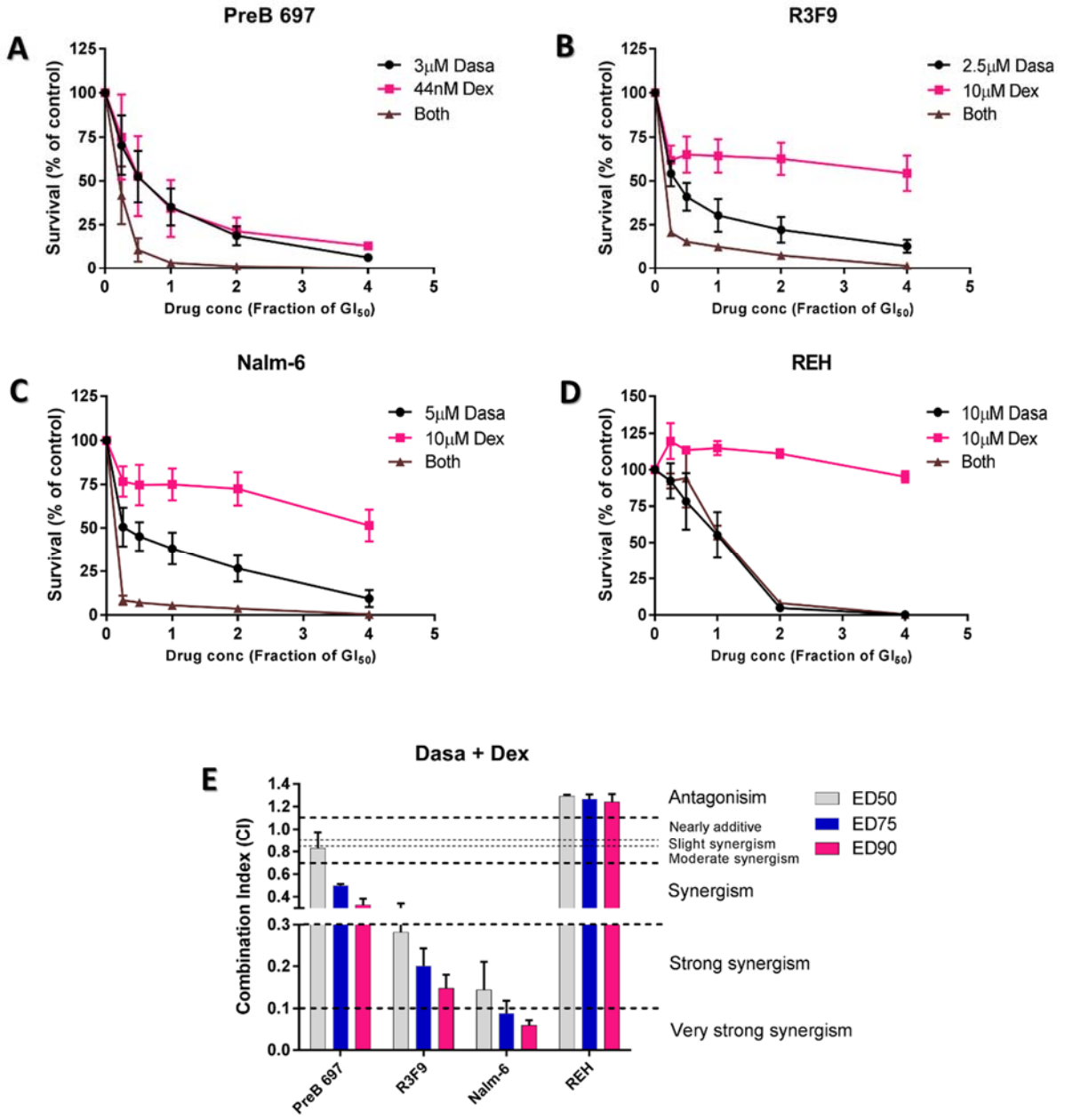

Figure 5.18: Dasatinib synergises with dexamethasone in Pre-BCR$^+$ BCP-ALL cell lines.

Dose response curves of **(A)** PreB 697, **(B)** R3F9, **(C)** Nalm-6 and **(D)** REH cell lines incubated with GI_{50} fractions of dasatinib (Dasa), dexamethasone (Dex) or both together for 96 hours followed by assessment by Alamar blue assay. **(E)** Histograms represent the mean combination indices calculated using CalcuSyn software at the effective doses (ED) that reduce 50, 75 and 90% of the cell viability. The viability curves and CI values represent the mean ± SEM of 3 independent experiments. GI_{50} concentrations were indicated for each cell line.

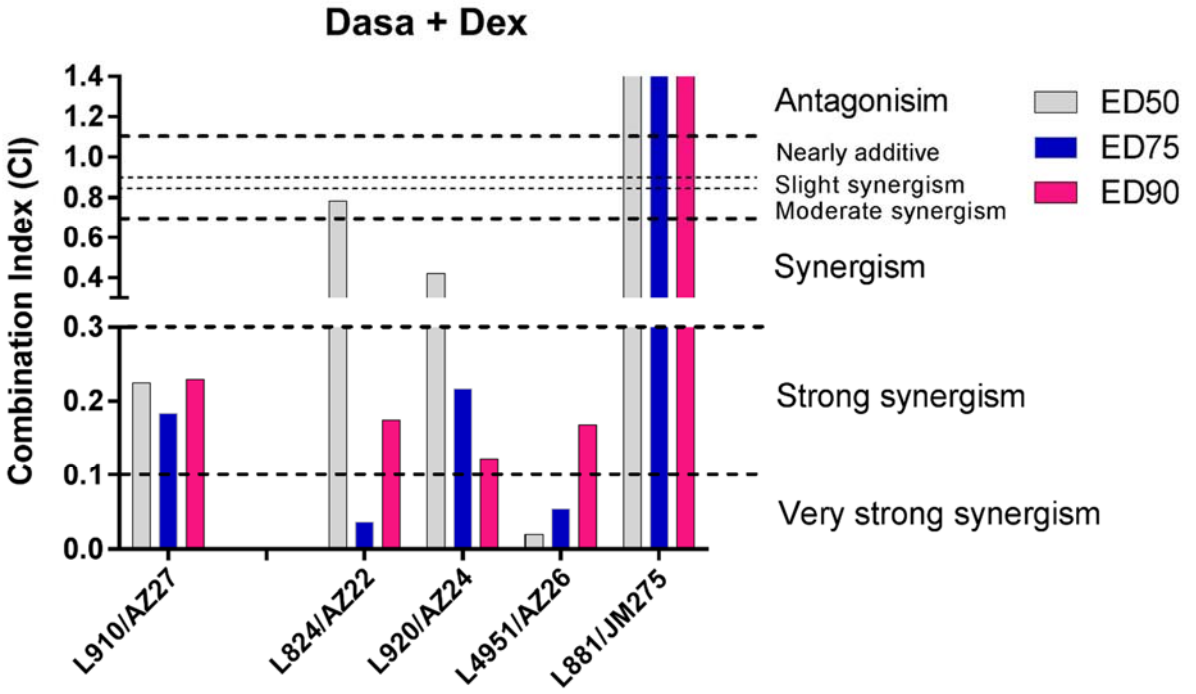

Figure 5.19: Dasatinib strongly synergises with dexamethasone in Pre-BCR$^+$ and Pre-BCR$^-$ PDX samples.

Histogram represent the combination indices calculated at 50, 75 and 90% effective doses (ED50, ED75 and ED90 respectively) using CalcuSyn software after PDX cells being exposed to GI_{50} fractions of dasatinib (Dasa), dexamethasone (Dex) or both together for 96 hours followed by Alamar blue assay. CI values were calculated from one replicate PDX.

5.6.2 Effect of dasatinib plus dexamethasone on cell cycle phases of BCP-ALL cell lines

In order to understand the mechanism of the synergistic effect seen after exposing BCP-ALL cells to dasatinib with dexamethasone mixture, the effect on distribution of cell cycle phases was studied by propidium iodide staining and flow cytometry (Section 2.3.3). To this end, R3F9 and PreB 697 cell lines were co-cultured with the GI_{50} concentrations of dasatinib (2.5µM and 3µM respectively), dexamethasone (25µM and 44nM respectively) alone or their mixture together. It was shown in chapter 4 that dasatinib treatment as a single inhibitor induced G1 arrest in multiple cell lines (Section 4.5.2). G1 arrest was also induced due to treatment with dexamethasone alone in the same cell lines (Figure 5.20). The combination of both drugs significantly enhanced G1 arrest. The mean percentage of R3F9 cells arrested at G1 ± SEM was 79.43 ± 0.72% after cells were incubated with dasatinib plus dexamethasone for 24 hours which was significantly higher than dasatinib (Mean ± SEM: 51.57 ± 4.02%; p=0.0024) or

dexamethasone (Mean ± SEM: 46.97 ± 1.28%; p<0.0001) treated cells. Interestingly, a similar trend of enhanced G1 arrest was maintained after 48 hours and was significant in combination when compared with single drugs treatments. In addition, 9.05 ± 1.25% of the cells co-cultured with combination for 48 hours were present in the sub-G1 peak which was significantly higher when compared with cells exposed to dasatinib (Mean ± SEM: 2.203 ± 0.26%; p=0.006) or dexamethasone (Mean ± SEM: 3.74 ± 0.72%; p=0.021) alone (Figure 5.20 A, B).

PreB 697 cells were also incubated with the dasatinib and dexamethasone combination and an increased percentage of cells arrested at G1 phase was observed after 24 hours (Mean ± SEM: 74.20 ± 2.91%) which was significant when compared with single drug treatment, dasatinib (Mean ± SEM: 43.30 ± 1.82%; p=0.0008) and dexamethasone (Mean ± SEM: 44.57 ± 3.5%; p=0.0029). However, after 48 hours the same combination induced G1 arrest (Mean ± SEM: 53.27 ± 0.29%) and the percentage of cells was only significantly higher than dasatinib treated cells (Mean ± SEM: 48.97 ± 0.98%; p=0.014). Moreover, a clear increase in the percentage of cells in the sub-G1 peak was seen after 48 hours incubation with the drug combination (Mean ± SEM: 30.60 ± 3.14%) when compared with dasatinib (Mean ± SEM: 2.27 ± 0.12%; p=0.0008) or dexamethasone (Mean ± SEM: 5.757 ± 1.17%; p=0.0018) alone indicating apoptosis induction (Figure 5.20 C).

To sum up, the combination of dasatinib and dexamethasone induced an enhanced increase in G1 arrest and an accumulation of cells in asub-G1 peak in comparison with treatment with single drugs.

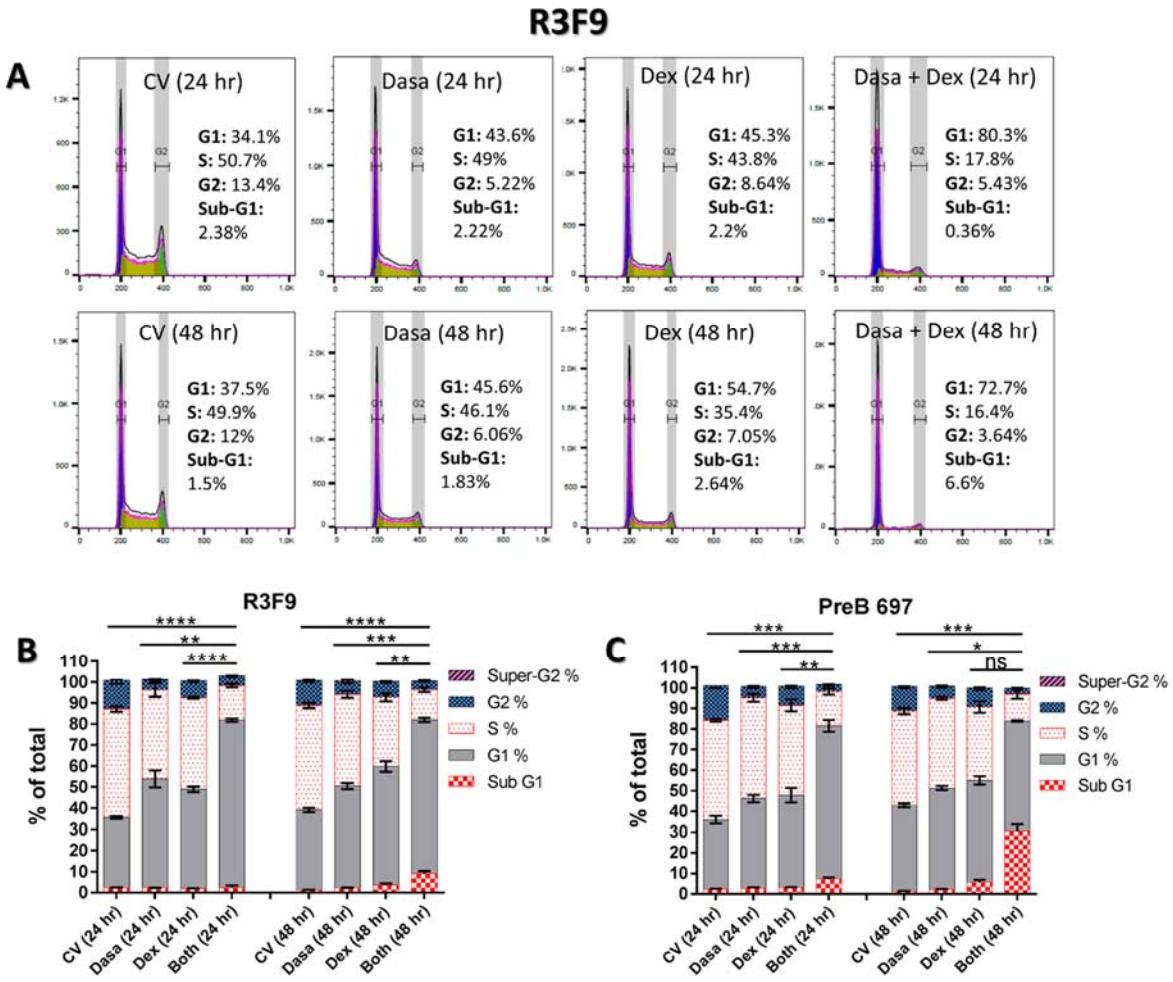

Figure 5.20: Dasatinib co-exposure with dexamethasone induces robust G1 arrest in BCP-ALL cell lines.

Cell cycle phases were assessed by flow cytometry using propidium iodide staining after incubating **(A, B)** R3F9 and **(C)** PreB 697 cells with dasatinib (Dasa), dexamethasone (Dex) alone or in combination. BCP-ALL cell lines were exposed to vehicle, dasatinib (R3F9: 2.5µM and PreB 697: 3µM), dexamethasone (R3F9: 25µM and PreB 697: 44nM) or a mixture of both drugs for 24 and 48 hours. Histograms of one representative cell cycle run of 3 independent experiments is presented for R3F9. The bar graphs show the mean percentage of cells distributed at different phases of the cell cycle ± SEM (n=3). FlowJo software was used to analyse cell cycle data. Asterisks denote the student`s t-test statistical analysis of the G1 phase for all cell lines. *p<0.05, **p<0.01, ***p<0.001, ****p<0.0001 and ns= not significant.

5.6.3 Apoptotic effect of dasatinib plus dexamethasone on BCP-ALL cell lines

As shown in section 5.6.1, a great synergy was seen in multiple cell lines exposed to dasatinib plus dexamethasone, hence, to characterise the mechanism of action of this drug combination, Annexin V-FITC staining (Section 2.3.2) was carried out to measure the percentage of apoptotic BCP-ALL cells by flow cytometry. To this end, R3F9 and PreB 697 cell lines were co-cultured with dasatinib (3µM and 2.5µM respectively), dexamethasone (25µM and 44nM respectively) alone or their mixture together for 48 and 72 hours.

In R3F9 cells, the combination of dasatinib and dexamethasone enhanced the percentage of apoptotic cells at 48 hours (Mean ± SEM: 26.80 ± 2.48%) and was nearly 2 fold higher than single agents [Dasatinib (Mean ± SEM: 10.75 ± 2.0%; p=0.007) or dexamethasone (Mean ± SEM: 13.38 ± 1.31%; p=0.008)]. Moreover, the effect of enhanced apoptosis was sustained after 72 hours and the proportion of cells was greater than 48 hour time point for all treatments. For cells cultured with the combination, the percentage of Annexin V positive cells (Mean ± SEM: 47.56 ± 1.2%) was significantly higher than cells exposed to dasatinib (Mean ± SEM: 30.59 ± 2.06%; p=0.0001) or dexamethasone (Mean ± SEM: 24.61 ± 1.9%; p=0.001) alone (Figure 5.21 A, B).

The combination effect was also studied in GC-sensitive PreB 697 cells. Interestingly, a similar trend of enhanced apoptosis was seen in PreB 697 cells treated with drug combination (Mean ± SEM: 51.04 ± 0.51%) for 48 hours which was significantly higher than single agent treatment [Dasatinib (Mean ± SEM: 9.53 ± 1.148%; p<0.0001) and dexamethasone (Mean ± SEM: 18.23 ± 2.62%; p=0.0003)]. Moreover, the percentage of Annexin V positive in cells treated with mixture of drugs was increased to 77.09 ± 3.9% after 72 hours which was robustly higher than the proportion of apoptosis induced by dasatinib (Mean ± SEM: 13.38 ± 0.99%; p<0.0001) or dexamethasone (Mean ± SEM: 36.29 ± 0.28%; p=0.0005) alone (Figure 5.21 C).

In conclusion, the combination of dasatinib and dexamethasone enhanced apoptosis induction in dexamethasone resistant and sensitive cell lines.

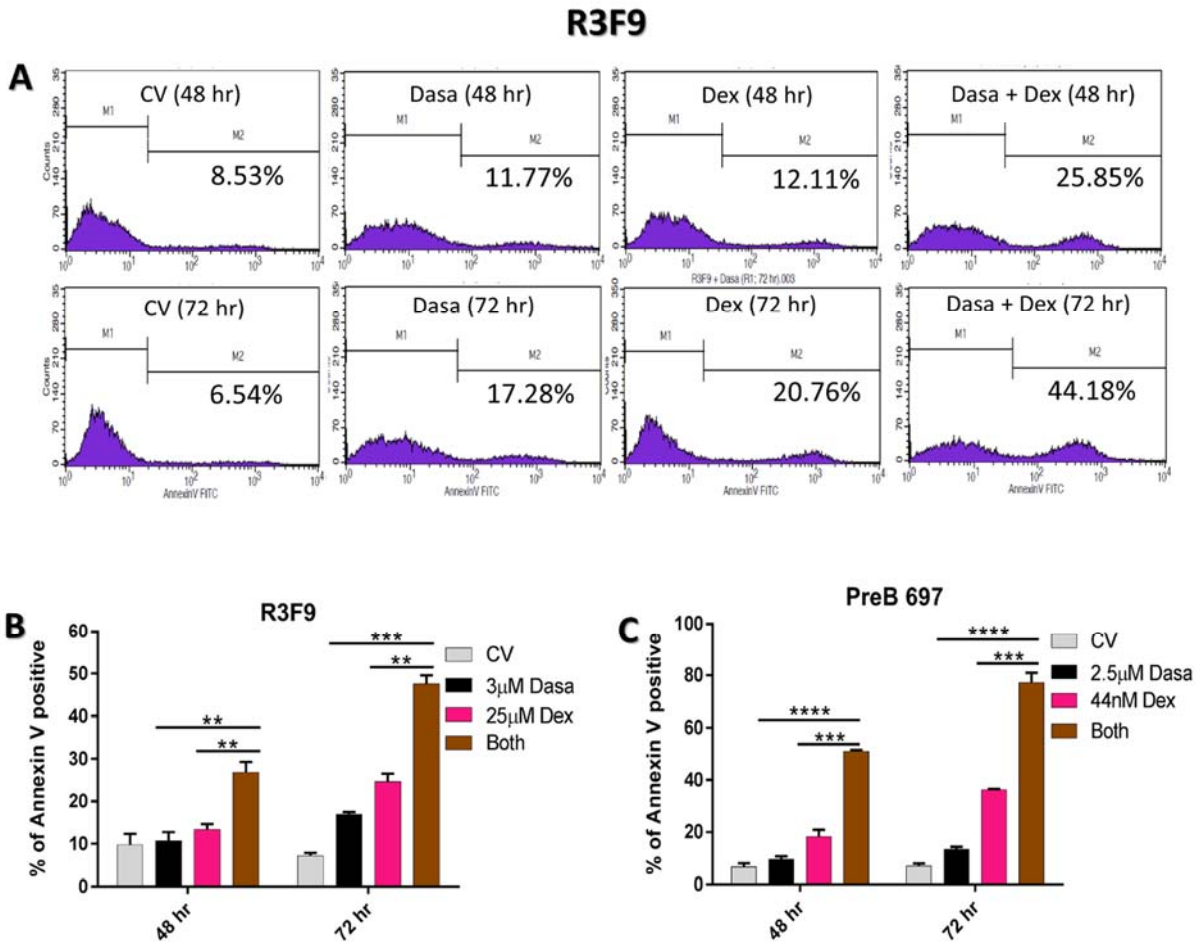

Figure 5.21: Dasatinib plus dexamethasone combination enhanced apoptosis in BCP-ALL cell lines.

Cell lines were co-treated with the indicated concentrations of dasatinib (Dasa), dexamethasone (Dex) alone or their combination for 48, 72 hours before Annexin V-FITC staining and assessment by flow cytometry. **(A)** Representative histograms of Annexin V staining are shown for R3F9 cells for two time points. Bar charts denote the mean ± SEM (n=3) of **(B)** R3F9 and **(C)** PreB 697. CellQuest software was used to analyse Annexin V data. Student`s t-test was carried out to calculate p values. **p<0.01, ***p<0.001, ****p<0.0001.

5.6.4 Pharmacodynamic effects of dasatinib plus dexamethasone on BCP-ALL cell lines

5.6.4.1 The effect of dasatinib/dexamethasone combination on the dasatinib targets inhibition

To further understand the synergistic effect seen after exposing BCP-ALL cell lines to dasatinib plus dexamethasone, the inhibition of potential pharmacological targets of dasatinib [pBTK(Y223), pSYK(Y348), pBLNK(Y84) and pPLC-ɣ2(Y759)] were investigated by intracellular phospho flow cytometry (Section 2.3.5). To this end, R3F9 was incubated with dasatinib (3µM) or dexamethasone (25µM) or with their mixture together for 24 hours. Consistent to data shown in chapter 4 (Figure 4.23), dasatinib alone significantly inhibited all phospho proteins investigated in both cell lines. Unexpectedly, dexamethasone alone also inhibited most of the tyrosine kinases in both cell lines. There was no additional inhibition seen with the drug combination when compared with single drugs (Figure 5.22) except for a subtle decrease in pSYK(Y348) phosphorylation (Mean MFI normalised to CV ± SEM: 60.0 ± 1.33%) with the drug combination in comparison with dasatinib (Mean MFI normalised to CV ± SEM: 65.16 ± 0.13%; p=0.018) or dexamethasone (Mean MFI normalised to CV ± SEM: 76.10 ± 1.76%; p=0.001) (Figure 5.22 B).

Taken together, the synergism seen in dasatinib plus dexamethasone did not appear to be due to enhanced inhibition of dasatinib Pre-BCR downstream signaling targets.

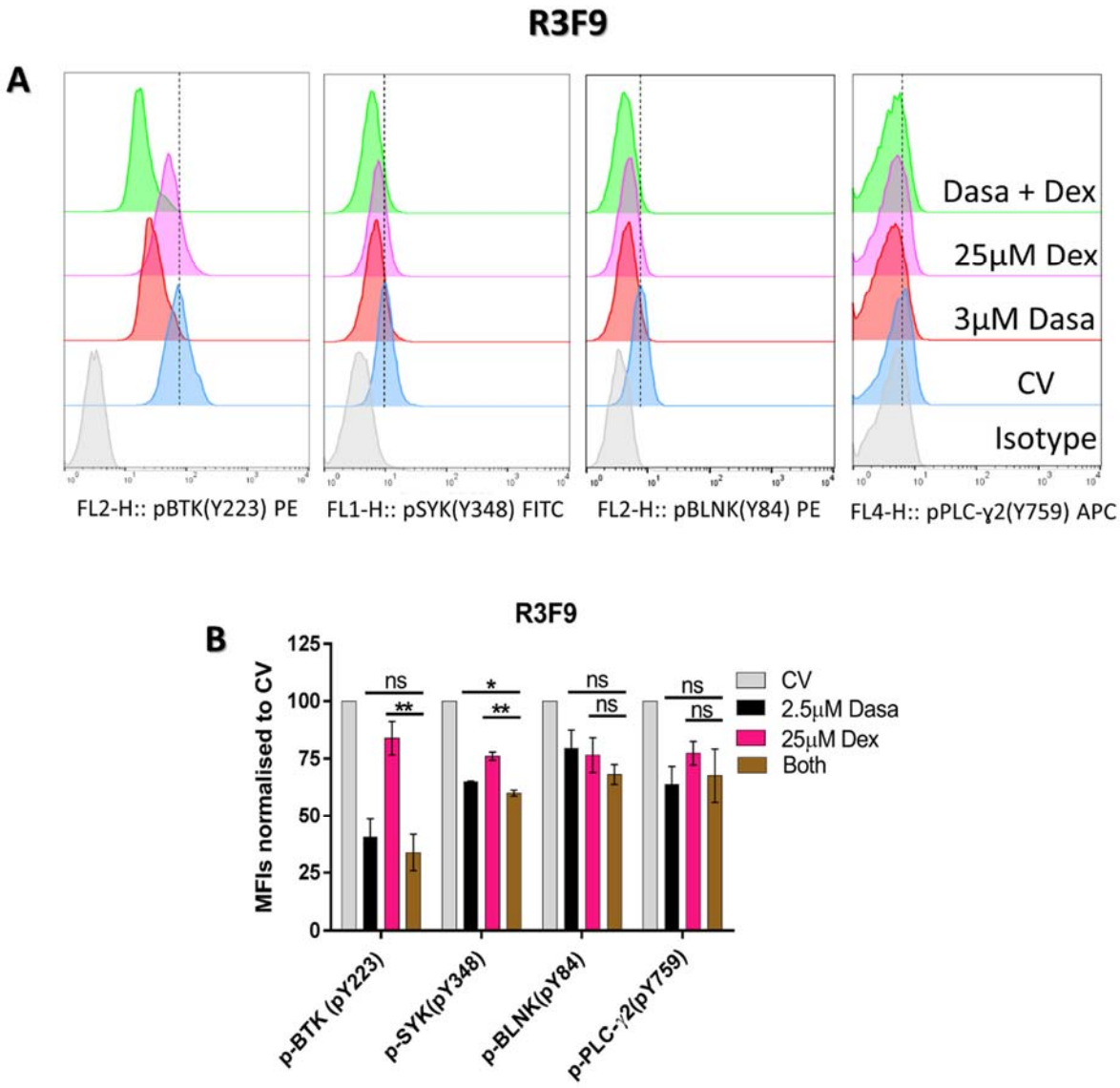

Figure 5.22: The pharmacodynamic effect of dasatinib plus dexamethasone mixture on R3F9 cell line.

Intracellular staining with anti-pBTK(Y233) PE, anti-pSYK(Y348) FITC, anti-pBLNK(Y84) PE and anti-pPLC-ɣ2(Y759) was performed on treated cells and acquired on a FACSCalibur with indicated concentrations of dasatinib (Dasa), dexamethasone (Dex) or their mixture together for 24 hours. **(A)** One representative overlay histograms show the phosphorylation levels of different phospho kinases in R3F9 cells treated with different drug treatments. Bar charts represent the mean ± SEM (n=2-3) of MFIs normalised to CV **(B)**. FlowJo software was used to generate histograms overlays. Student`s t-test was used to calculate p values. $p>0.05$ not significant (ns), *$p<0.05$, **$p<0.01$.

5.6.4.2 Effect of dasatinib plus dexamethasone mixture on the transcription of GR target gene *GILZ*

To further investigate the mechanism behind the synergistic effect of dasatinib plus dexamethasone combination, the level of *GILZ* transcription was studied. R3F9 cells were co-cultured with 2.5µM dasatinib, 25µM dexamethasone or with their mixture together for 24 hours before assessment of *GILZ* expression by QRT-PCR (Section 2.4). For cells exposed to single drugs (Dasatinib or dexamethasone), significant induction of *GILZ* expression was obtained in comparison with CV treated cells (~ 8 fold, p=0.0033 and ~117 fold, p=0.0017, respectively). Moreover, significantly higher induction of *GILZ* was detected in cells treated with combination compared with cells exposed to dasatinib (~81 fold, p=0.0007) or dexamethasone (~5 fold, p=0.0016) alone (Figure 5.23 A).

A similar experiment was repeated with R3F9 and Nalm-6 cells using dasatinib (3µM and 2.5µM respectively), and a lower dexamethasone concentration (10µM for both cell lines) or mixture of both drugs. Interestingly, a similar trend of enhanced transcriptional activity of *GILZ* was observed in R3F9 cells cultured with the drug combination compared to dasatinib (~75 fold) or dexamethasone (~4 fold) alone (Figure 5.23 B). Moreover, *GILZ* mRNA in Nalm-6 cells treated with combination was nearly 105 and 8 fold higher than cells exposed to dasatinib or dexamethasone, respectively (Figure 5.23 C).

As shown in section 5.6.1, the combination between dasatinib and dexamethasone was non-effective in the GR negative REH cell line (Figure 5.18 D, E). Hence, to confirm if these findings are also mirrored in the transcriptional activity of GR target gene, *GILZ* level was measured and used as negative control. REH cells were incubated with 6µM dasatinib, 10µM dexamethasone or with their mixture for 24 hours. Similar to REH cells exposed to dexamethasone combined with R406 (Section 5.5.5.4), no further induction in the transcription of *GILZ* gene was observed in cells treated with dexamethasone combination with dasatinib when compared with cells treated with dasatinib alone. Compared to CV, there was no change in the level of *GILZ* mRNA in cells treated with dexamethasone alone but was nearly 5 fold higher in cells incubated with dasatinib alone (Figure 5.23 D).

In summary, the combination of dasatinib with dexamethasone significantly enhanced the induction of *GILZ* mRNA in GC-resistant cell lines that express GR protein.

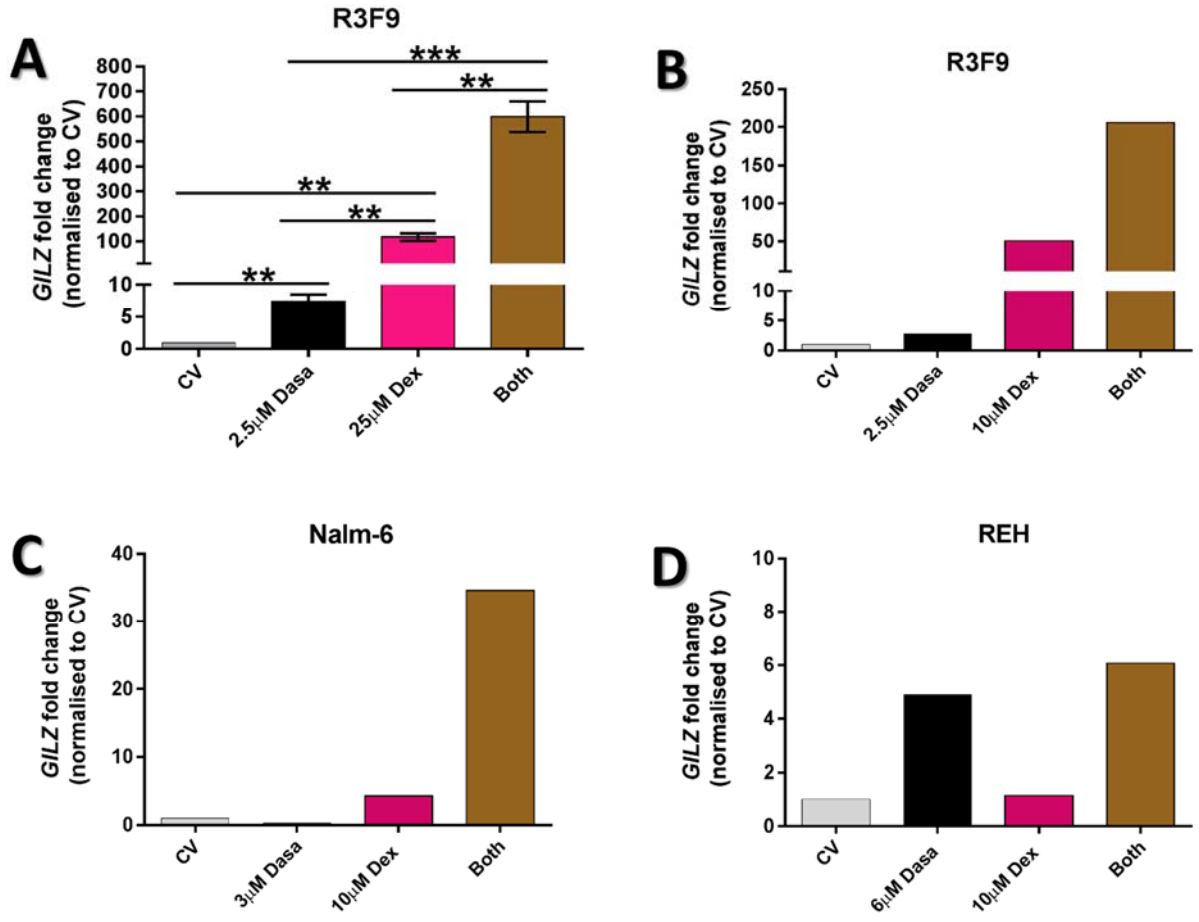

Figure 5.23: Dasatinib plus dexamethasone combination enhances the levels of *GILZ* mRNA.

(A, B) R3F9, **(C)** Nalm-6 and **(D)** REH cells were treated with the indicated concentrations of dasatinib (Dasa), dexamethasone (Dex) alone or their combination for 24 hours. The level of *GILZ* gene mRNA was measured in relation to the endogenous control gene *TBP* by QRT-PCR, *GILZ* transcription in different treatments was then normalised to CV. Bar chart **(A)** shows the mean fold change of *GILZ* ± SEM (n=3). Histograms **(B, C and D)** show the mean fold change of *GILZ* of one replicate run. Student`s t-test was used to calculate p values **p<0.01, ***p<0.001.

5.6.5 Mechanistic study of the combination between dasatinib and dexamethasone in BCP-ALL cell lines at the GR level

In order to investigate the mechanism behind the synergistic apoptosis (Section 5.6.3) and enhanced *GILZ* expression (Section 5.6.4.2) seen in cells co-incubated with dasatinib plus dexamethasone, several parameters involved in GR pathway such as GR expression and phosphorylation, GR nuclear translocation, GRE binding were studied in GC-resistant lines that previously exhibited synergy (Sections 5.6.1 and 5.6.3).

5.6.5.1 Effect of dasatinib plus dexamethasone on GR expression and phosphorylation

To confirm if GR expression and phosphorylation were modulated, GC-resistant cell lines were exposed to dasatinib plus dexamethasone. Nalm-6 and R3F9 were incubated with dasatinib alone (3µM and 2.5µM respectively), dexamethasone alone (10µM) or both together for 4 hours prior to immunoblotting detection (Section 2.6.1). REH cells were used as negative control because they lack GR expression (Bachmann *et al.*, 2007). Immunoblots of both cell lines depicted that no effect was observed on the GR protein level in all different treatments (Figure 5.24). Moreover, dexamethasone alone and in combination equally induced phosphorylation of GR in both cell lines (Figure 5.24), hence, the combination of dasatinib with dexamethasone does not enhance GR protein levels expression or activation as assessed by GR ser211 phosphorylation in BCP-ALL cells.

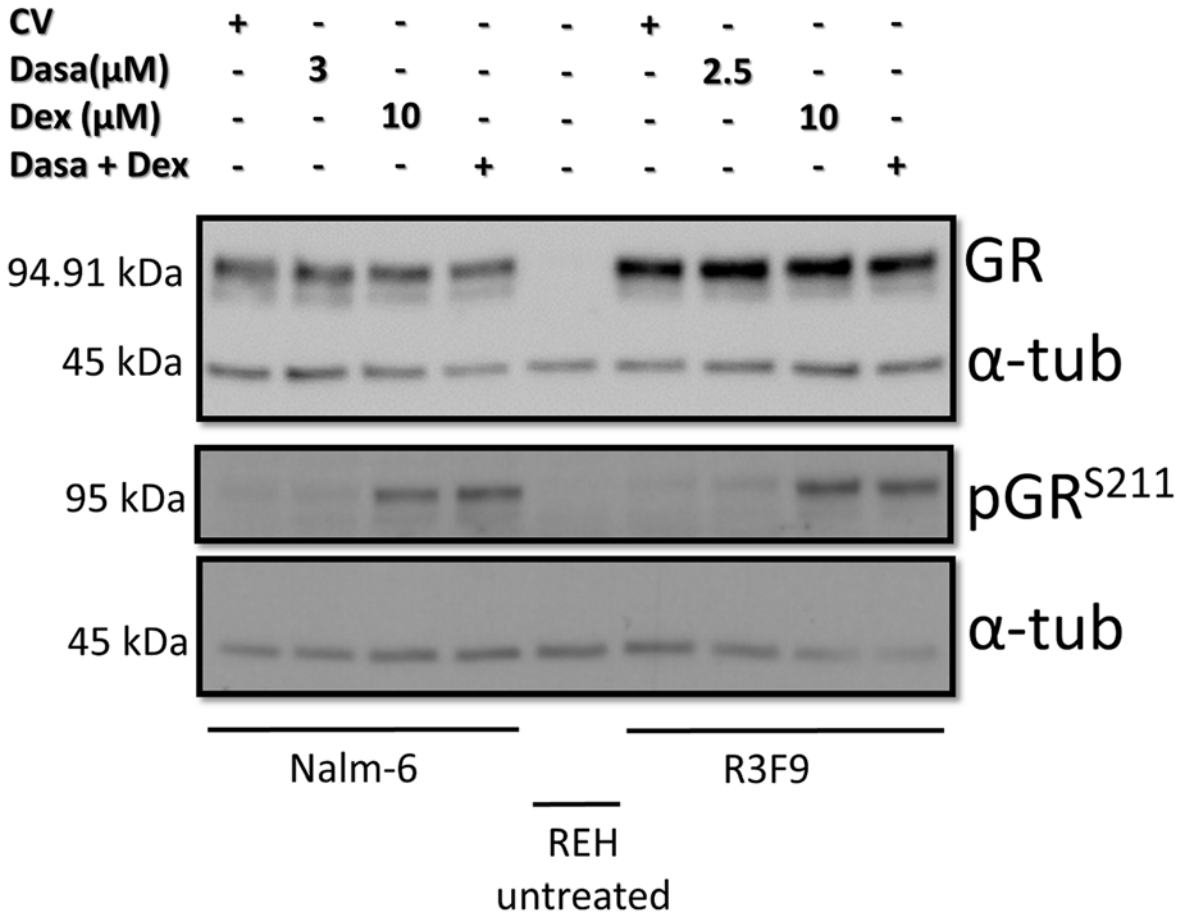

Figure 5.24: Dasatinib and dexamethasone combination does not enhance GR expression and phosphorylation at ser211 in BCP-ALL cell lines.

Effects of dasatinib (Dasa) alone or dexamethasone (Dex) alone or their mixture together using the indicated concentrations on GR expression and phosphorylation in Nalm-6 and R3F9 cells after 4 hours incubation. Total proteins were extracted from whole cell lysates before detection by western blotting, α-tubulin was used as a loading control. Untreated REH cells served as a negative control for GR and pGR.

5.6.5.2 Effect of dasatinib plus dexamethasone on GR translocation from the cytosol to the nucleus

To explore the mechanism of synergy at the level of GC receptor, GR localisation from cytosol to the nucleus was evaluated. R3F9, a glucocorticoid resistant cell line, was incubated with dasatinib (2.5µM), dexamethasone (10µM) and with both together for 4 hours before extracting cytosolic and nuclear proteins (Section 2.6.2) and detection by western blotting (Section 2.6.1). Proteins extracted from whole REH cell lysate (Section 2.6.1.1) were also loaded and considered as a GR protein negative control. As expected, dexamethasone alone induced significant translocation of GR protein from the cytoplasm to the nucleus, and similar amount of GR protein were translocated in cells exposed to the drug combination. On the other hand, cells incubated with dasatinib did not show translocation of GR from cytoplasm to the nucleus when compared to CV treated cells (Figure 5.25). Thus the synergism due to the dexamethasone/dasatinib combination is not due to enhance GR nuclear translocation.

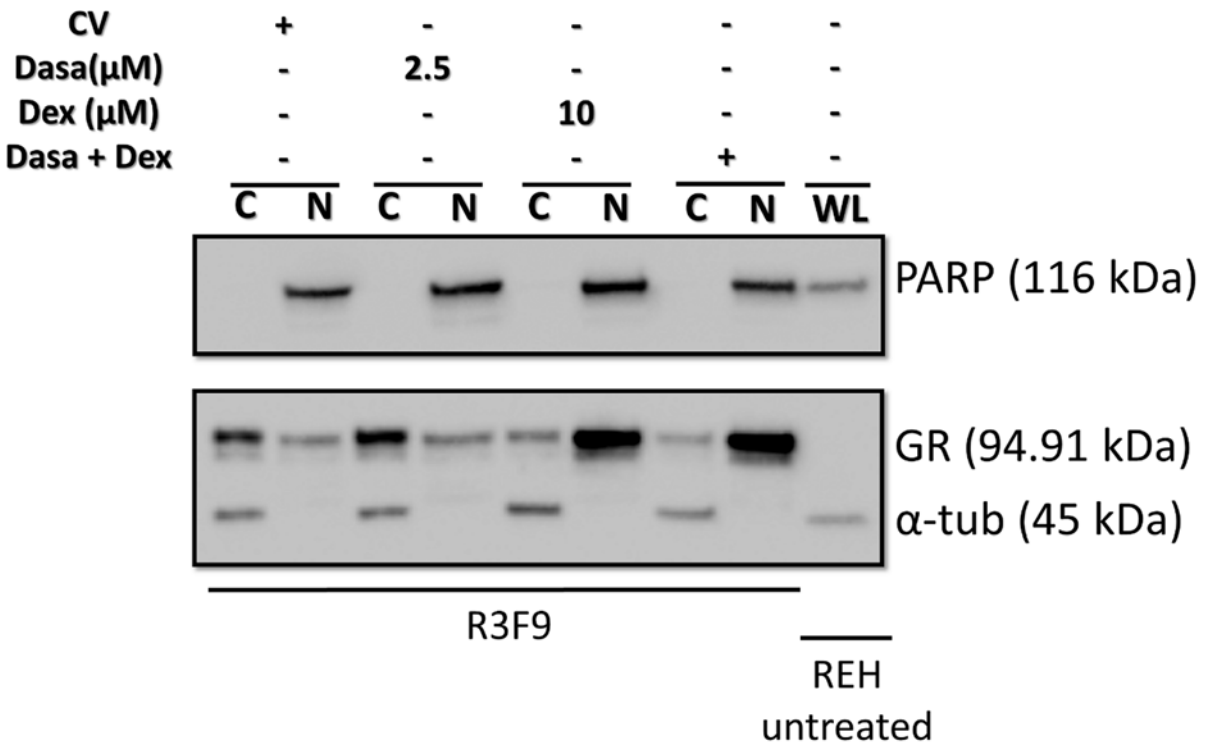

Figure 5.25: Dasatinib plus dexamethasone has no effect on GR nuclear translocation in R3F9 cells.

R3F9 cells were incubated with the indicated concentrations of dasatinib (Dasa), dexamethasone (Dex) or both together for 4 hours followed by cytoplasmic (C) and nuclear (N) proteins extraction to detect GR translocation by western blotting. Proteins extracted from the whole cells lysates (WL) of untreated REH cells served as a negative control for GR protein. Cytoplasmic (α-tubulin) and nuclear (PARP) loading controls were used. One representative immunoblot of 2 biological replicates is presented.

5.6.5.3 Effect of dasatinib plus dexamethasone on GRE binding activity

The GR localisation experiment (Section 2.6.6.2) evidenced that similar levels of GR translocated to the nucleus upon treatment of R3F9 cells with dexamethasone alone or with the drug combination. To further investigate GR function, GRE binding activity to the DNA was assessed by ELISA (Section 2.6.3).

R3F9 cells were incubated with dasatinib (2.5µM), dexamethasone (10µM) or with their combination together for 4 hours. Nuclear proteins were then extracted (Section 2.6.3.1) and an aliquot of 10µg was used for ELISA assay. Nuclear protein extracted from HeLa cells exposed to dexamethasone (100nM, 1 hour) was used as positive control. In comparison with CV treated cells (Abs. at 450nm: 0.313), both dexamethasone alone and dasatinib and dexamethasone treated cells showed increased GRE binding activity (Abs. at 450nm: 0.398 and 0.74 respectively) but to similar levels (Figure 5.26). These data suggest no effect on GRE binding activity in cells treated with the combination.

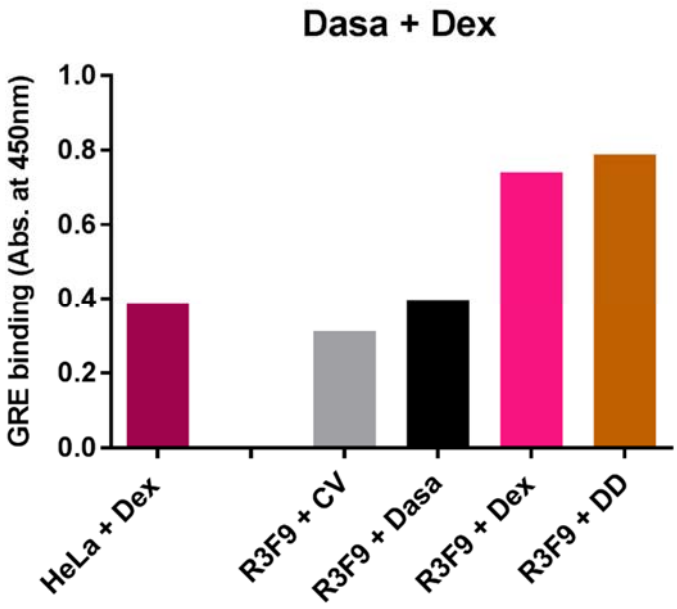

Figure 5.26: Dasatinib plus dexamethasone combination has no effect on GRE binding activity in R3F9 cells.

R3F9 cells were cultured with dasatinib (Dasa) (2.5µM) or dexamethasone (Dex) (10µM) or both (DD) for 4 hours before extracting nuclear proteins to assess GRE binding activity by ELISA. Columns represent the absorbance at 450nm for different treatments of one replicate experiment.

5.6.5.4 Effect of dasatinib plus dexamethasone on the Pro-apoptotic target BIM

As shown earlier in this chapter, enhanced apoptosis was seen in cell lines exposed to the dasatinib/dexamethasone combination (Section 5.6.3), in addition to enhanced transcription of the GR-target gene (*GILZ*) (Section 5.6.4.2). Therefore, to further investigate the mechanism of dasatinib-dexamethasone synergy, the pro-apoptotic factor (BIM) was assessed by immune-blotting (Section 2.6.1). R3F9 cells were treated with 2.5µM dasatinib, 25µM dexamethasone or with the drug mixture for 48 hours. Interestingly, apparent increase in all BIM isoforms was observed in cells treated with combination compared to dexamethasone treated cells (Figure 5.27).

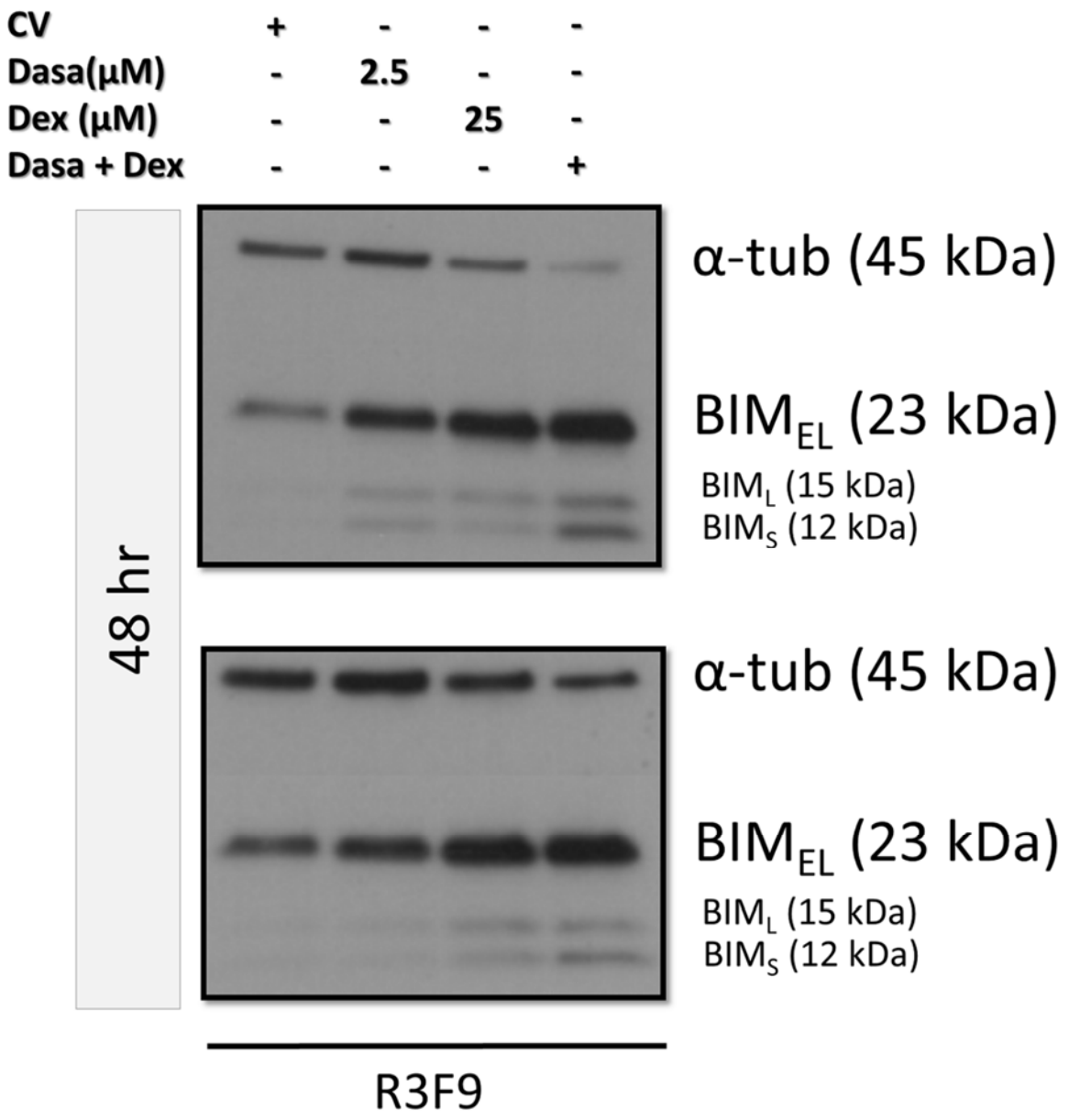

Figure 5.27: Dasatinib plus dexamethasone enhances BIM expression in R3F9 cells.

R3F9 cells were co-cultured with the indicated concentrations of dasatinib (Dasa), dexamethasone (Dex) alone or with their mixture for 48 hours to study the effect of combination on the pro-apoptotic factor BIM by western blotting. Two blots of 2 independent biological replicates are shown, α-tubulin was used as a loading control.

Similar experiments were repeated in R3F9 and Nalm-6 cells using dasatinib (2.5μM and 3μM, respectively), less dexamethasone concentration (10μM for both cell lines) or mixture of both drugs for 48 hours. Interestingly, R3F9 incubated with combination (2.5μM Dasatinib plus 10μM Dexamethasone) for 48 hours showed enhanced BIM induction in all isoforms (Figure 5.28) compared to dexamethasone or dasatinib alone.

In Nalm-6 cells treated with combination for 48 hours, no further induction of BIM isoforms (BIM_{EL}, BIM_L and BIM_S) was depicted when compared with dexamethasone treated cells (Figure 5.29 A), however, after 72 hours, a clear induction of BIM (all isoforms) was observed in cells exposed to combination compared to dasatinib or dexamethasone (Figure 5.29 B).

Taken together, enhanced BIM induction was seen in GC-resistant lines which was associated with apoptosis after exposure to dasatinib plus dexamethasone.

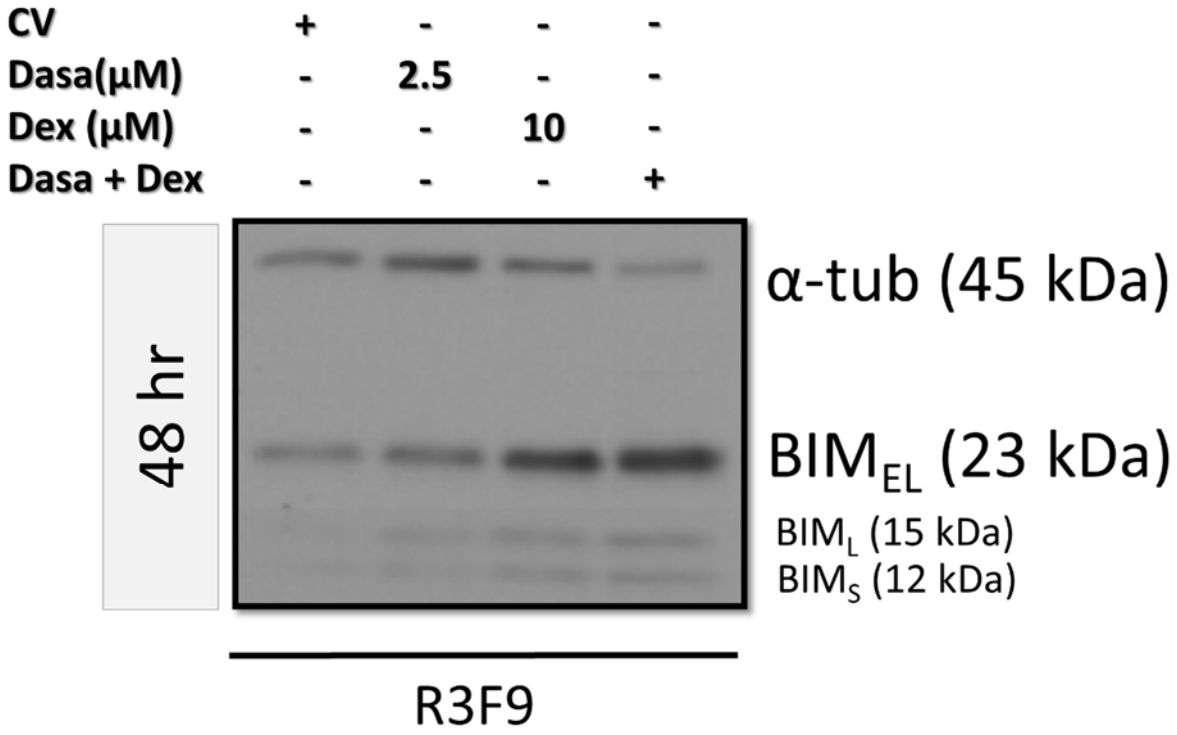

Figure 5.28: The pro-apoptotic protein BIM is upregulated upon treatment with dasatinib and dexamethasone combination in R3F9 cells.

R3F9 cells were incubated with the depicted concentrations of dasatinib (Dasa), dexamethasone (Dex) alone or with their mixture for 48 hours to study the effect of combination on the pro-apoptotic factor BIM by western blotting. Blot of one biological replicate is shown, α-tubulin was used as a loading control.

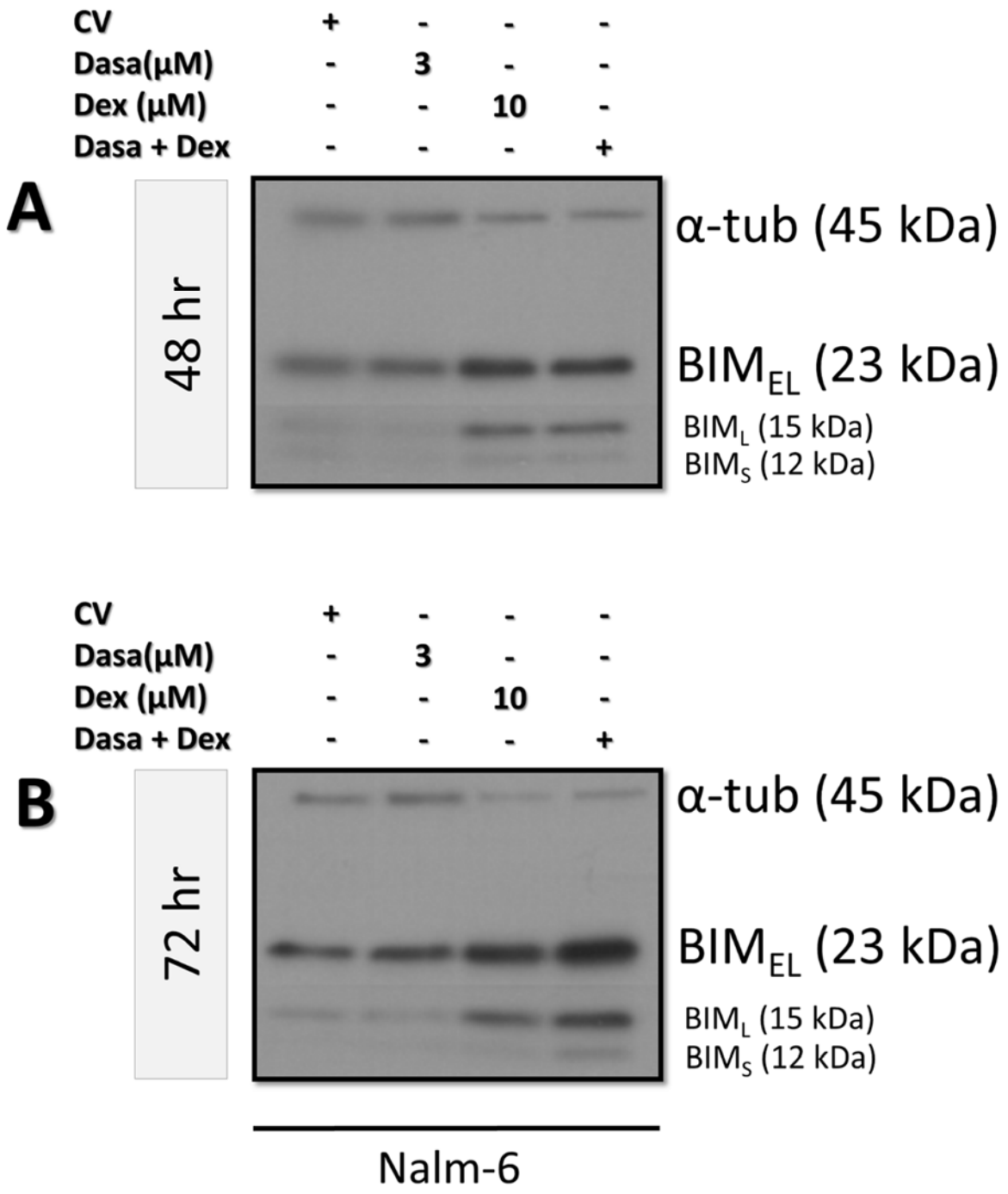

Figure 5.29: The effect of dasatinib plus dexamethasone combination on BIM induction in Nalm-6 cells.

Nalm-6 cells were dosed with the indicated concentrations of dasatinib (Dasa), dexamethasone (Dex) alone or with their mixture for 48 **(A)** and 72 **(B)** hours to study the effect of combination on the pro-apoptotic factor BIM by western blotting. Blots of one biological replicate are shown, α-tubulin was used as a loading control.

5.7 Discussion

The sensitivity seen in some ALL cell lines and PDX samples after exposure to single TKI inhibitors provided the rationale to explore potential synergism with key ALL drugs. Dexamethasone was selected based on prior evidence for synergism with other TKIs such as JNK and MEK inhibitors (Jones *et al.*, 2015; Nicholson *et al.*, 2015; Elizabeth C. Matheson) with prioritisation of dasatinib and fostamatinib R406 plus dexamethasone combinations in BCP-ALL cells. To achieve this objective, viability, cell cycle, apoptosis, pharmacodynamics and mechanism of synergism at the level of GR and its downstream pathways were investigated in BCP-ALL cells.

As presented earlier in chapter 4, an exclusive effect on proliferation/viability was noticed in 3 Pre-BCR$^+$ cell lines and 6 out of 15 PDX samples (2 Pre-BCR$^+$ and 4 Pre-BCR$^-$) after treatment with fostamatinib R406. Combination of R406 plus dexamethasone on BCP-ALL cells resulted in synergism both in Pre-BCR$^+$ (3 cell lines and 1 PDX sample) and Pre-BCR$^-$ (3 PDX samples) cells. Synergism of this combination was associated with enhancement of cell cycle arrest but no significant induction of apoptosis was observed. There was no additional inhibition of pharmacological targets in cells exposed to the drug combination compared to cells treated with single agents. As part of pharmacodynamics study, the effect of R406 plus dexamethasone was also investigated on the GR target gene, *GILZ* which was upregulated in cells demonstrated synergy. Hence, the mechanism of synergism was explored at the level of GR. In cells treated with combination compared to single agents, no differences were seen in the levels of GR, phosphorylation as a marker of activation, translocation to the nucleus or GRE binding activity. In addition, in contrast to the synergism seen with dasatinib, there was no increase in the expression of the pro-apoptotic factor BIM and this in keeping with the lack of apoptosis induced by the R406 plus dexamethasone in both PreB 697 and R3F9 cell lines. In other studies, the GR target gene *GILZ* was associated with apoptosis (Schmidt *et al.*, 2004; Kruth *et al.*, 2017) but in this study it was upregulated in cells treated with the drug combination but without BIM expression and apoptosis induction. However, *GILZ* induction was associated with cell cycle arrest in cells showed synergy which is in keeping to what has been suggested before that the long variant of GILZ (L-GILZ) activates P53, a mediator of cell cycle arrest (Lane, 1992; Levine, 1997; Ayroldi *et al.*, 2015). Moreover, upregulation of GILZ was shown to have an inhibitory effect on components of multiple pathways involved in cell

survival and proliferation (such as PI3K/AKT and MAPK) (Figure 5.30) with these effects being translated into growth inhibition (Ayroldi *et al.*, 2002; Asselin-Labat *et al.*, 2005; Ayroldi *et al.*, 2007; Latre de Late *et al.*, 2010). In fact, a significant reduction in apoptosis was seen in the GC sensitive PreB 697 cells exposed to the drug combination compared to cells treated with dexamethasone alone and this is in agreement with the finding of Asselin-Labat and colleagues who stated that BIM expression could be downregulated by GILZ and thus apoptosis was negatively affected (Asselin-Labat *et al.*, 2004). As discussed in chapter 4, R406 inhibits several targets in addition to SYK (Table 4.16) (Davis *et al.*, 2010b; Maude *et al.*, 2012; Roberts *et al.*, 2012; Roberts *et al.*, 2014; Rolf *et al.*, 2015) and recently some of these targets such as SYK, FLT3, PI3K-δ, BLK and ERK/MAPK have been shown to sensitize BCP-ALL cells to glucocorticoids (Figure: 5.30) (Piovan *et al.*, 2013; Silveira *et al.*, 2015; Kim *et al.*, 2017; Kruth *et al.*, 2017). FLT3 is a receptor tyrosine kinase that can activate the downstream signalling cascades involved in leukaemogenesis such as PI3K and RAS pathways (Stirewalt and Radich, 2003; Scholl *et al.*, 2008) (Figure 5.30). The synergism between dexamethasone and fostamatinib has been reported in WM cells (Kuiatse *et al.*, 2015). The viability of WM cell lines exposed to the drug combination for 48 hours was reduced to about 25% but no mechanistic studies were performed.

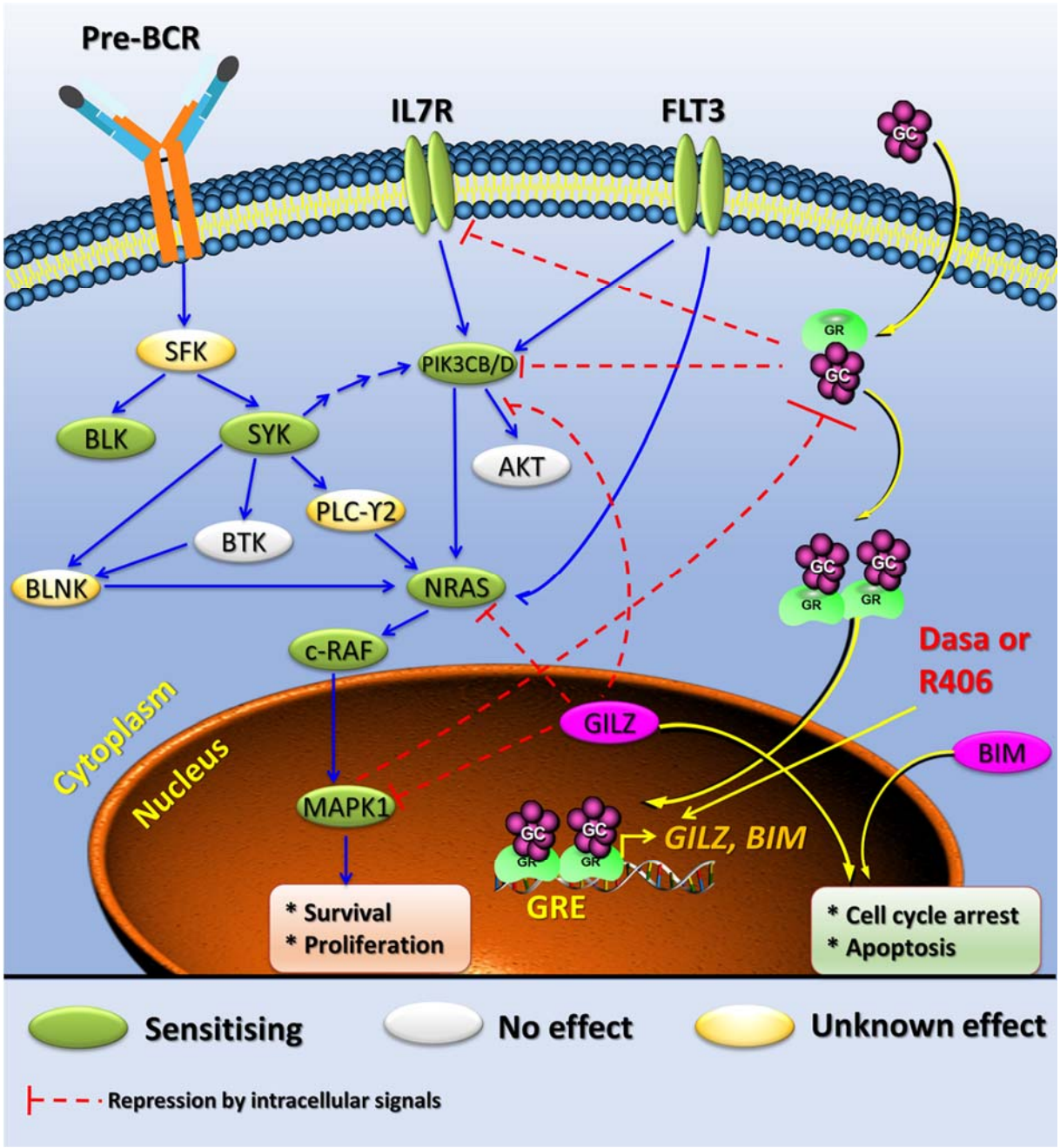

Figure 5.30: Suppression of Pre-BCR downstream signals enhances sensitivity of BCP-ALL cells to dexamethasone.

This diagram summarises the mechanism of synergy of TKI combinations with GC which could be attributed to the interplay between GR and Pre-BCR pathways based on data acquired throughout this study and data from the literature (Nahar and Muschen, 2009; Piovan *et al.*, 2013; Buchner *et al.*, 2015; Silveira *et al.*, 2015; Hall *et al.*, 2016; Kruth *et al.*, 2017; Serafin *et al.*, 2017). GC mediated apoptosis via GR pathway (Right side) is triggered by GC binding with GR, phosphorylation, activation before translocation to the nucleus. Inside the nucleus, GR-GC molecules dimerize and bind to the consensus DNA sequences binding sites (GREs) and enhance transcription of multiple genes involved in cell cycle arrest and apoptosis (e.g. *GILZ* and *BIM*). Interestingly, dasatinib or fostamatinib R406 alone could also upregulate *GILZ* mRNA level. In addition, components of multiple pathways (such as PI3K/AKT and MAPK) were found to be associated with *GILZ* induction. On the other hand, inhibition of components

downstream of Pre-BCR checkpoint (Pharmacological inhibition by TKIs/gene knockdown) was found to sensitize BCP-ALL cells to dexamethasone (Left side). It has been found that TKIs may inhibit targets other than the primary target(s) such as fostamatinib which inhibits FLT3. FLT3 is a receptor tyrosine kinase that can activate PI3K and RAS pathways. Activated PI3K-δ (via SYK or IL-7R or FLT3) inhibits GR function through activation of MAPK pathway. Interestingly, GC may interfere with this double negative feedback loop between PI3K-δ and GR and therefore enhance or restore the regulation of programmed cell death genes.

As presented in chapter 4, sensitivity to dasatinib was seen in multiple Pre-BCR$^+$ and this sensitivity was correlated with the inhibition of key kinases downstream of Pre-BCR signalling. Other studies have also reported successful preclinical potential of dasatinib in re-sensitizing T-ALL to dexamethasone both *in vitro* and *in vivo* through LCK inhibition (Serafin *et al.*, 2017) or overcoming the stromal cells-mediated resistance of myeloma cells to dexamethasone (Ramasamy, 2012). Therefore, dasatinib plus dexamethasone mixture was investigated in BCP-ALL. Strikingly, both Pre-BCR$^+$ (3 cell lines out of 3 and 1 PDX sample) and Pre-BCR$^-$ (3 PDX samples out of 4, 2 of them were Ph$^+$ and Ph-like cytogenetics) cells exhibited synergism after exposure to this combination. Furthermore, a robust induction of G1 arrest associated with an increase in the non-viable population (sub-G1) which indicate programmed cell death in both GC sensitive and resistant cell lines. Moreover, with dasatinib and dexamethasone, there was significant apoptosis over that for dasatinib or dexamethasone alone in both tested cell lines (PreB 697 and R3F9), confirming the cell cycle findings (sub-G1 arrest) in the same cells. The mechanism of drug action was studied and a similar degree of pharmacological targets (pBTK, pSYK, pBLNK and pPLC-ɣ2) inhibition was observed in cells incubated with combination compared to cells treated with dasatinib alone. On the GR level, no further GR expression, phosphorylation, translocation and GRE binding activity to the nucleus were detected, however, there was a significant *GILZ* upregulation, which was associated with further apoptosis (Schmidt *et al.*, 2004; Bruscoli *et al.*, 2015; Kruth *et al.*, 2017) in cells co-treated with dasatinib and dexamethasone combination. Moreover, an increase in the expression of BIM, the pro-apoptotic BCL-2 family factor which regulates the activation of cell death pathway in mitochondria (Cory and Adams, 2002), was also seen and explains programmed cell death and cytotoxicity observed in cells exposed to combination (Joha *et al.*, 2012). In line with results presented in this chapter, preclinical data of dasatinib plus dexamethasone combination found similar synergism in cells viability/proliferation in addition to enhanced effect on cell

cycle (G1 arrest) and or apoptosis induction in myeloma cells (Ramasamy, 2012) and T-ALL cells (Serafin *et al.*, 2017). A recent clinical trial carried out in elderly patients with Ph-positive ALL found that dexamethasone combination with dasatinib is well tolerated and increased long term survival in one third of patients (Rousselot *et al.*, 2016).

Since the mechanism of glucocorticoid resistance in clinical samples is not yet fully understood, based on the findings presented here and by others, one could hypothesize that the mechanism of synergy in all TKI combinations with dexamethasone is attributed to the cooperative role of two independent pathways, GR pathway (GC-mediated) and Pre-BCR downstream signaling (Some components are targeted by TKIs) (Figure 5.30). The role of GR pathway from GC binding to GR phosphorylation, translocation, GRE binding and eventually *GILZ* induction after treatment with dexamethasone is outlined in figure 5.30. The enhanced induction of *GILZ* was observed in cells treated with the drug combination. Surprisingly, dasatinib or R406 single drug treatment were also found to upregulate *GILZ* mRNA to some extent in the GR positive cells and this may suggest that these inhibitors influence GR phosphorylation at phosphorylation site(s) (S203 or S226) other than S211 (Chen *et al.*, 2008) or modify GR transcriptional enhancers or repressors. On the other hand, by using TKI inhibitors, multiple targets downstream of Pre-BCR signaling could be inhibited by TKIs (including primary and off target effects) (Tables 4.14 to 4.17), and these targets may play a pivotal role in re-sensitising cells to glucocorticoids as evidenced by several studies in BCP-ALL, T-ALL (Figure: 5.30) (Piovan *et al.*, 2013; Silveira *et al.*, 2015; Hall *et al.*, 2016; Kruth *et al.*, 2017; Serafin *et al.*, 2017). However, similar to GR pathway components, no further inhibition of pharmacological target(s) was observed in cells exposed to dexamethasone combination with R406 or with dasatinib compared to single TKI treatment. Taken together, these findings provide the evidence that synergy mechanism was functional only if drug combination was affecting both GR pathway and Pre-BCR signaling simultaneously (Figure 5.30). As a proof of this concept, no synergy was seen in REH cells treated with dexamethasone combined with any of the 4 TKIs (CAL-101, ibrutinib, R406 and dasatinib), because REH cells are reported to be GR negative and this was confirmed by western blotting in figure 5.14 but is also confirmed by the observation that no GC or combination-mediated induction of *GILZ* was obtained. Endogenous GCs (e.g. cortisol) play a physiological role in maintaining a steady state of lymphocytes production. Cortisol, in addition to synthetic GCs, induce selective apoptotic effect on B cells at early maturation stage (early progenitor stage) rather than more mature B

cells (Lill-Elghanian *et al.*, 2002; Igarashi *et al.*, 2005) and this may suggest an impact of GCs (endogenous or synthetic) on Pre-BCR or downstream signaling.

In addition to R406 or dasatinib combinations with dexamethasone, other Pre-BCR inhibitors (CAL-101 and ibrutinib) were also investigated in this study after combining them with dexamethasone and unexpectedly, synergism was seen in both combinations in some ALL samples.

Several reports found that PI3K-δ/AKT inhibition may reverse resistance or enhance sensitivity of B and T-ALL cells to glucocorticoids (Piovan *et al.*, 2013; Hall *et al.*, 2016; Kruth *et al.*, 2017). In addition, increased GC-induced programmed cell death was reported in a human follicular lymphoma cell line in the presence of PI3K-δ/AKT inhibitors (Nuutinen *et al.*, 2006). In section 4.2.1 of this study, sensitivity was noticed in some PDX samples within clinical ranges when treated with CAL-101 alone, therefore, synergism was assessed with dexamethasone. Interestingly, synergy was found in cells resistant to either drug alone and included Pre-BCR^{+} (2 cell lines and 1 PDXs) and Pre-BCR^{-} (2 PDXs) cells. As these cells were found to be resistant to CAL-101 alone, they were exposed to fractions of CAL-101 GI_{50} (GI_{50}=10μM) in synergy experiments and the least concentration was 2.5 micromolar, therefore, inhibition of PI3K-δ was expected especially when these samples exhibited higher levels of baseline AKT phosphorylation as evidenced in chapter 3 (Table 3.1). Recently, Kruth and co-workers (Kruth *et al.*, 2017) found that dexamethasone treatment strongly inhibited PI3K-δ, which can be activated downstream of Pre-BCR through proximal SYK or through IL-7 receptor signaling or downstream of FLT3 (Figure 5.30) (Stirewalt and Radich, 2003; Herzog *et al.*, 2009). On the other hand, activated PI3K-δ inhibits GR function through downstream activation of MAPK signalling (Figure 5.30) (Kruth *et al.*, 2017). GCs may interfere with this double negative feedback loop between GR and PI3K-δ and hence restore or enhance the regulation of apoptotic genes (Figure 5.30) (Kruth *et al.*, 2017). Therefore, they postulated that knockdown of PI3K-δ would support sensitising BCP-ALL cells to dexamethasone and inhibit growth. As a proof of concept and in line with findings of this study, the same authors (Kruth *et al.*, 2017) tested a combination of CAL-101 with dexamethasone on BCP-ALL cells from variety of genetic backgrounds and it was super-additive both *in vitro* and *in vivo* and synergy was seen in cells regardless of Pre-BCR status. Similarly, Piovan and others (Piovan *et al.*, 2013) tested the AKT

inhibitor MK2206 combination with dexamethasone on T-ALL cells and they found that the inhibition of AKT reversed the resistance to GCs both *in vitro* and *in vivo*.

As shown in chapter 4, some PDX samples were sensitive to ibrutinib treatment as a single inhibitor and the GI_{50} values obtained were within clinically achievable concentration in a Pre-BCR^+ PDX sample and sensitivity was associated with the inhibition of the target (pBTK). Therefore ibrutinib combined with dexamethasone was explored in this chapter and shown to be synergistic in Pre-BCR^+ cell lines and PDX cells. Recent reports have revealed synergistic effects in CLL and Pre-BCR^+ ALL cells exposed to dexamethasone combined with ibrutinib *in vitro* (Manzoni *et al.*, 2016; Kim *et al.*, 2017). Synergy experiments were carried out in both Pre-BCR^+ and Pre-BCR^- cells. The cells used in synergy experiments were found to be resistant to either drug alone (ibrutinib or dexamethasone) but Pre-BCR^+ cells exhibited sensitivity to drugs when combined together. However, it is unclear if synergism could be also seen in ibrutinib-sensitive PDX samples due to the limitation of cell number and/or PDX samples availability. In addition, the synergy was further investigated using the GC-resistant Pre-BCR^+ cell line R3F9 which showed significant G1 arrest and apoptosis induction when co-treated with combination compared to single agents alone. In line with these results, a recent report found that ibrutinib has sensitised Pre-BCR^+ ALL cells to dexamethasone treatment (Kim *et al.*, 2017). Moreover, another report exhibited a similar trend of synergistic effect in CLL cells treated with the same combination (Manzoni *et al.*, 2016), but interestingly, cell cycle arrest and apoptosis induction were more potent in the BCP-ALL cell line (R3F9) investigated in these data presented here. Compared to CV, the induction of apoptosis in cells treated with combined drugs was 5 fold in BCP-ALL cells whereas it was 3 fold in CLL cells. In addition, the BCP-ALL cells arrested at S phase were reduced to 70% while in CLL cells it was only reduced by 50%. As evidenced in chapter 4, the sensitivity seen in cell lines and some PDX samples was associated with significant inhibition of pBTK. Interestingly, Kim and co-authors (Kim *et al.*, 2017) noticed that both BTK and BLK were inhibited by ibrutinib alone and the drug was mainly effective in Pre-BCR^+ BCP-ALL cells whether single or combined with dexamethasone *in vitro* (Kim *et al.*, 2017). This may explain the synergy observed in the study presented here in Pre-BCR^+ cells (2 cell lines and 1 PDX sample). Interestingly, BTK knockdown was found to be non-effective in re-sensitizing BCP-ALL cells to dexamethasone, thus inhibition of BLK may be more relevant (Figure: 5.30) (Kruth *et al.*, 2017). Moreover, an *in vitro* kinase assay performed by

two groups showed that other tyrosine kinases, other than BTK, such as SRC (Table 4.15) were also irreversibly inhibited by ibrutinib (Honigberg *et al.*, 2010; Lanning *et al.*, 2014).

In summary, this is the first study to evaluate the dual exposure of dexamethasone with 4 TKIs in BCP-ALL cells. Evidence of better reduced viability *in vitro* (growth inhibition and/or apoptosis) was provided using dexamethasone in combination with R406 or with dasatinib in both GC sensitive and resistant cells, regardless of Pre-BCR status. In addition, the mechanism of synergy was associated with enhanced *GILZ* expression and may involve BIM induction as seen with the dasatinib/dexamethasone combination, in addition to the inhibition of multiple Pre-BCR downstream targets. Further studies are needed to define the precise 'effector' targets that are inhibited and how that correlates with re-sensitising ALL cells to dexamethasone. The preclinical data of dexamethasone combined with dasatinib shown here, warrants confirmation in the orthotopic NSG mouse model, with appropriate pharmacokinetic and pharmacodynamic analyses and if positive, may open the door to translate this combination regimen for clinical use in Pre-BCR positive or Ph^+/Ph-like BCP-ALL.

Chapter 6: Overall Summary and Future Directions

Chapter 6: Overall summary and future directions

6.1 Overall summary and future directions

BCP-ALL is the most prevalent paediatric cancer, associated with a high number of mortalities and short and long term treatment toxicities (Inaba *et al.*, 2013) and there is a demand for more effective, targeted therapies with less toxicity (Nachman *et al.*, 2007; Locatelli *et al.*, 2012). The treatment outcome for some high risk groups of ALL has improved in recent years with the introduction of targeted therapies. For example, the use of small molecule TKI inhibitors targeting BCR-ABL has led to a remarkable increase in the outcome in Ph^+ patients treated with imatinib combined with chemotherapy, with no increase in toxicity (Schultz *et al.*, 2009; Ravandi *et al.*, 2010; Schultz *et al.*, 2014). The development of antibody therapies conjugated with drugs or toxins has also offered a different type of targeted treatment. More recently, the strategy of using T cells with chimeric antigen receptors (CAR T cells) has revealed interesting clinical results in refractory/relapsed patients, however, adverse reactions are associated with CAR T cell and antibody treatment (Irving, 2016; Papadantonakis and Advani, 2016).

Given that BCP-ALL malignancy is caused by key genetic lesions/mutations that interfere with the Pre-BCR signaling pathway (Herzog *et al.*, 2009; Clark *et al.*, 2014; Eswaran *et al.*, 2015), this may serve as an Achilles' heel that could be exploited therapeutically (Geng *et al.*, 2015). Therefore, TKIs targeting BCR signaling [CAL-101, ibrutinib, dasatinib (FDA-approved) and fostamatinib] which have demonstrated promising clinical effects with less toxicity in other B-cell malignancies, immune diseases and certain subtypes of BCP-ALL (Ph^+ ALL) were used in this study (Morales-Torres, 2012; Young and Staudt, 2013; Buchner and Muschen, 2014; Muschen, 2015; Trimarchi and Aifantis, 2015). The objective of this study was to characterise Pre-BCR function and activity in a cohort of cell lines and PDX samples derived from patients with high risk and relapse ALL subtypes followed by testing the effects of single TKIs and their synergism with essential ALL chemotherapy *in vitro*.

Initially, Pre-BCR expression and function were characterised in cell lines and PDX samples to see if these parameters were associated with prediction of sensitivity to certain TKIs. As expected, Pre-BCR was not expressed in the majority of cases despite their ability to replicate and self-renewal (Trageser *et al.*, 2009; Geng *et al.*, 2015). The Ca^{2+} flux assay after stimulation

with anti-μHC was utilised as a measure of Pre-BCR function and cell lines data showed that only cells with intact Pre-B and B cell receptor were able to induce calcium mobilisation (Kuwahara *et al.*, 1996; Wang *et al.*, 2002a; Trageser *et al.*, 2009). Importantly, monitoring of activated pathways integral to Pre-BCR signalling were also assessed as predictive biomarkers of response to the selected TKIs (Irving *et al.*, 2014; Dolai *et al.*, 2016) and therefore, basal and anti-μHC induced phosphorylation were quantified in this study for all cell lines and PDX models.

Generally, sensitivity to TKIs was observed in some ALLs irrespective of Pre-BCR status, the highest number of sensitive PDXs were observed with R406 or with dasatinib. For R406, sensitivity was associated with modest inhibition of known targets, i.e. pSYK in cell lines but for dasatinib, inhibition of pBTK, pSYK, pBLNK and p-PLC-ɣ2 was evidenced in both cell lines and PDX cells. Pre-BCR$^+$ usually responded to dasatinib but from the Pre-BCR$^-$ group, only Ph$^+$ or PDGFR translocation positive ALLs were sensitive. For R406, sensitivity was observed in Pre-BCR$^+$ and some Pre-BCR$^-$ cells, however predictive biomarkers were not identified.

In support of previous isolated kinase and *in vitro* studies, the pharmacodynamic data of TKIs investigated here depicted that other targets (beside the primary targets) could be also inhibited to achieve sensitivity of BCP-ALL cells to single TKIs (Tables 4.14 – 4.17) (Davis *et al.*, 2010b; Honigberg *et al.*, 2010; Maude *et al.*, 2012; Roberts *et al.*, 2012; Lanning *et al.*, 2014; Roberts *et al.*, 2014; Rolf *et al.*, 2015). Therefore, siRNA knockdown of potential targets associated with TKI activity would be an advisable option for fostamatinib where the target(s) is unclear and also in confirming ibrutinib and dasatinib targets. Moreover, it has been found in several studies that TKIs targets (primary and off targets) may play a vital role in re-sensitising BCP-ALL, T-ALL cells to glucocorticoids (Figure: 5.30) (Piovan *et al.*, 2013; Silveira *et al.*, 2015; Hall *et al.*, 2016; Kim *et al.*, 2017; Kruth *et al.*, 2017; Serafin *et al.*, 2017).

Interestingly, dexamethasone combinations with single TKIs enhanced sensitivity and the synergistic effect was reflected in enhanced cell cycle arrest and/or programmed cell death, with the prioritisation of dexamethasone combinations with R406 or with dasatinib. The synergism of dexamethasone combined with R406 or with dasatinib was associated with the induction of the GR target gene (*GILZ*) which was thought to play a role in enhanced cell cycle and/or apoptosis (Schmidt *et al.*, 2004; Ayroldi *et al.*, 2015; Kruth *et al.*, 2017). In addition, BIM (pro-apoptotic factor) induction was observed in dasatinib and dexamethasone

combination and explains the observation of apoptosis induction along with *GILZ* (Joha *et al.*, 2012). Interestingly, recent reports have suggested that inhibition of key components downstream of Pre-BCR checkpoint may represent a therapeutic option for BCP-ALL (Perova *et al.*, 2014; Geng *et al.*, 2015; Irving, 2016; Eldfors *et al.*, 2017; Kim *et al.*, 2017), also, others have found that downregulation/pharmacological inhibition of these effectors increased sensitivity of BCP-ALL cells to dexamethasone (Figure 5.30) (Piovan *et al.*, 2013; Kruth *et al.*, 2017). Moreover, a physiological role for endogenous GCs has been observed during B lymphocytes maturation to maintain a steady state. Cortisol (or synthetic GCs) was found to induce selective programmed cell death in early progenitor B cells which express Pre-BCR over more mature B cells (Lill-Elghanian *et al.*, 2002; Igarashi *et al.*, 2005). This may indicate that GCs may interfere with the Pre-BCR pathway.

Although R406 and dasatinib (single or combined with dexamethasone) showed efficacy in Pre-BCR$^+$ cells (apart from *TCF3-HLF* positive PDX sample) and some Pre-BCR$^-$ cells, constitutive target(s) activation (such as pAKT, pBTK, pSYK) were not associated with sensitivity to relevant inhibitor(s). Thus, the lack of predictive biomarkers may necessitate the *in vitro* testing of primary or PDX cells from refractory patients using candidate drug libraries. Alternatively, a recent paper described the use of 'real-time' PDX *in vivo* testing in the orthotopic mouse model to identify active drugs (Trahair *et al.*, 2016). Antibody therapies have the advantage of easily identifiable predictive biomarkers.

6.2 Overview

This study investigated the impact of small molecule TKI inhibitors in targeting effectors downstream of the Pre-BCR checkpoint, using ALL cell lines and PDX models. The data presented in this thesis showed good activity of dasatinib and R406 in Pre-BCR$^+$ cells at clinically achievable drug concentrations, with the exception of the highly resistant t(17;19) sample (Fischer *et al.*, 2015). A significant proportion of Pre-BCR$^-$ were also sensitive to these inhibitors, although predictive biomarkers remain to be established. Moreover, significant synergy was obtained in combining fostamatinib and dasatinib with dexamethasone, the latter resulting in a profound induction of apoptosis due to the enhanced induction of *GILZ* and the pro-apoptotic BIM. Confirmation of these synergistic data *in vivo* using an orthotopic mouse model engrafted with well-characterised PDX cells, may offer alternative therapies for

Pre-BCR$^+$ ALL, particularly the Pre-BCR positive t(1;19) subgroup, which have a dismal outcome after relapse (Jeha *et al.*, 2009). Thus, these data may pave the way for new, less toxic treatment options for refractory ALLs.

Appendix

Appendix

Published abstracts

1. **American Society for Hematology Annual Meeting 2016, San Diego Convention Center, San Diego**

Exploring Pre-B Cell Receptor Signalling As a Therapeutic Target in Acute Lymphoblastic Leukaemia

Ali Alhammer, M.Sc[1,2*] , Marian Case, MSc[1*] , Helen J Blair, PhD[1*] , Josef Vormoor, MD, FRCPCH[1] and Julie Irving, PhD[1]

[1] Northern Institute for Cancer Research, Newcastle University, Newcastle upon Tyne, United Kingdom

[2] Biotechnology Research Center, Al-Nahrain University, Baghdad, Iraq

Acute Lymphoblastic Leukemia: Biology, Cytogenetics, and Molecular Markers in Diagnosis and Prognosis

Program: Oral and Poster Abstracts

Session: 618. Acute Lymphoblastic Leukemia: Biology, Cytogenetics, and Molecular Markers in Diagnosis and

Prognosis: Poster III

Monday, December 5, 2016, 6:00 PM-8:00 PM

Hall GH (San Diego Convention Center)

Introduction:

Acute lymphoblastic leukaemia (ALL) is a clonal disorder of developing lymphocytes and is the most common malignancy in children and adolescents. While cure rates are high, treatment is associated with significant morbidity and relapsed ALL remains one of the leading causes of cancer-related deaths in children. New, less toxic therapies are clearly needed for refractory ALL.

There are a number of lines of evidence to suggest that ALL cells hijack components of precursor-B cell receptor (Pre-BCR) signalling and this dependency may be amenable to therapeutic exploitation. There are a number of tyrosine kinase inhibitors (TKIs) targeting Pre-

BCR signalling that are showing great promise in the clinic for other leukemia subtypes which warrant preclinical evaluation in childhood ALL.[1] These include CAL-101 (PI3K-δ inhibitor), Ibrutinib (BTK inhibitor), Fostamatinib R406 (SYK inhibitor) and Dasatinib (BCR-ABL/SRC inhibitor).

Methods:

TKIs were evaluated in ALL cells, including cell lines (PreB 697 and its glucocorticoid resistant descendant, R3F9; Nalm-6 and Reh) and 25 patient derived xenograft samples (PDX) from 12 predominantly high risk/relapse children ALLs. Resazurin was used to assess cell viability. Flow cytometry was used to detect Pre-BCR expression (μHc, Vpreb and λ5) and functionality using a Calcium flux assay. Phospho-flow cytometry was performed to monitor constitutive phosphorylation and response to Pre-BCR activation and to assess pharmacodynamic drug action (p-AKT, p-BLNK, p-BTK, p-SYK, p-ERK, and p-PLC-ϒ2). *GILZ* expression was measured by RQ-PCR. Cell cycle and apoptosis were determined by flow cytometry using Propidium Iodide and Annexin V staining.

Results:

ALL cell lines were resistant to CAL-101 (mean GI50 52.08 μM, range 25 μM-77.83 μM) and Ibrutinib (mean GI50 15.9 μM, range 11.47 μM-18.3 μM). However, modest sensitivity was seen to R406 (mean GI50 4.32 μM, range 2.88 μM-5.83 μM) and Dasatinib (mean GI50 5.33 μM, range 2.45 μM-12.5 μM). CAL-101 and Dasatinib were shown to be cytostatic, causing G1 arrest but no significant apoptosis, while Ibrutinib and R406 were associated with cell cycle arrest and significant apoptosis after 72 hours incubation with GI50 concentrations (16.81±1.71 % and 31.34±5.78 % apoptosis, respectively). Pre-B receptor positive cells were more sensitive to Dasatinib and Fostamatinib. Pharmacodynamic assessment using Phospho-flow cytometry and Western blotting showed inhibition of the relevant targets at the GI50 concentrations. PDX ALL cells were generally more sensitive than the cell lines; CAL-101 (mean GI50 25.56 μM, range 76 nM-100 μM; 2 out of 12 patient samples <2μM); Ibrutinib (mean GI50 14.23 μM, range 490 nM-100 μM; 3 out of 12 patient samples <5μM); R406 (mean GI50 11.52 μM and range 56 nM-25 μM, 4 out of 12 patient samples <4μM); Dasatinib (mean GI50 25.56 μM, range 76 nM-100 μM; 3 out of 12 patient samples <0.5μM). ALLs sensitive to Dasatinib were Ph+ or Pre-BCR positive and the latter were also sensitive to Fostamatinib.

Synergism was seen after co-treatment of TKIs with the glucocorticoid (GC), Dexamethasone (CAL-101 CI mean 0.7, range 0.056-1.34; Ibrutinib CI mean 0.71, range 0.41-0.97; R406 CI mean 0.27, range 0.1-0.6 and Dasatinib CI mean 0.63, range 0.14-1.29). No synergism was observed in the glucocorticoid receptor negative, Reh cell line. For R406 and Dasatinib, co- exposure was strongly synergistic and was associated with increased apoptosis in PreB 697 and the GC resistant lines, Nalm-6 and R3F9. Synergism was associated with a significant increase in expression of the GR target, *GILZ* and an enhanced downregulation of R406 and Dasatinib targets (p-SYK for R406 and p-BTK, p-SYK for Dasatinib).

Conclusion:

We have identified significant sensitivity of TKIs impacting on Pre-BCR signalling in ALL cells at clinically relevant concentrations; Pre-BCR positive ALLs were associated with Dasatinib and Fostamatinib sensitivity; Pre-BCR negative ALL cells were also sensitive to some TKIs, although predictive biomarkers remain to be established. Marked synergism was observed in combination with dexamethasone, even in GC resistant cells. In vivo preclinical confirmation of these data may offer new therapies for refractory ALL.

1. Young, R.M. and L.M. Staudt, Targeting pathological B cell receptor signalling in lymphoid malignancies. Nature Reviews Drug Discovery, 2013. 12(3): p. 229-243.

2. 22nd Congress of the European Hematology Association, IFEMA – Feria de Madrid, Madrid, Spain

THERAPEUTIC TARGETING OF PRE-B CELL RECEPTOR SIGNALLING IN CHILDHOOD ACUTE LYMPHOBLASTIC LEUKEMIA

Ali Alhammer[*, 1, 2], Marian Case[1], Elizabeth Matheson[1], Helen Blair[1], Josef Vormoor[1], Julie Irving[1]

[1]Newcastle University, Northern Institute for Cancer research, Newcastle upon Tyne, United Kingdom, [2]Al-Nahrain University, Biotechnology research Center, Baghdad, Iraq

(Abstract release date: May 18, 2017) EHA Learning Center. Alhammer A. Jun 24, 2017; 181799

Abstract: P512

Type: Poster Presentation

Presentation during EHA22: On Saturday, June 24, 2017 from 17:30 - 19:00

Location: Poster area (Hall 7)

Background: Acute lymphoblastic leukaemia (ALL) is the most common malignancy in children and adolescents and relapsed ALL remains one of the leading causes of cancer-related deaths in children. Components of the precursor-B cell receptor (Pre-BCR) signalling pathway are hijacked in ALL cells and this dependence may be therapeutically targeted. A number of tyrosine kinase inhibitors (TKIs) targeting effectors of this signalling pathway are showing great promise in the clinic and warrant preclinical evaluation in paediatric ALL. They include Dasatinib (BCR-ABL/SRC inhibitor), Fostamatinib R406 (SYK inhibitor), Ibrutinib (BTK inhibitor) and CAL-101 (PI3K-δ inhibitor).

Aims: To preclinically evaluate these candidate TKIs, as novel, targeted drugs for high risk and relapsed ALL.

Methods: ALL cell lines (Reh, Nalm-6, PreB 697 and its glucocorticoid resistant descendant, R3F9) and 36 primary-derived xenograft (PDX) cells from 16 ALL were used in the study. Cell

viability was assessed by Resazurin. Pre-BCR expression (μHC, Vpreb and λ5) and functionality using a Calcium flux assay were detected by Flow cytometry. Intracellular phospho-flow cytometry was used to detect constitutive phosphorylation and activation in response to anti-Igμ antibody, as well as drug pharmacodynamic measures (p-BTK, p-SYK, p-AKT, p-ERK, p-PLC-ϒ2, p-BLNK). Apoptosis and cell cycle were analysed by flow cytometry using Annexin V and Propidium Iodide. RQ-PCR was used to measure *GILZ* expression. Bim induction, GR expression and phosphorylation were detected by western blotting.

Results: ALL cell lines were modestly sensitive to Dasatinib (mean GI50 5.33 μM, range 2.45 μM-12.5 μM) and R406 (mean GI50 4.32 μM, range 2.88 μM-5.83 μM). However, cells were resistant to Ibrutinib (mean GI50 15.9 μM, range 11.47 μM-18.3 μM) and CAL-101 (mean GI50 52.08 μM, range 25 μM-77.83 μM). Cell cycle arrest and significant apoptosis was seen with R406 and Ibrutinib treatment, while Dasatinib and CAL-101 were cytostatic, causing G1 arrest with no substantial cell death. Pharmacodynamic assays confirmed inhibition of the relevant drug targets. PDX cells showed greater sensitivity than the cell lines to Dasatinib (4 out of 16 patient samples <0.5μM), R406 (7 out of 16 patient samples <5μM), Ibrutinib (3 out of 15 patient samples <5μM) and CAL-101 (3 out of 15 patient samples <2μM). Pre-BCR positive ALL cell lines and PDX cells were sensitive to R406 and Dasatinib, with a Ph+ PDX confirming sensitivity to the latter. Combining TKIs with the glucocorticoid (GC), Dexamethasone showed synergism in ALL cell lines and was particularly notable for Dasatinib and R406 in PreB cell receptor positive lines. Synergism was associated with significantly enhanced apoptosis, an increase in expression of the GR target gene, *GILZ* and for Dasatinib, enhanced expression of the pro-apoptotic, Bim. Control REH cells (GC receptor negative) showed no synergism.

Summary/Conclusion: Significant sensitivity of TKIs targeting Pre-BCR signalling have been identified at clinically achievable concentrations. Dasatinib and R406 sensitivity was associated with Pre-BCR positive ALL and combination with Dexamethasone showed significant synergism in GC resistant cell lines and PDX samples. TKIs were also effective in some Pre-BCR negative ALL cells, however, predictive biomarkers need to be established. Confirmation of these data in preclinical models in vivo may define new therapies for high risk ALLs.

Keywords: dexamethasone, Tyrosine kinase inhibitor.

References

References

(ECACC), E.C.o.C.C. *General Cell Collection Detail*. Available at: https://www.phe-culturecollections.org.uk/products/celllines/generalcell/detail.jsp?refId=95111735&collection=ecacc_gc.

Advani, R.H., Buggy, J.J., Sharman, J.P., Smith, S.M., Boyd, T.E., Grant, B., Kolibaba, K.S., Furman, R.R., Rodriguez, S., Chang, B.Y., Sukbuntherng, J., Izumi, R., Hamdy, A., Hedrick, E. and Fowler, N.H. (2013) 'Bruton tyrosine kinase inhibitor ibrutinib (PCI-32765) has significant activity in patients with relapsed/refractory B-cell malignancies', *J Clin Oncol*, 31(1), pp. 88-94.

Aiba, Y., Kameyama, M., Yamazaki, T., Tedder, T.F. and Kurosaki, T. (2008) 'Regulation of B-cell development by BCAP and CD19 through their binding to phosphoinositide 3-kinase', *Blood*, 111(3), pp. 1497-503.

Almqvist, N. and Martensson, I.L. (2012) 'The pre-B cell receptor; selecting for or against autoreactivity', *Scand J Immunol*, 76(3), pp. 256-62.

Amrein, P.C., Attar, E.C., Takvorian, T., Hochberg, E.P., Ballen, K.K., Leahy, K.M., Fisher, D.C., Lacasce, A.S., Jacobsen, E.D., Armand, P., Hasserjian, R.P., Werner, L., Neuberg, D. and Brown, J.R. (2011) 'Phase II study of dasatinib in relapsed or refractory chronic lymphocytic leukemia', *Clin Cancer Res*, 17(9), pp. 2977-86.

An, Q., Wright, S.L., Konn, Z.J., Matheson, E., Minto, L., Moorman, A.V., Parker, H., Griffiths, M., Ross, F.M., Davies, T., Hall, A.G., Harrison, C.J., Irving, J.A. and Strefford, J.C. (2008) 'Variable breakpoints target PAX5 in patients with dicentric chromosomes: a model for the basis of unbalanced translocations in cancer', *Proc Natl Acad Sci U S A*, 105(44), pp. 17050-4.

Arber, D.A., Orazi, A., Hasserjian, R., Thiele, J., Borowitz, M.J., Le Beau, M.M., Bloomfield, C.D., Cazzola, M. and Vardiman, J.W. (2016) 'The 2016 revision to the World Health Organization classification of myeloid neoplasms and acute leukemia', *Blood*, 127(20), pp. 2391-405.

Arico, M., Schrappe, M., Hunger, S.P., Carroll, W.L., Conter, V., Galimberti, S., Manabe, A., Saha, V., Baruchel, A., Vettenranta, K., Horibe, K., Benoit, Y., Pieters, R., Escherich, G., Silverman, L.B., Pui, C.H. and Valsecchi, M.G. (2010) 'Clinical outcome of children with newly diagnosed Philadelphia chromosome-positive acute lymphoblastic leukemia treated between 1995 and 2005', *J Clin Oncol*, 28(31), pp. 4755-61.

Armstrong, S.A. and Look, A.T. (2005) 'Molecular genetics of acute lymphoblastic leukemia', *J Clin Oncol*, 23(26), pp. 6306-15.

Arya, M., Shergill, I.S., Williamson, M., Gommersall, L., Arya, N. and Patel, H.R. (2005) 'Basic principles of real-time quantitative PCR', *Expert Rev Mol Diagn*, 5(2), pp. 209-19.

Aspland, S.E., Bendall, H.H. and Murre, C. (2001) 'The role of E2A-PBX1 in leukemogenesis', *Oncogene*, 20(40), pp. 5708-17.

Asselin-Labat, M.L., Biola-Vidamment, A., Kerbrat, S., Lombes, M., Bertoglio, J. and Pallardy, M. (2005) 'FoxO3 mediates antagonistic effects of glucocorticoids and interleukin-2 on glucocorticoid-induced leucine zipper expression', *Mol Endocrinol*, 19(7), pp. 1752-64.

Asselin-Labat, M.L., David, M., Biola-Vidamment, A., Lecoeuche, D., Zennaro, M.C., Bertoglio, J. and Pallardy, M. (2004) 'GILZ, a new target for the transcription factor FoxO3, protects T lymphocytes from interleukin-2 withdrawal-induced apoptosis', *Blood*, 104(1), pp. 215-23.

Aubry, J.P., Blaecke, A., Lecoanet-Henchoz, S., Jeannin, P., Herbault, N., Caron, G., Moine, V. and Bonnefoy, J.Y. (1999) 'Annexin V used for measuring apoptosis in the early events of cellular cytotoxicity', *Cytometry*, 37(3), pp. 197-204.

Ayroldi, E., Petrillo, M.G., Bastianelli, A., Marchetti, M.C., Ronchetti, S., Nocentini, G., Ricciotti, L., Cannarile, L. and Riccardi, C. (2015) 'L-GILZ binds p53 and MDM2 and suppresses tumor growth through p53 activation in human cancer cells', *Cell Death Differ*, 22(1), pp. 118-30.

Ayroldi, E., Zollo, O., Bastianelli, A., Marchetti, C., Agostini, M., Di Virgilio, R. and Riccardi, C. (2007) 'GILZ mediates the antiproliferative activity of glucocorticoids by negative regulation of Ras signaling', *J Clin Invest*, 117(6), pp. 1605-15.

Ayroldi, E., Zollo, O., Macchiarulo, A., Di Marco, B., Marchetti, C. and Riccardi, C. (2002) 'Glucocorticoid-induced leucine zipper inhibits the Raf-extracellular signal-regulated kinase pathway by binding to Raf-1', *Mol Cell Biol*, 22(22), pp. 7929-41.

Bachmann, P.S., Gorman, R., Mackenzie, K.L., Lutze-Mann, L. and Lock, R.B. (2005) 'Dexamethasone resistance in B-cell precursor childhood acute lymphoblastic leukemia occurs downstream of ligand-induced nuclear translocation of the glucocorticoid receptor', *Blood*, 105(6), pp. 2519-26.

Bachmann, P.S., Gorman, R., Papa, R.A., Bardell, J.E., Ford, J., Kees, U.R., Marshall, G.M. and Lock, R.B. (2007) 'Divergent mechanisms of glucocorticoid resistance in experimental models of pediatric acute lymphoblastic leukemia', *Cancer Res*, 67(9), pp. 4482-90.

Baluom, M., Grossbard, E.B., Mant, T. and Lau, D.T.W. (2013) 'Pharmacokinetics of fostamatinib, a spleen tyrosine kinase (SYK) inhibitor, in healthy human subjects following single and multiple oral dosing in three phase I studies', *British Journal of Clinical Pharmacology*, 76(1), pp. 78-88.

Bavetsias, V. and Linardopoulos, S. (2015) 'Aurora Kinase Inhibitors: Current Status and Outlook', *Front Oncol*, 5, p. 278.

Beato, M., Chalepakis, G., Schauer, M. and Slater, E.P. (1989) 'DNA regulatory elements for steroid hormones', *J Steroid Biochem*, 32(5), pp. 737-47.

Beeler, T.J., Jona, I., van and Martonosi, A. (1979) 'The effect of ionomycin on calcium fluxes in sarcoplasmic reticulum vesicles and liposomes', *Journal of Biological Chemistry*, 254(14), pp. 6229-6231.

Bercovich, D., Ganmore, I., Scott, L.M., Wainreb, G., Birger, Y., Elimelech, A., Shochat, C., Cazzaniga, G., Biondi, A., Basso, G., Cario, G., Schrappe, M., Stanulla, M., Strehl, S., Haas, O.A., Mann, G., Binder, V., Borkhardt, A., Kempski, H., Trka, J., Bielorei, B., Avigad, S., Stark, B., Smith, O., Dastugue, N., Bourquin, J.P., Tal, N.B., Green, A.R. and Izraeli, S. (2008) 'Mutations of JAK2 in acute lymphoblastic leukaemias associated with Down's syndrome', *Lancet*, 372(9648), pp. 1484-92.

Berridge, M.J., Bootman, M.D. and Roderick, H.L. (2003) 'Calcium signalling: dynamics, homeostasis and remodelling', *Nat Rev Mol Cell Biol*, 4(7), pp. 517-29.

Bicocca, V.T., Chang, B.H., Masouleh, B.K., Muschen, M., Loriaux, M.M., Druker, B.J. and Tyner, J.W. (2012) 'Crosstalk between ROR1 and the Pre-B cell receptor promotes survival of t(1;19) acute lymphoblastic leukemia', *Cancer Cell*, 22(5), pp. 656-67.

Bijnsdorp, I.V., Giovannetti, E. and Peters, G.J. (2011) 'Analysis of drug interactions', *Methods Mol Biol*, 731, pp. 421-34.

Borowitz, M.J., Devidas, M., Hunger, S.P., Bowman, W.P., Carroll, A.J., Carroll, W.L., Linda, S., Martin, P.L., Pullen, D.J., Viswanatha, D., Willman, C.L., Winick, N. and Camitta, B.M. (2008) 'Clinical significance of minimal residual disease in childhood acute lymphoblastic

leukemia and its relationship to other prognostic factors: a Children's Oncology Group study', *Blood*, 111(12), pp. 5477-85.

Bradford, M.M. (1976) 'A rapid and sensitive method for the quantitation of microgram quantities of protein utilizing the principle of protein-dye binding', *Anal Biochem*, 72, pp. 248-54.

Braselmann, S., Taylor, V., Zhao, H., Wang, S., Sylvain, C., Baluom, M., Qu, K., Herlaar, E., Lau, A., Young, C., Wong, B.R., Lovell, S., Sun, T., Park, G., Argade, A., Jurcevic, S., Pine, P., Singh, R., Grossbard, E.B., Payan, D.G. and Masuda, E.S. (2006) 'R406, an orally available spleen tyrosine kinase inhibitor blocks fc receptor signaling and reduces immune complex-mediated inflammation', *J Pharmacol Exp Ther*, 319(3), pp. 998-1008.

Brave, M., Goodman, V., Kaminskas, E., Farrell, A., Timmer, W., Pope, S., Harapanhalli, R., Saber, H., Morse, D., Bullock, J., Men, A., Noory, C., Ramchandani, R., Kenna, L., Booth, B., Gobburu, J., Jiang, X., Sridhara, R., Justice, R. and Pazdur, R. (2008) 'Sprycel for chronic myeloid leukemia and Philadelphia chromosome-positive acute lymphoblastic leukemia resistant to or intolerant of imatinib mesylate', *Clin Cancer Res*, 14(2), pp. 352-9.

Brown, P. (2013) 'Treatment of infant leukemias: challenge and promise', *Hematology Am Soc Hematol Educ Program*, 2013, pp. 596-600.

Brown, R., Yang, S., Weatherburn, C., Gibson, J., Ho, P.J., Suen, H., Hart, D. and Joshua, D. (2015) 'Phospho-flow detection of constitutive and cytokine-induced pSTAT3/5, pAKT and pERK expression highlights novel prognostic biomarkers for patients with multiple myeloma', *Leukemia*, 29(2), pp. 483-90.

Brunner, C., Muller, B. and Wirth, T. (2005) 'Bruton's Tyrosine Kinase is involved in innate and adaptive immunity', *Histol Histopathol*, 20(3), pp. 945-55.

Bruscoli, S., Biagioli, M., Sorcini, D., Frammartino, T., Cimino, M., Sportoletti, P., Mazzon, E., Bereshchenko, O. and Riccardi, C. (2015) 'Lack of glucocorticoid-induced leucine zipper (GILZ) deregulates B-cell survival and results in B-cell lymphocytosis in mice', *Blood*, 126(15), pp. 1790-801.

Buchner, M. and Muschen, M. (2014) 'Targeting the B-cell receptor signaling pathway in B lymphoid malignancies', *Curr Opin Hematol*, 21(4), pp. 341-9.

Buchner, M., Swaminathan, S., Chen, Z. and Muschen, M. (2015) 'Mechanisms of pre-B-cell receptor checkpoint control and its oncogenic subversion in acute lymphoblastic leukemia', *Immunol Rev*, 263(1), pp. 192-209.

Burger, J.A. (2012) 'Targeting the microenvironment in chronic lymphocytic leukemia is changing the therapeutic landscape', *Curr Opin Oncol*, 24(6), pp. 643-9.

Burger, J.A., Li, K.W., Keating, M.J., Sivina, M., Amer, A.M., Garg, N., Ferrajoli, A., Huang, X., Kantarjian, H., Wierda, W.G., O'Brien, S., Hellerstein, M.K., Turner, S.M., Emson, C.L., Chen, S.S., Yan, X.J., Wodarz, D. and Chiorazzi, N. (2017) 'Leukemia cell proliferation and death in chronic lymphocytic leukemia patients on therapy with the BTK inhibitor ibrutinib', *JCI Insight*, 2(2), p. e89904.

Burnette, W.N. (1981) '"Western blotting": electrophoretic transfer of proteins from sodium dodecyl sulfate--polyacrylamide gels to unmodified nitrocellulose and radiographic detection with antibody and radioiodinated protein A', *Anal Biochem*, 112(2), pp. 195-203.

Burrows, P.D., Stephan, R.P., Wang, Y.H., Lassoued, K., Zhang, Z. and Cooper, M.D. (2002) 'The transient expression of pre-B cell receptors governs B cell development', *Semin Immunol*, 14(5), pp. 343-9.

Bustin, S.A., Benes, V., Garson, J.A., Hellemans, J., Huggett, J., Kubista, M., Mueller, R., Nolan, T., Pfaffl, M.W., Shipley, G.L., Vandesompele, J. and Wittwer, C.T. (2009) 'The MIQE

guidelines: minimum information for publication of quantitative real-time PCR experiments', *Clin Chem*, 55(4), pp. 611-22.

Byrd, J.C., Furman, R.R., Coutre, S., Flinn, I.W., Burger, J.A., Blum, K.A., Sharman, J., Grant, B., Jones, J.A. and Wierda, W.G. (2012) *ASH annual meeting abstracts*.

Calo, V., Migliavacca, M., Bazan, V., Macaluso, M., Buscemi, M., Gebbia, N. and Russo, A. (2003) 'STAT proteins: from normal control of cellular events to tumorigenesis', *J Cell Physiol*, 197(2), pp. 157-68.

Campana, D. (2012) 'Minimal residual disease monitoring in childhood acute lymphoblastic leukemia', *Curr Opin Hematol*, 19(4), pp. 313-8.

Cardullo, R.A., Agrawal, S., Flores, C., Zamecnik, P.C. and Wolf, D.E. (1988) 'Detection of nucleic acid hybridization by nonradiative fluorescence resonance energy transfer', *Proceedings of the National Academy of Sciences of the United States of America*, 85(23), pp. 8790-8794.

Cario, G., Zimmermann, M., Romey, R., Gesk, S., Vater, I., Harbott, J., Schrauder, A., Moericke, A., Izraeli, S., Akasaka, T., Dyer, M.J., Siebert, R., Schrappe, M. and Stanulla, M. (2010) 'Presence of the P2RY8-CRLF2 rearrangement is associated with a poor prognosis in non-high-risk precursor B-cell acute lymphoblastic leukemia in children treated according to the ALL-BFM 2000 protocol', *Blood*, 115(26), pp. 5393-7.

Carpinelli, P. and Moll, J. (2008) 'Aurora kinase inhibitors: identification and preclinical validation of their biomarkers', *Expert Opin Ther Targets*, 12(1), pp. 69-80.

Case, M., Matheson, E., Minto, L., Hassan, R., Harrison, C.J., Bown, N., Bailey, S., Vormoor, J., Hall, A.G. and Irving, J.A. (2008) 'Mutation of genes affecting the RAS pathway is common in childhood acute lymphoblastic leukemia', *Cancer Res*, 68(16), pp. 6803-9.

Chen, D., Zheng, J., Gerasimcik, N., Lagerstedt, K., Sjogren, H., Abrahamsson, J., Fogelstrand, L. and Martensson, I.L. (2016) 'The Expression Pattern of the Pre-B Cell Receptor Components Correlates with Cellular Stage and Clinical Outcome in Acute Lymphoblastic Leukemia', *PLoS One*, 11(9), p. e0162638.

Chen, L., Widhopf, G., Huynh, L., Rassenti, L., Rai, K.R., Weiss, A. and Kipps, T.J. (2002) 'Expression of ZAP-70 is associated with increased B-cell receptor signaling in chronic lymphocytic leukemia', *Blood*, 100(13), pp. 4609-14.

Chen, W., Dang, T., Blind, R.D., Wang, Z., Cavasotto, C.N., Hittelman, A.B., Rogatsky, I., Logan, S.K. and Garabedian, M.J. (2008) 'Glucocorticoid receptor phosphorylation differentially affects target gene expression', *Mol Endocrinol*, 22(8), pp. 1754-66.

Cheng, S., Ma, J., Guo, A., Lu, P., Leonard, J.P., Coleman, M., Liu, M., Buggy, J.J., Furman, R.R. and Wang, Y.L. (2014) 'BTK inhibition targets in vivo CLL proliferation through its effects on B-cell receptor signaling activity', *Leukemia*, 28(3), pp. 649-57.

Chessells, J.M., Harrison, C.J., Kempski, H., Webb, D.K., Wheatley, K., Hann, I.M., Stevens, R.F., Harrison, G. and Gibson, B.E. (2002) 'Clinical features, cytogenetics and outcome in acute lymphoblastic and myeloid leukaemia of infancy: report from the MRC Childhood Leukaemia working party', *Leukemia*, 16(5), pp. 776-84.

Chiaretti, S., Zini, G. and Bassan, R. (2014) 'Diagnosis and Subclassification of Acute Lymphoblastic Leukemia', *Mediterranean Journal of Hematology and Infectious Diseases*, 6(1), p. e2014073.

Choi, M.Y. and Kipps, T.J. (2012) 'Inhibitors of B-cell receptor signaling for patients with B-cell malignancies', *Cancer J*, 18(5), pp. 404-10.

Choi, S., Henderson, M.J., Kwan, E., Beesley, A.H., Sutton, R., Bahar, A.Y., Giles, J., Venn, N.C., Pozza, L.D., Baker, D.L., Marshall, G.M., Kees, U.R., Haber, M. and Norris, M.D. (2007)

'Relapse in children with acute lymphoblastic leukemia involving selection of a preexisting drug-resistant subclone', *Blood*, 110(2), pp. 632-9.

Chou, T.-C. and Talalay, P. (1984) 'Quantitative analysis of dose-effect relationships: the combined effects of multiple drugs or enzyme inhibitors', *Advances in enzyme regulation*, 22, pp. 27-55.

Chou, T.C. (2010) 'Drug combination studies and their synergy quantification using the Chou-Talalay method', *Cancer Res*, 70(2), pp. 440-6.

Cilloni, D. and Saglio, G. (2012) 'Molecular pathways: BCR-ABL', *Clin Cancer Res*, 18(4), pp. 930-7.

Clark, M.R., Mandal, M., Ochiai, K. and Singh, H. (2014) 'Orchestrating B cell lymphopoiesis through interplay of IL-7 receptor and pre-B cell receptor signalling', *Nat Rev Immunol*, 14(2), pp. 69-80.

Conter, V., Bartram, C.R., Valsecchi, M.G., Schrauder, A., Panzer-Grümayer, R., Möricke, A., Aricò, M., Zimmermann, M., Mann, G. and De Rossi, G. (2010) 'Molecular response to treatment redefines all prognostic factors in children and adolescents with B-cell precursor acute lymphoblastic leukemia: results in 3184 patients of the AIEOP-BFM ALL 2000 study', *Blood*, 115(16), pp. 3206-3214.

Corfe, S.A. and Paige, C.J. (2012) 'The many roles of IL-7 in B cell development; mediator of survival, proliferation and differentiation', *Semin Immunol*, 24(3), pp. 198-208.

Cory, S. and Adams, J.M. (2002) 'The Bcl2 family: regulators of the cellular life-or-death switch', *Nat Rev Cancer*, 2(9), pp. 647-56.

Coustan-Smith, E., Sancho, J., Hancock, M.L., Boyett, J.M., Behm, F.G., Raimondi, S.C., Sandlund, J.T., Rivera, G.K., Rubnitz, J.E., Ribeiro, R.C., Pui, C.H. and Campana, D. (2000) 'Clinical importance of minimal residual disease in childhood acute lymphoblastic leukemia', *Blood*, 96(8), pp. 2691-6.

Cox, C.V., Evely, R.S., Oakhill, A., Pamphilon, D.H., Goulden, N.J. and Blair, A. (2004) 'Characterization of acute lymphoblastic leukemia progenitor cells', *Blood*, 104(9), pp. 2919-25.

Crespo, M., Villamor, N., Gine, E., Muntanola, A., Colomer, D., Marafioti, T., Jones, M., Camos, M., Campo, E., Montserrat, E. and Bosch, F. (2006) 'ZAP-70 expression in normal pro/pre B cells, mature B cells, and in B-cell acute lymphoblastic leukemia', *Clin Cancer Res*, 12(3 Pt 1), pp. 726-34.

Crissman, H.A. and Steinkamp, J.A. (1973) 'Rapid, simultaneous measurement of DNA, protein, and cell volume in single cells from large mammalian cell populations', *J Cell Biol*, 59(3), pp. 766-71.

Davis, M.I., Hunt, J.P., Herrgard, S., Ciceri, P., Wodicka, L.M., Pallares, G., Hocker, M., Treiber, D.K. and Zarrinkar, P.P. (2011) 'Comprehensive analysis of kinase inhibitor selectivity', *Nat Biotechnol*, 29(11), pp. 1046-51.

Davis, R.E., Ngo, V.N., Lenz, G., Tolar, P., Young, R.M., Romesser, P.B., Kohlhammer, H., Lamy, L., Zhao, H., Yang, Y., Xu, W., Shaffer, A.L., Wright, G., Xiao, W., Powell, J., Jiang, J.-k., Thomas, C.J., Rosenwald, A., Ott, G., Muller-Hermelink, H.K., Gascoyne, R.D., Connors, J.M., Johnson, N.A., Rimsza, L.M., Campo, E., Jaffe, E.S., Wilson, W.H., Delabie, J., Smeland, E.B., Fisher, R.I., Braziel, R.M., Tubbs, R.R., Cook, J.R., Weisenburger, D.D., Chan, W.C., Pierce, S.K. and Staudt, L.M. (2010a) 'Chronic active B-cell-receptor signalling in diffuse large B-cell lymphoma', *Nature*, 463(7277), pp. 88-92.

Davis, R.E., Ngo, V.N., Lenz, G., Tolar, P., Young, R.M., Romesser, P.B., Kohlhammer, H., Lamy, L., Zhao, H., Yang, Y., Xu, W., Shaffer, A.L., Wright, G., Xiao, W., Powell, J., Jiang, J.K., Thomas, C.J., Rosenwald, A., Ott, G., Muller-Hermelink, H.K., Gascoyne, R.D., Connors,

J.M., Johnson, N.A., Rimsza, L.M., Campo, E., Jaffe, E.S., Wilson, W.H., Delabie, J., Smeland, E.B., Fisher, R.I., Braziel, R.M., Tubbs, R.R., Cook, J.R., Weisenburger, D.D., Chan, W.C., Pierce, S.K. and Staudt, L.M. (2010b) 'Chronic active B-cell-receptor signalling in diffuse large B-cell lymphoma', *Nature*, 463(7277), pp. 88-92.

de Labarthe, A., Rousselot, P., Huguet-Rigal, F., Delabesse, E., Witz, F., Maury, S., Rea, D., Cayuela, J.M., Vekemans, M.C., Reman, O., Buzyn, A., Pigneux, A., Escoffre, M., Chalandon, Y., MacIntyre, E., Lheritier, V., Vernant, J.P., Thomas, X., Ifrah, N. and Dombret, H. (2007) 'Imatinib combined with induction or consolidation chemotherapy in patients with de novo Philadelphia chromosome-positive acute lymphoblastic leukemia: results of the GRAAPH-2003 study', *Blood*, 109(4), pp. 1408-13.

De Luca, A. and Normanno, N. (2010) 'Predictive biomarkers to tyrosine kinase inhibitors for the epidermal growth factor receptor in non-small-cell lung cancer', *Curr Drug Targets*, 11(7), pp. 851-64.

de Weers, M., Verschuren, M.C., Kraakman, M.E., Mensink, R.G., Schuurman, R.K., van Dongen, J.J. and Hendriks, R.W. (1993) 'The Bruton's tyrosine kinase gene is expressed throughout B cell differentiation, from early precursor B cell stages preceding immunoglobulin gene rearrangement up to mature B cell stages', *Eur J Immunol*, 23(12), pp. 3109-14.

Deane, J.A. and Fruman, D.A. (2004) 'Phosphoinositide 3-kinase: diverse roles in immune cell activation', *Annu Rev Immunol*, 22, pp. 563-98.

Dellis, O., Arbabian, A., Brouland, J.-P., Kovàcs, T., Rowe, M., Chomienne, C., Joab, I. and Papp, B. (2009) 'Modulation of B-cell endoplasmic reticulum calcium homeostasis by Epstein-Barr virus latent membrane protein-1', *Mol Cancer*, 8, p. 59.

Den Boer, M.L., van Slegtenhorst, M., De Menezes, R.X., Cheok, M.H., Buijs-Gladdines, J.G., Peters, S.T., Van Zutven, L.J., Beverloo, H.B., Van der Spek, P.J., Escherich, G., Horstmann, M.A., Janka-Schaub, G.E., Kamps, W.A., Evans, W.E. and Pieters, R. (2009) 'A subtype of childhood acute lymphoblastic leukaemia with poor treatment outcome: a genome-wide classification study', *Lancet Oncol*, 10(2), pp. 125-34.

Ding, J.Y., Takano, T., Gao, S.Y., Han, W.H., Noda, C., Yanagi, S. and Yamamura, H. (2000) *Syk Is Required for the Activation of Akt Survival Pathway in B Cells Exposed to Oxidative Stress*.

Do, B., Mace, M. and Rexwinkle, A. (2016) 'Idelalisib for treatment of B-cell malignancies', *Am J Health Syst Pharm*, 73(8), pp. 547-55.

Dolai, S., Sia, K.C., Robbins, A.K., Zhong, L., Heatley, S.L., Vincent, T.L., Hochgrafe, F., Sutton, R., Kurmasheva, R.T., Revesz, T., White, D.L., Houghton, P.J., Smith, M.A., Teachey, D.T., Daly, R.J., Raftery, M.J. and Lock, R.B. (2016) 'Quantitative phosphotyrosine profiling of patient-derived xenografts identifies therapeutic targets in pediatric leukemia', *Cancer Res*.

Dorak, M.T. (2006) 'Real-time PCR (Advanced methods series)', *Leong SL, Hocking AD & Scott ES (2006) Survival and growth of*.

Dordelmann, M., Reiter, A., Borkhardt, A., Ludwig, W.D., Gotz, N., Viehmann, S., Gadner, H., Riehm, H. and Schrappe, M. (1999) 'Prednisone response is the strongest predictor of treatment outcome in infant acute lymphoblastic leukemia', *Blood*, 94(4), pp. 1209-17.

Drexler, H.G. and Uphoff, C.C. (2002) 'Mycoplasma contamination of cell cultures: Incidence, sources, effects, detection, elimination, prevention', *Cytotechnology*, 39(2), pp. 75-90.

Druker, B.J., Talpaz, M., Resta, D.J., Peng, B., Buchdunger, E., Ford, J.M., Lydon, N.B., Kantarjian, H., Capdeville, R., Ohno-Jones, S. and Sawyers, C.L. (2001) 'Efficacy and safety

of a specific inhibitor of the BCR-ABL tyrosine kinase in chronic myeloid leukemia', *N Engl J Med*, 344(14), pp. 1031-7.

Duque-Afonso, J., Lin, C.H., Han, K., Wei, M.C., Feng, J., Kurzer, J.H., Schneidawind, C., Wong, S.H., Bassik, M.C. and Cleary, M.L. (2016) 'E2A-PBX1 Remodels Oncogenic Signaling Networks in B-cell Precursor Acute Lymphoid Leukemia', *Cancer Res*, 76(23), pp. 6937-6949.

Duy, C., Hurtz, C., Shojaee, S., Cerchietti, L., Geng, H., Swaminathan, S., Klemm, L., Kweon, S.M., Nahar, R., Braig, M., Park, E., Kim, Y.M., Hofmann, W.K., Herzog, S., Jumaa, H., Koeffler, H.P., Yu, J.J., Heisterkamp, N., Graeber, T.G., Wu, H., Ye, B.H., Melnick, A. and Muschen, M. (2011) 'BCL6 enables Ph+ acute lymphoblastic leukaemia cells to survive BCR-ABL1 kinase inhibition', *Nature*, 473(7347), pp. 384-8.

Duy, C., Yu, J.J., Nahar, R., Swaminathan, S., Kweon, S.M., Polo, J.M., Valls, E., Klemm, L., Shojaee, S., Cerchietti, L., Schuh, W., Jack, H.M., Hurtz, C., Ramezani-Rad, P., Herzog, S., Jumaa, H., Koeffler, H.P., de Alboran, I.M., Melnick, A.M., Ye, B.H. and Muschen, M. (2010) 'BCL6 is critical for the development of a diverse primary B cell repertoire', *J Exp Med*, 207(6), pp. 1209-21.

Eckert, C., Flohr, T., Koehler, R., Hagedorn, N., Moericke, A., Stanulla, M., Kirschner-Schwabe, R., Cario, G., Stackelberg, A., Bartram, C.R., Henze, G., Schrappe, M. and Schrauder, A. (2011) 'Very early/early relapses of acute lymphoblastic leukemia show unexpected changes of clonal markers and high heterogeneity in response to initial and relapse treatment', *Leukemia*, 25(8), pp. 1305-13.

Eldfors, S., Kuusanmaki, H., Kontro, M., Majumder, M.M., Parsons, A., Edgren, H., Pemovska, T., Kallioniemi, O., Wennerberg, K., Gokbuget, N., Burmeister, T., Porkka, K. and Heckman, C.A. (2017) 'Idelalisib sensitivity and mechanisms of disease progression in relapsed TCF3-PBX1 acute lymphoblastic leukemia', *Leukemia*, 31(1), pp. 51-57.

Elizabeth C. Matheson, H.T., Marian Case, Helen Blair, Rosanna K. Jackson, Gareth Veal, Chris Halsey, David R Newell, Josef Vormoor and Julie A.E Irving (Manuscript submitted) *Glucocorticoids and selumetinib are highly synergistic in RAS pathway mutated childhood ALL through upregulation of bim: a preclinical data package supporting the Seludex trial.*

Ensor, H.M., Schwab, C., Russell, L.J., Richards, S.M., Morrison, H., Masic, D., Jones, L., Kinsey, S.E., Vora, A.J., Mitchell, C.D., Harrison, C.J. and Moorman, A.V. (2011) 'Demographic, clinical, and outcome features of children with acute lymphoblastic leukemia and CRLF2 deregulation: results from the MRC ALL97 clinical trial', *Blood*, 117(7), pp. 2129-36.

Eschbach, C., Bach, M.P., Fidler, I., Pelanda, R., Kohler, F., Rajewsky, K. and Jumaa, H. (2011) 'Efficient generation of B lymphocytes by recognition of self-antigens', *Eur J Immunol*, 41(8), pp. 2397-403.

Eswaran, J., Sinclair, P., Heidenreich, O., Irving, J., Russell, L.J., Hall, A., Calado, D.P., Harrison, C.J. and Vormoor, J. (2015) 'The pre-B-cell receptor checkpoint in acute lymphoblastic leukaemia', *Leukemia*, 29(8), pp. 1623-31.

Fadok, V.A., Voelker, D.R., Campbell, P.A., Cohen, J.J., Bratton, D.L. and Henson, P.M. (1992) 'Exposure of phosphatidylserine on the surface of apoptotic lymphocytes triggers specific recognition and removal by macrophages', *J Immunol*, 148(7), pp. 2207-16.

Fei, F., Stoddart, S., Muschen, M., Kim, Y.M., Groffen, J. and Heisterkamp, N. (2010) 'Development of resistance to dasatinib in Bcr/Abl-positive acute lymphoblastic leukemia', *Leukemia*, 24(4), pp. 813-20.

Feldhahn, N., Klein, F., Mooster, J.L., Hadweh, P., Sprangers, M., Wartenberg, M., Bekhite, M.M., Hofmann, W.K., Herzog, S., Jumaa, H., Rowley, J.D. and Muschen, M. (2005)

'Mimicry of a constitutively active pre-B cell receptor in acute lymphoblastic leukemia cells', *J Exp Med*, 201(11), pp. 1837-52.

Feske, S. (2007) 'Calcium signalling in lymphocyte activation and disease', *Nat Rev Immunol*, 7(9), pp. 690-702.

Fielding, A.K., Rowe, J.M., Buck, G., Foroni, L., Gerrard, G., Litzow, M.R., Lazarus, H., Luger, S.M., Marks, D.I., McMillan, A.K., Moorman, A.V., Patel, B., Paietta, E., Tallman, M.S. and Goldstone, A.H. (2014) 'UKALLXII/ECOG2993: addition of imatinib to a standard treatment regimen enhances long-term outcomes in Philadelphia positive acute lymphoblastic leukemia', *Blood*, 123(6), pp. 843-50.

Findley, H.W., Jr., Cooper, M.D., Kim, T.H., Alvarado, C. and Ragab, A.H. (1982) 'Two new acute lymphoblastic leukemia cell lines with early B-cell phenotypes', *Blood*, 60(6), pp. 1305-1309.

Fine, B.M., Stanulla, M., Schrappe, M., Ho, M., Viehmann, S., Harbott, J. and Boxer, L.M. (2004) 'Gene expression patterns associated with recurrent chromosomal translocations in acute lymphoblastic leukemia', *Blood*, 103(3), pp. 1043-9.

Fischer, M., Schwieger, M., Horn, S., Niebuhr, B., Ford, A., Roscher, S., Bergholz, U., Greaves, M., Lohler, J. and Stocking, C. (2005) 'Defining the oncogenic function of the TEL/AML1 (ETV6/RUNX1) fusion protein in a mouse model', *Oncogene*, 24(51), pp. 7579-91.

Fischer, U., Forster, M., Rinaldi, A., Risch, T., Sungalee, S., Warnatz, H.J., Bornhauser, B., Gombert, M., Kratsch, C., Stutz, A.M., Sultan, M., Tchinda, J., Worth, C.L., Amstislavskiy, V., Badarinarayan, N., Baruchel, A., Bartram, T., Basso, G., Canpolat, C., Cario, G., Cave, H., Dakaj, D., Delorenzi, M., Dobay, M.P., Eckert, C., Ellinghaus, E., Eugster, S., Frismantas, V., Ginzel, S., Haas, O.A., Heidenreich, O., Hemmrich-Stanisak, G., Hezaveh, K., Holl, J.I., Hornhardt, S., Husemann, P., Kachroo, P., Kratz, C.P., Te Kronnie, G., Marovca, B., Niggli, F., McHardy, A.C., Moorman, A.V., Panzer-Grumayer, R., Petersen, B.S., Raeder, B., Ralser, M., Rosenstiel, P., Schafer, D., Schrappe, M., Schreiber, S., Schutte, M., Stade, B., Thiele, R., von der Weid, N., Vora, A., Zaliova, M., Zhang, L., Zichner, T., Zimmermann, M., Lehrach, H., Borkhardt, A., Bourquin, J.P., Franke, A., Korbel, J.O., Stanulla, M. and Yaspo, M.L. (2015) 'Genomics and drug profiling of fatal TCF3-HLF-positive acute lymphoblastic leukemia identifies recurrent mutation patterns and therapeutic options', *Nat Genet*, 47(9), pp. 1020-1029.

Fisher, A.G., Burdet, C., LeMeur, M., Haasner, D., Gerber, P. and Ceredig, R. (1993) 'Lymphoproliferative disorders in an IL-7 transgenic mouse line', *Leukemia*, 7 Suppl 2, pp. S66-8.

Flemming, A., Brummer, T., Reth, M. and Jumaa, H. (2003) 'The adaptor protein SLP-65 acts as a tumor suppressor that limits pre-B cell expansion', *Nat Immunol*, 4(1), pp. 38-43.

Flinn, I.W., Bartlett, N.L., Blum, K.A., Ardeshna, K.M., LaCasce, A.S., Flowers, C.R., Shustov, A.R., Thress, K.S., Mitchell, P., Zheng, F., Skolnik, J.M. and Friedberg, J.W. (2016) 'A phase II trial to evaluate the efficacy of fostamatinib in patients with relapsed or refractory diffuse large B-cell lymphoma (DLBCL)', *Eur J Cancer*, 54, pp. 11-17.

Foa, R., Vitale, A., Vignetti, M., Meloni, G., Guarini, A., De Propris, M.S., Elia, L., Paoloni, F., Fazi, P., Cimino, G., Nobile, F., Ferrara, F., Castagnola, C., Sica, S., Leoni, P., Zuffa, E., Fozza, C., Luppi, M., Candoni, A., Iacobucci, I., Soverini, S., Mandelli, F., Martinelli, G. and Baccarani, M. (2011) 'Dasatinib as first-line treatment for adult patients with Philadelphia chromosome-positive acute lymphoblastic leukemia', *Blood*, 118(25), pp. 6521-8.

Fowler, N. and Davis, E. (2013) 'Targeting B-cell receptor signaling: changing the paradigm', *Hematology Am Soc Hematol Educ Program*, 2013, pp. 553-60.

Friedberg, J.W., Sharman, J., Sweetenham, J., Johnston, P.B., Vose, J.M., Lacasce, A., Schaefer-Cutillo, J., De Vos, S., Sinha, R., Leonard, J.P., Cripe, L.D., Gregory, S.A., Sterba, M.P., Lowe, A.M., Levy, R. and Shipp, M.A. (2010) 'Inhibition of Syk with fostamatinib disodium has significant clinical activity in non-Hodgkin lymphoma and chronic lymphocytic leukemia', *Blood*, 115(13), pp. 2578-85.

Frismantas, V., Dobay, M.P., Rinaldi, A., Tchinda, J., Dunn, S.H., Kunz, J., Richter-Pechanska, P., Marovca, B., Pail, O., Jenni, S., Diaz-Flores, E., Chang, B.H., Brown, T.J., Collins, R.H., Uhrig, S., Balasubramanian, G.P., Bandapalli, O.R., Higi, S., Eugster, S., Voegeli, P., Delorenzi, M., Cario, G., Loh, M.L., Schrappe, M., Stanulla, M., Kulozik, A.E., Muckenthaler, M.U., Saha, V., Irving, J.A., Meisel, R., Radimerski, T., Von Stackelberg, A., Eckert, C., Tyner, J.W., Horvath, P., Bornhauser, B.C. and Bourquin, J.P. (2017) 'Ex vivo drug response profiling detects recurrent sensitivity patterns in drug-resistant acute lymphoblastic leukemia', *Blood*, 129(11), pp. e26-e37.

Furman, R.R., Sharman, J.P., Coutre, S.E., Cheson, B.D., Pagel, J.M., Hillmen, P., Barrientos, J.C., Zelenetz, A.D., Kipps, T.J., Flinn, I., Ghia, P., Eradat, H., Ervin, T., Lamanna, N., Coiffier, B., Pettitt, A.R., Ma, S., Stilgenbauer, S., Cramer, P., Aiello, M., Johnson, D.M., Miller, L.L., Li, D., Jahn, T.M., Dansey, R.D., Hallek, M. and O'Brien, S.M. (2014) 'Idelalisib and rituximab in relapsed chronic lymphocytic leukemia', *N Engl J Med*, 370(11), pp. 997-1007.

Gandemer, V., Chevret, S., Petit, A., Vermylen, C., Leblanc, T., Michel, G., Schmitt, C., Lejars, O., Schneider, P., Demeocq, F., Bader-Meunier, B., Bernaudin, F., Perel, Y., Auclerc, M.F., Cayuela, J.M., Leverger, G. and Baruchel, A. (2012) 'Excellent prognosis of late relapses of ETV6/RUNX1-positive childhood acute lymphoblastic leukemia: lessons from the FRALLE 93 protocol', *Haematologica*, 97(11), pp. 1743-50.

Garnett, M.J., Edelman, E.J., Heidorn, S.J., Greenman, C.D., Dastur, A., Lau, K.W., Greninger, P., Thompson, I.R., Luo, X., Soares, J., Liu, Q., Iorio, F., Surdez, D., Chen, L., Milano, R.J., Bignell, G.R., Tam, A.T., Davies, H., Stevenson, J.A., Barthorpe, S., Lutz, S.R., Kogera, F., Lawrence, K., McLaren-Douglas, A., Mitropoulos, X., Mironenko, T., Thi, H., Richardson, L., Zhou, W., Jewitt, F., Zhang, T., O'Brien, P., Boisvert, J.L., Price, S., Hur, W., Yang, W., Deng, X., Butler, A., Choi, H.G., Chang, J.W., Baselga, J., Stamenkovic, I., Engelman, J.A., Sharma, S.V., Delattre, O., Saez-Rodriguez, J., Gray, N.S., Settleman, J., Futreal, P.A., Haber, D.A., Stratton, M.R., Ramaswamy, S., McDermott, U. and Benes, C.H. (2012) 'Systematic identification of genomic markers of drug sensitivity in cancer cells', *Nature*, 483(7391), pp. 570-5.

Gauthier, L., Rossi, B., Roux, F., Termine, E. and Schiff, C. (2002) 'Galectin-1 is a stromal cell ligand of the pre-B cell receptor (BCR) implicated in synapse formation between pre-B and stromal cells and in pre-BCR triggering', *Proc Natl Acad Sci U S A*, 99(20), pp. 13014-9.

Gee, K.R., Brown, K.A., Chen, W.N., Bishop-Stewart, J., Gray, D. and Johnson, I. (2000) 'Chemical and physiological characterization of fluo-4 Ca(2+)-indicator dyes', *Cell Calcium*, 27(2), pp. 97-106.

Geier, J.K. and Schlissel, M.S. (2006) 'Pre-BCR signals and the control of Ig gene rearrangements', *Semin Immunol*, 18(1), pp. 31-9.

Genevier, H.C. and Callard, R.E. (1997) 'Impaired Ca(2+) mobilization by X-linked agammaglobulinaemia (XLA) B cells in response to ligation of the B cell receptor (BCR)', *Clin Exp Immunol*, 110(3), pp. 386-91.

Geng, H., Hurtz, C., Lenz, K.B., Chen, Z., Baumjohann, D., Thompson, S., Goloviznina, N.A., Chen, W.Y., Huan, J., LaTocha, D., Ballabio, E., Xiao, G., Lee, J.W., Deucher, A., Qi, Z., Park,

E., Huang, C., Nahar, R., Kweon, S.M., Shojaee, S., Chan, L.N., Yu, J., Kornblau, S.M., Bijl, J.J., Ye, B.H., Ansel, K.M., Paietta, E., Melnick, A., Hunger, S.P., Kurre, P., Tyner, J.W., Loh, M.L., Roeder, R.G., Druker, B.J., Burger, J.A., Milne, T.A., Chang, B.H. and Muschen, M. (2015) 'Self-enforcing feedback activation between BCL6 and pre-B cell receptor signaling defines a distinct subtype of acute lymphoblastic leukemia', *Cancer Cell*, 27(3), pp. 409-25.

Girdler, F., Gascoigne, K.E., Eyers, P.A., Hartmuth, S., Crafter, C., Foote, K.M., Keen, N.J. and Taylor, S.S. (2006) 'Validating Aurora B as an anti-cancer drug target', *J Cell Sci*, 119(Pt 17), pp. 3664-75.

Gobessi, S., Laurenti, L., Longo, P.G., Carsetti, L., Berno, V., Sica, S., Leone, G. and Efremov, D.G. (2009) 'Inhibition of constitutive and BCR-induced Syk activation downregulates Mcl-1 and induces apoptosis in chronic lymphocytic leukemia B cells', *Leukemia*, 23(4), pp. 686-97.

Greaves, M. (2005) 'In utero origins of childhood leukaemia', *Early Hum Dev*, 81(1), pp. 123-9.

Greaves, M.F., Maia, A.T., Wiemels, J.L. and Ford, A.M. (2003) 'Leukemia in twins: lessons in natural history', *Blood*, 102(7), pp. 2321-33.

Guo, B., Kato, R.M., Garcia-Lloret, M., Wahl, M.I. and Rawlings, D.J. (2000) 'Engagement of the human pre-B cell receptor generates a lipid raft-dependent calcium signaling complex', *Immunity*, 13(2), pp. 243-53.

Hall, C.P., Reynolds, C.P. and Kang, M.H. (2016) 'Modulation of Glucocorticoid Resistance in Pediatric T-cell Acute Lymphoblastic Leukemia by Increasing BIM Expression with the PI3K/mTOR Inhibitor BEZ235', *Clin Cancer Res*, 22(3), pp. 621-32.

Han, T., Dadey, B. and Minowada, J. (1978) 'Unique leukemic non-T/non-B lymphoid cell lines (REH and KM-3): absence of MLR-S and presence of suppressor cell activity for normal T-cell response', *J Clin Lab Immunol*, 1(3), pp. 237-43.

Hantschel, O., Rix, U., Schmidt, U., Burckstummer, T., Kneidinger, M., Schutze, G., Colinge, J., Bennett, K.L., Ellmeier, W., Valent, P. and Superti-Furga, G. (2007) 'The Btk tyrosine kinase is a major target of the Bcr-Abl inhibitor dasatinib', *Proc Natl Acad Sci U S A*, 104(33), pp. 13283-8.

Harrison, C. (2011) 'New genetics and diagnosis of childhood B-cell precursor acute lymphoblastic leukemia', *Pediatr Rep*, 3(Suppl 2).

Harrison, C.J. (2015) 'Blood Spotlight on iAMP21 acute lymphoblastic leukemia (ALL), a high-risk pediatric disease', *Blood*, 125(9), pp. 1383-6.

Harrison, C.J., Moorman, A.V., Schwab, C., Carroll, A.J., Raetz, E.A., Devidas, M., Strehl, S., Nebral, K., Harbott, J., Teigler-Schlegel, A., Zimmerman, M., Dastuge, N., Baruchel, A., Soulier, J., Auclerc, M.F., Attarbaschi, A., Mann, G., Stark, B., Cazzaniga, G., Chilton, L., Vandenberghe, P., Forestier, E., Haltrich, I., Raimondi, S.C., Parihar, M., Bourquin, J.P., Tchinda, J., Haferlach, C., Vora, A., Hunger, S.P., Heerema, N.A. and Haas, O.A. (2014) 'An international study of intrachromosomal amplification of chromosome 21 (iAMP21): cytogenetic characterization and outcome', *Leukemia*, 28(5), pp. 1015-21.

Heerema, N.A., Carroll, A.J., Devidas, M., Loh, M.L., Borowitz, M.J., Gastier-Foster, J.M., Larsen, E.C., Mattano, L.A., Jr., Maloney, K.W., Willman, C.L., Wood, B.L., Winick, N.J., Carroll, W.L., Hunger, S.P. and Raetz, E.A. (2013) 'Intrachromosomal amplification of chromosome 21 is associated with inferior outcomes in children with acute lymphoblastic leukemia treated in contemporary standard-risk children's oncology group studies: a report from the children's oncology group', *J Clin Oncol*, 31(27), pp. 3397-402.

Hendriks, R.W. and Kersseboom, R. (2006) 'Involvement of SLP-65 and Btk in tumor suppression and malignant transformation of pre-B cells', *Semin Immunol*, 18(1), pp. 67-76.

Hendriks, R.W. and Middendorp, S. (2004) 'The pre-BCR checkpoint as a cell-autonomous proliferation switch', *Trends Immunol*, 25(5), pp. 249-56.

Hendriks, R.W., Yuvaraj, S. and Kil, L.P. (2014) 'Targeting Bruton's tyrosine kinase in B cell malignancies', *Nat Rev Cancer*, 14(4), pp. 219-32.

Henel, G. and Schmitz, J.L. (2007) 'Basic Theory and Clinical Applications of Flow Cytometry', *Laboratory Medicine*, 38(7), pp. 428-436.

Herishanu, Y., Perez-Galan, P., Liu, D., Biancotto, A., Pittaluga, S., Vire, B., Gibellini, F., Njuguna, N., Lee, E., Stennett, L., Raghavachari, N., Liu, P., McCoy, J.P., Raffeld, M., Stetler-Stevenson, M., Yuan, C., Sherry, R., Arthur, D.C., Maric, I., White, T., Marti, G.E., Munson, P., Wilson, W.H. and Wiestner, A. (2011) 'The lymph node microenvironment promotes B-cell receptor signaling, NF-kappaB activation, and tumor proliferation in chronic lymphocytic leukemia', *Blood*, 117(2), pp. 563-74.

Herman, S.E., Gordon, A.L., Hertlein, E., Ramanunni, A., Zhang, X., Jaglowski, S., Flynn, J., Jones, J., Blum, K.A., Buggy, J.J., Hamdy, A., Johnson, A.J. and Byrd, J.C. (2011) 'Bruton tyrosine kinase represents a promising therapeutic target for treatment of chronic lymphocytic leukemia and is effectively targeted by PCI-32765', *Blood*, 117(23), pp. 6287-96.

Herman, S.E., Gordon, A.L., Wagner, A.J., Heerema, N.A., Zhao, W., Flynn, J.M., Jones, J., Andritsos, L., Puri, K.D., Lannutti, B.J., Giese, N.A., Zhang, X., Wei, L., Byrd, J.C. and Johnson, A.J. (2010) 'Phosphatidylinositol 3-kinase-delta inhibitor CAL-101 shows promising preclinical activity in chronic lymphocytic leukemia by antagonizing intrinsic and extrinsic cellular survival signals', *Blood*, 116(12), pp. 2078-88.

Herman, S.E. and Johnson, A.J. (2012) 'Molecular pathways: targeting phosphoinositide 3-kinase p110-delta in chronic lymphocytic leukemia', *Clin Cancer Res*, 18(15), pp. 4013-8.

Herman, S.E., Mustafa, R.Z., Gyamfi, J.A., Pittaluga, S., Chang, S., Chang, B., Farooqui, M. and Wiestner, A. (2014a) 'Ibrutinib inhibits BCR and NF-kappaB signaling and reduces tumor proliferation in tissue-resident cells of patients with CLL', *Blood*, 123(21), pp. 3286-95.

Herman, S.E., Niemann, C.U., Farooqui, M., Jones, J., Mustafa, R.Z., Lipsky, A., Saba, N., Martyr, S., Soto, S., Valdez, J., Gyamfi, J.A., Maric, I., Calvo, K.R., Pedersen, L.B., Geisler, C.H., Liu, D., Marti, G.E., Aue, G. and Wiestner, A. (2014b) 'Ibrutinib-induced lymphocytosis in patients with chronic lymphocytic leukemia: correlative analyses from a phase II study', *Leukemia*, 28(11), pp. 2188-96.

Herman, S.E., Sun, X., McAuley, E.M., Hsieh, M.M., Pittaluga, S., Raffeld, M., Liu, D., Keyvanfar, K., Chapman, C.M., Chen, J., Buggy, J.J., Aue, G., Tisdale, J.F., Perez-Galan, P. and Wiestner, A. (2013) 'Modeling tumor-host interactions of chronic lymphocytic leukemia in xenografted mice to study tumor biology and evaluate targeted therapy', *Leukemia*, 27(12), pp. 2311-21.

Herzog, S., Hug, E., Meixlsperger, S., Paik, J.H., DePinho, R.A., Reth, M. and Jumaa, H. (2008) 'SLP-65 regulates immunoglobulin light chain gene recombination through the PI(3)K-PKB-Foxo pathway', *Nat Immunol*, 9(6), pp. 623-31.

Herzog, S., Reth, M. and Jumaa, H. (2009) 'Regulation of B-cell proliferation and differentiation by pre-B-cell receptor signalling', *Nat Rev Immunol*, 9(3), pp. 195-205.

Hidalgo, M., Amant, F., Biankin, A.V., Budinska, E., Byrne, A.T., Caldas, C., Clarke, R.B., de Jong, S., Jonkers, J., Maelandsmo, G.M., Roman-Roman, S., Seoane, J., Trusolino, L. and Villanueva, A. (2014) 'Patient-derived xenograft models: an emerging platform for translational cancer research', *Cancer Discov*, 4(9), pp. 998-1013.

Hiebert, S.W., Sun, W., Davis, J.N., Golub, T., Shurtleff, S., Buijs, A., Downing, J.R., Grosveld, G., Roussell, M.F., Gilliland, D.G., Lenny, N. and Meyers, S. (1996) 'The t(12;21) translocation converts AML-1B from an activator to a repressor of transcription', *Mol Cell Biol*, 16(4), pp. 1349-55.

Hoellenriegel, J., Coffey, G.P., Sinha, U., Pandey, A., Sivina, M., Ferrajoli, A., Ravandi, F., Wierda, W.G., O'Brien, S., Keating, M.J. and Burger, J.A. (2012) 'Selective, novel spleen tyrosine kinase (Syk) inhibitors suppress chronic lymphocytic leukemia B-cell activation and migration', *Leukemia*, 26(7), pp. 1576-83.

Hoellenriegel, J., Meadows, S.A., Sivina, M., Wierda, W.G., Kantarjian, H., Keating, M.J., Giese, N., O'Brien, S., Yu, A., Miller, L.L., Lannutti, B.J. and Burger, J.A. (2011) 'The phosphoinositide 3'-kinase delta inhibitor, CAL-101, inhibits B-cell receptor signaling and chemokine networks in chronic lymphocytic leukemia', *Blood*, 118(13), pp. 3603-12.

Hogan, P.G., Lewis, R.S. and Rao, A. (2010) 'Molecular basis of calcium signaling in lymphocytes: STIM and ORAI', *Annual review of immunology*, 28, p. 491.

Hongo, T., Yajima, S., Sakurai, M., Horikoshi, Y. and Hanada, R. (1997) 'In vitro drug sensitivity testing can predict induction failure and early relapse of childhood acute lymphoblastic leukemia', *Blood*, 89(8), pp. 2959-65.

Honigberg, L.A., Smith, A.M., Sirisawad, M., Verner, E., Loury, D., Chang, B., Li, S., Pan, Z., Thamm, D.H., Miller, R.A. and Buggy, J.J. (2010) 'The Bruton tyrosine kinase inhibitor PCI-32765 blocks B-cell activation and is efficacious in models of autoimmune disease and B-cell malignancy', *Proc Natl Acad Sci U S A*, 107(29), pp. 13075-80.

Houghton, P.J., Morton, C.L., Tucker, C., Payne, D., Favours, E., Cole, C., Gorlick, R., Kolb, E.A., Zhang, W., Lock, R., Carol, H., Tajbakhsh, M., Reynolds, C.P., Maris, J.M., Courtright, J., Keir, S.T., Friedman, H.S., Stopford, C., Zeidner, J., Wu, J., Liu, T., Billups, C.A., Khan, J., Ansher, S., Zhang, J. and Smith, M.A. (2007) 'The pediatric preclinical testing program: description of models and early testing results', *Pediatr Blood Cancer*, 49(7), pp. 928-40.

Howlader, N., Noone, A.M., Krapcho, M., Garshell, J., Neyman, N. and Aletkruse, S. (2013) 'SEER Cancer Statistics Review, 1975-2010,[Online] National Cancer Institute. Bethesda, MD'.

Huettner, C.S., Zhang, P., Van Etten, R.A. and Tenen, D.G. (2000) 'Reversibility of acute B-cell leukaemia induced by BCR-ABL1', *Nat Genet*, 24(1), pp. 57-60.

Hulspas, R., O'Gorman, M.R., Wood, B.L., Gratama, J.W. and Sutherland, D.R. (2009) 'Considerations for the control of background fluorescence in clinical flow cytometry', *Cytometry B Clin Cytom*, 76(6), pp. 355-64.

Hunger, S.P., Lu, X., Devidas, M., Camitta, B.M., Gaynon, P.S., Winick, N.J., Reaman, G.H. and Carroll, W.L. (2012) 'Improved survival for children and adolescents with acute lymphoblastic leukemia between 1990 and 2005: a report from the children's oncology group', *Journal of Clinical Oncology*, p. JCO. 2011.37. 8018.

Hurwitz, R., Hozier, J., LeBien, T., Minowada, J., Gajl-Peczalska, K., Kubonishi, I. and Kersey, J. (1979) 'Characterization of a leukemic cell line of the pre-B phenotype', *Int J Cancer*, 23(2), pp. 174-80.

Huse, M. and Kuriyan, J. (2002) 'The conformational plasticity of protein kinases', *Cell*, 109(3), pp. 275-82.

Iacobucci, I. and Mullighan, C.G. (2017) 'Genetic Basis of Acute Lymphoblastic Leukemia', *J Clin Oncol*, 35(9), pp. 975-983.

Igarashi, H., Medina, K.L., Yokota, T., Rossi, M.I., Sakaguchi, N., Comp, P.C. and Kincade, P.W. (2005) 'Early lymphoid progenitors in mouse and man are highly sensitive to glucocorticoids', *Int Immunol*, 17(5), pp. 501-11.

Imamura, Y., Oda, A., Katahira, T., Bundo, K., Pike, K.A., Ratcliffe, M.J. and Kitamura, D. (2009) 'BLNK binds active H-Ras to promote B cell receptor-mediated capping and ERK activation', *J Biol Chem*, 284(15), pp. 9804-13.

Inaba, H., Greaves, M. and Mullighan, C.G. (2013) 'Acute lymphoblastic leukaemia', *Lancet*, 381(9881), pp. 1943-55.

Inaba, H. and Pui, C.H. (2010) 'Glucocorticoid use in acute lymphoblastic leukaemia', *Lancet Oncol*, 11(11), pp. 1096-106.

Inthal, A., Krapf, G., Beck, D., Joas, R., Kauer, M.O., Orel, L., Fuka, G., Mann, G. and Panzer-Grumayer, E.R. (2008) 'Role of the erythropoietin receptor in ETV6/RUNX1-positive acute lymphoblastic leukemia', *Clin Cancer Res*, 14(22), pp. 7196-204.

Iritani, B.M., Forbush, K.A., Farrar, M.A. and Perlmutter, R.M. (1997) 'Control of B cell development by Ras-mediated activation of Raf', *Embo j*, 16(23), pp. 7019-31.

Irving, J., Matheson, E., Minto, L., Blair, H., Case, M., Halsey, C., Swidenbank, I., Ponthan, F., Kirschner-Schwabe, R., Groeneveld-Krentz, S., Hof, J., Allan, J., Harrison, C., Vormoor, J., von Stackelberg, A. and Eckert, C. (2014) 'Ras pathway mutations are prevalent in relapsed childhood acute lymphoblastic leukemia and confer sensitivity to MEK inhibition', *Blood*, 124(23), pp. 3420-30.

Irving, J.A. (2016) 'Towards an understanding of the biology and targeted treatment of paediatric relapsed acute lymphoblastic leukaemia', *Br J Haematol*, 172(5), pp. 655-66.

Ishibashi, T., Yaguchi, A., Terada, K., Ueno-Yokohata, H., Tomita, O., Iijima, K., Kobayashi, K., Okita, H., Fujimura, J., Ohki, K., Shimizu, T. and Kiyokawa, N. (2016) 'Ph-like ALL-related novel fusion kinase ATF7IP-PDGFRB exhibits high sensitivity to tyrosine kinase inhibitors in murine cells', *Exp Hematol*, 44(3), pp. 177-88.e5.

Jabbour, E., Ottmann, O.G., Deininger, M. and Hochhaus, A. (2014) 'Targeting the phosphoinositide 3-kinase pathway in hematologic malignancies', *haematologica*, 99(1), pp. 7-18.

Jeha, S., Pei, D., Raimondi, S.C., Onciu, M., Campana, D., Cheng, C., Sandlund, J.T., Ribeiro, R.C., Rubnitz, J.E., Howard, S.C., Downing, J.R., Evans, W.E., Relling, M.V. and Pui, C.H. (2009) 'Increased risk for CNS relapse in pre-B cell leukemia with the t(1;19)/TCF3-PBX1', *Leukemia*, 23(8), pp. 1406-9.

Joha, S., Nugues, A.L., Hetuin, D., Berthon, C., Dezitter, X., Dauphin, V., Mahon, F.X., Roche-Lestienne, C., Preudhomme, C., Quesnel, B. and Idziorek, T. (2012) 'GILZ inhibits the mTORC2/AKT pathway in BCR-ABL(+) cells', *Oncogene*, 31(11), pp. 1419-30.

Johnson, K., Hashimshony, T., Sawai, C.M., Pongubala, J.M., Skok, J.A., Aifantis, I. and Singh, H. (2008) 'Regulation of immunoglobulin light-chain recombination by the transcription factor IRF-4 and the attenuation of interleukin-7 signaling', *Immunity*, 28(3), pp. 335-45.

Jones, C.L., Gearheart, C.M., Fosmire, S., Delgado-Martin, C., Evensen, N.A., Bride, K., Waanders, A.J., Pais, F., Wang, J., Bhatla, T., Bitterman, D.S., de Rijk, S.R., Bourgeois, W., Dandekar, S., Park, E., Burleson, T.M., Madhusoodhan, P.P., Teachey, D.T., Raetz, E.A., Hermiston, M.L., Muschen, M., Loh, M.L., Hunger, S.P., Zhang, J., Garabedian, M.J., Porter, C.C. and Carroll, W.L. (2015) 'MAPK signaling cascades mediate distinct glucocorticoid resistance mechanisms in pediatric leukemia', *Blood*, 126(19), pp. 2202-12.

Jumaa, H., Bossaller, L., Portugal, K., Storch, B., Lotz, M., Flemming, A., Schrappe, M., Postila, V., Riikonen, P., Pelkonen, J., Niemeyer, C.M. and Reth, M. (2003) 'Deficiency of the adaptor SLP-65 in pre-B-cell acute lymphoblastic leukaemia', *Nature*, 423(6938), pp. 452-456.

Kandoth, C., McLellan, M.D., Vandin, F., Ye, K., Niu, B., Lu, C., Xie, M., Zhang, Q., McMichael, J.F., Wyczalkowski, M.A., Leiserson, M.D.M., Miller, C.A., Welch, J.S., Walter, M.J., Wendl, M.C., Ley, T.J., Wilson, R.K., Raphael, B.J. and Ding, L. (2013) 'Mutational landscape and significance across 12 major cancer types', *Nature*, 502(7471), pp. 333-339.

Kantarjian, H., Jabbour, E., Grimley, J. and Kirkpatrick, P. (2006) 'Dasatinib', *Nature Reviews Drug Discovery*, 5, p. 717.

Kantarjian, H., Shah, N.P., Hochhaus, A., Cortes, J., Shah, S., Ayala, M., Moiraghi, B., Shen, Z., Mayer, J. and Pasquini, R. (2010a) 'Dasatinib versus imatinib in newly diagnosed chronic-phase chronic myeloid leukemia', *New England Journal of Medicine*, 362(24), pp. 2260-2270.

Kantarjian, H., Shah, N.P., Hochhaus, A., Cortes, J., Shah, S., Ayala, M., Moiraghi, B., Shen, Z., Mayer, J., Pasquini, R., Nakamae, H., Huguet, F., Boque, C., Chuah, C., Bleickardt, E., Bradley-Garelik, M.B., Zhu, C., Szatrowski, T., Shapiro, D. and Baccarani, M. (2010b) 'Dasatinib versus imatinib in newly diagnosed chronic-phase chronic myeloid leukemia', *N Engl J Med*, 362(24), pp. 2260-70.

Karasuyama, H., Kudo, A. and Melchers, F. (1990) 'The proteins encoded by the VpreB and lambda 5 pre-B cell-specific genes can associate with each other and with mu heavy chain', *J Exp Med*, 172(3), pp. 969-72.

Kaspers, G.J., Pieters, R., Klumper, E., De Waal, F.C. and Veerman, A.J. (1994) 'Glucocorticoid resistance in childhood leukemia', *Leuk Lymphoma*, 13(3-4), pp. 187-201.

Kaspers, G.J., Pieters, R., Van Zantwijk, C.H., Van Wering, E.R., Van Der Does-Van Den Berg, A. and Veerman, A.J. (1998) 'Prednisolone resistance in childhood acute lymphoblastic leukemia: vitro-vivo correlations and cross-resistance to other drugs', *Blood*, 92(1), pp. 259-66.

Katz, F.E., Lovering, R.C., Bradley, L.A., Rigley, K.P., Brown, D., Cotter, F., Chessells, J.M., Levinsky, R.J. and Kinnon, C. (1994) 'Expression of the X-linked agammaglobulinemia gene, btk in B-cell acute lymphoblastic leukemia', *Leukemia*, 8(4), pp. 574-7.

Kauffman, R.F., Taylor, R.W. and Pfeiffer, D.R. (1980) 'Cation transport and specificity of ionomycin. Comparison with ionophore A23187 in rat liver mitochondria', *J Biol Chem*, 255(7), pp. 2735-9.

Kawamata, N., Pennella, M.A., Woo, J.L., Berk, A.J. and Koeffler, H.P. (2012) 'Dominant-negative mechanism of leukemogenic PAX5 fusions', *Oncogene*, 31(8), pp. 966-77.

Kersseboom, R., Middendorp, S., Dingjan, G.M., Dahlenborg, K., Reth, M., Jumaa, H. and Hendriks, R.W. (2003) 'Bruton's tyrosine kinase cooperates with the B cell linker protein SLP-65 as a tumor suppressor in Pre-B cells', *J Exp Med*, 198(1), pp. 91-8.

Kim, E., Hurtz, C., Koehrer, S., Wang, Z., Balasubramanian, S., Chang, B.Y., Muschen, M., Davis, R.E. and Burger, J.A. (2017) 'Ibrutinib inhibits pre-BCR+ B-cell acute lymphoblastic leukemia progression by targeting BTK and BLK', *Blood*, 129(9), pp. 1155-1165.

Kim, E., Koehrer, S., Rosin, N.Y., Thomas, D.A., Ravandi, F., Kornblau, S.M., Kantarjian, H.M., O'Brien, S., Estrov, Z. and Buggy, J.J. (2012) *ASH Annual Meeting Abstracts*.

King, L.B. and Freedman, B.D. (2009) 'B-lymphocyte calcium influx', *Immunol Rev*, 231(1), pp. 265-77.

Klein, E., Klein, G., Nadkarni, J.S., Nadkarni, J.J., Wigzell, H. and Clifford, P. (1968) 'Surface IgM-kappa specificity on a Burkitt lymphoma cell in vivo and in derived culture lines', *Cancer Res*, 28(7), pp. 1300-10.

Klein, F., Feldhahn, N., Harder, L., Wang, H., Wartenberg, M., Hofmann, W.K., Wernet, P., Siebert, R. and Muschen, M. (2004a) 'The BCR-ABL1 kinase bypasses selection for the

expression of a pre-B cell receptor in pre-B acute lymphoblastic leukemia cells', *J Exp Med*, 199(5), pp. 673-85.

Klein, F., Feldhahn, N. and Muschen, M. (2004b) 'Interference of BCR-ABL1 kinase activity with antigen receptor signaling in B cell precursor leukemia cells', *Cell Cycle*, 3(7), pp. 858-60.

Klein, G., Giovanella, B., Westman, A., Stehlin, J.S. and Mumford, D. (1975) 'An EBV-genome-negative cell line established from an American Burkitt lymphoma; receptor characteristics. EBV infectibility and permanent conversion into EBV-positive sublines by in vitro infection', *Intervirology*, 5(6), pp. 319-34.

Knight, T. and Irving, J.A. (2014) 'Ras/Raf/MEK/ERK Pathway Activation in Childhood Acute Lymphoblastic Leukemia and Its Therapeutic Targeting', *Front Oncol*, 4, p. 160.

Kobayashi, K., Miyagawa, N., Mitsui, K., Matsuoka, M., Kojima, Y., Takahashi, H., Ootsubo, K., Nagai, J., Ueno, H., Ishibashi, T., Sultana, S., Okada, Y., Akimoto, S., Okita, H., Matsumoto, K., Goto, H., Kiyokawa, N. and Ohara, A. (2015) 'TKI dasatinib monotherapy for a patient with Ph-like ALL bearing ATF7IP/PDGFRB translocation', *Pediatr Blood Cancer*, 62(6), pp. 1058-60.

Koerber, R.M., Held, S.A.E., Heine, A., Kotthoff, P., Daecke, S.N., Bringmann, A. and Brossart, P. (2015) 'Analysis of the anti-proliferative and the pro-apoptotic efficacy of Syk inhibition in multiple myeloma', *Exp Hematol Oncol*, 4, p. 21.

Kofler, R. (2000) 'The molecular basis of glucocorticoid-induced apoptosis of lymphoblastic leukemia cells', *Histochem Cell Biol*, 114(1), pp. 1-7.

Kohrer, S., Havranek, O., Seyfried, F., Hurtz, C., Coffey, G.P., Kim, E., Ten Hacken, E., Jager, U., Vanura, K., O'Brien, S., Thomas, D.A., Kantarjian, H., Ghosh, D., Wang, Z., Zhang, M., Ma, W., Jumaa, H., Debatin, K.M., Muschen, M., Meyer, L.H., Davis, R.E. and Burger, J.A. (2016) 'Pre-BCR signaling in precursor B-cell acute lymphoblastic leukemia regulates PI3K/AKT, FOXO1 and MYC, and can be targeted by SYK inhibition', *Leukemia*, 30(6), pp. 1246-54.

Kouro, T., Nagata, K., Takaki, S., Nisitani, S., Hirano, M., Wahl, M.I., Witte, O.N., Karasuyama, H. and Takatsu, K. (2001) 'Bruton's tyrosine kinase is required for signaling the CD79b-mediated pro-B to pre-B cell transition', *Int Immunol*, 13(4), pp. 485-93.

Krause, D.S. and Van Etten, R.A. (2005) 'Tyrosine kinases as targets for cancer therapy', *N Engl J Med*, 353(2), pp. 172-87.

Krishan, A. (1975) 'Rapid flow cytofluorometric analysis of mammalian cell cycle by propidium iodide staining', *J Cell Biol*, 66(1), pp. 188-93.

Kruth, K.A., Fang, M., Shelton, D.N., Abu-Halawa, O., Mahling, R., Yang, H., Weissman, J.S., Loh, M.L., Muschen, M., Tasian, S.K., Bassik, M.C., Kampmann, M. and Pufall, M.A. (2017) 'Suppression of B-cell development genes is key to glucocorticoid efficacy in treatment of acute lymphoblastic leukemia', *Blood*, 129(22), pp. 3000-3008.

Krutzik, P.O., Irish, J.M., Nolan, G.P. and Perez, O.D. (2004) 'Analysis of protein phosphorylation and cellular signaling events by flow cytometry: techniques and clinical applications', *Clin Immunol*, 110(3), pp. 206-21.

Kuiatse, I., Baladandayuthapani, V., Lin, H.Y., Thomas, S.K., Bjorklund, C.C., Weber, D.M., Wang, M., Shah, J.J., Zhang, X.D., Jones, R.J., Ansell, S.M., Yang, G., Treon, S.P. and Orlowski, R.Z. (2015) 'Targeting the Spleen Tyrosine Kinase with Fostamatinib as a Strategy against Waldenstrom Macroglobulinemia', *Clin Cancer Res*, 21(11), pp. 2538-45.

Kuiper, R.P., Schoenmakers, E.F., van Reijmersdal, S.V., Hehir-Kwa, J.Y., van Kessel, A.G., van Leeuwen, F.N. and Hoogerbrugge, P.M. (2007) 'High-resolution genomic profiling of

childhood ALL reveals novel recurrent genetic lesions affecting pathways involved in lymphocyte differentiation and cell cycle progression', *Leukemia*, 21(6), pp. 1258-66.

Kulathu, Y., Grothe, G. and Reth, M. (2009) 'Autoinhibition and adapter function of Syk', *Immunol Rev*, 232(1), pp. 286-99.

Kurosaki, T. and Okada, T. (2001) 'Regulation of phospholipase C-gamma2 and phosphoinositide 3-kinase pathways by adaptor proteins in B lymphocytes', *Int Rev Immunol*, 20(6), pp. 697-711.

Kurosaki, T. and Tsukada, S. (2000) 'BLNK: connecting Syk and Btk to calcium signals', *Immunity*, 12(1), pp. 1-5.

Kuwahara, K., Kawai, T., Mitsuyoshi, S., Matsuo, Y., Kikuchi, H., Imajoh-Ohmi, S., Hashimoto, E., Inui, S., Cooper, M.D. and Sakaguchi, N. (1996) 'Cross-linking of B cell antigen receptor-related structure of pre-B cell lines induces tyrosine phosphorylation of p85 and p110 subunits and activation of phosphatidylinositol 3-kinase', *Int Immunol*, 8(8), pp. 1273-85.

Laemmli, U.K. (1970) 'Cleavage of structural proteins during the assembly of the head of bacteriophage T4', *Nature*, 227(5259), pp. 680-5.

Lane, D.P. (1992) 'Cancer. p53, guardian of the genome', *Nature*, 358(6381), pp. 15-6.

Lanning, B.R., Whitby, L.R., Dix, M.M., Douhan, J., Gilbert, A.M., Hett, E.C., Johnson, T.O., Joslyn, C., Kath, J.C., Niessen, S., Roberts, L.R., Schnute, M.E., Wang, C., Hulce, J.J., Wei, B., Whiteley, L.O., Hayward, M.M. and Cravatt, B.F. (2014) 'A road map to evaluate the proteome-wide selectivity of covalent kinase inhibitors', *Nat Chem Biol*, 10(9), pp. 760-767.

Lannutti, B.J., Meadows, S.A., Herman, S.E., Kashishian, A., Steiner, B., Johnson, A.J., Byrd, J.C., Tyner, J.W., Loriaux, M.M., Deininger, M., Druker, B.J., Puri, K.D., Ulrich, R.G. and Giese, N.A. (2011) 'CAL-101, a p110delta selective phosphatidylinositol-3-kinase inhibitor for the treatment of B-cell malignancies, inhibits PI3K signaling and cellular viability', *Blood*, 117(2), pp. 591-4.

Larson, R.A. and Anastasi, J. (2008) 'Acute Lymphoblastic Leukemia: Clinical Presentation, Diagnosis, and Classification', in *Acute Leukemias*. Springer, pp. 109-118.

Latre de Late, P., Pepin, A., Assaf-Vandecasteele, H., Espinasse, C., Nicolas, V., Asselin-Labat, M.L., Bertoglio, J., Pallardy, M. and Biola-Vidamment, A. (2010) 'Glucocorticoid-induced leucine zipper (GILZ) promotes the nuclear exclusion of FOXO3 in a Crm1-dependent manner', *J Biol Chem*, 285(8), pp. 5594-605.

Ledderose, C., Heyn, J., Limbeck, E. and Kreth, S. (2011) 'Selection of reliable reference genes for quantitative real-time PCR in human T cells and neutrophils', *BMC Research Notes*, 4, pp. 427-427.

Lee, E.M., Bachmann, P.S. and Lock, R.B. (2007) 'Xenograft models for the preclinical evaluation of new therapies in acute leukemia', *Leuk Lymphoma*, 48(4), pp. 659-68.

Levine, A.J. (1997) 'p53, the cellular gatekeeper for growth and division', *Cell*, 88(3), pp. 323-31.

Levy, J.A., Virolainen, M. and Defendi, V. (1968) 'Human lymphoblastoid lines from lymph node and spleen', *Cancer*, 22(3), pp. 517-24.

Li, J., Lin, B., Li, X., Tang, X., He, Z. and Zhou, K. (2015) 'Biomarkers for predicting response to tyrosine kinase inhibitors in drug-sensitive and drug-resistant human bladder cancer cells', *Oncol Rep*, 33(2), pp. 951-7.

Li, Y., Schwab, C., Ryan, S., Papaemmanuil, E., Robinson, H.M., Jacobs, P., Moorman, A.V., Dyer, S., Borrow, J., Griffiths, M., Heerema, N.A., Carroll, A.J., Talley, P., Bown, N., Telford, N., Ross, F.M., Gaunt, L., McNally, R.J.Q., Young, B.D., Sinclair, P., Rand, V., Teixeira, M.R.,

Joseph, O., Robinson, B., Maddison, M., Dastugue, N., Vandenberghe, P., Stephens, P.J., Cheng, J., Van Loo, P., Stratton, M.R., Campbell, P.J. and Harrison, C.J. (2014) 'Constitutional and somatic rearrangement of chromosome 21 in acute lymphoblastic leukaemia', *Nature*, 508(7494), pp. 98-102.

Liem, N.L., Papa, R.A., Milross, C.G., Schmid, M.A., Tajbakhsh, M., Choi, S., Ramirez, C.D., Rice, A.M., Haber, M., Norris, M.D., MacKenzie, K.L. and Lock, R.B. (2004) 'Characterization of childhood acute lymphoblastic leukemia xenograft models for the preclinical evaluation of new therapies', *Blood*, 103(10), pp. 3905-14.

Lill-Elghanian, D., Schwartz, K., King, L. and Fraker, P. (2002) 'Glucocorticoid-induced apoptosis in early B cells from human bone marrow', *Exp Biol Med (Maywood)*, 227(9), pp. 763-70.

Liston, D.R. and Davis, M. (2017) 'Clinically Relevant Concentrations of Anticancer Drugs: A Guide for Nonclinical Studies', *Clin Cancer Res*, 23(14), pp. 3489-3498.

Liu, J., Xie, W., Lange, M.D., Hong, S.Y., Su, K. and Zhang, Z. (2013) 'Internalization of B cell receptors in human EU12 muHC(+) immature B cells specifically alters downstream signaling events', *Biomed Res Int*, 2013, p. 807240.

Locatelli, F., Schrappe, M., Bernardo, M.E. and Rutella, S. (2012) 'How I treat relapsed childhood acute lymphoblastic leukemia', *Blood*, 120(14), pp. 2807-16.

Lock, R.B., Liem, N., Farnsworth, M.L., Milross, C.G., Xue, C., Tajbakhsh, M., Haber, M., Norris, M.D., Marshall, G.M. and Rice, A.M. (2002) 'The nonobese diabetic/severe combined immunodeficient (NOD/SCID) mouse model of childhood acute lymphoblastic leukemia reveals intrinsic differences in biologic characteristics at diagnosis and relapse', *Blood*, 99(11), pp. 4100-8.

Loh, M.L., Zhang, J., Harvey, R.C., Roberts, K., Payne-Turner, D., Kang, H., Wu, G., Chen, X., Becksfort, J., Edmonson, M., Buetow, K.H., Carroll, W.L., Chen, I.M., Wood, B., Borowitz, M.J., Devidas, M., Gerhard, D.S., Bowman, P., Larsen, E., Winick, N., Raetz, E., Smith, M., Downing, J.R., Willman, C.L., Mullighan, C.G. and Hunger, S.P. (2013) 'Tyrosine kinome sequencing of pediatric acute lymphoblastic leukemia: a report from the Children's Oncology Group TARGET Project', *Blood*, 121(3), pp. 485-8.

Lombardo, L.J., Lee, F.Y., Chen, P., Norris, D., Barrish, J.C., Behnia, K., Castaneda, S., Cornelius, L.A., Das, J., Doweyko, A.M., Fairchild, C., Hunt, J.T., Inigo, I., Johnston, K., Kamath, A., Kan, D., Klei, H., Marathe, P., Pang, S., Peterson, R., Pitt, S., Schieven, G.L., Schmidt, R.J., Tokarski, J., Wen, M.L., Wityak, J. and Borzilleri, R.M. (2004) 'Discovery of N-(2-chloro-6-methyl- phenyl)-2-(6-(4-(2-hydroxyethyl)- piperazin-1-yl)-2-methylpyrimidin-4-ylamino)thiazole-5-carboxamide (BMS-354825), a dual Src/Abl kinase inhibitor with potent antitumor activity in preclinical assays', *J Med Chem*, 47(27), pp. 6658-61.

Look, A.T. (1997) 'Oncogenic transcription factors in the human acute leukemias', *Science*, 278(5340), pp. 1059-64.

Lu, Q. and Kamps, M.P. (1997) 'Heterodimerization of Hox proteins with Pbx1 and oncoprotein E2a-Pbx1 generates unique DNA-binding specifities at nucleotides predicted to contact the N-terminal arm of the Hox homeodomain--demonstration of Hox-dependent targeting of E2a-Pbx1 in vivo', *Oncogene*, 14(1), pp. 75-83.

Lu, R., Medina, K.L., Lancki, D.W. and Singh, H. (2003) 'IRF-4,8 orchestrate the pre-B-to-B transition in lymphocyte development', *Genes Dev*, 17(14), pp. 1703-8.

Maia, A.T., van der Velden, V.H., Harrison, C.J., Szczepanski, T., Williams, M.D., Griffiths, M.J., van Dongen, J.J. and Greaves, M.F. (2003) 'Prenatal origin of hyperdiploid acute lymphoblastic leukemia in identical twins', *Leukemia*, 17(11), pp. 2202-6.

Manzoni, D., Catallo, R., Chebel, A., Baseggio, L., Michallet, A.S., Roualdes, O., Magaud, J.P., Salles, G. and Ffrench, M. (2016) 'The ibrutinib B-cell proliferation inhibition is

potentiated in vitro by dexamethasone: Application to chronic lymphocytic leukemia', *Leuk Res*, 47, pp. 1-7.

Marani, M., Tenev, T., Hancock, D., Downward, J. and Lemoine, N.R. (2002) 'Identification of Novel Isoforms of the BH3 Domain Protein Bim Which Directly Activate Bax To Trigger Apoptosis', *Molecular and Cellular Biology*, 22(11), pp. 3577-3589.

Marshall, A.J., Niiro, H., Yun, T.J. and Clark, E.A. (2000) 'Regulation of B-cell activation and differentiation by the phosphatidylinositol 3-kinase and phospholipase Cgamma pathway', *Immunol Rev*, 176, pp. 30-46.

Mårtensson, I.-L., Almqvist, N., Grimsholm, O. and Bernardi, A.I. (2010) 'The pre-B cell receptor checkpoint', *FEBS letters*, 584(12), pp. 2572-2579.

Martensson, I.L., Almqvist, N., Grimsholm, O. and Bernardi, A.I. (2010) 'The pre-B cell receptor checkpoint', *FEBS Lett*, 584(12), pp. 2572-9.

Maude, S.L., Dolai, S., Delgado-Martin, C., Vincent, T., Robbins, A., Selvanathan, A., Ryan, T., Hall, J., Wood, A.C., Tasian, S.K., Hunger, S.P., Loh, M.L., Mullighan, C.G., Wood, B.L., Hermiston, M.L., Grupp, S.A., Lock, R.B. and Teachey, D.T. (2015) 'Efficacy of JAK/STAT pathway inhibition in murine xenograft models of early T-cell precursor (ETP) acute lymphoblastic leukemia', *Blood*, 125(11), pp. 1759-67.

Maude, S.L., Tasian, S.K., Vincent, T., Hall, J.W., Sheen, C., Roberts, K.G., Seif, A.E., Barrett, D.M., Chen, I.M., Collins, J.R., Mullighan, C.G., Hunger, S.P., Harvey, R.C., Willman, C.L., Fridman, J.S., Loh, M.L., Grupp, S.A. and Teachey, D.T. (2012) 'Targeting JAK1/2 and mTOR in murine xenograft models of Ph-like acute lymphoblastic leukemia', *Blood*, 120(17), pp. 3510-8.

McHale, C.M., Wiemels, J.L., Zhang, L., Ma, X., Buffler, P.A., Guo, W., Loh, M.L. and Smith, M.T. (2003) 'Prenatal origin of TEL-AML1-positive acute lymphoblastic leukemia in children born in California', *Genes Chromosomes Cancer*, 37(1), pp. 36-43.

McMillin, D.W., Negri, J.M. and Mitsiades, C.S. (2013) 'The role of tumour-stromal interactions in modifying drug response: challenges and opportunities', *Nat Rev Drug Discov*, 12(3), pp. 217-28.

Meadows, S.A., Vega, F., Kashishian, A., Johnson, D., Diehl, V., Miller, L.L., Younes, A. and Lannutti, B.J. (2012) 'PI3Kδ inhibitor, GS-1101 (CAL-101), attenuates pathway signaling, induces apoptosis, and overcomes signals from the microenvironment in cellular models of Hodgkin lymphoma', *Blood*, 119(8), pp. 1897-1900.

Melchers, F. (2005) 'The pre-B-cell receptor: selector of fitting immunoglobulin heavy chains for the B-cell repertoire', *Nat Rev Immunol*, 5(7), pp. 578-84.

Melo, J.V. (1996) 'The diversity of BCR-ABL fusion proteins and their relationship to leukemia phenotype', *Blood*, 88(7), pp. 2375-84.

Mertsching, E., Grawunder, U., Meyer, V., Rolink, T. and Ceredig, R. (1996) 'Phenotypic and functional analysis of B lymphopoiesis in interleukin-7-transgenic mice: expansion of pro/pre-B cell number and persistence of B lymphocyte development in lymph nodes and spleen', *Eur J Immunol*, 26(1), pp. 28-33.

Meyer, C., Hofmann, J., Burmeister, T., Groger, D., Park, T.S., Emerenciano, M., Pombo de Oliveira, M., Renneville, A., Villarese, P., Macintyre, E., Cave, H., Clappier, E., Mass-Malo, K., Zuna, J., Trka, J., De Braekeleer, E., De Braekeleer, M., Oh, S.H., Tsaur, G., Fechina, L., van der Velden, V.H., van Dongen, J.J., Delabesse, E., Binato, R., Silva, M.L., Kustanovich, A., Aleinikova, O., Harris, M.H., Lund-Aho, T., Juvonen, V., Heidenreich, O., Vormoor, J., Choi, W.W., Jarosova, M., Kolenova, A., Bueno, C., Menendez, P., Wehner, S., Eckert, C., Talmant, P., Tondeur, S., Lippert, E., Launay, E., Henry, C., Ballerini, P., Lapillone, H., Callanan, M.B., Cayuela, J.M., Herbaux, C., Cazzaniga, G., Kakadiya, P.M., Bohlander, S.,

Ahlmann, M., Choi, J.R., Gameiro, P., Lee, D.S., Krauter, J., Cornillet-Lefebvre, P., Te Kronnie, G., Schafer, B.W., Kubetzko, S., Alonso, C.N., zur Stadt, U., Sutton, R., Venn, N.C., Izraeli, S., Trakhtenbrot, L., Madsen, H.O., Archer, P., Hancock, J., Cerveira, N., Teixeira, M.R., Lo Nigro, L., Moricke, A., Stanulla, M., Schrappe, M., Sedek, L., Szczepanski, T., Zwaan, C.M., Coenen, E.A., van den Heuvel-Eibrink, M.M., Strehl, S., Dworzak, M., Panzer-Grumayer, R., Dingermann, T., Klingebiel, T. and Marschalek, R. (2013) 'The MLL recombinome of acute leukemias in 2013', *Leukemia*, 27(11), pp. 2165-76.

Meyer, C., Kowarz, E., Hofmann, J., Renneville, A., Zuna, J., Trka, J., Ben Abdelali, R., Macintyre, E., De Braekeleer, E., De Braekeleer, M., Delabesse, E., de Oliveira, M.P., Cave, H., Clappier, E., van Dongen, J.J., Balgobind, B.V., van den Heuvel-Eibrink, M.M., Beverloo, H.B., Panzer-Grumayer, R., Teigler-Schlegel, A., Harbott, J., Kjeldsen, E., Schnittger, S., Koehl, U., Gruhn, B., Heidenreich, O., Chan, L.C., Yip, S.F., Krzywinski, M., Eckert, C., Moricke, A., Schrappe, M., Alonso, C.N., Schafer, B.W., Krauter, J., Lee, D.A., Zur Stadt, U., Te Kronnie, G., Sutton, R., Izraeli, S., Trakhtenbrot, L., Lo Nigro, L., Tsaur, G., Fechina, L., Szczepanski, T., Strehl, S., Ilencikova, D., Molkentin, M., Burmeister, T., Dingermann, T., Klingebiel, T. and Marschalek, R. (2009) 'New insights to the MLL recombinome of acute leukemias', *Leukemia*, 23(8), pp. 1490-9.

Meyer, L.H. and Debatin, K.M. (2011) 'Diversity of human leukemia xenograft mouse models: implications for disease biology', *Cancer Res*, 71(23), pp. 7141-4.

Middendorp, S., Zijlstra, A.J., Kersseboom, R., Dingjan, G.M., Jumaa, H. and Hendriks, R.W. (2005) 'Tumor suppressor function of Bruton tyrosine kinase is independent of its catalytic activity', *Blood*, 105(1), pp. 259-65.

Mielenz, D., Vettermann, C., Hampel, M., Lang, C., Avramidou, A., Karas, M. and Jack, H.M. (2005) 'Lipid rafts associate with intracellular B cell receptors and exhibit a B cell stage-specific protein composition', *J Immunol*, 174(6), pp. 3508-17.

Miller, B.W., Przepiorka, D., de Claro, R.A., Lee, K., Nie, L., Simpson, N., Gudi, R., Saber, H., Shord, S., Bullock, J., Marathe, D., Mehrotra, N., Hsieh, L.S., Ghosh, D., Brown, J., Kane, R.C., Justice, R., Kaminskas, E., Farrell, A.T. and Pazdur, R. (2015) 'FDA approval: idelalisib monotherapy for the treatment of patients with follicular lymphoma and small lymphocytic lymphoma', *Clin Cancer Res*, 21(7), pp. 1525-9.

Milne, C.D. and Paige, C.J. (2006) 'IL-7: a key regulator of B lymphopoiesis', *Semin Immunol*, 18(1), pp. 20-30.

Mocsai, A., Ruland, J. and Tybulewicz, V.L. (2010) 'The SYK tyrosine kinase: a crucial player in diverse biological functions', *Nat Rev Immunol*, 10(6), pp. 387-402.

Monroe, J.G. (2006) 'ITAM-mediated tonic signalling through pre-BCR and BCR complexes', *Nat Rev Immunol*, 6(4), pp. 283-94.

Moorman, A.V. (2012) 'The clinical relevance of chromosomal and genomic abnormalities in B-cell precursor acute lymphoblastic leukaemia', *Blood Rev*, 26(3), pp. 123-35.

Moorman, A.V., Ensor, H.M., Richards, S.M., Chilton, L., Schwab, C., Kinsey, S.E., Vora, A., Mitchell, C.D. and Harrison, C.J. (2010) 'Prognostic effect of chromosomal abnormalities in childhood B-cell precursor acute lymphoblastic leukaemia: results from the UK Medical Research Council ALL97/99 randomised trial', *Lancet Oncol*, 11(5), pp. 429-38.

Moorman, A.V., Raimondi, S.C., Pui, C.H., Baruchel, A., Biondi, A., Carroll, A.J., Forestier, E., Gaynon, P.S., Harbott, J., Harms, D.O., Heerema, N., Pieters, R., Schrappe, M., Silverman, L.B., Vilmer, E. and Harrison, C.J. (2005) 'No prognostic effect of additional chromosomal abnormalities in children with acute lymphoblastic leukemia and 11q23 abnormalities', *Leukemia*, 19(4), pp. 557-63.

Moorman, A.V., Robinson, H., Schwab, C., Richards, S.M., Hancock, J., Mitchell, C.D., Goulden, N., Vora, A. and Harrison, C.J. (2013) 'Risk-directed treatment intensification significantly reduces the risk of relapse among children and adolescents with acute lymphoblastic leukemia and intrachromosomal amplification of chromosome 21: a comparison of the MRC ALL97/99 and UKALL2003 trials', *J Clin Oncol*, 31(27), pp. 3389-96.

Morales-Torres, J. (2012) 'The status of fostamatinib in the treatment of rheumatoid arthritis', *Expert Rev Clin Immunol*, 8(7), pp. 609-15.

Mori, H., Colman, S.M., Xiao, Z., Ford, A.M., Healy, L.E., Donaldson, C., Hows, J.M., Navarrete, C. and Greaves, M. (2002) 'Chromosome translocations and covert leukemic clones are generated during normal fetal development', *Proc Natl Acad Sci U S A*, 99(12), pp. 8242-7.

Morrow, M., Horton, S., Kioussis, D., Brady, H.J. and Williams, O. (2004) 'TEL-AML1 promotes development of specific hematopoietic lineages consistent with preleukemic activity', *Blood*, 103(10), pp. 3890-6.

Mullighan, C.G. (2012) 'The molecular genetic makeup of acute lymphoblastic leukemia', *Hematology Am Soc Hematol Educ Program*, 2012, pp. 389-96.

Mullighan, C.G., Collins-Underwood, J.R., Phillips, L.A., Loudin, M.G., Liu, W., Zhang, J., Ma, J., Coustan-Smith, E., Harvey, R.C., Willman, C.L., Mikhail, F.M., Meyer, J., Carroll, A.J., Williams, R.T., Cheng, J., Heerema, N.A., Basso, G., Pession, A., Pui, C.H., Raimondi, S.C., Hunger, S.P., Downing, J.R., Carroll, W.L. and Rabin, K.R. (2009a) 'Rearrangement of CRLF2 in B-progenitor- and Down syndrome-associated acute lymphoblastic leukemia', *Nat Genet*, 41(11), pp. 1243-6.

Mullighan, C.G. and Downing, J.R. (2009) 'Genome-wide profiling of genetic alterations in acute lymphoblastic leukemia: recent insights and future directions', *Leukemia*, 23(7), pp. 1209-18.

Mullighan, C.G., Goorha, S., Radtke, I., Miller, C.B., Coustan-Smith, E., Dalton, J.D., Girtman, K., Mathew, S., Ma, J., Pounds, S.B., Su, X., Pui, C.H., Relling, M.V., Evans, W.E., Shurtleff, S.A. and Downing, J.R. (2007) 'Genome-wide analysis of genetic alterations in acute lymphoblastic leukaemia', *Nature*, 446(7137), pp. 758-64.

Mullighan, C.G., Miller, C.B., Radtke, I., Phillips, L.A., Dalton, J., Ma, J., White, D., Hughes, T.P., Le Beau, M.M., Pui, C.H., Relling, M.V., Shurtleff, S.A. and Downing, J.R. (2008) 'BCR-ABL1 lymphoblastic leukaemia is characterized by the deletion of Ikaros', *Nature*, 453(7191), pp. 110-4.

Mullighan, C.G., Zhang, J., Harvey, R.C., Collins-Underwood, J.R., Schulman, B.A., Phillips, L.A., Tasian, S.K., Loh, M.L., Su, X., Liu, W., Devidas, M., Atlas, S.R., Chen, I.M., Clifford, R.J., Gerhard, D.S., Carroll, W.L., Reaman, G.H., Smith, M., Downing, J.R., Hunger, S.P. and Willman, C.L. (2009b) 'JAK mutations in high-risk childhood acute lymphoblastic leukemia', *Proc Natl Acad Sci U S A*, 106(23), pp. 9414-8.

Muschen, M. (2015) 'Rationale for targeting the pre-B-cell receptor signaling pathway in acute lymphoblastic leukemia', *Blood*, 125(24), pp. 3688-93.

Muto, A., Hoshino, H., Madisen, L., Yanai, N., Obinata, M., Karasuyama, H., Hayashi, N., Nakauchi, H., Yamamoto, M., Groudine, M. and Igarashi, K. (1998) 'Identification of Bach2 as a B-cell-specific partner for small maf proteins that negatively regulate the immunoglobulin heavy chain gene 3' enhancer', *EMBO J*, 17(19), pp. 5734-43.

Muzio, M., Apollonio, B., Scielzo, C., Frenquelli, M., Vandoni, I., Boussiotis, V., Caligaris-Cappio, F. and Ghia, P. (2008) 'Constitutive activation of distinct BCR-signaling pathways in a subset of CLL patients: a molecular signature of anergy', *Blood*, 112(1), pp. 188-95.

Nachman, J.B., Heerema, N.A., Sather, H., Camitta, B., Forestier, E., Harrison, C.J., Dastugue, N., Schrappe, M., Pui, C.H., Basso, G., Silverman, L.B. and Janka-Schaub, G.E. (2007) 'Outcome of treatment in children with hypodiploid acute lymphoblastic leukemia', *Blood*, 110(4), pp. 1112-5.

Nagaoka, H., Takahashi, Y., Hayashi, R., Nakamura, T., Ishii, K., Matsuda, J., Ogura, A., Shirakata, Y., Karasuyama, H., Sudo, T., Nishikawa, S., Tsubata, T., Mizuochi, T., Asano, T., Sakano, H. and Takemori, T. (2000) 'Ras mediates effector pathways responsible for pre-B cell survival, which is essential for the developmental progression to the late pre-B cell stage', *J Exp Med*, 192(2), pp. 171-82.

Nahar, R. and Muschen, M. (2009) 'Pre-B cell receptor signaling in acute lymphoblastic leukemia', *Cell Cycle*, 8(23), pp. 3874-7.

Nahar, R., Ramezani-Rad, P., Mossner, M., Duy, C., Cerchietti, L., Geng, H., Dovat, S., Jumaa, H., Ye, B.H., Melnick, A. and Muschen, M. (2011) 'Pre-B cell receptor-mediated activation of BCL6 induces pre-B cell quiescence through transcriptional repression of MYC', *Blood*, 118(15), pp. 4174-8.

Nakata, Y., Ueda, T., Nagamachi, A., Yamasaki, N., Ikeda, K.I., Sera, Y., Takubo, K., Kanai, A., Oda, H., Sanada, M., Ogawa, S., Tsuji, K., Ebihara, Y., Wolff, L., Honda, Z.I., Suda, T., Inaba, T. and Honda, H. (2017) 'Acquired expression of CblQ367P in mice induces dysplastic myelopoiesis mimicking chronic myelomonocytic leukemia', *Blood*, 129(15), pp. 2148-2160.

Nakayama, J., Yamamoto, M., Hayashi, K., Satoh, H., Bundo, K., Kubo, M., Goitsuka, R., Farrar, M.A. and Kitamura, D. (2009) 'BLNK suppresses pre-B-cell leukemogenesis through inhibition of JAK3', *Blood*, 113(7), pp. 1483-92.

Newland, A., Lee, E.J., McDonald, V. and Bussel, J.B. (2018) 'Fostamatinib for persistent/chronic adult immune thrombocytopenia', *Immunotherapy*, 10(1), pp. 9-25.

Nicholson, L., Evans, C.A., Matheson, E., Minto, L., Keilty, C., Sanichar, M., Case, M., Schwab, C., Williamson, D., Rainer, J., Harrison, C.J., Kofler, R., Hall, A.G., Redfern, C.P., Whetton, A.D. and Irving, J.A. (2015) 'Quantitative proteomic analysis reveals maturation as a mechanism underlying glucocorticoid resistance in B lineage ALL and re-sensitization by JNK inhibition', *Br J Haematol*, 171(4), pp. 595-605.

Nicholson, L., Knight, T., Matheson, E., Minto, L., Case, M., Sanichar, M., Bomken, S., Vormoor, J., Hall, A. and Irving, J. (2012) 'Casitas B lymphoma mutations in childhood acute lymphoblastic leukemia', *Genes Chromosomes Cancer*, 51(3), pp. 250-6.

Nicolaides, N.C., Galata, Z., Kino, T., Chrousos, G.P. and Charmandari, E. (2010) 'The human glucocorticoid receptor: molecular basis of biologic function', *Steroids*, 75(1), pp. 1-12.

Niiro, H. and Clark, E.A. (2002) 'Regulation of B-cell fate by antigen-receptor signals', *Nat Rev Immunol*, 2(12), pp. 945-56.

Nuutinen, U., Postila, V., Matto, M., Eeva, J., Ropponen, A., Eray, M., Riikonen, P. and Pelkonen, J. (2006) 'Inhibition of PI3-kinase-Akt pathway enhances dexamethasone-induced apoptosis in a human follicular lymphoma cell line', *Exp Cell Res*, 312(3), pp. 322-30.

O'Shea, J.J. and Plenge, R. (2012) 'JAK and STAT signaling molecules in immunoregulation and immune-mediated disease', *Immunity*, 36(4), pp. 542-50.

Oakley, R.H. and Cidlowski, J.A. (2013a) 'The Biology of the Glucocorticoid Receptor: New Signaling Mechanisms in Health and Disease', *The Journal of allergy and clinical immunology*, 132(5), pp. 1033-1044.

Oakley, R.H. and Cidlowski, J.A. (2013b) 'The biology of the glucocorticoid receptor: new signaling mechanisms in health and disease', *J Allergy Clin Immunol*, 132(5), pp. 1033-44.

Ochiai, K., Maienschein-Cline, M., Mandal, M., Triggs, J.R., Bertolino, E., Sciammas, R., Dinner, A.R., Clark, M.R. and Singh, H. (2012) 'A self-reinforcing regulatory network triggered by limiting IL-7 activates pre-BCR signaling and differentiation', *Nat Immunol*, 13(3), pp. 300-7.

Ohnishi, K. and Melchers, F. (2003) 'The nonimmunoglobulin portion of lambda5 mediates cell-autonomous pre-B cell receptor signaling', *Nat Immunol*, 4(9), pp. 849-56.

Okkenhaug, K. and Vanhaesebroeck, B. (2003) 'PI3K in lymphocyte development, differentiation and activation', *Nat Rev Immunol*, 3(4), pp. 317-30.

Okuda, T., van Deursen, J., Hiebert, S.W., Grosveld, G. and Downing, J.R. (1996) 'AML1, the target of multiple chromosomal translocations in human leukemia, is essential for normal fetal liver hematopoiesis', *Cell*, 84(2), pp. 321-30.

Onciu, M. (2009) 'Acute lymphoblastic leukemia', *Hematol Oncol Clin North Am*, 23(4), pp. 655-74.

Osmond, D.G. (1991) 'Proliferation kinetics and the lifespan of B cells in central and peripheral lymphoid organs', *Curr Opin Immunol*, 3(2), pp. 179-85.

Ottmann, O.G. and Pfeifer, H. (2009) 'Management of Philadelphia chromosome-positive acute lymphoblastic leukemia (Ph+ ALL)', *Hematology Am Soc Hematol Educ Program*, pp. 371-81.

Oyake, T., Itoh, K., Motohashi, H., Hayashi, N., Hoshino, H., Nishizawa, M., Yamamoto, M. and Igarashi, K. (1996) 'Bach proteins belong to a novel family of BTB-basic leucine zipper transcription factors that interact with MafK and regulate transcription through the NF-E2 site', *Mol Cell Biol*, 16(11), pp. 6083-95.

Pan, Z., Scheerens, H., Li, S.J., Schultz, B.E., Sprengeler, P.A., Burrill, L.C., Mendonca, R.V., Sweeney, M.D., Scott, K.C., Grothaus, P.G., Jeffery, D.A., Spoerke, J.M., Honigberg, L.A., Young, P.R., Dalrymple, S.A. and Palmer, J.T. (2007) 'Discovery of selective irreversible inhibitors for Bruton's tyrosine kinase', *ChemMedChem*, 2(1), pp. 58-61.

Papadantonakis, N. and Advani, A.S. (2016) 'Recent advances and novel treatment paradigms in acute lymphocytic leukemia', *Therapeutic Advances in Hematology*, 7(5), pp. 252-269.

Parker, C., Waters, R., Leighton, C., Hancock, J., Sutton, R., Moorman, A.V., Ancliff, P., Morgan, M., Masurekar, A., Goulden, N., Green, N., Revesz, T., Darbyshire, P., Love, S. and Saha, V. (2010) 'Effect of mitoxantrone on outcome of children with first relapse of acute lymphoblastic leukaemia (ALL R3): an open-label randomised trial', *Lancet*, 376(9757), pp. 2009-17.

Parker, M.J., Licence, S., Erlandsson, L., Galler, G.R., Chakalova, L., Osborne, C.S., Morgan, G., Fraser, P., Jumaa, H. and Winkler, T.H. (2005) 'The pre-B-cell receptor induces silencing of VpreB and λ5 transcription', *The EMBO journal*, 24(22), pp. 3895-3905.

Passegue, E., Jamieson, C.H., Ailles, L.E. and Weissman, I.L. (2003) 'Normal and leukemic hematopoiesis: are leukemias a stem cell disorder or a reacquisition of stem cell characteristics?', *Proc Natl Acad Sci U S A*, 100 Suppl 1, pp. 11842-9.

Pemovska, T., Kontro, M., Yadav, B., Edgren, H., Eldfors, S., Szwajda, A., Almusa, H., Bespalov, M.M., Ellonen, P., Elonen, E., Gjertsen, B.T., Karjalainen, R., Kulesskiy, E., Lagstrom, S., Lehto, A., Lepisto, M., Lundan, T., Majumder, M.M., Marti, J.M., Mattila, P., Murumagi, A., Mustjoki, S., Palva, A., Parsons, A., Pirttinen, T., Ramet, M.E., Suvela, M., Turunen, L., Vastrik, I., Wolf, M., Knowles, J., Aittokallio, T., Heckman, C.A., Porkka, K., Kallioniemi, O. and Wennerberg, K. (2013) 'Individualized systems medicine strategy to tailor

treatments for patients with chemorefractory acute myeloid leukemia', *Cancer Discov*, 3(12), pp. 1416-29.

Perez-Vera, P., Reyes-Leon, A. and Fuentes-Panana, E.M. (2011) 'Signaling proteins and transcription factors in normal and malignant early B cell development', *Bone Marrow Res*, 2011, p. 502751.

Perova, T., Grandal, I., Nutter, L.M., Papp, E., Matei, I.R., Beyene, J., Kowalski, P.E., Hitzler, J.K., Minden, M.D., Guidos, C.J. and Danska, J.S. (2014) 'Therapeutic potential of spleen tyrosine kinase inhibition for treating high-risk precursor B cell acute lymphoblastic leukemia', *Sci Transl Med*, 6(236), p. 236ra62.

Petlickovski, A., Laurenti, L., Li, X., Marietti, S., Chiusolo, P., Sica, S., Leone, G. and Efremov, D.G. (2005) 'Sustained signaling through the B-cell receptor induces Mcl-1 and promotes survival of chronic lymphocytic leukemia B cells', *Blood*, 105(12), pp. 4820-7.

Pieters, R., Schrappe, M., De Lorenzo, P., Hann, I., De Rossi, G., Felice, M., Hovi, L., LeBlanc, T., Szczepanski, T., Ferster, A., Janka, G., Rubnitz, J., Silverman, L., Stary, J., Campbell, M., Li, C.K., Mann, G., Suppiah, R., Biondi, A., Vora, A. and Valsecchi, M.G. (2007) 'A treatment protocol for infants younger than 1 year with acute lymphoblastic leukaemia (Interfant-99): an observational study and a multicentre randomised trial', *Lancet*, 370(9583), pp. 240-50.

Pillai, S. and Baltimore, D. (1987) 'Formation of disulphide-linked mu 2 omega 2 tetramers in pre-B cells by the 18K omega-immunoglobulin light chain', *Nature*, 329(6135), pp. 172-4.

Piovan, E., Yu, J., Tosello, V., Herranz, D., Ambesi-Impiombato, A., Da Silva, A.C., Sanchez-Martin, M., Perez-Garcia, A., Rigo, I., Castillo, M., Indraccolo, S., Cross, J.R., de Stanchina, E., Paietta, E., Racevskis, J., Rowe, J.M., Tallman, M.S., Basso, G., Meijerink, J.P., Cordon-Cardo, C., Califano, A. and Ferrando, A.A. (2013) 'Direct reversal of glucocorticoid resistance by AKT inhibition in acute lymphoblastic leukemia', *Cancer Cell*, 24(6), pp. 766-76.

Ponader, S., Chen, S.S., Buggy, J.J., Balakrishnan, K., Gandhi, V., Wierda, W.G., Keating, M.J., O'Brien, S., Chiorazzi, N. and Burger, J.A. (2012) 'The Bruton tyrosine kinase inhibitor PCI-32765 thwarts chronic lymphocytic leukemia cell survival and tissue homing in vitro and in vivo', *Blood*, 119(5), pp. 1182-9.

Popat, U. and Abraham, J. (2011) *Leukemia*. Demos Medical Publishing. Available at: http://NCL.eblib.com/patron/FullRecord.aspx?p=782031.

Porkka, K., Koskenvesa, P., Lundan, T., Rimpilainen, J., Mustjoki, S., Smykla, R., Wild, R., Luo, R., Arnan, M., Brethon, B., Eccersley, L., Hjorth-Hansen, H., Hoglund, M., Klamova, H., Knutsen, H., Parikh, S., Raffoux, E., Gruber, F., Brito-Babapulle, F., Dombret, H., Duarte, R.F., Elonen, E., Paquette, R., Zwaan, C.M. and Lee, F.Y. (2008) 'Dasatinib crosses the blood-brain barrier and is an efficient therapy for central nervous system Philadelphia chromosome-positive leukemia', *Blood*, 112(4), pp. 1005-12.

Pozarowski, P. and Darzynkiewicz, Z. (2004) 'Analysis of cell cycle by flow cytometry', *Checkpoint Controls and Cancer: Volume 2: Activation and Regulation Protocols*, pp. 301-311.

Pui, C.-H. and Evans, W.E. (2006) 'Treatment of acute lymphoblastic leukemia', *New England Journal of Medicine*, 354(2), pp. 166-178.

Pui, C.-H., Mullighan, C.G., Evans, W.E. and Relling, M.V. (2012a) 'Pediatric acute lymphoblastic leukemia: where are we going and how do we get there?', *Blood*, 120(6), pp. 1165-1174.

Pui, C.-H., Robison, L.L. and Look, A.T. (2008) 'Acute lymphoblastic leukaemia', *The Lancet*, 371(9617), pp. 1030-1043.

Pui, C.H. (2013) 'Reducing delayed intensification therapy in childhood ALL', *Lancet Oncol*, 14(3), pp. 178-9.

Pui, C.H., Campana, D., Pei, D., Bowman, W.P., Sandlund, J.T., Kaste, S.C., Ribeiro, R.C., Rubnitz, J.E., Raimondi, S.C., Onciu, M., Coustan-Smith, E., Kun, L.E., Jeha, S., Cheng, C., Howard, S.C., Simmons, V., Bayles, A., Metzger, M.L., Boyett, J.M., Leung, W., Handgretinger, R., Downing, J.R., Evans, W.E. and Relling, M.V. (2009) 'Treating childhood acute lymphoblastic leukemia without cranial irradiation', *N Engl J Med*, 360(26), pp. 2730-41.

Pui, C.H. and Jeha, S. (2007) 'New therapeutic strategies for the treatment of acute lymphoblastic leukaemia', *Nat Rev Drug Discov*, 6(2), pp. 149-65.

Pui, C.H., Mullighan, C.G., Evans, W.E. and Relling, M.V. (2012b) 'Pediatric acute lymphoblastic leukemia: where are we going and how do we get there?', *Blood*, 120(6), pp. 1165-74.

Pui, C.H., Pei, D., Coustan-Smith, E., Jeha, S., Cheng, C., Bowman, W.P., Sandlund, J.T., Ribeiro, R.C., Rubnitz, J.E., Inaba, H., Bhojwani, D., Gruber, T.A., Leung, W.H., Downing, J.R., Evans, W.E., Relling, M.V. and Campana, D. (2015) 'Clinical utility of sequential minimal residual disease measurements in the context of risk-based therapy in childhood acute lymphoblastic leukaemia: a prospective study', *Lancet Oncol*, 16(4), pp. 465-74.

Pui, C.H., Relling, M.V. and Downing, J.R. (2004) 'Acute lymphoblastic leukemia', *N Engl J Med*, 350(15), pp. 1535-48.

Quiroga, M.P., Balakrishnan, K., Kurtova, A.V., Sivina, M., Keating, M.J., Wierda, W.G., Gandhi, V. and Burger, J.A. (2009) 'B-cell antigen receptor signaling enhances chronic lymphocytic leukemia cell migration and survival: specific targeting with a novel spleen tyrosine kinase inhibitor, R406', *Blood*, 114(5), pp. 1029-37.

Raedler, L.A. (2016) 'Imbruvica (Ibrutinib): First Drug Approved for the Treatment of Patients with Waldenström's Macroglobulinemia', *American Health & Drug Benefits*, 9(Spec Feature), p. 89.

Ramadani, F., Bolland, D.J., Garcon, F., Emery, J.L., Vanhaesebroeck, B., Corcoran, A.E. and Okkenhaug, K. (2010) 'The PI3K isoforms p110alpha and p110delta are essential for pre-B cell receptor signaling and B cell development', *Sci Signal*, 3(134), p. ra60.

Ramasamy, K.A. (2012) *Combination of Dasatinib and Dexamethasone targets the myeloma plasma cell through its interaction with the bone marrow microenvironment* Haemato-Oncology thesis. King's College London.

Rand, V., Parker, H., Russell, L.J., Schwab, C., Ensor, H., Irving, J., Jones, L., Masic, D., Minto, L., Morrison, H., Ryan, S., Robinson, H., Sinclair, P., Moorman, A.V., Strefford, J.C. and Harrison, C.J. (2011) 'Genomic characterization implicates iAMP21 as a likely primary genetic event in childhood B-cell precursor acute lymphoblastic leukemia', *Blood*, 117(25), pp. 6848-55.

Ravandi, F., O'Brien, S., Thomas, D., Faderl, S., Jones, D., Garris, R., Dara, S., Jorgensen, J., Kebriaei, P., Champlin, R., Borthakur, G., Burger, J., Ferrajoli, A., Garcia-Manero, G., Wierda, W., Cortes, J. and Kantarjian, H. (2010) 'First report of phase 2 study of dasatinib with hyper-CVAD for the frontline treatment of patients with Philadelphia chromosome-positive (Ph+) acute lymphoblastic leukemia', *Blood*, 116(12), pp. 2070-7.

Rebecca, V.W. and Smalley, K.S. (2014) 'Change or die: targeting adaptive signaling to kinase inhibition in cancer cells', *Biochem Pharmacol*, 91(4), pp. 417-25.

Reth, M. and Nielsen, P. (2014) 'Chapter Four - Signaling Circuits in Early B-Cell Development', in Frederick, W.A. (ed.) *Advances in Immunology*. Academic Press, pp. 129-175.

Ribeiro, R.C., Abromowitch, M., Raimondi, S.C., Murphy, S.B., Behm, F. and Williams, D.L. (1987) 'Clinical and biologic hallmarks of the Philadelphia chromosome in childhood acute lymphoblastic leukemia', *Blood*, 70(4), pp. 948-53.

Riccaboni, M., Bianchi, I. and Petrillo, P. (2010) 'Spleen tyrosine kinases: biology, therapeutic targets and drugs', *Drug Discov Today*, 15(13-14), pp. 517-30.

Rickert, R.C. (2013) 'New insights into pre-BCR and BCR signalling with relevance to B cell malignancies', *Nat Rev Immunol*, 13(8), pp. 578-91.

Ries, L.A.G., Smith, M.A., Gurney, J.G., Linet, M., Tamra, T., Young, J.L. and Bunin, G. (1999) 'Cancer incidence and survival among children and adolescents: United States SEER Program 1975-1995', *Cancer incidence and survival among children and adolescents: United States SEER Program 1975-1995*.

Roberts, K.G., Li, Y., Payne-Turner, D., Harvey, R.C., Yang, Y.L., Pei, D., McCastlain, K., Ding, L., Lu, C., Song, G., Ma, J., Becksfort, J., Rusch, M., Chen, S.C., Easton, J., Cheng, J., Boggs, K., Santiago-Morales, N., Iacobucci, I., Fulton, R.S., Wen, J., Valentine, M., Cheng, C., Paugh, S.W., Devidas, M., Chen, I.M., Reshmi, S., Smith, A., Hedlund, E., Gupta, P., Nagahawatte, P., Wu, G., Chen, X., Yergeau, D., Vadodaria, B., Mulder, H., Winick, N.J., Larsen, E.C., Carroll, W.L., Heerema, N.A., Carroll, A.J., Grayson, G., Tasian, S.K., Moore, A.S., Keller, F., Frei-Jones, M., Whitlock, J.A., Raetz, E.A., White, D.L., Hughes, T.P., Guidry Auvil, J.M., Smith, M.A., Marcucci, G., Bloomfield, C.D., Mrozek, K., Kohlschmidt, J., Stock, W., Kornblau, S.M., Konopleva, M., Paietta, E., Pui, C.H., Jeha, S., Relling, M.V., Evans, W.E., Gerhard, D.S., Gastier-Foster, J.M., Mardis, E., Wilson, R.K., Loh, M.L., Downing, J.R., Hunger, S.P., Willman, C.L., Zhang, J. and Mullighan, C.G. (2014) 'Targetable kinase-activating lesions in Ph-like acute lymphoblastic leukemia', *N Engl J Med*, 371(11), pp. 1005-15.

Roberts, K.G., Morin, R.D., Zhang, J., Hirst, M., Zhao, Y., Su, X., Chen, S.C., Payne-Turner, D., Churchman, M.L., Harvey, R.C., Chen, X., Kasap, C., Yan, C., Becksfort, J., Finney, R.P., Teachey, D.T., Maude, S.L., Tse, K., Moore, R., Jones, S., Mungall, K., Birol, I., Edmonson, M.N., Hu, Y., Buetow, K.E., Chen, I.M., Carroll, W.L., Wei, L., Ma, J., Kleppe, M., Levine, R.L., Garcia-Manero, G., Larsen, E., Shah, N.P., Devidas, M., Reaman, G., Smith, M., Paugh, S.W., Evans, W.E., Grupp, S.A., Jeha, S., Pui, C.H., Gerhard, D.S., Downing, J.R., Willman, C.L., Loh, M., Hunger, S.P., Marra, M.A. and Mullighan, C.G. (2012) 'Genetic alterations activating kinase and cytokine receptor signaling in high-risk acute lymphoblastic leukemia', *Cancer Cell*, 22(2), pp. 153-66.

Roederer, M. (2001) 'Spectral compensation for flow cytometry: visualization artifacts, limitations, and caveats', *Cytometry*, 45(3), pp. 194-205.

Rolf, M.G., Curwen, J.O., Veldman-Jones, M., Eberlein, C., Wang, J., Harmer, A., Hellawell, C.J. and Braddock, M. (2015) 'In vitro pharmacological profiling of R406 identifies molecular targets underlying the clinical effects of fostamatinib', *Pharmacol Res Perspect*, 3(5), p. e00175.

Rousselot, P., Coude, M.M., Gokbuget, N., Gambacorti Passerini, C., Hayette, S., Cayuela, J.M., Huguet, F., Leguay, T., Chevallier, P., Salanoubat, C., Bonmati, C., Alexis, M., Hunault, M., Glaisner, S., Agape, P., Berthou, C., Jourdan, E., Fernandes, J., Sutton, L., Banos, A., Reman, O., Lioure, B., Thomas, X., Ifrah, N., Lafage-Pochitaloff, M., Bornand, A., Morisset, L., Robin, V., Pfeifer, H., Delannoy, A., Ribera, J., Bassan, R., Delord, M., Hoelzer, D., Dombret, H. and Ottmann, O.G. (2016) 'Dasatinib and low-intensity chemotherapy in elderly patients with Philadelphia chromosome-positive ALL', *Blood*, 128(6), pp. 774-82.

Rubnitz, J.E., Wichlan, D., Devidas, M., Shuster, J., Linda, S.B., Kurtzberg, J., Bell, B., Hunger, S.P., Chauvenet, A., Pui, C.H., Camitta, B. and Pullen, J. (2008) 'Prospective analysis of TEL gene rearrangements in childhood acute lymphoblastic leukemia: a Children's Oncology Group study', *J Clin Oncol*, 26(13), pp. 2186-91.

Russell, L.J., Capasso, M., Vater, I., Akasaka, T., Bernard, O.A., Calasanz, M.J., Chandrasekaran, T., Chapiro, E., Gesk, S., Griffiths, M., Guttery, D.S., Haferlach, C., Harder, L., Heidenreich, O., Irving, J., Kearney, L., Nguyen-Khac, F., Machado, L., Minto, L., Majid, A., Moorman, A.V., Morrison, H., Rand, V., Strefford, J.C., Schwab, C., Tonnies, H., Dyer, M.J., Siebert, R. and Harrison, C.J. (2009) 'Deregulated expression of cytokine receptor gene, CRLF2, is involved in lymphoid transformation in B-cell precursor acute lymphoblastic leukemia', *Blood*, 114(13), pp. 2688-98.

Ryan, S.L., Matheson, E., Grossmann, V., Sinclair, P., Bashton, M., Schwab, C., Towers, W., Partington, M., Elliott, A., Minto, L., Richardson, S., Rahman, T., Keavney, B., Skinner, R., Bown, N., Haferlach, T., Vandenberghe, P., Haferlach, C., Santibanez-Koref, M., Moorman, A.V., Kohlmann, A., Irving, J.A. and Harrison, C.J. (2016) 'The role of the RAS pathway in iAMP21-ALL', *Leukemia*, 30(9), pp. 1824-31.

Safaroghli-Azar, A., Bashash, D., Sadreazami, P., Momeny, M. and Ghaffari, S.H. (2017) 'PI3K-delta inhibition using CAL-101 exerts apoptotic effects and increases doxorubicin-induced cell death in pre-B-acute lymphoblastic leukemia cells', *Anticancer Drugs*, 28(4), pp. 436-445.

Sakaguchi, N. and Melchers, F. (1986) 'λ5, a new light-chain-related locus selectively expressed in pre-B lymphocytes', *Nature*, 324, p. 579.

Samuels, A.L., Peeva, V.K., Papa, R.A., Firth, M.J., Francis, R.W., Beesley, A.H., Lock, R.B. and Kees, U.R. (2010) 'Validation of a mouse xenograft model system for gene expression analysis of human acute lymphoblastic leukaemia', *BMC Genomics*, 11, p. 256.

Schaaf, M.J. and Cidlowski, J.A. (2002) 'Molecular mechanisms of glucocorticoid action and resistance', *J Steroid Biochem Mol Biol*, 83(1-5), pp. 37-48.

Schaink A, H.C. (2016) 'Minimal Residual Disease Evaluation in Childhood Acute Lymphoblastic Leukemia: A Clinical Evidence Review', *Ont Health Technol Assess Ser*, 16(7), pp. 1-52.

Scharenberg, A.M., Humphries, L.A. and Rawlings, D.J. (2007a) 'Calcium signalling and cell-fate choice in B cells', *Nat Rev Immunol*, 7(10), pp. 778-789.

Scharenberg, A.M., Humphries, L.A. and Rawlings, D.J. (2007b) 'Calcium signalling and cell-fate choice in B cells', *Nat Rev Immunol*, 7(10), pp. 778-89.

Schmidt, S., Rainer, J., Ploner, C., Presul, E., Riml, S. and Kofler, R. (2004) 'Glucocorticoid-induced apoptosis and glucocorticoid resistance: molecular mechanisms and clinical relevance', *Cell Death Differ*, 11 Suppl 1, pp. S45-55.

Schmidt, S., Rainer, J., Riml, S., Ploner, C., Jesacher, S., Achmuller, C., Presul, E., Skvortsov, S., Crazzolara, R., Fiegl, M., Raivio, T., Janne, O.A., Geley, S., Meister, B. and Kofler, R. (2006) 'Identification of glucocorticoid-response genes in children with acute lymphoblastic leukemia', *Blood*, 107(5), pp. 2061-9.

Schmiegelow, K., Forestier, E., Hellebostad, M., Heyman, M., Kristinsson, J., Soderhall, S. and Taskinen, M. (2010) 'Long-term results of NOPHO ALL-92 and ALL-2000 studies of childhood acute lymphoblastic leukemia', *Leukemia*, 24(2), pp. 345-54.

Schmittgen, T.D. and Livak, K.J. (2008) 'Analyzing real-time PCR data by the comparative C(T) method', *Nat Protoc*, 3(6), pp. 1101-8.

Schneider, D., Duhren-von Minden, M., Alkhatib, A., Setz, C., van Bergen, C.A., Benkisser-Petersen, M., Wilhelm, I., Villringer, S., Krysov, S., Packham, G., Zirlik, K., Romer, W., Buske, C., Stevenson, F.K., Veelken, H. and Jumaa, H. (2015) 'Lectins from opportunistic bacteria interact with acquired variable-region glycans of surface immunoglobulin in follicular lymphoma', *Blood*, 125(21), pp. 3287-96.

Scholl, C., Gilliland, D.G. and Frohling, S. (2008) 'Deregulation of signaling pathways in acute myeloid leukemia', *Semin Oncol*, 35(4), pp. 336-45.

Schreer, A., Tinson, C., Sherry, J.P. and Schirmer, K. (2005) 'Application of Alamar blue/5-carboxyfluorescein diacetate acetoxymethyl ester as a noninvasive cell viability assay in primary hepatocytes from rainbow trout', *Anal Biochem*, 344(1), pp. 76-85.

Schreiber, E., Matthias, P., Muller, M.M. and Schaffner, W. (1989) 'Rapid detection of octamer binding proteins with 'mini-extracts', prepared from a small number of cells', *Nucleic Acids Res*, 17(15), p. 6419.

Schultz, K.R., Bowman, W.P., Aledo, A., Slayton, W.B., Sather, H., Devidas, M., Wang, C., Davies, S.M., Gaynon, P.S., Trigg, M., Rutledge, R., Burden, L., Jorstad, D., Carroll, A., Heerema, N.A., Winick, N., Borowitz, M.J., Hunger, S.P., Carroll, W.L. and Camitta, B. (2009) 'Improved early event-free survival with imatinib in Philadelphia chromosome-positive acute lymphoblastic leukemia: a children's oncology group study', *J Clin Oncol*, 27(31), pp. 5175-81.

Schultz, K.R., Carroll, A., Heerema, N.A., Bowman, W.P., Aledo, A., Slayton, W.B., Sather, H., Devidas, M., Zheng, H.W., Davies, S.M., Gaynon, P.S., Trigg, M., Rutledge, R., Jorstad, D., Winick, N., Borowitz, M.J., Hunger, S.P., Carroll, W.L. and Camitta, B. (2014) 'Long-term follow-up of imatinib in pediatric Philadelphia chromosome-positive acute lymphoblastic leukemia: Children's Oncology Group study AALL0031', *Leukemia*, 28(7), pp. 1467-71.

Schwab, C.J., Chilton, L., Morrison, H., Jones, L., Al-Shehhi, H., Erhorn, A., Russell, L.J., Moorman, A.V. and Harrison, C.J. (2013) 'Genes commonly deleted in childhood B-cell precursor acute lymphoblastic leukemia: association with cytogenetics and clinical features', *Haematologica*, 98(7), pp. 1081-8.

Scott, C.L., Becker, M.A., Haluska, P. and Samimi, G. (2013) 'Patient-derived xenograft models to improve targeted therapy in epithelial ovarian cancer treatment', *Front Oncol*, 3, p. 295.

Scupoli, M.T. and Pizzolo, G. (2012) 'Signaling pathways activated by the B-cell receptor in chronic lymphocytic leukemia', *Expert Rev Hematol*, 5(3), pp. 341-8.

Serafin, V., Capuzzo, G., Milani, G., Minuzzo, S.A., Pinazza, M., Bortolozzi, R., Bresolin, S., Porcu, E., Frasson, C., Indraccolo, S., Basso, G. and Accordi, B. (2017) 'Glucocorticoid resistance is reverted by LCK inhibition in pediatric T-cell acute lymphoblastic leukemia', *Blood*.

Shaw, A.C., Swat, W., Davidson, L. and Alt, F.W. (1999a) 'Induction of Ig light chain gene rearrangement in heavy chain-deficient B cells by activated Ras', *Proc Natl Acad Sci U S A*, 96(5), pp. 2239-43.

Shaw, A.C., Swat, W., Ferrini, R., Davidson, L. and Alt, F.W. (1999b) 'Activated Ras signals developmental progression of recombinase-activating gene (RAG)-deficient pro-B lymphocytes', *J Exp Med*, 189(1), pp. 123-9.

Shultz, L.D., Ishikawa, F. and Greiner, D.L. (2007) 'Humanized mice in translational biomedical research', *Nat Rev Immunol*, 7(2), pp. 118-30.

Silveira, A.B., Laranjeira, A.B., Rodrigues, G.O., Leal, P.C., Cardoso, B.A., Barata, J.T., Yunes, R.A., Zanchin, N.I., Brandalise, S.R. and Yunes, J.A. (2015) 'PI3K inhibition synergizes with glucocorticoids but antagonizes with methotrexate in T-cell acute lymphoblastic leukemia', *Oncotarget*, 6(15), pp. 13105-18.

Siolas, D. and Hannon, G.J. (2013) 'Patient-derived tumor xenografts: transforming clinical samples into mouse models', *Cancer Res*, 73(17), pp. 5315-9.

Sivina, M., Kreitman, R.J., Arons, E., Ravandi, F. and Burger, J.A. (2014) 'The bruton tyrosine kinase inhibitor ibrutinib (PCI-32765) blocks hairy cell leukaemia survival, proliferation

and B cell receptor signalling: a new therapeutic approach', *British journal of haematology*.

Skopek, T.R., Liber, H.L., Penman, B.W. and Thilly, W.G. (1978) 'Isolation of a human lymphoblastoid line heterozygous at the thymidine kinase locus: possibility for a rapid human cell mutation assay', *Biochem Biophys Res Commun*, 84(2), pp. 411-6.

Slinger, E., Thijssen, R., Kater, A.P. and Eldering, E. (2017) 'Targeting antigen-independent proliferation in chronic lymphocytic leukemia through differential kinase inhibition', *Leukemia*.

Smith, M., Arthur, D., Camitta, B., Carroll, A.J., Crist, W., Gaynon, P., Gelber, R., Heerema, N., Korn, E.L., Link, M., Murphy, S., Pui, C.H., Pullen, J., Reamon, G., Sallan, S.E., Sather, H., Shuster, J., Simon, R., Trigg, M., Tubergen, D., Uckun, F. and Ungerleider, R. (1996) 'Uniform approach to risk classification and treatment assignment for children with acute lymphoblastic leukemia', *J Clin Oncol*, 14(1), pp. 18-24.

Smith, P.K., Krohn, R.I., Hermanson, G.T., Mallia, A.K., Gartner, F.H., Provenzano, M.D., Fujimoto, E.K., Goeke, N.M., Olson, B.J. and Klenk, D.C. (1985) 'Measurement of protein using bicinchoninic acid', *Anal Biochem*, 150(1), pp. 76-85.

Staudt, L.M., Dunleavy, K., Buggy, J.J., Hedrick, E., Lucas, N., Pittaluga, S., Jhavar, S., Schmitz, R., Williams, M. and Lih, J. (2011) *ASH Annual Meeting Abstracts*.

Stirewalt, D.L. and Radich, J.P. (2003) 'The role of FLT3 in haematopoietic malignancies', *Nat Rev Cancer*, 3(9), pp. 650-65.

Strober, W. (2001) 'Trypan blue exclusion test of cell viability', *Curr Protoc Immunol*, Appendix 3, p. Appendix 3B.

Su, Y.W. and Jumaa, H. (2003) 'LAT links the pre-BCR to calcium signaling', *Immunity*, 19(2), pp. 295-305.

Suljagic, M., Longo, P.G., Bennardo, S., Perlas, E., Leone, G., Laurenti, L. and Efremov, D.G. (2010) 'The Syk inhibitor fostamatinib disodium (R788) inhibits tumor growth in the Emu- TCL1 transgenic mouse model of CLL by blocking antigen-dependent B-cell receptor signaling', *Blood*, 116(23), pp. 4894-905.

Sun, C. and Bernards, R. (2014) 'Feedback and redundancy in receptor tyrosine kinase signaling: relevance to cancer therapies', *Trends Biochem Sci*, 39(10), pp. 465-74.

Sun, C., Chang, L. and Zhu, X. (2017) 'Pathogenesis of ETV6/RUNX1-positive childhood acute lymphoblastic leukemia and mechanisms underlying its relapse', *Oncotarget*, 8(21), pp. 35445-35459.

Swaminathan, S., Huang, C., Geng, H., Chen, Z., Harvey, R., Kang, H., Ng, C., Titz, B., Hurtz, C., Sadiyah, M.F., Nowak, D., Thoennissen, G.B., Rand, V., Graeber, T.G., Koeffler, H.P., Carroll, W.L., Willman, C.L., Hall, A.G., Igarashi, K., Melnick, A. and Muschen, M. (2013a) 'BACH2 mediates negative selection and p53-dependent tumor suppression at the pre-B cell receptor checkpoint', *Nat Med*, 19(8), pp. 1014-1022.

Swaminathan, S., Huang, C., Geng, H., Chen, Z., Harvey, R., Kang, H., Ng, C., Titz, B., Hurtz, C., Sadiyah, M.F., Nowak, D., Thoennissen, G.B., Rand, V., Graeber, T.G., Koeffler, H.P., Carroll, W.L., Willman, C.L., Hall, A.G., Igarashi, K., Melnick, A. and Muschen, M. (2013b) 'BACH2 mediates negative selection and p53-dependent tumor suppression at the pre-B cell receptor checkpoint', *Nat Med*, 19(8), pp. 1014-22.

Sweeny, D.J., Li, W., Clough, J., Bhamidipati, S., Singh, R., Park, G., Baluom, M., Grossbard, E. and Lau, D.T. (2010) 'Metabolism of fostamatinib, the oral methylene phosphate prodrug of the spleen tyrosine kinase inhibitor R406 in humans: contribution of hepatic and gut bacterial processes to the overall biotransformation', *Drug Metab Dispos*, 38(7), pp. 1166-76.

Szczepanski, T., Harrison, C.J. and van Dongen, J.J. (2010) 'Genetic aberrations in paediatric acute leukaemias and implications for management of patients', *Lancet Oncol*, 11(9), pp. 880-9.

Ta, V.B., de Bruijn, M.J., ter Brugge, P.J., van Hamburg, J.P., Diepstraten, H.J., van Loo, P.F., Kersseboom, R. and Hendriks, R.W. (2010) 'Malignant transformation of Slp65-deficient pre-B cells involves disruption of the Arf-Mdm2-p53 tumor suppressor pathway', *Blood*, 115(7), pp. 1385-93.

Taguchi, T., Kiyokawa, N., Takenouch, H., Matsui, J., Tang, W.R., Nakajima, H., Suzuki, K., Shiozawa, Y., Saito, M., Katagiri, Y.U., Takahashi, T., Karasuyama, H., Matsuo, Y., Okita, H. and Fujimoto, J. (2004) 'Deficiency of BLNK hampers PLC-gamma2 phosphorylation and Ca2+ influx induced by the pre-B-cell receptor in human pre-B cells', *Immunology*, 112(4), pp. 575-82.

Takano, T., Sada, K. and Yamamura, H. (2002) 'Role of protein-tyrosine kinase syk in oxidative stress signaling in B cells', *Antioxid Redox Signal*, 4(3), pp. 533-41.

Talpaz, M., Shah, N.P., Kantarjian, H., Donato, N., Nicoll, J., Paquette, R., Cortes, J., O'Brien, S., Nicaise, C., Bleickardt, E., Blackwood-Chirchir, M.A., Iyer, V., Chen, T.T., Huang, F., Decillis, A.P. and Sawyers, C.L. (2006) 'Dasatinib in imatinib-resistant Philadelphia chromosome-positive leukemias', *N Engl J Med*, 354(24), pp. 2531-41.

Tan, S.C. and Yiap, B.C. (2009) 'DNA, RNA, and Protein Extraction: The Past and The Present', *Journal of Biomedicine and Biotechnology*, 2009, p. 574398.

Tang, T.T., Dowbenko, D., Jackson, A., Toney, L., Lewin, D.A., Dent, A.L. and Lasky, L.A. (2002) 'The forkhead transcription factor AFX activates apoptosis by induction of the BCL-6 transcriptional repressor', *J Biol Chem*, 277(16), pp. 14255-65.

Tasian, S.K., Doral, M.Y., Borowitz, M.J., Wood, B.L., Chen, I.M., Harvey, R.C., Gastier-Foster, J.M., Willman, C.L., Hunger, S.P., Mullighan, C.G. and Loh, M.L. (2012) 'Aberrant STAT5 and PI3K/mTOR pathway signaling occurs in human CRLF2-rearranged B-precursor acute lymphoblastic leukemia', *Blood*, 120(4), pp. 833-42.

Tataurov, A.V., You, Y. and Owczarzy, R. (2008) 'Predicting ultraviolet spectrum of single stranded and double stranded deoxyribonucleic acids', *Biophys Chem*, 133(1-3), pp. 66-70.

Tentler, J.J., Tan, A.C., Weekes, C.D., Jimeno, A., Leong, S., Pitts, T.M., Arcaroli, J.J., Messersmith, W.A. and Eckhardt, S.G. (2012) 'Patient-derived tumour xenografts as models for oncology drug development', *Nat Rev Clin Oncol*, 9(6), pp. 338-50.

Trageser, D., Iacobucci, I., Nahar, R., Duy, C., von Levetzow, G., Klemm, L., Park, E., Schuh, W., Gruber, T., Herzog, S., Kim, Y.M., Hofmann, W.K., Li, A., Storlazzi, C.T., Jack, H.M., Groffen, J., Martinelli, G., Heisterkamp, N., Jumaa, H. and Muschen, M. (2009) 'Pre-B cell receptor-mediated cell cycle arrest in Philadelphia chromosome-positive acute lymphoblastic leukemia requires IKAROS function', *J Exp Med*, 206(8), pp. 1739-53.

Trahair, T.N., Lock, R.B., Sutton, R., Sia, K.C., Evans, K., Richmond, J., Law, T., Venn, N.C., Irving, J.A., Moore, S., Nievergall, E., Dang, P., Heatley, S.L., White, D.L. and Revesz, T. (2016) 'Xenograft-directed personalized therapy for a patient with post-transplant relapse of ALL', *Bone Marrow Transplant*, 51(9), pp. 1279-82.

Trimarchi, T. and Aifantis, I. (2015) 'The pre-BCR to the rescue: therapeutic targeting of pre-B cell ALL', *Cancer Cell*, 27(3), pp. 321-3.

Tucker, D.L. and Rule, S.A. (2015) 'A critical appraisal of ibrutinib in the treatment of mantle cell lymphoma and chronic lymphocytic leukemia', *Therapeutics and Clinical Risk Management*, 11, pp. 979-990.

Tyner, J.W., Yang, W.F., Bankhead, A., 3rd, Fan, G., Fletcher, L.B., Bryant, J., Glover, J.M., Chang, B.H., Spurgeon, S.E., Fleming, W.H., Kovacsovics, T., Gotlib, J.R., Oh, S.T., Deininger, M.W., Zwaan, C.M., Den Boer, M.L., van den Heuvel-Eibrink, M.M., O'Hare, T., Druker, B.J. and Loriaux, M.M. (2013) 'Kinase pathway dependence in primary human leukemias determined by rapid inhibitor screening', *Cancer Res*, 73(1), pp. 285-96.

Ubelhart, R., Bach, M.P., Eschbach, C., Wossning, T., Reth, M. and Jumaa, H. (2010) 'N-linked glycosylation selectively regulates autonomous precursor BCR function', *Nat Immunol*, 11(8), pp. 759-65.

Uckun, F.M., Ek, R.O., Jan, S.T., Chen, C.L. and Qazi, S. (2010a) 'Targeting SYK kinase-dependent anti-apoptotic resistance pathway in B-lineage acute lymphoblastic leukaemia (ALL) cells with a potent SYK inhibitory pentapeptide mimic', *Br J Haematol*, 149(4), pp. 508-17.

Uckun, F.M. and Qazi, S. (2014) 'SYK as a New Therapeutic Target in B-Cell Precursor Acute Lymphoblastic Leukemia', *J Cancer Ther*, 5(1), pp. 124-131.

Uckun, F.M., Qazi, S., Ma, H., Tuel-Ahlgren, L. and Ozer, Z. (2010b) 'STAT3 is a substrate of SYK tyrosine kinase in B-lineage leukemia/lymphoma cells exposed to oxidative stress', *Proc Natl Acad Sci U S A*, 107(7), pp. 2902-7.

van Delft, F.W., Bellotti, T., Luo, Z., Jones, L.K., Patel, N., Yiannikouris, O., Hill, A.S., Hubank, M., Kempski, H., Fletcher, D., Chaplin, T., Foot, N., Young, B.D., Hann, I.M., Gammerman, A. and Saha, V. (2005) 'Prospective gene expression analysis accurately subtypes acute leukaemia in children and establishes a commonality between hyperdiploidy and t(12;21) in acute lymphoblastic leukaemia', *Br J Haematol*, 130(1), pp. 26-35.

van der Veer, A., van der Velden, V.H., Willemse, M.E., Hoogeveen, P.G., Petricoin, E.F., Beverloo, H.B., Escherich, G., Horstmann, M.A., Pieters, R. and den Boer, M.L. (2014) 'Interference with pre-B-cell receptor signaling offers a therapeutic option for TCF3-rearranged childhood acute lymphoblastic leukemia', *Blood Cancer J*, 4, p. e181.

Vanhaesebroeck, B., Welham, M.J., Kotani, K., Stein, R., Warne, P.H., Zvelebil, M.J., Higashi, K., Volinia, S., Downward, J. and Waterfield, M.D. (1997) 'P110delta, a novel phosphoinositide 3-kinase in leukocytes', *Proc Natl Acad Sci U S A*, 94(9), pp. 4330-5.

Vermes, I., Haanen, C., Steffens-Nakken, H. and Reutelingsperger, C. (1995) 'A novel assay for apoptosis. Flow cytometric detection of phosphatidylserine expression on early apoptotic cells using fluorescein labelled Annexin V', *J Immunol Methods*, 184(1), pp. 39-51.

Vora, A., Goulden, N., Mitchell, C., Hancock, J., Hough, R., Rowntree, C., Moorman, A.V. and Wade, R. (2014) 'Augmented post-remission therapy for a minimal residual disease-defined high-risk subgroup of children and young people with clinical standard-risk and intermediate-risk acute lymphoblastic leukaemia (UKALL 2003): a randomised controlled trial', *The lancet oncology*, 15(8), pp. 809-818.

Walker, N.J. (2002) 'Tech.Sight. A technique whose time has come', *Science*, 296(5567), pp. 557-9.

Wang, K., Sanchez-Martin, M., Wang, X., Knapp, K.M., Koche, R., Vu, L., Nahas, M.K., He, J., Hadler, M., Stein, E.M., Tallman, M.S., Donahue, A.L., Frampton, G.M., Lipson, D., Roels, S., Stephens, P.J., Sanford, E.M., Brennan, T., Otto, G.A., Yelensky, R., Miller, V.A., Kharas, M.G., Levine, R.L., Ferrando, A., Armstrong, S.A. and Krivtsov, A.V. (2017) 'Patient-derived xenotransplants can recapitulate the genetic driver landscape of acute leukemias', *Leukemia*, 31(1), pp. 151-158.

Wang, Y.H., Stephan, R.P., Scheffold, A., Kunkel, D., Karasuyama, H., Radbruch, A. and Cooper, M.D. (2002a) 'Differential surrogate light chain expression governs B-cell differentiation', *Blood*, 99(7), pp. 2459-67.

Wang, Z., Frederick, J. and Garabedian, M.J. (2002b) 'Deciphering the phosphorylation "code" of the glucocorticoid receptor in vivo', *J Biol Chem*, 277(29), pp. 26573-80.

Wang, Z., Malone, M.H., He, H., McColl, K.S. and Distelhorst, C.W. (2003) 'Microarray analysis uncovers the induction of the proapoptotic BH3-only protein Bim in multiple models of glucocorticoid-induced apoptosis', *J Biol Chem*, 278(26), pp. 23861-7.

Ward, E., DeSantis, C., Robbins, A., Kohler, B. and Jemal, A. (2014) 'Childhood and adolescent cancer statistics, 2014', *CA Cancer J Clin*, 64(2), pp. 83-103.

Weinblatt, M.E., Genovese, M.C., Ho, M., Hollis, S., Rosiak-Jedrychowicz, K., Kavanaugh, A., Millson, D.S., Leon, G., Wang, M. and van der Heijde, D. (2014) 'Effects of fostamatinib, an oral spleen tyrosine kinase inhibitor, in rheumatoid arthritis patients with an inadequate response to methotrexate: results from a phase III, multicenter, randomized, double-blind, placebo-controlled, parallel-group study', *Arthritis Rheumatol*, 66(12), pp. 3255-64.

Welsh, S.J., Churchman, M.L., Togni, M., Mullighan, C.G. and Hagman, J. (2017) 'Deregulation of kinase signaling and lymphoid development in EBF1-PDGFRB ALL leukemogenesis', *Leukemia*.

Werner, M., Hobeika, E. and Jumaa, H. (2010) 'Role of PI3K in the generation and survival of B cells', *Immunol Rev*, 237(1), pp. 55-71.

Wiemels, J. (2012) 'Perspectives on the causes of childhood leukemia', *Chem Biol Interact*, 196(3), pp. 59-67.

Wiemels, J.L., Cazzaniga, G., Daniotti, M., Eden, O.B., Addison, G.M., Masera, G., Saha, V., Biondi, A. and Greaves, M.F. (1999) 'Prenatal origin of acute lymphoblastic leukaemia in children', *Lancet*, 354(9189), pp. 1499-503.

Williams, S.A., Anderson, W.C., Santaguida, M.T. and Dylla, S.J. (2013) 'Patient-derived xenografts, the cancer stem cell paradigm, and cancer pathobiology in the 21st century', *Lab Invest*, 93(9), pp. 970-982.

Winick, N.J., Carroll, W.L. and Hunger, S.P. (2004) 'Childhood leukemia-new advances and challenges', *New England Journal of Medicine*, 351, pp. 601-602.

Winters, A.C. and Bernt, K.M. (2017) 'MLL-Rearranged Leukemias-An Update on Science and Clinical Approaches', *Front Pediatr*, 5, p. 4.

Woiterski, J., Ebinger, M., Witte, K.E., Goecke, B., Heininger, V., Philippek, M., Bonin, M., Schrauder, A., Rottgers, S., Herr, W., Lang, P., Handgretinger, R., Hartwig, U.F. and Andre, M.C. (2013) 'Engraftment of low numbers of pediatric acute lymphoid and myeloid leukemias into NOD/SCID/IL2Rcgammanull mice reflects individual leukemogenecity and highly correlates with clinical outcome', *Int J Cancer*, 133(7), pp. 1547-56.

Wong, N.C., Bhadri, V.A., Maksimovic, J., Parkinson-Bates, M., Ng, J., Craig, J.M., Saffery, R. and Lock, R.B. (2014) 'Stability of gene expression and epigenetic profiles highlights the utility of patient-derived paediatric acute lymphoblastic leukaemia xenografts for investigating molecular mechanisms of drug resistance', *BMC Genomics*, 15, p. 416.

Woo, J.S., Alberti, M.O. and Tirado, C.A. (2014) 'Childhood B-acute lymphoblastic leukemia: a genetic update', *Exp Hematol Oncol*, 3, p. 16.

Wossning, T., Herzog, S., Kohler, F., Meixlsperger, S., Kulathu, Y., Mittler, G., Abe, A., Fuchs, U., Borkhardt, A. and Jumaa, H. (2006) 'Deregulated Syk inhibits differentiation and induces growth factor-independent proliferation of pre-B cells', *J Exp Med*, 203(13), pp. 2829-40.

Yasuda, T., Sanjo, H., Pages, G., Kawano, Y., Karasuyama, H., Pouyssegur, J., Ogata, M. and Kurosaki, T. (2008) 'Erk kinases link pre-B cell receptor signaling to transcriptional events required for early B cell expansion', *Immunity*, 28(4), pp. 499-508.

Young, R.M. and Staudt, L.M. (2013) 'Targeting pathological B cell receptor signalling in lymphoid malignancies', *Nature Reviews Drug Discovery*, 12(3), pp. 229-243.

Yuan, T.L. and Cantley, L.C. (2008) 'PI3K pathway alterations in cancer: variations on a theme', *Oncogene*, 27(41), pp. 5497-510.

Zhang, J., Mullighan, C.G., Harvey, R.C., Wu, G., Chen, X., Edmonson, M., Buetow, K.H., Carroll, W.L., Chen, I.M., Devidas, M., Gerhard, D.S., Loh, M.L., Reaman, G.H., Relling, M.V., Camitta, B.M., Bowman, W.P., Smith, M.A., Willman, C.L., Downing, J.R. and Hunger, S.P. (2011) 'Key pathways are frequently mutated in high-risk childhood acute lymphoblastic leukemia: a report from the Children's Oncology Group', *Blood*, 118(11), pp. 3080-7.

Zhou, Y., You, M.J., Young, K.H., Lin, P., Lu, G., Medeiros, L.J. and Bueso-Ramos, C.E. (2012) 'Advances in the molecular pathobiology of B-lymphoblastic leukemia', *Hum Pathol*, 43(9), pp. 1347-62.